UNIVERSITY OF LEEDS

Regional modelling of coupled aerosol-cloud interactions and new particle formation in Amazonian convective environments

Xuemei Wang

Submitted in accordance with the requirements for the degree of Doctor of Philosophy

University of Leeds

School of Earth and Environment

March 2023

Declaration of Authorship

The candidate confirms that the work submitted is her own, except where works that formed part of jointly-authored publications have been included. The contributions of the candidate and the other authors to this work have been explicitly indicated below. The candidate confirms that appropriate credit has been given within the thesis where reference has been made to the work of others.

Chapter 3 in its entirety is based on a jointly-authored manuscript intended for publication, but is not yet submitted for review. The manuscript is jointly authored by K. S. Carslaw, D. P. Grosvenor, H. Gordon and M. O. Andreae. The text was written by the candidate with advice and edits from KSC, DPG, HG and MOA during the manuscript preparation. The regional configuration of UM-UKCA was provided by HG and DPG, and HG also provided the codes for pure biogenic nucleation. MOA calculated and corrected the CPC and UHSAS data from ACRIDICO-CHUVA campaign. KSC helped make the schematic diagram (Fig. 3.15) in discussion and conclusion section of Chapter 3. I am thankful to P. Field for advice regarding convection settings and providing meteorology data to run the model, to the Atmospheric and Cloud Dynamics group for helpful discussions on convection and transport, and to A. Ranjithkumar for providing Fortran codes to produce extra model output. The candidate ran the model simulations and analysed the model results with insights, comments, and advise from KSC, HG and DPG.

The text in Chapter 4 and 5 was written by the candidate with advice and edits from KSC, DPG, and HG during the preparation. HG and DPG provided the regional configuration of UM-UKCA for the two chapters and tested the time step setting in the global model for Chapter 5. HG provided the codes for pure biogenic nucleation and inorganic nucleation, and python scripts to interpolate model output in Chapter 4. The candidate ran the model simulations

and analysed the model results with insights, comments, and advise from KSC, HG and DPG. The GoAmazon2014/5 data in Chapter 4 (from CPC and PCASP) were obtained from ARM Climate Research Facility with advice from Jennifer Comstock. Thanks to AR for helping identify the oxidant fields for biogenic nucleation of UKCA for the two chapters.

Acknowledgements

I would like to give my deepest gratitude to my supervisors, Ken Carslaw, Dan Grosvenor and Hamish Gordon. The four-year PhD study would not have been possible without their support and guidance. They spent significant time in helping develop the structure of the PhD, supervision meetings, providing constructive feedback for reports, abstracts, thesis and presentations, helping me build the technical skills and background knowledge for the thesis.

Many thanks to the members of cloud and aerosol research group who have been kind and supportive. It has been great to be part of the team and enjoy all the discussions, meetings and chats which helped me build up background knowledge, provided tips for models and feedbacks that I could not have anywhere else. A special thanks to Ananth Ranjithkumar for providing the Fortran codes for model diagnostic outputs and the help to find oxidant fields, and thanks to Atmospheric and Cloud Dynamics group for advice regarding on the convection scheme.

I am grateful to the CLOUD consortium, CLOUD-MOTION and Marie Curie Initial Training Network fellowship which provided the funding and made this research possible. A special thanks to Joachim Curtius and Katja Ivanova for coordinating events and providing support for all that I needed to join the collaboration meetings.

Thank you to the JASMIN and Met Office group for providing support for UM-UKCA-CASIM and Monsoon Superco(o)mputing Node to run the simulations, and the JASMIN team with whose platform I processed the modelled data. A special thanks to Paul Field for providing the meteorology data files needed to run the model simulations and the advice for Chapter 4.

I would like to thank the co-author of Chapter 3, Meinrat O. Andreae, who provided the particle concentrations during the ACRIDICON-CHUVA campaign.

Finally, thanks to my family and friends for always being supportive and understanding.

Abstract

New particle formation (NPF) has been proven to significantly affect Earth's global radiation balance by forming new aerosols that can subsequently grow to cloud condensation nuclei (CCN). In a tropical convective environment like Amazonia, NPF involving biogenic gas precursors closely interacts with deep convection, which efficiently transports the precursors upward, leading to formation of new particles in the free and upper troposphere. Deep convection can potentially transport these new aerosols downward and supply CCN into the boundary layer. Global models have previously been used to investigate NPF and the contribution to global CCN of aerosols created by NPF. However, to better understand NPF-deep convection interactions, it is necessary to use high-resolution regional models that fully resolve processes that occur at sub-grid scales of a global model. Therefore, this thesis used a high-resolution regional model nested in a global model to investigate the relationships between NPF, aerosol, and deep convection in Amazonia.

Based on the results from CLOUD (Cosmics Leaving Outdoor Droplets) chamber experiments and the previous parameterisations of the nucleation mechanisms in the global models, several nucleation mechanisms were used in the model to investigate the sensitivities of particle profiles in a 1000 km Amazonian region. In Chapter 3, simulations were used to quantify and understand the role of deep convection in modulating NPF and particles during the dry-to-wet transition season. The results show that deep convection transports sufficient amounts of biogenic gas precursor to the upper troposphere to produce high NPF rates. However, the nested simulations within the global model show that more than 75% of the NPF-induced CCN in the boundary layer were originally formed by NPF outside the regional domain rather than in the upper troposphere in the regional domain. The fraction of CCN created by NPF in the regional domain is low because very few of the particles that are formed by NPF in the upper

troposphere can be transported downward to the boundary layer by deep convection within 1000 km.

Anthropogenic emissions can affect particle concentrations via NPF that involves sulfuric acid, and subsequent alteration of CCN concentrations may affect clouds. The sensitivity of aerosol and cloud properties to six anthropogenic emission scenarios in the Amazonian wet season was investigated in Chapter 4. Changes in aerosol and cloud properties in response to the increases in anthropogenic emissions from default emissions were calculated. The results showed that 13% higher aerosol particle concentrations caused by anthropogenic emissions led to 9% increases in cloud droplet number concentrations (CDNC), but cloud water and rain mass mixing ratio were insensitive to any changes in anthropogenic emissions. However, in a test simulation, more-distinct changes in cloud properties occurred when the number of cloud droplets was significantly reduced (by a factor of 2). The results imply that anthropogenic emission will only affect clouds in the Amazonian wet season if it causes significant changes to cloud droplet concentrations, or that there have already been enough particles to suppress rain in the pristine Amazonia, then cloud properties are not sensitive to the increasing anthropogenic emissions.

The biogenic nucleation rate in the upper troposphere is influenced by the concentrations and volatility of gas precursors that are transported upward by deep convection, as well as by the vapour/nuclei condensation sink, temperature, and oxidant concentrations. Nucleation rate is a non-linear function of the influencing factors which are all correlated and are not homogeneously distributed within a region. The non-linear relationship and inhomogeneous distribution cause nucleation rates to be sensitive to their spatial-temporal distribution. However, the spatial variability of the influencing factors may not be well represented by global models with coarse resolutions and parameterised convection. Chapter 5 aimed to investigate how coarse resolution or averaging of the influencing factors could affect the non-linear area-mean nucleation rate at coarse resolutions with different oxidation rates of monoterpenes. The results showed that averaging at coarse resolutions smeared out the monoterpene and condensation sink spatial variability, which was important to correctly calculate nucleation rates over a region. Nucleation rates were not significantly affected by averaging when the gas precursor, monoterpene, had a relatively long lifetime, but were significantly reduced when monoterpene had a shorter lifetime (typical of alpha-pinene). The difference occurs because the lifetime of the precursor gas affects whether it can be homogeneously mixed with the surrounding air.

Overall, the thesis showed the importance of deep convection to support and affect NPF with biogenic gas precursors, and influence particle concentrations over Amazonia. The results also improved our understandings of NPF-aerosol-deep convection interactions under the influence of anthropogenic emissions within Amazonian region. Eventually, the thesis highlights the necessity of using high resolution and resolved convection to better represent non-linear NPF and clouds that are associated with significant spatial variability in Amazonia.

Contents

List of Figures

List of Tables

Abbreviations

ACE	Aerosol Characterization Experiment
ACRIDICON-CHUVA	Aerosol, Cloud, Precipitation, and Radiation Interactions and Dynamics of Convective Cloud Systems - Cloud Processes of the Main Precipitation Systems in Brazil: A Contribution to Cloud Resolving Modeling
ATom	NASA Atmospheric Tomography Mission
ATTO	Amazon Tall Tower Observatory
BC	Black Carbon
BVOC	Biogenic Volatile Organic Compounds
CAM	Community Atmosphere Model
CASIM	Cloud-AeroSol Interacting Microphysics
CCN	Cloud Condensation Nuclei
CDNC	Cloud Droplet Number Concentration
CERN	Conseil Européen pour la Recherche Nucléaire
CLASSIC	Coupled Large-scale Aerosol Simulator for Studies In Climate
CLOUD	Cosmics Leaving Outdoor Droplets
CMIP	Coupled Model Intercomparison Project
CPC	Condensation Particle Counter
COSMO	Consortium for Small-scale Modeling
EDGAR	Emissions Database for Global Atmospheric Research
ENDGame	Even Newer Dynamics for General atmospheric modelling of the environment dynamics
G-1	Gulfstream I
GA	Global Atmosphere
GFED	Global Fire Emissions Database
GLOMAP	Global Model of Aerosol Processes
GoAmazon2014/5	Observations and Modeling of the Green Ocean Amazon 2014-2015
GOES	Geostationary Operational Environmental Satellites
GPM	Global Precipitation Measurement
HadGEM3	Hadley Centre Global Environment Model version 3
HALO	High Altitude and Long Range Research Aircraft
HOM	Highly-Oxygenated Molecule
ICON	Icosahedral Nonhydrostatic

IMPACT	Integrated Massively Parallel Atmospheric Chemical Transport
INC	Ice number concentration
IPCC	Intergovernmental Panel on Climate Change
JULES	Joint UK Land Environment Simulator
KDE	Kernel Distribution Estimation
LES	Large-Eddy Simulation
LWP	Liquid Water Path
MACCity MEGAN	Monitoring Atmospheric Composition and Climate project. The Model of Emissions of Gases and Aerosols from Nature
MODIS	Moderate Resolution Imaging Spectroradiometer
NASA	National Aeronautics and Space Administration
NCAR	National Center for Atmospheric Research
NPF	New Particle Formation
NVOC	Non-Volatile Organic Compounds
OC	Organic carbon
OPC	Optical Particle Counter
PCASP	Passive Cavity Aerosol Spectrometer Probe
PDF	Probability Distribution Function
PUG	Probability of Ultrafine particle Growth
RAMS	Regional Atmospheric Modeling System
SAM	System for Atmospheric Modeling
SOCRATES	Southern Ocean Clouds, Radiation, Aerosol Transport Experimental Study
STP	Standard Temperature and Pressure
UHSAS	Ultra-High Sensitivity Aerosol Spectrometer
UM	Unified Model
UKCA	United Kingdom Chemistry and Aerosol
UT	Upper Troposphere
UTC	Universal Time Coordinated
WRF-Chem	Weather Research and Forecasting (WRF) model coupled with Chemistry

Chapter 1

Motivation and background

1.1 Aerosol and climate

Aerosol particles affect climate by directly altering radiation balance (Ångström 1929; Charlson et al. 1992) and acting as cloud condensation nuclei (CCN) (Twomey 1977; Albrecht 1989; Gordon et al. 2016). Anthropogenic aerosols produce one of the greatest uncertainties in evaluating global radiative forcing and understanding climate change (Jones et al. 1994; Yu et al. 2013).

The importance of aerosols to the climate has been reported by the Intergovernmental Panel on Climate Change (IPCC) Assessment Reports. The fifth IPCC Assessment Report (AR5) evaluated forcings from different forcing agents (Stocker et al. 2013). It quantitatively shows the radiative forcing and effective radiative forcing (ERF). The ERF is the difference in radiative flux at the top of the atmosphere caused by forcing agents such as carbon dioxide, ozone, methane, aerosol, cloud etc. with fixed surface temperature. For ERF calculations, the forcing agents are generally varied between pre-industrial and present day values. The ERF will also cause changes to the atmosphere which includes the adjustments of the cloud structure, precipitation etc. which occur over relatively short time scales, i.e. quicker than the responses that would occur due to surface temperature changes. Figure 1.1 shows that aerosol causes a large negative ERF ($\sim$ 1.3 W m^{-2}) with a high level of uncertainty of around 1.4 W m^{-2} in AR6 (Arias et al. 2021). Therefore, a better understanding of aerosol-cloud interactions will improve the performance of models to quantify aerosol forcing, and this thesis aims to investigate the physical processes of aerosol and clouds.

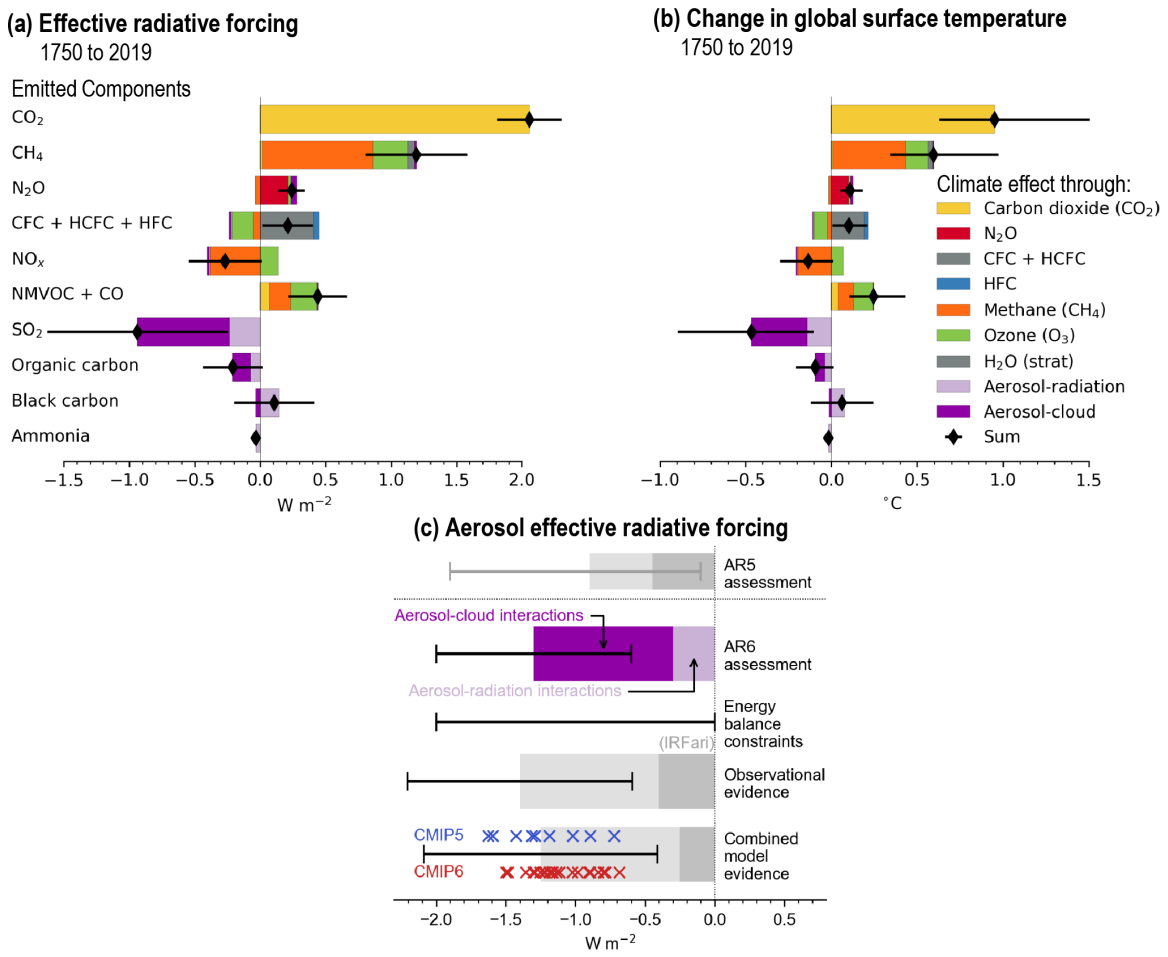

Figure 1.1: Radiative forcing, effective forcing and temperature changes from IPCC AR6 report. The original caption is as follows: 'Contribution to (a) effective radiative forcing (ERF) and (b) global surface temperature change from component emissions for 1750–2019 based on Coupled Model Intercomparison Project Phase 6 (CMIP6) models and (c) net aerosol ERF for 1750–2014 from different lines of evidence. The intent of this figure is to show advances since AR5 in the understanding of (a) emissions-based ERF, (b) global surface temperature response for short-lived climate forcers as estimated in Chapter 6, and (c) aerosol ERF from different lines of evidence as assessed in Chapter 7. In panel (a), ERFs for well-mixed greenhouse gases (WMGHGs) are from the analytical formulae. ERFs for other components are multi-model means based on Earth system model simulations that quantify the effect of individual components. The derived emissions-based ERFs are rescaled to match the concentration-based ERFs in Figure 7.6. Error bars are 5–95% and for the ERF account for uncertainty in radiative efficiencies and multi-model error in the means. In panel (b), the global mean temperature response is calculated from the ERF time series using an impulse response function. In panel (c), the AR6 assessment is based on energy balance constraints, observational evidence from satellite retrievals, and climate model-based evidence. For each line of evidence, the assessed best-estimate contributions from ERF due to aerosol–radiation interactions (ERFari) and aerosol–cloud interactions (ERFaci) are shown with darker and paler shading, respectively. Estimates from individual CMIP Phase 5 (CMIP5) and CMIP6 models are depicted by blue and red crosses, respectively. The observational assessment for ERFari is taken from the instantaneous forcing due to aerosol–radiation interactions (IRFari). Uncertainty ranges are given in black bars for the total aerosol ERF and depict very likely ranges.' (Arias et al. 2021)

Globally, aerosol particles are either directly emitted into the atmosphere (primary aerosols) or are newly formed via gas-to-particle conversion processes (Boucher 2015). This PhD thesis is focused on the newly formed aerosols.

Primary aerosols account for more than 80% of the global aerosol mass emission (Boucher et al. 2013) and are emitted from both natural (sea salt, mineral dust, terrestrial and marine organic aerosols) and anthropogenic sources (black carbon and biomass burning events). Secondary aerosols are newly formed and account for more than 50% of the global low-altitude CCN at 0.2% supersaturation in the present-day environment (Gordon et al. 2017).

1.1.1 New particle formation and growth

The formation of new particles is called nucleation or new particle formation (NPF), which produces new particles via the gas-to-particle conversion process (Boucher 2015). The precursor gases can form clusters of oxidised inorganic gases (Weber et al. 1995; Vehkamäki et al. 2002; Dunne et al. 2016), and highly-oxygenated biogenic gases. Because the ability of organic vapours to nucleate depends on the volatility, the lower volatility, the greater the capacity to nucleate (Riccobono et al. 2014; Kirkby et al. 2016; Tröstl et al. 2016; Simon et al. 2020). Nucleation is then followed by the initial growth of particles by condensation of gases, depending on gas volatility. Gases with lower volatility are more likely to condense on existing particle surface as long as the partial vapour pressure is greater than saturation vapour pressure (Donahue et al. 2006; Lipsky and Robinson 2006; Shrivastava et al. 2006). Condensable gases with high vapour pressure can also easily evaporate from particles. Common gases that can be involved in nucleation or condensation include sulfuric acid (H_2SO_4), ammonia (NH_3), iodic acid (HIO_3), various oxidation products of biogenic volatile organic compounds (BVOCs) etc. (Vehkamäki et al. 2002; Kirkby et al. 2011; Kirkby et al. 2016; He et al. 2021).

Nucleation of particles and their initial growth are affected by the condensation sink (CS) (Kulmala et al. 2001b; Kulmala et al. 2001a; Dal Maso et al. 2002). The condensation sink works to suppress the nucleation rate by allowing the gases to condense on existing particle surfaces instead of nucleating new particles (Kulmala et al. 2001b; Kulmala et al. 2001a; Dal Maso et al. 2002). The magnitude of the condensation sink usually depends on the pre-existing aerosol particle surface area as established by several early studies (Gelbard and Seinfeld 1978; Gelbard and Seinfeld 1979; McMurry and Friedlander 1979; McMurry 1983). The condensation sink

term was incorporated in a box model by Pirjola and Kulmala (1998), so that the model could simulate different environments, and they proved that the background aerosol could act as a condensation sink for the gas-phase H_2SO_4. Cloud droplets and ice crystals, which are much greater in size and surface area than aerosol particles, are also potentially large condensation sink for NPF gases (Lee et al. 2004; Kazil et al. 2011), but are usually not accounted for during the NPF process in modelling studies. Scavenging of gases by cloud and rain has been included in many studies, but most of them do not focus on particle nucleation (Wurzler et al. 1995; Wurzler 1998; Zhang et al. 2006; Kazil et al. 2011; Baklanov et al. 2013; Elperin et al. 2015; Elperin et al. 2017). The inclusion of a condensation sink from cloud hydrometeors will improve modelling of the NPF process in convective environments and achieve a better representation of the particle population.

Coagulation is the process by which aerosol particles collide due to Brownian motion, turbulence and gravitational forces etc, and stick to each other in the atmosphere (Carslaw 2022). It is a sink for particle number concentrations because coagulation with larger particles may reduce the concentrations of tiny particles, and thereby allows growth in mass and size for large particles (Carslaw 2022).

Other environmental conditions, such as temperature and relative humidity have strong influences on NPF (Simon et al. 2020; Hamed et al. 2011). Low temperature usually slows down the gas oxidation rate, and thus stablises the nucleation gases which then increases the probability of nucleation (Zhao et al. 2020), while relative humidity indirectly affects NPF by increasing the condensation sink or by blocking sunlight which suppresses NPF (Hamed et al. 2011).

Observations of NPF

Large number of sub-micron aerosols as well as the subsequent growth have been observed by aircraft and ground-based measurements in the marine; boreal forest; free and upper tropospheric; urban polluted; polar environments etc. NPF events usually occur during the daytime and is driven by solar radiation which allows photochemistry to produce oxidants which then oxidise the gaseous precursors of nucleation, such as SO_2, monoterpene, NO_2 etc. (Vehkamäki et al. 2004; Hamed et al. 2007; Wu et al. 2007; Asmi et al. 2011; Weigel et al. 2011; Qi et al. 2015; Crumeyrolle et al. 2022).

In marine environments, aircraft measurements have detected newly formed particles in the free troposphere that are related to cloud outflow regions with particle populations up to 10000 cm^{-3} greater than in the boundary layer where no new particle is found (Clarke et al. 1998). Two follow up studies found that these newly formed aerosol particles are likely to be formed by binary nucleation which involves nucleating sulfuric acid and water clusters, and the studies suggested the importance of clouds in promoting the nucleation process (Clarke et al. 1999a; Clarke et al. 1999b). Apart from cloud outflow regions, a substantial number of particles with diameter 4-9 nm were detected in the interstitial regions of clouds over Florida (Lee et al. 2004). Clarke et al. (2013) also implied the role of the subsidence of particles in supplying boundary layer CCN, but the NPF that generated these particles could have occurred either in the local atmosphere or further afield. Similar findings have been published in a global observational-modelling study called ATom (NASA Atmospheric Tomography Mission), which detected significant NPF in the upper troposphere and showed their important contribution to low-altitude CCN (Williamson et al. 2019). Observations have proven that precipitation may enhance NPF by scavenging existing large aerosol particles and creating an environment with a lower condensation sink (Zheng et al. 2021). Marine boundary layer NPF has also been observed over the New Zealand coastal region, and it was found to be influenced by the air masses from both land and the sea (Peltola et al. 2022).

In the forest environment, nucleation in the boundary layer has been detected at several observational sites (Hyytiälä (Mäkelä et al. 1997; Kulmala et al. 2001a), Idaho Hill in Colorado (Weber et al. 1997), in Duke forest (Pillai et al. 2013), in British Columbia Canada (Andreae et al. 2022) etc.). Nucleation has also been observed in the free troposphere over mountainous regions, such as Jungfraujoch in Switzerland (Bianchi et al. 2016) where the particles were composed of BVOCs, sulfuric acid and ammonia. In Himalaya regions, newly formed aerosol particles mainly involve biogenic compounds (Bianchi et al. 2020). Both of these two sites are influenced by the air masses from the surrounding environments. In the tropical Amazonian rainforest, NPF is rarely observed within the boundary layer and thus, the boundary layer is not likely to produce smaller sized particle populations (Krejci et al. 2003; Rizzo et al. 2010; Andreae et al. 2018; Wimmer et al. 2018; Rizzo et al. 2018). Instead, newly formed aerosol particles have been detected in the free and upper troposphere over Amazonia by aircraft measurements during the ACRIDICON-CHUVA campaign in September and October 2014 (Andreae et al. 2018).

ACRIDICON-CHUVA stands for Aerosol, Cloud, Precipitation, and Radiation Interactions and Dynamics of Convective Cloud Systems–Cloud Processes of the Main Precipitation Systems in Brazil: A Contribution to Cloud Resolving Modeling and to the GPM (Global Precipitation Measurement) (Wendisch et al. 2016). 80% of the total observed particle concentrations in the free and upper troposphere during ACRIDICON-CHUVA campaign have diameters between 20 and 90 nm, meaning that the majority of the particles here are newly formed by NPF (Andreae et al. 2018).

In polluted urban areas, newly formed aerosol particles were observed over India and the nucleation rate was found to be a factor of 10 greater in the urban regions than in measurements over the mountainous regions during the campaign period (Sebastian et al. 2022). NPF associated with H_2SO_4 was detected in Beijing in 2018 and 2019 (Zhou et al. 2021). In in an urban observational site in Lille France, NPF events occurred in conditions with a high condensation sink, temperature, solar radiation and with a relative humidity smaller than 45% (Crumeyrolle et al. 2022).

NPF mechanisms

Several nucleation mechanisms that involve anthropogenic and biogenic gas precursors have been widely used or have been established by experiments (Vehkamäki et al. 2002; Kirkby et al. 2011; Riccobono et al. 2014; Kirkby et al. 2016).

Binary nucleation is a well known nucleation mechanism that forms particles from H_2SO_4-H_2O clusters and is most efficient in the upper troposphere where the temperature and condensation sink are low (Vehkamäki et al. 1994; Kreidenweis and Seinfeld 1988; Pirjola et al. 2000; Vehkamäki et al. 2002). Progress in understanding other nucleation mechanisms has been made by experiments in the CLOUD (Cosmics Leaving Outdoor Droplets) chamber, which is an experimental facility based at CERN (Conseil Européen pour la Recherche Nucléaire) with the ability to operate the relative humidity (around 80%-180%), pressure (up to 220 hPa above 1 standard atmosphere pressure) and temperature (183-300 K), and to introduce ions by galactic cosmic rays, to study a wide range of nucleation environments (Guida et al. 2013; Dias et al. 2017; Pierce 2017). The experiments investigated the effects of ions; quantified the rates of ternary nucleation and identified pure biogenic nucleation; the nucleation of organic and inorganic gas mixtures; and nucleation with iodic acid; amine etc. (Kirkby et al. 2011; Almeida

et al. 2013; Riccobono et al. 2014; Kirkby et al. 2016; He et al. 2021; Duplissy et al. 2016; Wagner et al. 2017).

The CLOUD experiment started with the investigation of the effects of galactic cosmic rays on climate, because cosmic rays can produce charged ions which may enhance new particle formation rate by stabilising neutral clusters and can enhance NPF at room temperatures (Duplissy et al. 2016; Pierce 2017; Wagner et al. 2017). Based on the CLOUD chamber experiments, Gordon et al. (2017) found that ion-induced nucleation contributed to around 50% of NPF globally. Ternary nucleation involves H_2SO_4-NH_3-H_2O clusters, and experimental results show that the nucleation rate is 100 to 1000 times faster than binary nucleation in producing new particles when around 100 ppbv of NH_3 is present (Kirkby et al. 2011). With the addition of amines, nucleation rates are further enhanced by a factor of 1000 compared to the rate with only NH_3 added (Almeida et al. 2013) because the H_2SO_4-amine nucleation reaches the collision limit due to significantly reduced evaporation, meaning that nucleation will occur whenever collision happens (Laakso et al. 2004; Almeida et al. 2013; Dingilian et al. 2021). However, such nucleation is only important at the local amine emission source (Almeida et al. 2013). In the regions with less pollution or in pristine environments, a nucleation mechanism that involves H_2SO_4 and highly-oxygenated biogenic gas molecules, or simply the highly-oxygenated biogenic gas molecules have also been discovered by CLOUD chamber experiments and applied in several modelling studies (Riccobono et al. 2014; Kirkby et al. 2016; Dunne et al. 2016; Gordon et al. 2016). Here, CLOUD chamber experiments recognized the importance of highly-oxygenated volatile organic compounds (HOMs), which are the oxidation products of BVOCs, as part of biogenic nucleation mechanisms. HOMs can nucleate most efficiently in the upper tropospheric environment. The biogenic nucleation mechanisms are especially important for Amazonian environment which is in a polluted state from time to time and has abundant BVOC emissions from the forest (Riccobono et al. 2014; Kirkby et al. 2016).

Modelling NPF

The importance of NPF to global low-level CCN and aerosol particles has been confirmed by modelling studies. With the inclusion of nucleation processes, an aerosol formation model predicted that less than half of the newly-formed particles in the boundary layer had the potential to form CCN (Pierce and Adams 2007). An early modelling study Wang and Penner (2009) at-

tempted to simulate binary nucleation in the boundary layer using the global NCAR (National Center for Atmospheric Research) Community Atmosphere Model (CAM) coupled with the IMPACT (Integrated Massively Parallel Atmospheric Chemical Transport) aerosol model, and found that binary nucleation produced around 5% of the boundary layer CCN. In the free troposphere, results from the CAM6 model along with comparisons with aircraft measurements from the SOCRATES (Southern Ocean Clouds, Radiation, Aerosol Transport Experimental Study) field campaign showed that free tropospheric nucleation could significantly affect CCN mass over the Southern Ocean (McCoy et al. 2021). Observations have also shown that nucleation occurs in the upper troposphere (UT), and the global aerosol microphysics model GLOMAP (Global Model of Aerosol Processes), which incorporated the Kulmala et al. (1998) nucleation mechanism showed that nucleation events in the UT could account for 35% of global low-level CCN concentrations (Vehkamäki et al. 2002; Spracklen et al. 2005; Merikanto et al. 2009). With the ATom3 observational dataset and chemical transport model simulations, Williamson et al. (2019) showed that tropical UT nucleation could be an important source of low-level CCN for many regions.

Including nucleation mechanisms in global models has improved the model observation comparisons in different aspects. The GLOMAP aerosol model had a better comparison with observations from South Africa and was able to capture well the yearly averaged CCN (Laakso et al. 2013); GLOMAP was also able to produce aerosol particle seasonal cycles when incorporating nucleation with biogenic gases and sulfuric acid (Riccobono et al. 2014). Based on the results from CLOUD chamber experiments and the GLOMAP model, Dunne et al. (2016) and Gordon et al. (2016) simulated the ternary and pure biogenic nucleation mechanisms, and found strong effects on CCN formation and global radiative forcing between preindustrial and present-day environments. Gordon et al. (2017) also quantified the contribution of various gas sources to global NPF. In the CAM model, with various combinations of binary nucleation, boundary layer nucleation with sulfate, and the emissions of sulfate aerosols, the global first aerosol indirect radiative forcing was found to be between -1.22 and -2.03 W m^{-2}, indicating the necessity of including nucleation in the global models (Wang and Penner 2009).

NPF has been included in several smaller-scale modelling studies which are able to investigate more fine-scale processes which may present different results from the global models. With a chemistry model, Pirjola et al. (2000) investigated the binary and ternary nucleation mechanisms

under different marine boundary layer environments, and concluded that the marine boundary layer was unlikely to allow binary nucleation to occur or allow the particles formed by ternary nucleation to grow to 3 nm diameter, unless the environment was cold and had extremely high DMS concentrations, or a very low condensation sink. Simulations with the AEROFOR model over a boreal forest in Finland confirmed that ion concentrations could affect the NPF process (Laakso et al. 2002). A regional air quality model also showed the importance of NPF on CCN by affecting the aerosol size distributions in Athens and Marseille (Sotiropoulou et al. 2006). Over the United States, the fraction of CCN formed by NPF were found to vary with height and to have reached a maximum in the upper troposphere (Yu et al. 2020). Regional WRF-Chem (Weather Research and Forecasting model coupled with Chemistry) simulations revealed stronger aerosol radiative forcings, with an average of -10 W m^{-2} at the top of the atmosphere, when including NPF, and showed the effect of strong NPF in suppressing particle growth to CCN sizes by consuming large amounts of H_2SO_4 (Sullivan et al. 2018).

Consequently, including NPF in global and regional models is important because it will help the models to better reproduce particle concentration, mass and size distribution.

1.1.2 Aerosol-cloud interactions

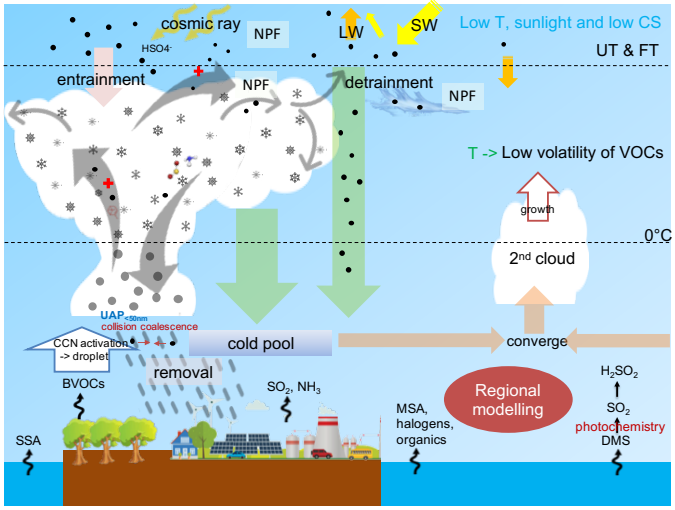

Figure 1.2: A schematic diagram of aerosol-deep convection interaction.

Aerosols interact with and affect clouds in many ways. For example, as highlighted in Fig. 1.2 for deep convection, they can be activated as CCN and form cloud droplets, be transported by convection and removed from the atmosphere by precipitation. Various factors including the

concentration, size distribution, and chemical composition of aerosol particles can affect aerosol-cloud interactions. Other environmental factors such as temperature and supersaturation are important for droplet formation from CCN and such processes are complex and vary with cloud types.

Aerosols acting as CCN

Aerosols need to exceed certain sizes under supersaturated environments to be activated as cloud droplets. The activation process is described by the combination of the Kelvin effect (for particles with curvature) and Raoult's law (accounting for the hygroscopicity of the particle material) in Köhler theory (Köhler 1936; Boucher 2015). The Kelvin effect encapsulates the fact that the vapour pressure is higher for a curved surface than for a flat surface and thus supersaturation can occur over the surface of the wet particles (Boucher 2015). Raoult's law describes how the saturation vapour pressure is reduced when a solute is added to pure water with a negative relationship between the saturation vapour pressure and the mole fraction of the solute in the solution. Köhler theory combines the Kelvin and Raoult effects and describes the saturation vapour pressure as a function of particle diameter. Köhler theory is used to derive the growth of particles under different ambient relative humidities. In Köhler theory, the critical radius and critical supersaturation define the conditions above which the particles can be activated and will continue growing into droplets unless the ambient air has insufficient relative humidity (Köhler 1936). Supersaturation occurs when an air parcel goes through expansion and a rapid reduction in temperature (Wallace and Hobbs 2006). The higher the supersaturation, the smaller the aerosols that can be activated (Fan et al. 2018; Grabowski and Morrison 2020; Pan et al. 2021; Zhang et al. 2021). The ability of aerosols to allow moisture to condense onto them partly depends on their composition, also referred to as hygroscopicity. Examples of hygroscopic compounds include sodium chloride, ammonium sulfate etc. (Wallace and Hobbs 2006). Organic compounds have very low hygroscopicity (Ajith et al. 2022), but the hygroscopicity may increase if these aerosols are aged or coated with hygroscopic compounds.

(1) Effects of CCN on shallow convection

The effects of aerosol on cloud and radiative forcing were first elaborated by Twomey (1977) and Albrecht (1989) who mainly considered low-altitude clouds. Twomey (1977) explains that the enhanced cloud droplet number concentration (N_d) caused by an increased CCN concentration

leads to an enhancement of cloud albedo because of the enhanced droplet surface area for a fixed cloud liquid water content. Albrecht (1989) showed that enhanced CCN may reduce droplet size, which then slows down the collision-coalescence process, and eventually delays the onset of precipitation, reduces rain intensity, and may consequently increase liquid water path (LWP) and cloud fraction which has a large impact on radiation balance (Cahalan et al. 1994; Chen et al. 2022). The Twomey and Albrecht effects were found in the 2014 Holuhraun volcano eruption that aerosols from the eruption plume caused increased cloud brightness and cover (Chen et al. 2022). Some observational and modelling studies found that increasing aerosol number concentration could form greater concentrations but smaller sized droplets which subsequently suppressed rain and thereby enhanced liquid water path (LWP) for shallow, non-precipitating clouds (Zhao et al. 2006; Lee et al. 2014). In contrast to increases in LWP by enhanced aerosols, Ackerman et al. (2004) found that increasing aerosol concentration could reduce cloud water because of enhanced entrainment unless the entrained air had a high relative humidity (Ackerman et al. 2004). A few later studies confirmed the increased droplet evaporation due to the smaller sizes with more aerosols, and it could subsequently cause cloud erosion or suppress rain (Hill et al. 2008; Xue et al. 2008; Wyant et al. 2022). Stevens and Feingold (2009) proposed using different cloud regimes to understand aerosol effects because factors including cloud development stage, cloud depth, whether in a land or marine environment, whether the atmosphere is polluted or clean, and latitude might affect the formation of precipitation and aerosol-cloud interactions. Furthermore, clouds could potentially buffer the impact of the aerosol changes in ways that depend on the cloud regime.

(2) Effects of CCN on deep convection

The response of deep convection to aerosol (or CCN) concentration is more complicated than shallow clouds because of the following aspects. The great vertical extent of deep convection allows varied cloud responses to aerosols at different heights; deep convection has strong updraft which allows rapid vertical transport and high supersaturations (including the potential for secondary activation above cloud base); phase changes may occur within deep convective clouds; and rain and/or snow can be formed within the clouds, which can also evaporate before the rain or snow reaches the surface. In general, higher concentrations of CCN can cause enhanced cloud droplet number concentrations with reduced sizes which is similar to shallow clouds. Subsequently, more smaller cloud droplets can be transported upward, and they may

lead to increased number concentrations of small-sized ice crystals (Fan et al. 2013; Herbert et al. 2015; Grabowski and Morrison 2020). Because the smaller ice crystals are less likely to fall out, clouds tend to persist longer (Grabowski and Morrison 2020). By affecting cloud microphysics, aerosol can further modulate the release of latent heat and thereby can potentially affect deep convective cloud dynamics. The following paragraphs briefly review the studies that have focused on aerosol-deep convection interactions.

The increased cloud droplet number concentration caused by higher aerosol concentration (Zhao et al. 2006; Kawamoto and Suzuki 2012) is expected to affect cloud liquid and ice water content, cloud cover and other cloud features, but demonstrating a deep convective response to aerosol using observations is complicated. Studies that use observations have confirmed that aerosols could change cloud optical depth, cloud thickness, LWP, and precipitation for both shallow and deep clouds (Kawamoto 2006; Sporre et al. 2012; Douglas and L'Ecuyer 2021), but cannot rule out the effect of meteorology, cloud type, background aerosols, retrieval artifacts, analysis methods etc. Satellite observations also have such difficulties that may hamper our understanding of the effects of aerosol, although some studies have identified the relationship between aerosol concentrations and cloud fraction, lifetime and precipitation using MODIS (Moderate Resolution Imaging Spectroradiometer) (Koren et al. 2005; Koren et al. 2010; Pan et al. 2021; Pan et al. 2022). One study used radar observations and found that biomass burning aerosol concentrations tend to more significantly influence cloud and precipitation under higher levels of background environmental instability (Gonçalves et al. 2015).

Idealised model simulations can separate the effects of aerosol and background meteorology. Cotton and Walko (2021) compared LES experiments with and without anthropogenic aerosols for clouds over Florida and found that more aerosols caused greater cloud liquid water content and updrafts, and explained that enhanced condensation could release extra latent heat and thereby enhanced warm cloud updrafts (Seiki and Nakajima 2014; Koren et al. 2014; Sheffield et al. 2015). However, the findings from idealised simulations may not always be applicable to reflect real-world aerosol-cloud interactions. This is because the responses of several interacting clouds under the influence of large-scale forcing within a region are different from an individual single-cloud. Here and after, the large-scale forcing refers to the advection of heat, moisture, wind, subsidence etc. from a large spatial and temporal scale. The strength of the large-scale forcing and whether it is realistic or idealised will influence the effect of aerosol on convective

clouds (Kipling et al. 2020; Dagan et al. 2022). Dagan et al. (2022) showed that with aerosol changes, the specific humidity was much smaller under realistic rather than idealised boundary conditions in several models (System for Atmospheric Modeling (SAM), ICON model etc.).

Apart from the varied background influences, deep convective clouds are complex by nature and may not exhibit linear response to increasing aerosol concentrations. For example, Ekman et al. (2007), Heever and Cotton (2007), and Connolly et al. (2013) found that precipitation could either increase or decrease with more aerosols due to a non-linear response of deep convective cloud. Similar to shallow clouds, stronger evaporation of smaller droplets that have been formed by more aerosols can cancel out the extra liquid water content from more smaller droplets, and thereby cause little change in cloud water content (Wang et al. 2022). A WRF model study also showed that aerosols could be effective in invigorating the initial stage of deep convection, but were not effective in changing the macrophysical aspects, such as cloud cover and thicknesses (Fan et al. 2013).

The invigoration of deep convection by increasing aerosol concentrations still needs to be better understood. Rosenfeld et al. (2008) proposed a cold-phase invigoration theory for deep convection which suggests that increasing aerosol concentrations can cause smaller droplets, and thus suppress and delay the conversion of cloud droplets to rain. Subsequently, more liquid condensate can reach higher altitudes where it can freeze and release more latent heat which eventually will enhance convection, deepen clouds and increase ice mass (Rosenfeld et al. 2008). In contrast, other studies found that the invigoration mainly occurred in the liquid and mixed-phase clouds (Fan et al. 2007; Sheffield et al. 2015; Chen et al. 2017; Fan et al. 2018). Such warm-phase invigoration is caused by extra condensation due to the enhanced number of smaller size cloud droplets which then releases latent heat.

Aerosols that are activated above the cloud base can contribute to deep convection invigoration (Ekman et al. 2004; Fan et al. 2018). Using a cloud-resolving model, Ekman et al. (2004) found that Aitken mode aerosols could be transported from the boundary layer to the free and upper troposphere where they formed ice crystals which helped sustain the deep convection. With the WRF-Chem model, Fan et al. (2018) found that sub-micron particles could be activated above the cloud base where supersaturation reached much higher levels; the deep convection could then be subsequently invigorated due to latent heat release from the extra droplet acti-

vation and subsequent ice formation. Evidence for the invigoration of deep convection in the warm phase was again provided by a subsequent study which found that sub-micron particles enhanced vertical velocity within deep convection, but only weakly and below the freezing level height (Grabowski and Morrison 2020). A similar conclusion was made in Igel and Heever (2021), which split the deep convective clouds into warm- and cold-based, and concluded with theoretical calculations that increasing aerosols was likely to cause only trivial invigoration of the cold-based convection and a weakening of the warm-based convection. Increases in the updraft velocity of deep convection is usually used to as a metric for invigoration and recent studies found that it mostly occurs in the warm phases of deep convection. Marinescu et al. (2021) compared several modelling studies and concluded that updraft velocities differed by a maximum of 15% between high- and low-aerosol concentrations below 8 km altitude via the alteration of buoyancy and pressure gradients by aerosols, and half of the analysed models showed weak effects above 8 km altitude. Such increases in updraft velocity caused by anthropogenic aerosols was also found in a comparison between simulated preindustrial and present-day environments over central Amazonia, (Fan et al. 2018).

The mechanisms of how aerosols affect convective precipitation is perhaps one of the most complicated processes in aerosol-cloud interactions (Rosenfeld et al. 2008; Tao et al. 2012) and the interactions involve changes in both microphysics and dynamics (Beydoun and Hoose 2019; Heikenfeld et al. 2019). There are no conclusive answers for the correlation between aerosol and precipitation for several reasons. The first is that more aerosols do not necessarily cause more cloud liquid and ice water content, which are essential for rain formation as stated above. Second, the collision and coalescence processes of cloud droplets to form rain are not well understood, and thus, uncertainties exist in the modelling of such processes. Lastly, how aerosol affects cloud and rain strongly depends on meteorology and background aerosols as well as whether model runs use idealised boundary forcings or not, etc. (Heever and Cotton 2007; Connolly et al. 2013; Wellmann et al. 2018; Dagan et al. 2022).

Background conditions and the scale of models to simulate aerosol-cloud processes represent large uncertainties for us to understand the response of precipitation to aerosol concentration dues to strongly varied the thermodynamic and dynamic conditions across different regions and thus it is important to study the effects of aerosols in the context of background meteorology. Under strong large-scale forcing, the simulated precipitation over Germany was found to have

negligible changes with aerosol concentrations using a weather forecast model (COSMO, Consortium for Small-scale Modeling) (Seifert et al. 2012). Over Asia, the dominant monsoon season is found to introduce extra complexity to our understandings of aerosol-cloud-precipitation systems (Furtado and Field 2022). However, with idealised boundary conditions, the significant perturbations of moisture content due to aerosol changes in a cloud-resolving model (Dagan et al. 2022) may lead to more evident response of precipitation. It is because the real-world background environment has diurnal and seasonal variations, and the air is additionally affected by human perturbations, exchange of energy between land and ocean etc., and such complexity is usually simplified in single-cloud models. Unlike single-cloud model, regional models that simulate several interactive clouds in a region are usually driven by boundary conditions provided by global models, reanalysis or real-time data which include much higher levels of complexity and uncertainty. Therefore, the response of precipitation to aerosol loading within a region that consists of several cloud systems is usually different from individual cloud systems.

Clouds with different rain intensities have different responses to changes in aerosol concentrations, because rain intensity is closely related to the strength of convection. Alizadeh-Choobari (2018) made an effort to isolate the aerosol effect on rain intensity, and concluded that heavy rainfall was enhanced but light rainfall was suppressed with a greater loading of hygroscopic aerosols. Similar conclusions that are built upon the separation of weak and heavy rain events, as well as of high and low cloud liquid contents have also been made by Li et al. (2011), Fan et al. (2012), and Wang et al. (2011).

Ice formation is an important factor for precipitation production. With increasing CCN concentration, enhanced deep convective clouds will contain more ice mass and thus are more likely to produce hail, snow and graupel that can eventually form rain (Carrio and Cotton 2011; Khain et al. 2011; Loftus and Cotton 2014). Therefore, whether deep convection is invigorated by higher aerosol concentrations will affect the response of rain.

Transport and scavenging of aerosols by clouds

Aerosol particles as well as some gas precursors can be transported vertically by convective clouds (Dickerson et al. 1987; Dye et al. 2000; Barth et al. 2015; Li et al. 2017). Aircraft measurements of particle concentrations over the marine environment during ACE (Aerosol Characterization Experiment) have shown that newly formed particles were formed close to the

cloud outflows (Clarke et al. 1998). The study also showed that newly formed aerosol particles measured in the free troposphere may undergo subsidence after the passage of a frontal system to reach the boundary layer. Similar results have also been found by Williamson et al. (2019) who analysed the global observational dataset ATom as well as model simulations. With radar measurements, Wang et al. (2016) have shown that aerosols that are formed in the free and upper troposphere can be rapidly transported into the boundary layer. Andreae et al. (2018) also hypothesised that deep convection over Amazonia transported insoluble gas precursors upward from the surface to the upper troposphere where aerosols were formed. Then, the newly formed aerosol particles could be transported downwards to supply the boundary layer particles (Andreae et al. 2018).

Model and experimental results show evidence of vertical transport of gas and aerosol by convective clouds. With a cloud-resolving model, Ekman et al. (2004) found that around 10% of the boundary layer Aitken mode aerosol concentrations could be transported by convective clouds into the free troposphere. Efficient upward transport of aerosol particles was also found in Yin et al. (2005) and Yin et al. (2012) using a cloud-resolving model which consequently affected the concentration and size distributions of aerosols in the upper troposphere. The results showed that aerosol upward transport was more efficient than downward transport, and the transported aerosols could subsequently result in increased rain. The upward transported aerosols were found to significantly affect total aerosol mass at high altitudes (Cui and Carslaw 2006). For gas transport, laboratory experiments tested and found that insoluble organic gases could be easily transported to reach the free and upper troposphere from the surface, paving way for us to understand high-altitude NPF (Kulmala et al. 2006). With a cloud-resolving model, which is able to well represent cloud-scale processes as well as tracer transport, Devine et al. (2006) found that the spatial distributions of insoluble DMS was closely related to updraughts. Investigations of vertical transport have also been designed with trajectory and global models (Tyson 1997; Williamson et al. 2019), or air quality models (Oshima et al. 2013), but large-scale models usually do not resolve cloud convection due to the coarse resolution and computational cost. Thus, many of them may not involve vertical transport at cloud scales and mainly focus on horizontal long-range transport (Eguchi et al. 2009; Vijayakumar et al. 2016; Das et al. 2017).

Wet scavenging is an efficient way of removing aerosol and trace gases from the atmosphere (Loosmore and Cederwall 2004; Yu et al. 2019) and it is dependent on aerosol particle size.

Scavenging acts to clean the atmosphere, reduce the trace gas condensation sink and thereby enhance NPF. A good representations of wet scavenging in models can improve results by better reproducing observed aerosol profiles (Kipling et al. 2013). Ekman et al. (2004) used a cloud-resolving model and found almost all particles within the simulated convective cloud with diameter greater than 30 nm were removed by activation and impact scavenging. Similarly, aircraft measurements have shown that scavenging efficiencies are positively correlated with particle sizes (Yang et al. 2015). Gases including CH_2O, and H_2O_2 are efficiently removed by convective scavenging within storms (Bela et al. 2016; Bela et al. 2018). Below the clouds, the removal efficiency increases with rain intensity, which greatly affects aerosol size distributions in the air (Andronache 2003). Cloud droplets can also remove aerosol particles and trace gases. With the Probability of Ultrafine particle Growth (PUG) model, Pierce et al. (2015) found that cloud droplets and ice affected the coagulation of small aerosol particles, significantly reducing global-mean small particle concentrations (by 15%-21%) and 80 nm particle concentrations (by 10%-12%). The coalescence of cloud droplets can reduce cloud droplet number concentrations by as much as 90% (Kang et al. 2022). A WRF-Chem study showed that H_2SO_4 was almost completely depleted by clouds and rain over the ocean (Kazil et al. 2011).

Many aspects of aerosol-cloud interactions are still not well understood. Therefore, improving the understandings will help global and regional models to better reproduce the real environment and better predict for the future climate.

1.2 Research questions

The aims of this study are to investigate aerosol-deep convection interactions over Amazonia and the potential contribution of new particle formation to the CCN budget in this convective environment. The study focuses on deep convection because it has the potential to support NPF by transporting gas precursors into the UT where NPF is efficient. Deep convection may also transport newly formed aerosols downwards to low altitudes where they may act as CCN. Aerosol-deep convection interactions likely affect the global radiation balance and are not well understood. NPF, aerosols and clouds have been widely investigated with global modelling and observational studies. However, many sub-grid cloud-scale processes that are important for individual regions are not resolved in the global models and thus, a high-resolution regional model with explicit convection is needed to investigate these processes. A regional version of

the Unified Model is used here because it is able to resolve convection, provide explicit tracer transport, and therefore can be used to investigate cloud-scale processes. It can also be coupled with aerosol microphysics, chemistry, and cloud microphysics schemes. The regional model is nested inside a global model, allowing the investigation of both regional-scale and global-scale processes. This thesis will address three main research questions in separate chapters as outlined below.

1.2.1 Chapter 3: Where do Amazonian aerosol particles come from?

Boundary layer nucleation has been proven to be insufficient to sustain the boundary layer aerosol particle population (Zhou et al. 2002; Krejci et al. 2003; Rissler et al. 2006; Spracklen et al. 2006; Rizzo et al. 2010; Andreae et al. 2018; Wimmer et al. 2018; Rizzo et al. 2018). Observations have also shown that new particle formation in the upper troposphere could be an important source (Wang et al. 2016; Andreae et al. 2018) of boundary layer particles. However, it is unknown whether such particles are formed within Amazonia or originated far afield and were transported into the region. In Chapter 3, a nested regional atmospheric model with aerosol microphysics is used to quantify the contribution of upper tropospheric NPF to boundary layer particle concentrations. The research questions investigated in this chapter are as follows:

(1) How do NPF-deep convection interactions on regional scales (around 1000 km) affect the vertical distributions of particles in the Amazonian tropical rainforest?

(2) How much does NPF occurring on a regional scale affect the CCN budget of the region? What fraction of CCN is created regionally versus being transported into a region from outside?

(3) How effective is deep convection at transporting particles downwards to low-levels?

(4) How are particle concentrations, nucleation and growth rates in the regional domain sensitive to changes in nucleation mechanisms?

1.2.2 Chapter 4: How do anthropogenic emissions and newly formed particles affect cloud and rain?

Anthropogenic emissions significantly affect aerosol mass and number concentrations in Amazonia, partly via NPF that makes use of gas precursors from pollution plumes (Shrivastava et al. 2019; Zhao et al. 2021). The affected aerosols are expected to influence aerosol-cloud interactions by adjusting cloud droplet number concentration, cloud properties and moisture

profiles. In reality, the response of clouds to increases in anthropogenic emissions may be non-monotonic and may strongly depend on the environmental conditions. Thus, in Chapter 4, I will use the nested regional model with coupled chemistry and a high-resolution anthropogenic emission inventory to investigate the effects of anthropogenic emissions on clouds and discuss the mechanisms involved. The research questions for this chapter are as follows:

(1) What are the effects of anthropogenic emissions on aerosol, cloud and rain in Amazonia?

(2) What mechanisms drive the changes in cloud water and rain?

1.2.3 Chapter 5: How is non-linear new particle formation affected by coarse resolutions?

Observations have shown that biogenic new particle formation (NPF) in Amazonia upper troposphere (UT) can produce substantial number of aerosols (Wang et al. 2016; Andreae et al. 2018). Biogenic NPF involves the nucleation of the oxidised biogenic gas precursors, and is a non-linear function of gas concentrations, temperature and condensation sink. In the UT, biogenic NPF is significantly affected by deep convection which transports gas precursors (monoterpenes), creates condensation sink, and perturbs the environments (Thornton et al. 1997; Sassi et al. 2001; Twohy et al. 2002; Kulmala et al. 2006; Johnston et al. 2018). The dependence of NPF in Amazonian UT on deep convection leads to significant spatial variability that may not be well represented by coarse-resolution global models. The lifetime of gas precursors may also affect whether the non-linear process can be simulated by global models. To investigate how the non-linear NPF is affected by coarse resolution, Chapter 5 used high-resolution regional model results and compared to the averaged results. The research questions are as follows:

(1) How are nucleation rates affected by averaging the input variables?

(2) What are the causes of the changes in nucleation rates by averaging?

(3) How will monoterpene oxidation rate affect the spatially non-linear nucleation rate?

Chapter 2

Model description

In this chapter I will introduce the general model configurations, coupling and pure biogenic nucleation mechanism that were used for all the results of the thesis. Other specific settings for the three topics are introduced separately within each chapter.

2.1 Global and regional model configurations

A a nested regional model located in central Amazonia, embedded in a global model is used in this thesis. The global model is the atmosphere-only configuration of the Hadley Centre Global Environment Model version 3 (HadGEM3) which are based on Unified Model (UM) framework, and both models incorporate the United Kingdom Chemistry and Aerosol (UKCA) model. The UKCA model was first run at kilometer-scale resolution by Planche et al. (2017) and tested in the one-way nesting configuration by Gordon et al. (2018). The one-way coupling allows the global model to drive the regional model with hourly boundary conditions generated from the global model, including aerosols, trace gases, and meteorology conditions (temperature, 3D wind, cloud liquid, cloud ice, humidity and rain), while the global model is not affected by the regional model. The nested regional model can be configured to several spatial resolutions.

The global model is based on GA7 (Global Atmosphere v7) of UM with an Even Newer Dynamics for General atmospheric modelling of the environment (ENDGame) dynamics (Walters et al. 2019). Parameterised convection is used in the global model (Fritsch and Chappell 1980; Gregory and Rowntree 1990; Stratton et al. 2009; Derbyshire et al. 2011; Walters et al. 2019), which simplifies the transport processes. The global model uses a single-moment cloud micro-

physics scheme for stratiform cloud (Wilson and Ballard 1999) that activates aerosol particles according to Abdul-Razzak and Ghan (2000) and works separately from convection. The activation process is based on the PDF (probability distribution function) of the updraft velocities centred around the large-scale vertical velocity to derive cloud droplet number concentrations for each time step (West et al. 2014). The simplified microphysics has prognostic rain which is affected by the 3D wind field. A fixed sea surface temperature is used and the land surface has been defined from a land surface model JULES (Joint UK Land Environment Simulator) (Walters et al. 2019).

The convection in the regional model is explicit which allows heat transfer and tracer transport to be resolved on the model grid. The regional model is also coupled with CASIM (Cloud-AeroSol Interacting Microphysics) model for both stratiform and resolved convective cloud (Field et al. 2023). CASIM is a two-moment cloud microphysics model with five types of hydrometeor (cloud droplets, rain, ice, snow and graupel) (Shipway and Hill 2012; Hill et al. 2015; Grosvenor et al. 2017). All hydrometeor distributions are defined by gamma distributions. CASIM activates aerosols to form cloud droplets depending on the mean updraft velocity in the grid box (Grosvenor et al. 2017; Miltenberger et al. 2018a). The droplet number concentrations are prognostic, which means that they are stored at each timestep, but if the model activates more droplets in the new timestep than the previous one, the old number concentration is overwritten (Gordon et al. 2020).

UKCA uses the GLOMAP-mode (Global Model of Aerosol Processes), a two-moment aerosol microphysics model which allows aerosol to form from gaseous precursors, grow to larger sizes, and be transported and removed (Mann et al. 2010). The aerosols are represented by four water-soluble modes (nucleation, Aitken, accumulation and coarse) and an insoluble Aitken mode which are specified by the number and mass (or equivalently size) depending on a fixed-width log-normal distribution. The chemical composition of the aerosol includes sulfate, sea-salt, black carbon and organic carbon.

Aerosol particles are scavenged by precipitation through rainout and washout. Rainout represents the reduction of aerosol concentrations in the cloud droplets due to collision and coalescence which form rain, and eventually aerosols are removed from the atmosphere. Washout, or impaction scavenging, is the removal of below-cloud aerosol particles because falling rain

droplets can collect aerosols and remove them from the atmosphere. The removal processes of aerosols are size-dependent, and are determined by a collection efficiency look-up table (Mann et al. 2010; Kipling et al. 2013). In the original version of the model, these processes only scavenge particles larger than 10 nm diameter. Here the influence of cloud hydrometeors on NPF (new particle formation) through their effect on the condensation sink is also investigated, as described in Section 2.2.

The UKCA and CASIM models are coupled to allow UKCA to pass aerosol particle number and mass to CASIM for activation, with the mass of different chemical components (sea-salt, sulfate, organic carbon and black carbon) used to derive the hygroscopicity for aerosol activation in CASIM (Gordon et al. 2020). CASIM also passes the rates of autoconversion and accretion to UKCA in order to affect the convective scavenging of aerosols by precipitation (Miltenberger et al. 2018a).

2.2 New particle formation

NPF represents the conversion processes from gas vapour to the particle phase. One of the NPF mechanisms used in this study is the pure biogenic nucleation which uses oxidised organic gas molecules (Kirkby et al. 2016). NPF in the UKCA model serves to produce aerosol particles up to 3 nm in diameter.

The pure biogenic nucleation mechanism along with the nucleation gas (HOMs, highly-oxygenated molecules) is added to UKCA. The definition of HOMs is based on the chamber experiment from CLOUD (Cosmics Leaving Outdoor Droplets) (Ehn et al. 2014; Kirkby et al. 2016; Bianchi et al. 2019) which found that a wide range of oxidised organic vapours were able to nucleate particles and that particle growth varies depending upon the volatility of the organic vapours (Tröstl et al. 2016; Stolzenburg et al. 2018; Simon et al. 2020). The experiments showed that HOMs can be formed from α-pinene, which is a subset of the monoterpenes, by reaction with OH and O_3. Based on CLOUD chamber experiments (Kirkby et al. 2016), the pure biogenic nucleation mechanism has been parameterised in Gordon et al. (2016). UKCA allows HOMs to nucleate new particles (Ehn et al. 2014; Kirkby et al. 2016; Tröstl et al. 2016; Stolzenburg et al. 2018; Bianchi et al. 2019) and continue with their subsequent growth with secondary organics, HOMs and H_2SO_4. This mechanism has been applied to several models (GLOMAP,

Community Earth System Model with IMPACT, and WRF-Chem) (Gordon et al. 2016; Zhu et al. 2019; Zhao et al. 2020).

In the parameterisations, HOM is oxidised from monoterpenes by OH and O_3, one of the BVOCs (Biogenic Volatile Organic Compounds) emitted from the forest (Gordon et al. 2016). In the original UKCA setup, monoterpenes are oxidised to SecOrg (secondary organics) which can grow particles by condensation. With the new parameterisation, monoterpenes are first oxidised to SecOrg, then the rest of the monoterpenes in the environment are used to derive HOM concentrations using the same steady-state approximation as used by Gordon et al. (2016). A schematic diagram in Fig. 2.1 shows the oxidation, nucleation and particle growth pathways of biogenic nucleation mechanism in UKCA.

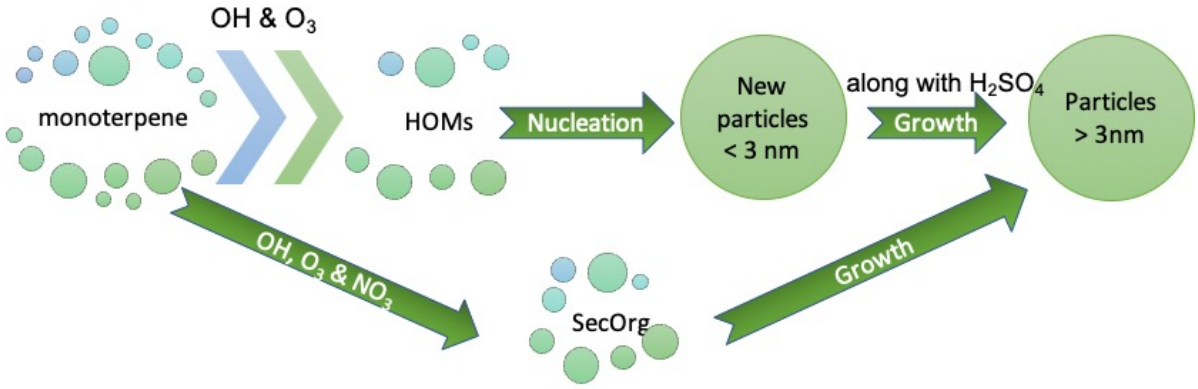

Figure 2.1: A schematic diagram showing oxidation pathways and their roles in biogenic nucleation mechanism and particle growth in the UKCA.

Yields of HOM are 1.2% when monoterpenes are oxidised by OH and 2.9% by O_3, and the concentrations of HOM are used to derive nucleation rates for particles at 1.7 nm in diameter following Gordon et al. (2016). The nucleation rate is the sum of the neutral and ion-induced nucleation rates (Eq. 2.1). The ion-induced nucleation uses a constant ion concentration at 400 cm^{-3} ([Ion] in eq. 2.1).

$$J_{Bio_{1.7nm}} = \exp(-(T - T_0)/A_6) \times (A_1 \times ([HOM]/A_7)^{A_2 + \frac{A_5}{[HOM]/A_7}} + [Ion] \times A_3 \times ([HOM]/A_7)^{A_4 + \frac{A_5}{[HOM]/A_7}}), \quad (2.1)$$

where $J_{Bio_{1.7nm}}$ is the nucleation rates at 1.7 nm in cm^{-3} s^{-1}, HOM represents the concentrations of pure biogenic nucleation gas in molecules cm^{-3}, T is the temperature in K, T_0

is a constant reference temperature (278 K), and A_{1-7} are constant parameters (Gordon et al. 2016). Both neutral and ion-induced rates are multiplied with a temperature dependency $\exp(-(T - T_0)/A_6))$ as a rough estimate such that nucleation rates vary with temperature at different heights (Gordon et al. 2016; Simon et al. 2020). A_6 is a dimensionless constant equals to 10 and A_7 is also a dimensionless constant equals to 10^7. The calculation of particles of 1.7 nm diameter growing to 3 nm, through the condensation of HOMs and H_2SO_4 is based on Kerminen and Kulmala (2002).

An additional condensation sink from cloud droplets and ice crystals is added to UKCA, and the value is added to the condensation sink from existing aerosols, which then suppresses nucleation rates in the cloudy regions (Kazil et al. 2011). A common condensation sink allows gases to condense on to existing aerosol particle surfaces instead of nucleate new particles. The addition of this term enables gases to also condense on cloud hydrometeor surfaces. The cloud hydrometeor condensation sink given in Eq. 2.2 is defined by assuming a fixed number concentration (100 cm^{-3}) of cloud droplets and ice particles to calculate radii that enter the Fuchs and Sutugin (1971) expression.

$$CCS = 4\pi D_v \times N_d \text{ (or } N_i) \times (r_{cloud} + r_{ice}), \tag{2.2}$$

where, CCS denotes cloud condensation sink in s^{-1}, D_v is gas diffusion coefficient in m^2 s^{-1}, N_d (or N_i) is a constant concentration of cloud droplets and ice (10^8 m^{-3}), r_{cloud} and r_{ice} are radius of cloud droplets and ice in m.

Chapter 3

The contribution of regional aerosol nucleation and transport to low-level CCN in an Amazonian deep convective environment

3.1 Introduction

Nucleation, or new particle formation (NPF), is important for aerosol-cloud interactions and thus climate, as the newly formed particles can grow to form cloud condensation nuclei (CCN) that affect cloud droplet number concentrations and cloud properties (Pierce and Adams 2007; Merikanto et al. 2009; Wang and Penner 2009; Kazil et al. 2010; Gordon et al. 2016; Dunne et al. 2016; Gordon et al. 2017). Global model studies have shown that NPF contributes around 54% of the global present-day CCN in the boundary layer (Gordon et al. 2017), and that 35% of the CCN were formed by NPF in the free and upper troposphere and later transported into the boundary layer (Merikanto et al. 2009). The downward transport can take place in large-scale subsidence in the general circulation such as in the Hadley cell, which is resolved by global models, or in the downdrafts of deep convection, which is a parameterised process in global models. These global-scale studies clearly show that high-altitude NPF contributes to low-level CCN, but the relative roles of these two transport mechanisms for the NPF-aerosol-CCN process is

unknown.

NPF involves inorganic species such as H_2SO_4-H_2O and H_2SO_4-NH_3-H_2O (Weber et al. 1995; Vehkamäki et al. 2002; Kirkby et al. 2011; Dunne et al. 2016) and the oxidation products of volatile organic carbon vapours such as monoterpenes producing HOMs, or highly-oxygenated molecules, (Kirkby et al. 2016; Tröstl et al. 2016). Previous studies have found that NPF is affected by precursor gas concentrations as well as by temperature and the condensation sink. Low temperatures in the UT (upper troposphere) usually slow down the chemical reaction of extremely low volatility organic compounds, but also reduce the vapour pressure of the gas precursors and thereby enhance NPF (Simon et al. 2020; Zhao et al. 2020). Yu et al. (2017) also reported that the low-altitude CCN that are generated by NPF from H_2SO_4-H_2O and organic gas molecules, were changed by 10%-30% when the temperature dependence of NPF was added. The condensation sink is also an important factor that affects the production and concentration of particles smaller than 3 nm in diameter (Kulmala et al. 2001a; Kulmala et al. 2001b; Dal Maso et al. 2002) by modulating the concentration of nucleating and condensing vapours. Many studies use cloud droplets or precipitation scavenging to act as a sink for the gases in the atmosphere (Wurzler et al. 1995; Wurzler 1998; Zhang et al. 2006; Kazil et al. 2011; Baklanov et al. 2013; Elperin et al. 2015; Elperin et al. 2017), although most of them do not focus on particle nucleation. Here the role of hydrometeors within convective clouds as a sink for the condensable gases is also investigated (Kazil et al. 2011).

In Amazonia, it has been shown that NPF was rarely observed in the boundary layer and thus is insufficient to sustain CCN during the dry-to-wet transition season (Zhou et al. 2002; Krejci et al. 2003; Rissler et al. 2006; Spracklen et al. 2006; Rizzo et al. 2010; Andreae et al. 2018; Wimmer et al. 2018; Rizzo et al. 2018). However, aircraft measurements have shown that strong NPF in the upper troposphere (UT) (from precursor vapours transported upwards by deep convection) can create an abundant supply of small nuclei that, following downward transport and particle growth, could account for some boundary layer CCN (Clarke et al. 1998; Clarke et al. 1999a; Clarke et al. 1999b; Clarke and Kapustin 2002; Weigel et al. 2011; Wang et al. 2016; Andreae et al. 2018; Williamson et al. 2019). However, from the observations alone it is unknown whether the transport is predominantly via convective downdrafts on the spatial scale of the deep convective cells, or via large-scale subsidence that takes days to transport particles to lower altitudes.

The CCN concentration at 0.4% supersaturation in the Amazonian boundary layer is around 185 cm^{-3} in the wet season and 2500 cm^{-3} during the dry season (Andreae 2009). The total particle concentration is around 300 cm^{-3} in the wet season and 3000 cm^{-3} in the dry season (Andreae 2009; Pöhlker et al. 2016; Pöhlker et al. 2018). Aircraft measurements show that more than 80% of the particles were between 20 and 90 nm in diameter in the UT during the dry season, suggesting that they are formed by NPF (Andreae et al. 2018). Particle concentrations exceeding 20000 cm^{-3} were observed above 8 km during the ACRIDICON-CHUVA (Aerosol, Cloud, Precipitation, and Radiation Interactions and Dynamics of Convective Cloud Systems - Cloud Processes of the Main Precipitation Systems in Brazil: A Contribution to Cloud Resolving Modeling) campaign in September and October 2014. Therefore, it is plausible that this high-altitude aerosol may contribute to the aerosol populations in this region through downward transport in an environment with strong vertical motion.

Andreae et al. (2018) hypothesised that the newly formed aerosol particles in Amazonian UT could be mixed and transported into the lower troposphere and contribute to boundary layer particles. Based on the observations from ACRIDICON-CHUVA in the dry season, they proposed that the organic compounds in UT particles were derived from gas-phase oxidation of insoluble gas precursors which were emitted from the rainforest and transported upwards by deep convection. In the wet season, based on GoAmazon2014/5 (Observations and Modeling of the Green Ocean Amazon 2014-2015) observations, Wang et al. (2016) concluded that the rapid vertical transport allowed newly formed particles in the free troposphere to enter the boundary layer in downdrafts associated with precipitation.

To understand the formation of aerosol and its vertical transport in a convective environment it is necessary to use a model that resolves cloud motion. Global models have shown that the UT is a major source of CCN in the boundary layer (Merikanto et al. 2009), but the results may only be reliable in regions where aerosol is transported in the types of synoptic-scale circulation that are resolved by the model, such as in the descending branch of the Hadley cell in sub-tropical regions. Deep convection is a regional- to local-scale system. Due to the strong vertical velocities, deep convection can potentially transport particles and vapours upwards and downwards on scales of a few kilometers that are unresolved by a global model (global models parameterize the vertical exchange of trace gases, but they do not resolve coherent updrafts and downdrafts and the associated clouds). Most studies have focused on upward transport.

Ekman et al. (2004) used a cloud-resolving model and found that only small particles (5.84 to 31.0 nm) were transported to the UT by a deep convective updraft, while larger particles were scavenged. Some of the smaller particles eventually grew and served as CCN or ice-nucleating particles (INP). Using an axisymmetric dynamic cloud model Yin et al. (2005) reported that aerosols were transported from the boundary layer to mid-cloud level and contributed to the aerosol mass within the hydrometeors in the deep convection. The analysis of Zhao et al. (2020) of ACRIDICON-CHUVA and GoAmazon2014/5 observations using a regional-scale chemical transport model with a detailed treatment of organic vapours suggested the importance of fast convective transport for low-altitude particles and CCN. However, to understand the spatial scales over which the NPF-aerosol-CCN pathway takes place, i.e. over a large-scale or within the regional convective domain, it is necessary to combine a global and regional model to represent both processes.

The previous studies are well designed and help to understand aerosol sources on global and regional scales. However, to address the questions about the relative importance of regional and global-scale transport I will use a model that combines high resolution (to resolve convection) with interactive aerosol microphysics that represents aerosol diameters as low as 3 nm and allows the simulation of NPF and growth. This is accompanied by a broader view from the global model. The model will simulate 3 days of the ACRIDICON-CHUVA campaign as a case study and investigate the role of deep convection in supporting the UT NPF and the boundary layer aerosols. Therefore, this chapter aims to quantify the extent to which the supply of aerosol to the Amazonian boundary layer is generated from local nucleation or from aerosol produced further afield. The effectiveness of convective transport to influence aerosol particles in the boundary layer will also be quantified, inspired by measurements made over Amazonia showing a free-tropospheric source of aerosol into the boundary layer in a convective environment (Wang et al. 2016). The questions for this chapter are as follows:

(1) How do NPF-deep convection interactions on regional scales (around 1000 km) affect the vertical distributions of particles in the Amazonian tropical rainforest?

(2) How much does NPF occurring on a regional scale affect the CCN budget of the region? What fraction of CCN is created regionally versus being transported into a region from outside?

(3) How effective is deep convection at transporting particles downwards to low-levels?

(4) How sensitive are particle concentrations, nucleation and growth rates in the regional domain to changes in the nucleation mechanisms?

3.2 Methods

3.2.1 Observations

ACRIDICON-CHUVA campaign

This study is motivated by the measurements made during ACRIDICON-CHUVA (Aerosol, Cloud, Precipitation, and Radiation Interactions and Dynamics of Convective Cloud Systems - Cloud Processes of the Main Precipitation Systems in Brazil: A Contribution to Cloud Resolving Modeling). Measurements from the GPM (Global Precipitation Measurement) satellite mission, and monoterpenes observations from aircraft measurements and ATTO (Amazon Tall Tower Observatory) tower are used (Kuhn et al. 2007; Yáñez-Serrano et al. 2018; Zannoni et al. 2020). The aim of ACRIDICON-CHUVA was to study the relationships between trace gases, particles and radiation in Amazonian convective environment. The campaign included 14 flights from early September until the beginning of October in 2014, centred around Manaus in Brazil (3.1°S, 60.0°W). They measured cloud, aerosol and trace gas properties in forest, urban and marine environments using the HALO (High Altitude and Long Range Research Aircraft) (Wendisch et al. 2016; Andreae et al. 2018); see Fig. 3.1.

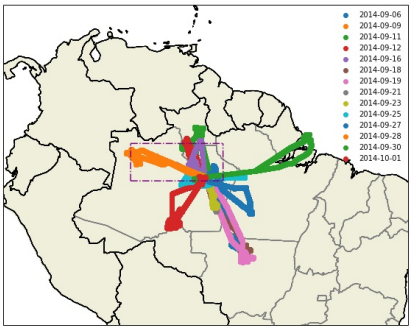

Figure 3.1: A map of the flight tracks during ACRIDICON-CHUVA campaign. The flight track in purple is AC11 (on 16 September 2014), and the purple dashed box denotes the regional domain used in this study.

Meteorology

The campaign took place during the transition season in Amazonia, which was towards the end of the dry season and the onset of the wet season. General subsidence caused by a northward-shifted ITCZ dominated the dry season during this period, but during the transition in September, moisture advection from the Atlantic Ocean was sufficient to cause the large-scale circulation to shift leading to an increase in rainfall (Li and Fu 2004). North-easterly and easterly wind dominated this period, bringing in moist air from the South Atlantic Ocean (Martin et al. 2016). The surface temperature was at its highest for the year in September 2014 and moisture started to increase from September onwards. The monthly averages of surface temperature reached 28°C and the specific humidity was over 19 g kg^{-1} (Collow et al. 2016). The UT equivalent potential temperature in September ranged from 60°C to 80°C and relative humidity was around 20% in September and rose to 100% in early October favouring the development of deep convection (Collow et al. 2016). Warm sea surface temperatures occurred during the campaign (Martin et al. 2016; Andreae et al. 2018).

During the simulation period (16 to 18 September 2014), MODIS (Moderate Resolution Imaging Spectroradiometer) images show that on 16 September, the sky was partially cloudy with shallow cumulus clouds. A deep convective cell formed to the northeast of Manaus with a large anvil above 12 km in altitude on 17 September. On this day, cloud fraction at the location of the regional domain reached 100%. A squall line passed Manaus and it extended as far as 240 km to the northwest of Manaus. On 18 September 2014, the sky became partially cloudy and the convective cells were diminished or left the region.

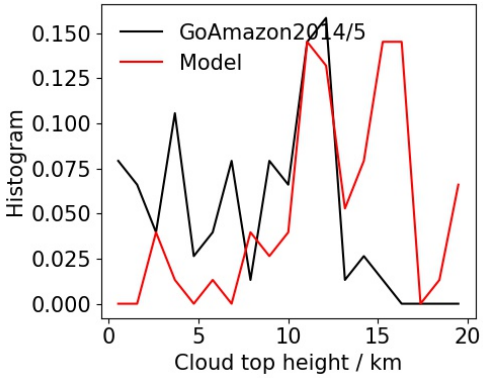

Figure 3.2: Histograms of hourly mean cloud top height from the GoAmazon2014/5 campaign observations (black) and the maximum cloud top heights of one of the regional model simulations, BioOxEmCCS (red; see Table 3.2) between 16-18 September 2014. The observations are from the Geostationary Operational Environmental Satellites (GOES; (Chen and Xie 1996)).

Figure 3.2 shows histograms of the hourly mean cloud top height obtained from the Geostationary Operational Environmental Satellites (GOES) from Atmospheric Radiation Measurement (ARM) user facility database for the time period of the GoAmazon2014/5 field campaign (16-18 September 2014, (Chen and Xie 1996)) and from a model simulation (BioOxEmCCS, see Table 3.2). GOES measured many cloud top heights at around 2-4 km, 6 km, and 8-13 km altitude during the three days. The model result does not show many cloud top heights at lower altitudes, because I only compared the maximum cloud top heights at each of the 3-hourly model output in the analysis. The model shows many cloud top heights at around 11-13 km, with the GOES observations also showing many clouds at these heights. However, the regional model generates many high clouds with cloud top heights around or above 15 km, indicating very deep clouds or thin clouds at high altitudes, which may potentially cause strong vertical transport.

Aerosol measurements

The measurements of particle number concentrations from ACRIDICON-CHUVA are used in this study. The instruments aboard the HALO aircraft measured aerosol particle concentrations up to around 14 km in altitude, approximately where boundary of the upper troposphere and lower stratosphere locates, and the flight area covered the region of interest (Fig. 3.3) as well as wider regions of Amazonian basin. Four butanol-based CPCs (condensation particle counters) and a UHSAS (Ultra-High Sensitivity Aerosol Spectrometer) were used to measure particles of various sizes. The measured particles are split into two size ranges by diameter: those larger than 20 nm dry diameter ($N_{D>20nm}$) and those larger than 90 nm diameter ($N_{D>90nm}$). The $N_{D>20nm}$ data consist of measurements with lower cut-off diameters that vary with pressure because of inlet loss: 9.2 nm at 1000 hPa, 11.2 nm at 500 hPa, and 18.5 nm at 150 hPa (Andreae et al. 2018). $N_{D>90nm}$ were measured using a UHSAS and an OPC (optical particle counter). For a more extensive description of the measurements, see Andreae et al. (2018).

3.2.2 Models and simulations

Global and regional model configurations

Based on GA7.1 (Global Atmosphere v7.1) of Unified Model version 11.3, a global model with a nested regional model configuration is used in this chapter (see also Chapter 2). The global model uses the N216 grid (around 65 km horizontal resolution) with 70 vertical levels up to 80 km altitude. The nested regional domain is centred at (1.5°S, 63°W) and has 4 km horizontal

resolution. The domain size is 440 km north-south and 1080 km east-west (Fig. 3.3) to align approximately with the mean wind direction. There are 70 vertical levels to 40 km altitude, with 63 levels in the lowest 20 km, the region of interest of this study. The residence time of air in the regional domain is determined by horizontal wind speed and is between 20 and 40 hours, which is around half of the total simulation time. As has been introduced in Chapter 2, the regional model is driven by hourly boundary conditions generated from the global model. The global model uses parameterised convection which simplifies the transport process (Fritsch and Chappell 1980; Gregory and Rowntree 1990; Stratton et al. 2009; Derbyshire et al. 2011; Walters et al. 2019) while the regional model is able to resolve convection. The global model has a simplified microphysics (Wilson and Ballard 1999; Abdul-Razzak and Ghan 2000; West et al. 2014) and regional model uses CASIM (Cloud-AeroSol Interacting Microphysics) microphysics model (Shipway and Hill 2012; Hill et al. 2015; Grosvenor et al. 2017; Miltenberger et al. 2018a; Gordon et al. 2020; Field et al. 2023).

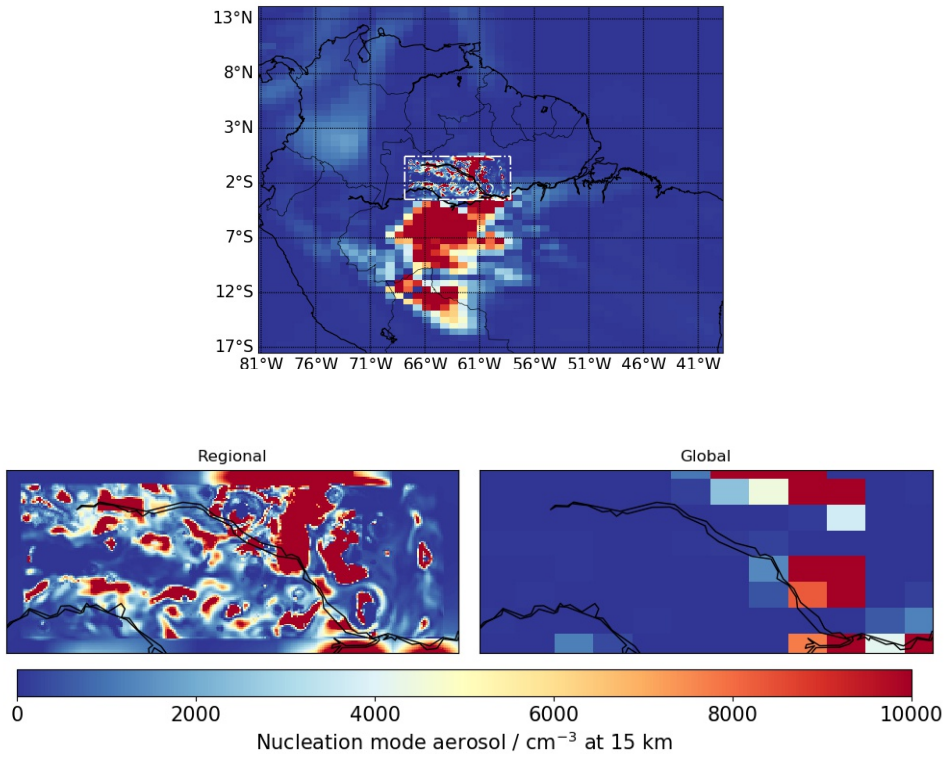

Figure 3.3: Maps of nucleation mode aerosol number concentrations from the regional and global models at a height of 15 km and at 15 UTC on 17 September, 2014. The map in the upper panel presents a broader view of South America and shows the location of the regional domain (dotted dashed box). All three maps share the same colourbar.

UKCA (United Kingdom Chemistry and Aerosol) is coupled to both global and regional model. The emissions used in this chapter includes organic carbon and black carbon emissions from

biomass and fossil fuel burning from the GFED (Global Fire Emissions Database) version 3.1 and CMIP5 (Coupled Model Intercomparison Project) inventories (Van Der Werf et al. 2003; Kanakidou et al. 2005). UKCA uses monthly averages of SO_2 and DMS from CMIP5 emission inventories in both the global and regional models. The marine source of DMS has been parameterised based on Lana et al. (2011) and land biomass burning (Werf et al. 2006; Lamarque et al. 2010; Granier et al. 2011; Diehl et al. 2012); SO_2 comes from volcano eruptions (Andres and Kasgnoc 1998; Halmer et al. 2002), biomass burning (GFEDv3.1 inventory), bio-fuel burning, fossil-fuel burning and industrial emissions (Cofala et al. 2005). The monoterpene emissions mainly come from the monthly averages of vegetation (Guenther et al. 1995).

New particle formation

In this chapter, binary nucleation and biogenic nucleation mechanisms are used to investigate the particle concentrations in the dry-to-wet transition season in Amazonia. The schematic diagrams in Fig. 2.1 and Fig. 3.4 show the oxidation, nucleation and particle growth pathways of the binary and biogenic nucleation mechanisms.

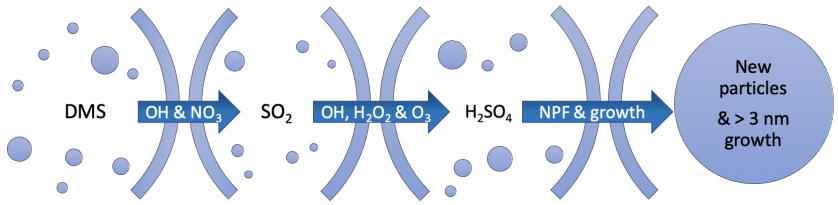

Figure 3.4: A schematic diagram showing oxidation pathways and their roles in binary nucleation mechanism and particle growth in the UKCA.

Binary nucleation follows the parameterisation of sulfuric acid-water (H_2SO_4-H_2O) in Vehkamäki et al. (2002). In the UKCA model, the binary nucleation gas H_2SO_4 mainly comes from the oxidation of SO_2 and DMS. It also condenses on to existing aerosols, contributing to their growth.

Details of biogenic nucleation can be found in Chapter 2. Here, biogenic nucleation is used to simulate Amazonian NPF, focussing on the environmental conditions for, and the consequences

of new particle formation rather than the chemical mechanism.

Table 3.1: The chemical reactions in the offline chemistry and the corresponding rate constants.

Reactions	Rate constants
DMS + OH $\rightarrow SO_2$	9.6×10^{-12}
DMS + OH $\rightarrow SO_2$ + DMSO	3.04×10^{-12}
DMS + NO_3 $\rightarrow SO_2$	1.9×10^{-13}
DMSO + OH $\rightarrow SO_2$	5.8×10^{-11}
SO_2 + OH $\rightarrow H_2SO_4$	3.00×10^{-31}
Monoterpene + OH $\rightarrow$SecOrg	1.2×10^{-11}
Monoterpene + O_3 $\rightarrow$SecOrg	1.01×10^{-15}
Monoterpene + NO_3 $\rightarrow$SecOrg	1.19×10^{-12}
HO_2 + HO_2 $\rightarrow H_2O_2$	2.2×10^{-13}
OH + H_2O_2 $\rightarrow H_2O$	2.9×10^{-12}

A simplified (offline) chemistry scheme is used to reduce computational cost. Here, the oxidants (OH, O_3, HO_2, H_2O_2 and NO_3) are read in from monthly mean ancillary files generated from a full chemistry simulation (Walters et al. 2019), then OH and HO_2 concentrations are modulated according to the diurnal cycle of solar radiation. The chemical reactions and rate constants are summarised in Table 3.1. In the Amazonian environment, apart from monoterpene, isoprene is another BVOC (biogenic volatile organic compounds) that significantly affects upper tropospheric aerosol mass (Schulz et al. 2018), but the simplified chemistry scheme does not include isoprene and the related chemistry. This representation of the chemical mechanism is one of the many uncertainties associated with biogenic particle formation.

Simulation details

Both the global and regional models are run from 16 to 18 September 2014, which is close to the end of Amazonia dry season and is the time when the ACRIDICON-CHUVA field campaign took place (Wendisch et al. 2016). The global model was spun-up for 15 days (1-15 September 2014) in order to allow the model to initialise the aerosol fields.

During the 3-day simulation, deep convection usually occurs at 15 UTC (11 LT) and reaches a maximum two hours later. The domain averaged surface rain rate reaches a maximum (approximately 118 mm hr^{-1}) within an hour after the start of the deep convection. The rain lasts for 5 to 6 hours, then the convective clouds start to dissipate and completely disappear by midnight. During the most vigorous phase, cloud top height reaches a maximum of 20 km in altitude. In the initial stages of cloud development, at below 2 km in altitude, the cloud coverage is around

50%-70%. As the clouds deepen, the low-level clouds are transformed into deep clouds within an hour, with the low-level cloud cover being reduced to approximately 10%. At the same time, mid-level cloud covers around 10% of the horizontal domain and the high-level cloud fraction reaches 100%.

In this chapter, I will test the binary and pure biogenic nucleation mechanisms and investigate the sensitivity of the particle number concentrations to the nucleation rate, oxidation rate, emission rate and condensation sink. I will also study the source and the vertical distribution of the particles in the regional domain. Table 3.2 shows the name and components of the nucleation mechanisms used for all the simulations in this study. The first five simulations use (1) binary sulfuric acid-water nucleation (denoted as Bn), (2) binary nucleation with the nucleation rate increased by a factor of 10 (Bn×10), (3) pure biogenic nucleation from Gordon et al. (2016) (Bio), (4) pure biogenic nucleation with the oxidation rates of monoterpenes reduced by a factor of 10 (BioOx), and (5) reduced monoterpenes oxidation and the monoterpenes emission rate increased by a factor of 10 (BioOxEm).

Table 3.2: A table of all simulations and the NPF mechanisms. The monoterpenes (MT) oxidation÷10 denotes that the oxidation rates of monoterpenes (to secondary organics) are reduced by a factor of 10, and 10×MT emission denotes increasing the monoterpenes emission rate by a factor of 10. CCS = condensation sink from clouds.

	Binary	Biogenic	MT oxidation÷10	10×MT emission	CCS	NPF notes
1. Bn	✓					
2. Bn×10	✓					Bn NPF rate×10
3. Bio		✓				
4. BioOx		✓	✓			
5. BioOxEm		✓	✓	✓		
6. BioOxCCS		✓	✓		✓	
7. BioOxEmCCS		✓	✓	✓	✓	
8. off_allNPF		✓	✓	✓	✓	NPF off everywhere
9. off_regNPF		✓	✓	✓	✓	NPF off in regional
10. NPF_1-4km		✓	✓	✓	✓	NPF 1-4 km only
11. NPF_4-7km		✓	✓	✓	✓	NPF 4-7 km only
12. NPF_7-10km		✓	✓	✓	✓	NPF 7-10 km only
13. NPF_10-13km		✓	✓	✓	✓	NPF 10-13 km only
14. NPF_13-16km		✓	✓	✓	✓	NPF 13-16 km only

The justification for the changes in monoterpenes emissions is that biogenic volatile organic compounds (BVOCs) usually have various species and a wide range of abundances and volatilities, and the rates of BVOC emissions and their oxidation mechanisms are still not well understood

despite some progress reported in the literature (Sindelarova et al. 2014). Additionally, the oxidation rate of organics has large range of uncertainty (up to 10^{-10}) and the rate even differs by three orders of magnitude with the same oxidant (Kwok and Atkinson 1995). The comparisons with observed aerosol (Section 3.3.1) suggest that monoterpenes are oxidised too quickly in the default simulation (Bio) and are not transported to the UT where they could contribute to NPF. Therefore, the oxidation rates in the UKCA are reduced to allow for a longer monoterpene lifetime so that monoterpenes will be more likely to contribute to NPF (BioOx simulation). The oxidation rates are not increased because they will drive the simulations away from the observations by producing too few aerosols in the UT.

The averaged monoterpenes mixing ratios in the regional domain overestimate the ATTO tower observations at the surface and 75 m by a factor of 2, and by a factor of 1.5 at 155 m (Yáñez-Serrano et al. 2018; Zannoni et al. 2020). In contrast, between 1 and 2.5 km, the simulations underestimate aircraft measurements by a factor of 0.1 (Kuhn et al. 2007). There are no measurements of monoterpenes available in the UT, but a even stronger underestimation is expected there. The insufficient mixing ratios of monoterpenes are likely the cause of the very low nucleation rates (1.8×10^{-3} cm^{-3} s^{-1}) in the UT in the simulations with the default biogenic nucleation scheme and with reduced oxidation rates, such that these simulations cannot reproduce the observed concentrations (Section 3.3.1 and 3.3.2). For example, the BioOxCCS simulation underestimates the observed particle number concentrations at 12 km by a factor of 8.6. Therefore, for the simulation with reduced oxidation rates, the monoterpenes emission rate is also increased by a factor of 10 to allow more monoterpenes to be transported to the UT to further enhance NPF (BioOxEm simulation). This is the default simulation for most of the rest of the study to explore the factors controlling NPF and aerosol transport.

In September 2014, strong biomass burning events took place, which led to high condensation sinks and partly explained the reason why no NPF events were observed close to the surface (Andreae et al. 2018). However, the models do not capture the suppression due to a lack of high-resolution biomass burning emissions and the overestimated monoterpenes emission at surface. Thus, the NPF is eliminated below 100 m for all simulations here.

The second set of simulations is designed to examine the effect on NPF of the condensation sink on cloud particles. The default model includes only a sink of vapours and nuclei onto existing

aerosol but not onto cloud hydrometeors. Thus, an additional condensation sink from cloud droplets and ice crystals is added to UKCA (see Chapter 2).

To understand the source of particles in the regional domain, additional simulations were ran in which nucleation was switched off in both the regional and global models (off_allNPF) and in the regional model only (off_regNPF). These simulations allow me to quantify the effect of NPF within the 1080 km by 440 km regional model domain compared to that from outside of the regional domain.

A final set of five simulations was performed to understand how particles that are nucleated at a particular altitude are transported vertically and thereby affect aerosol at other altitudes. These simulations are also based upon the BioOxEmCCS simulation. For these five simulations, NPF will occur at all heights above 100 m in the global model, but only allow NPF in the regional model to occur at certain altitudes (1-4 km, 4-7 km, 7-10 km, 10-13 km and 13-16 km).

3.3 Results

3.3.1 Model-observation comparison

Figure 3.5 shows the measured profiles of median particle number concentrations from flight AC11 (16 September 2014) of the ACRIDICON-CHUVA campaign compared to five of the model simulations. All the data in this section are converted to standard temperature (273.15 K) and pressure (10^5 Pa; STP), using Eq. 3.1.

$$N_{STP} = \frac{N_{ambient} \times P_0 \times T}{P \times T_0}, \tag{3.1}$$

where N_{STP} is the number concentrations of particles converted to STP, $N_{ambient}$ is the number concentration at the current temperature and pressure, T is temperature in K, P is the pressure in Pa, P_0 is the constant pressure (10^5 Pa), and T_0 is the constant temperature (273.15 K). The data from flight AC11 are used because the flight track falls well within the regional domain and the date of measurement is within the simulation period. Supplementary Fig. A.1 shows the full campaign.

Below 3 km in altitude, the observed median $N_{D>20nm}$ is homogeneous with height, with a concentration of around 1600 cm^{-3}. The median of $N_{D>20nm}$ then increases with altitude to a

maximum at 11.8 km with a value of 19000 cm^{-3}. The observed profile of median $N_{D>90nm}$ is also homogeneous with height up until around 2 km and has a similar median concentration to $N_{D>20nm}$ (1400 cm^{-3}), which shows that the observed concentration of small particles is low at these low altitudes. Above 2 km, the observed $N_{D>90nm}$ decreases to around 6-8 km and then increases again with height and reaches around 1100 cm^{-3} at 12.5 km.

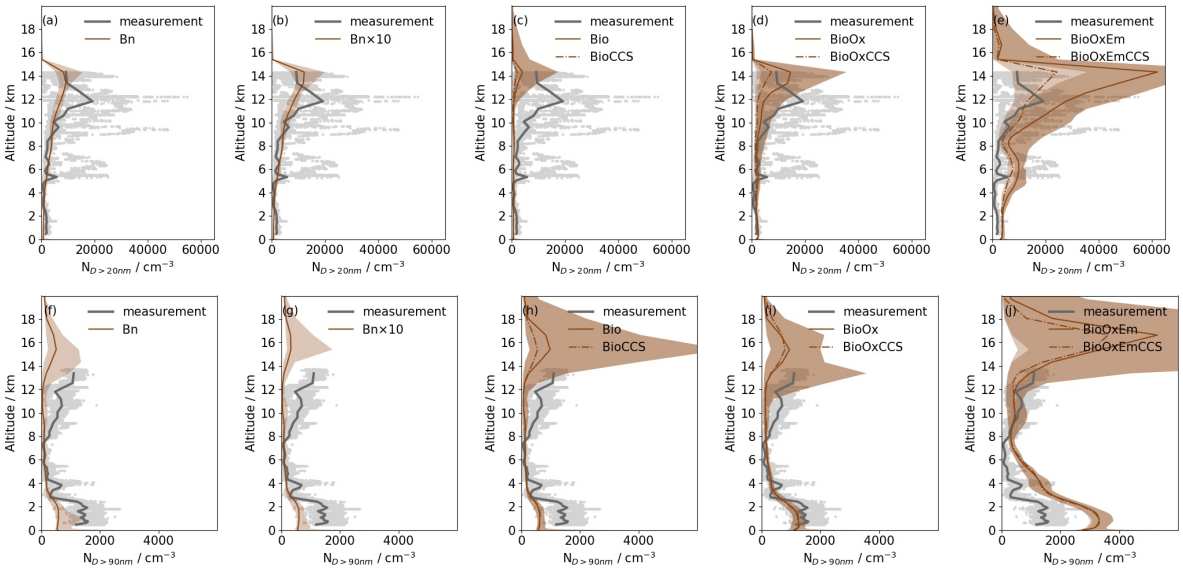

Figure 3.5: The observed and modelled vertical profiles of median number concentrations of particles with diameters >20 nm ($N_{D>20nm}$, top row) and >90 nm ($N_{D>90nm}$, bottom row). The observations are shown as grey dots and a grey line (repeated for all panels). The grey dots are individual observations from ACRIDICON-CHUVA flight AC11 (16 September 2014) with a time resolution of 1 minute, and the thick grey lines are the medians of the observations binned within the same height ranges as the regional model levels. The modelled results are from the various regional simulations averaged from 0 UTC on 17 September to 23 UTC on 18 September 2014, (a) Bn, (b) Bn×10, (c) Bio and BioCCS (dashed line), (d) BioOx and BioOxCCS (dashed line), and (e) BioOxEm and BioOxEmCCS (dashed line). The shading represents 2.5% and 97.5% percentiles from the modelling results.

In the simulation with the default binary nucleation mechanism (simulation Bn) and in that with a 10 times enhanced nucleation rate (Bn×10; Fig. 3.5 a and b) median number concentrations of $N_{D>20nm}$ are low at the surface, and then increase with height until they reach a maximum (9900 cm^{-3}) at 14 km in altitude where they start to decrease to almost zero at around 15 km in altitude. The two simulations exhibit similar number concentrations until 12 km. Throughout most of the profiles, both simulations reproduce the measurements well with an overall mean difference of -4.6% (Bn) and 2% (Bn×10). However, between 10 and 13 km the models underestimate the observations by 46% for the Bn and and 37% for the Bn×10 simulations. The profiles of $N_{D>90nm}$ (Fig. 3.5 f and g) show the highest concentrations below

2 km where the values are approximately constant with height (600 cm^{-3}). There is another peak at around 15.5-16 km (around 500 cm^{-3}) in altitude, and the concentrations are much lower between 4 and 13 km (< 100 cm^{-3}). These two simulations underestimate the observed $N_{D>90nm}$ by 46% (Bn) and 47% (Bn×10) when averaged over all altitudes.

In the simulations with biogenic nucleation (Bio, BioOx and BioOxEm) the median $N_{D>20nm}$ have low concentrations from the surface to around 10 km in altitude, where the particle number concentrations significantly increase. The profiles of $N_{D>90nm}$ have higher concentrations in the boundary layer and UT than at the altitudes in between. The Bio and BioCCS simulations (Fig. 3.5 c) underestimate the height-averaged observed $N_{D>20nm}$ (by 52%) and $N_{D>90nm}$ (by 36.7%) suggesting insufficient NPF and particle growth. When the monoterpenes oxidation rates are reduced (BioOx and BioOxCCS; Fig. 3.5 d), the aerosol number concentrations increase because the reduced oxidation rate enables the longer-lived monoterpenes to be transported to the UT. The BioOx and BioOxCCS simulations therefore match the observed concentrations below 8 km, but still underestimate concentrations above 8 km by an average of 28% (BioOx) and 50% (BioOxCCS) for $N_{D>20nm}$ and 76% for $N_{D>90nm}$ in both simulations. With an increased monoterpenes emission rate (BioOxEm and BioOxEmCCS simulations; Fig. 3.5 e) the model produces significantly higher particle concentrations than in the other simulations, as expected. The BioOxEm simulation overestimates $N_{D>20nm}$ at all altitudes with an averaged overestimation of a factor of 3 for heights below 14.3 km, and overestimates $N_{D>90nm}$ below 9 km by an average factor of 3 (Fig. 3.5 j). Adding the cloud condensation sink (BioOxEmCCS) improves overestimation of $N_{D>20nm}$ above 9 km and the modelled concentration is reduced to around 30% compared to the observations. The increased emission rate combined with the cloud condensation sink allows the model to reproduce the UT aerosol number concentrations but causes too many particles in the lower troposphere. Whether these particles are formed by NPF within the regional model or in the global model is discussed in Section 3.3.4.

The simulations with binary nucleation mechanisms (Bn and Bn×10) produce $N_{D>20nm}$ and $N_{D>90nm}$ in the UT that are up to 100 times smaller than the three simulations with biogenic nucleation (Bio, BioOx and BioOxEm). The smaller concentrations and variability occur because binary nucleation is determined by the SO_2 gas field that, due to its long lifetime relative to monoterpenes, is more controlled by the global model, whereas biogenic nucleation is controlled more by convective transport, mixing and oxidation in the regional model. I also ran a

simulation in which the regional SO_2 emission was removed and the SO_2 profiles were almost identical to the Bn simulation meaning that the SO_2 in the regional domain was hardly affected by the regional-scale processes.

The BioOxEmCCS simulation is chosen as the base model for the rest of this study for two reasons: (1) it matches the observed particle concentrations well in the UT (Section 3.3.1); (2) it includes the suppression of unrealistic NPF inside clouds via the cloud condensation sink. Various factors including oxidation rates, oxidant concentrations, emissions and the condensation sink affect the model performance and these simulations can only give a limited view of this sensitive environment since they lack the complexity to represent all of the processes that happen in reality. However, the overall reasonable match to observations shows that the chosen model is well suited to addressing the aims of this study.

3.3.2 Analysis of particle formation and growth

Figure 3.6 shows vertical profiles of particle concentrations, nucleation and growth rates, and trace gas volume mixing ratios. All the profiles are averaged from 0 UTC on 17 September to 23 UTC on 18 September 2014. For the rest of the chapter, ambient particle concentrations are quoted without the conversion to STP as performed for Fig. 3.5.

The NPF rates at 3 nm in diameter in all five simulations increase with height until 14.3 km, reaching a maximum of 3.5 cm^{-3} s^{-1} in the simulation with the most intensive nucleation (BioOxEm). The binary nucleation rates increase more sharply with height because of the strong temperature dependence of the binary nucleation rate (Vehkamäki et al. 2002). The nucleation rate in the simulation with the biogenic nucleation mechanism is higher in the boundary layer compared to the Bn simulation because of abundant monoterpene, but still, at around 0.03 cm^{-3} s^{-1}, too low to produce frequent NPF events. The rate then decreases until 2 km in altitude, where it starts to increase with height until 14 km. When the monoterpenes oxidation rate is decreased and the monoterpenes emission rate is increased (from Bio to BioOxEm), the NPF rate increases by up to a factor 160 and growth rates increase by a factor of 11 in the UT because more monoterpenes is transported to the UT. Averaged over all heights, the nucleation rates from these three biogenic simulations are factors of 160 to 200 larger than in the Bn and Bn×10 simulations.

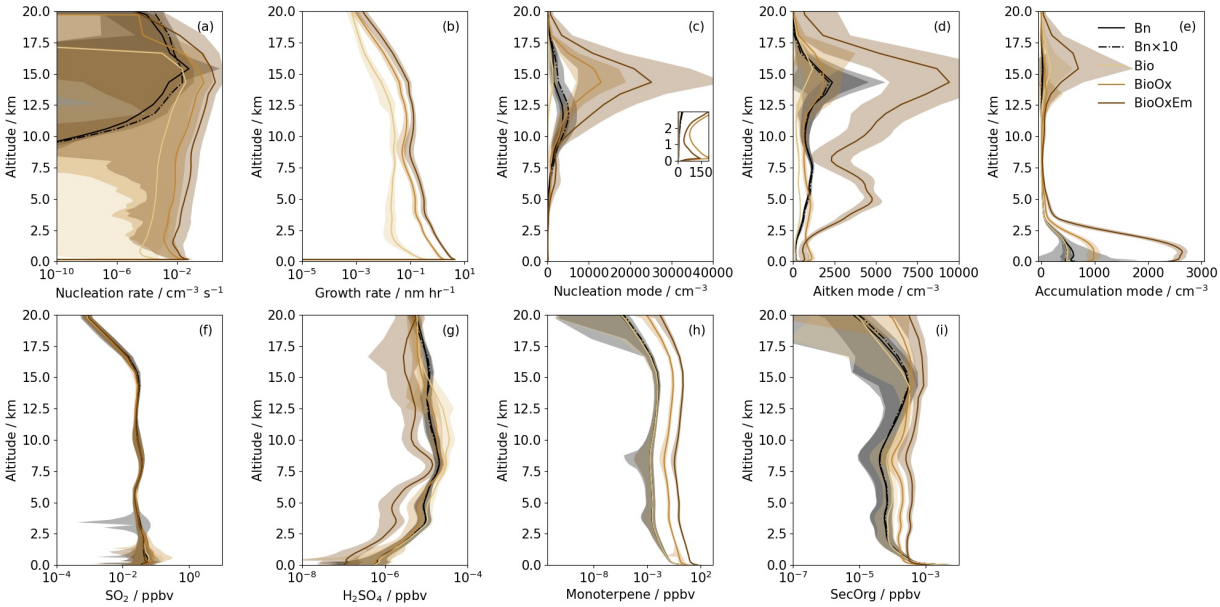

Figure 3.6: Regional domain- and time-averaged vertical profiles of ambient (a) nucleation rate (up to 3 nm in diameter), (b) growth rate in the biogenic nucleation mechanism (from 1.7 nm to 3 nm), (c) nucleation mode aerosol number concentrations (with the inset figure showing the number at lowest 3 km), (d) Aitken mode aerosol number concentrations, (e) accumulation mode aerosol number concentrations, (f) SO_2 volume mixing ratios, (g) H_2SO_4 volume mixing ratios, (h) monoterpenes volume mixing ratios, and (i) secondary organic (SecOrg; the oxidation product of monoterpene) volume mixing ratios. The results are from the simulations with binary nucleation (Bn; black solid), binary nucleation with 10 times nucleation rate (Bn×10; black dotted dashed), pure biogenic nucleation (Bio; light brown), biogenic nucleation with reduced (÷10) oxidation rate (BioOx; brown), and biogenic nucleation with reduced oxidation rate and enhanced (×10) monoterpenes emission (BioOxEm; dark brown). The shading represents one standard deviation either side of the mean at each height.

The growth rate for the biogenic nucleation between 1.7 nm and 3 nm in diameter is driven by the concentrations of the condensable gases. For binary nucleation, which is driven by H_2SO_4, there is no consideration of the growth rate between 1.7 nm and 3 nm in the model calculations and therefore it is not shown in Fig. 3.6. The growth rates in the simulations with biogenic nucleation (Bio, BioOx, and BioOxEm) decrease with height because the concentration of HOMs decreases by a factor of around 1000 from the surface to 14 km in all simulations.

The differences in the nucleation and growth rates between the binary and biogenic nucleation mechanisms are generally reflected in the aerosol number concentrations (Fig. 3.6 c, d, and e). Following the nucleation and growth rates, the nucleation mode aerosol number concentrations are very low below 4 km in all simulations. Above 4 km the concentration increases with height. The differences in nucleation mode aerosol number concentration between the two simulations with binary nucleation are small due to similar nucleation rates, except for those

between 10 and 16 km with a maximum enhancement of 73% for Bn×10 compared to the default Bn simulation. With biogenic nucleation (Bio, BioOx, and BioOxEm), the nucleation mode concentration peaks at around 14 km (25000 cm^{-3}). When the simulations with the most intensive nucleation (BioOxEm) to the standard biogenic nucleation simulation (Bio) are compared, the results show that the 1800 times higher nucleation rate and 10 times higher growth rate result in a factor of 18 higher nucleation mode concentration at 14 km.

The Aitken mode profiles in the simulations with binary nucleation mechanisms (Bn and Bn×10) have two peaks at around 8 km and 14 km. The concentrations in Bn and Bn×10 simulations are similar except for between 12 and 16 km in altitude where the difference is likely due to the higher nucleation mode aerosol concentrations. The simulations with biogenic nucleation mechanisms (Bio, BioOx and BioOxEm) also have two peaks at 5 km and 14 km. The concentrations in those peaks are 11 times higher in the BioOxEm than in the default Bio simulation. Interestingly, there is no corresponding peak in the nucleation and growth rates at 5 km in any of the three biogenic nucleation simulations. The Aitken mode peaks at 5 km are due to transport from outside of the regional domain (i.e., from the global model) from the same altitudes where nucleation rate is greater than 0.1 cm^{-3} s^{-1} (Supplementary Fig. A.2 and A.3). Whether particles are formed within or outside the regional domain is investigated in more detail in Section 3.3.4.

The accumulation mode aerosol number concentrations are greatest below 2 km (on average between 500-2500 cm^{-3}) in all simulations. They quickly decrease to almost-zero between 6 and 12 km in altitude above which the concentrations increase again to form a peak at around 14-15 km. The BioOxEm simulation has more accumulation mode aerosols below 2 km than the BioOx simulations even though the BioOxEm simulation has fewer Aitken mode particles to grow from in the regional domain. This suggests that the Aitken mode particles are not growing into the accumulation mode size range within the regional domain, but rather in the global domain and are then transported into the regional domain (Supplementary Fig. A.2). The peak in accumulation mode number concentration at around 14-15 km is also associated with peaks in nucleation and Aitken mode concentrations, implying that the newly nucleated particles can grow to larger sizes in the UT.

In the boundary layer both the binary and biogenic nucleation mechanisms produce similar

particle number concentrations in their default scenarios (Bn and Bio). When the monoterpenes oxidation and emission rates are changed (BioOx and BioOxEm), aerosol number concentrations increase by factors of 3-5, especially for Aitken and accumulation mode aerosols. This suggests that the aerosol concentrations are very sensitive to the representation of biogenic nucleation in the boundary layer. Conversely, the lack of binary nucleation in the boundary layer means that the details of the binary nucleation process are not important for the boundary layer.

3.3.3 Cloud condensation sink

The condensation sink suppresses NPF and models often calculate it using the aerosol surface area. An additional condensation sink due to cloud droplets and ice crystals is added to suppress in-cloud NPF in the global and regional model domains (Kazil et al. 2011). It is applied to the simulations with biogenic nucleation (BioOx and BioOxEm) to produce the simulations BioOxCCS and BioOxEmCCS. In the UKCA model, the typical aerosol condensation sink varies between 0.003 to around 0.01 s^{-1} over all heights, with a maximum domain average of 0.04 s^{-1}. After adding the condensation sink from cloud droplets and ice crystals, the overall condensation sink is doubled.

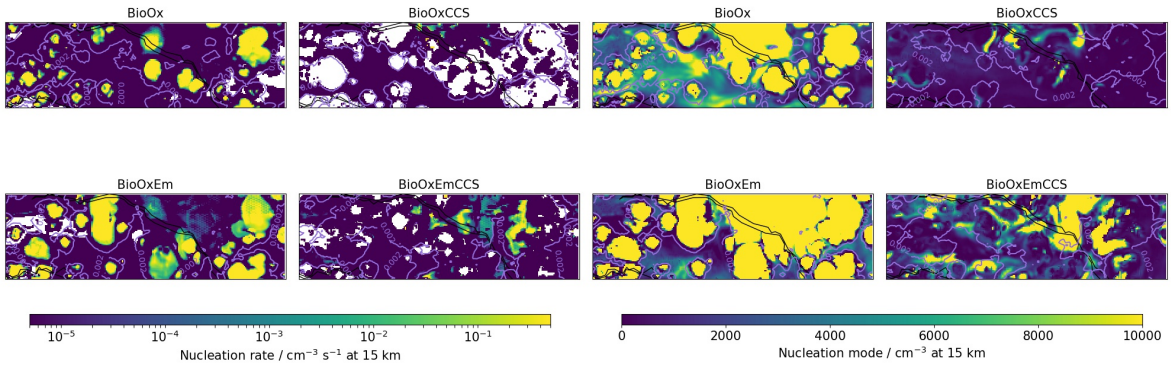

Figure 3.7: Maps of regional domain nucleation rate (left) and nucleation mode aerosol number concentrations (right) in the simulations BioOx, BioOxCCS, BioOxEm, and BioOxEmCCS at a height of 15 km and at 16 UTC on 17 September 2014. Contours highlight the locations of clouds and are drawn where the cloud water content is equal to 0.002 g kg^{-1}. The white areas in the nucleation rate maps have zero values and cannot be specified by a log-scale plot.

The addition of a cloud condensation sink substantially alters the spatial distribution of the nucleation rates and particle concentrations. Figure 3.7 shows that adding the cloud condensation sink almost completely suppresses NPF in the cloudy regions, which is evident from the holes in the spatial pattern of nucleation rate with rates lower than 10^{-5} cm^{-3} s^{-1} at 15 km. Consequently the addition of the cloud condensation sink results in lower nucleation and Aitken

mode particle concentrations (Fig. 3.8). NPF continues to occur in the non-cloudy regions because the upward-transported monoterpenes continue to be oxidised after the clouds evaporate, especially in the simulations with reduced oxidation rates. Holes in the NPF spatial distribution also occur in the BioOxEmCCS simulation (with both reduced monoterpenes oxidation and enhanced emissions). However, these empty areas do not cover the full extent of the clouds as they do in the BioOxCCS simulation. In the cloud outflow regions NPF rates reach 1 cm^{-3} s^{-1} in the BioOxEmCCS simulation.

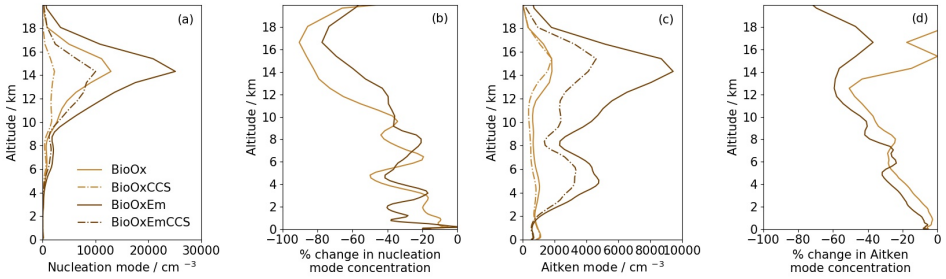

Figure 3.8: Regional time- and domain-averaged profiles from the BioOx, BioOxCCS, BioOxEm, and BioOxEmCCS simulations. Shown are the nucleation and Aitken mode aerosol number concentrations (a and c) and the percentage changes in nucleation and Aitken mode aerosol number concentrations due to the introduction of the cloud condensation sink (b and d).

3.3.4 Contribution of NPF to low-level regional particles

This section aims to quantify the number of aerosol particles in the regional domain that are formed due to NPF and growth occurring within the regional domain compared to those transported into the domain from the rest of the world. Thus, extra simulations are included where NPF is switched off in both the regional and global domains (off_allNPF) and only in the regional domain (off_regNPF) using the BioOxEmCCS as the baseline simulation. The percentage change is calculated as $100 \times$ (BioOxEmCCS $-$ off_XXNPF)/BioOxEmCCS, where off_XXNPF denotes the simulation with either NPF switched off in both models (off_allNPF), or NPF switched off in the regional model (off_regNPF) only.

The time series of the aerosol vertical profiles in Fig. 3.9 show how number concentrations in the nucleation, Aitken and accumulation modes change when nucleation is switched off. The number concentrations of particles of all sizes are often reduced greatly compared to the baseline simulation by switching off NPF regionally and globally. Reductions are smaller when switching off NPF in just the regional model (off_regNPF), particularly below about 14 km. The changes in aerosol number concentrations in the regional model mostly occur between 10 and 18 km. In

contrast, the changes in aerosol number concentrations are large at all heights when nucleation in both models is switched off (off_allNPF).

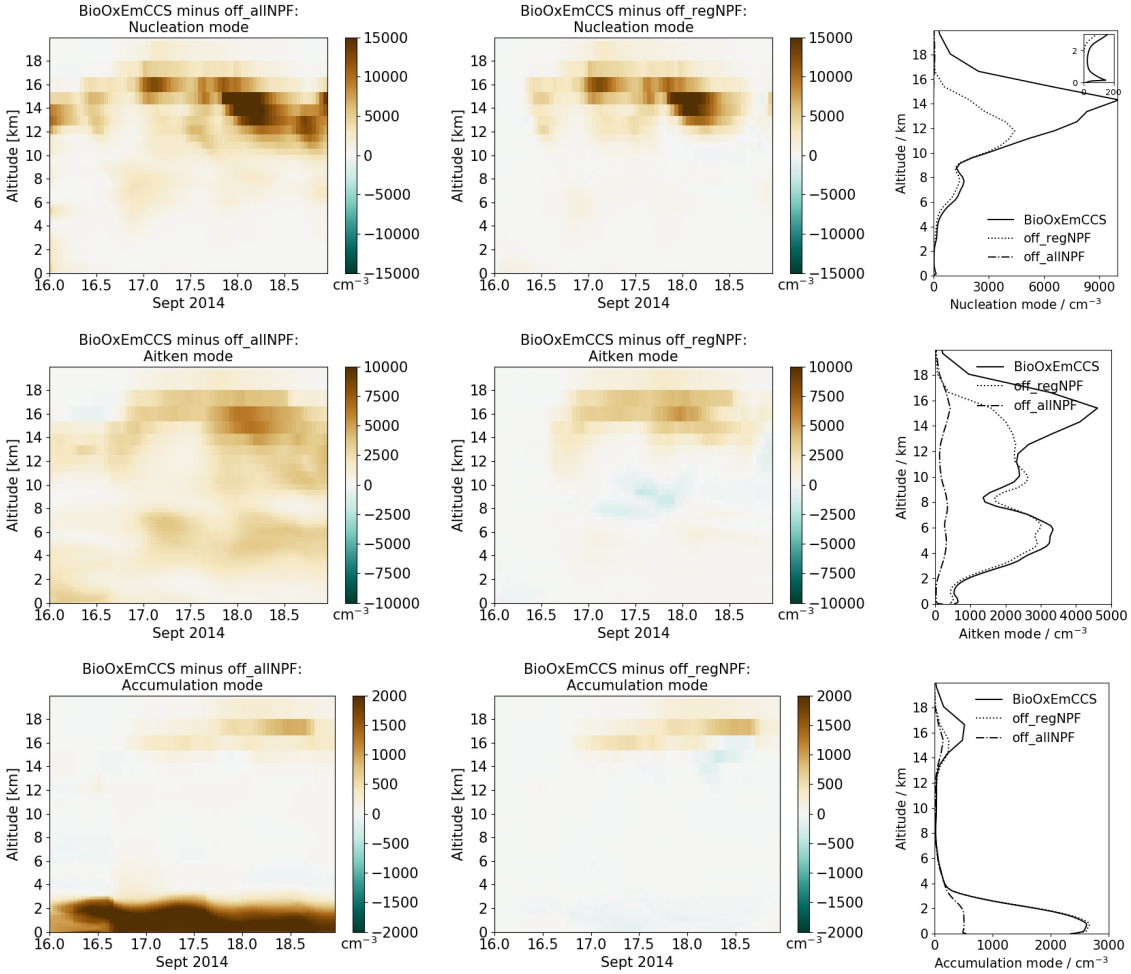

Figure 3.9: Time series of the regional domain averaged ambient aerosol number concentration profiles in the baseline BioOxEmCCS run minus those from a run in which nucleation is switched off in both the regional and global model (off_allNPF, left column) and minus those in which it is switched off in only the regional model (off_regNPF, middle column). The right column shows the time and domain-averaged profiles and the small panel embedded in the nucleation mode aerosol number concentration profiles (top right) shows details in the lowest 3 km in altitude. Values are shown for the nucleation mode aerosol (upper row), Aitken mode aerosol (middle row), and accumulation mode aerosol (bottom row). The regional domain averaged nucleation mode aerosol number concentrations in the simulation off_allNPF (top right plot) are all zero.

The percentage contribution of NPF to aerosol concentrations varies with the particle size and altitude (Fig. 3.10). The larger the particle size, the smaller the influence from NPF occurring in the regional model.

In this domain, NPF in the regional model has the dominant contribution to the nucleation mode particle concentration for all heights except 3-10 km, with contributions of more than

80% above 10 km in altitude. It demonstrates that formation of nucleation mode aerosol occurs on relatively short time scales and hence also small spatial scales. These results show that the increased nucleation mode aerosol concentrations seen in the UT in Fig. 3.6 when switching from the baseline biogenic nucleation (Bio) to the enhanced biogenic nucleation schemes (BioOx and BioOxEm) are mainly caused by additional biogenic NPF within the regional domain rather than outside of it. At 3-10 km, NPF in the regional model contributes to less than 45% of the nucleation mode concentration, so 55% is formed in the global model and advected in.

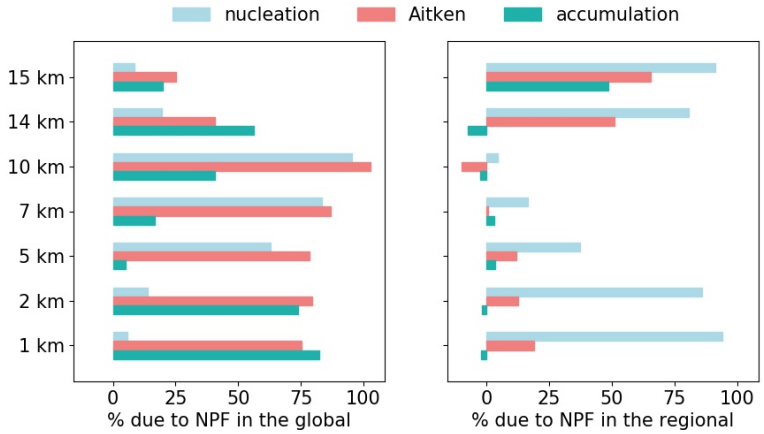

Figure 3.10: In the regional domain, the percentage contribution of NPF to the nucleation, Aitken and accumulation mode aerosol number concentrations from the global model (left) and regional model (right) at various altitudes.

The effect of advection of nucleation mode aerosol into the regional domain at different altitudes is determined partly by the different vertical profiles in the two domains. Nucleation rates in the global model at 3-10 km are on average 25 times greater than in the regional model in the BioOxEmCCS simulation (Supplementary Fig. A.3). The smaller nucleation rate in the regional model is likely due to the higher condensation sink generated by explicit cloud convection, and by the different vertical profiles of trace gases caused by resolved convection. For example, at around 8 km where the nucleation mode concentration is about a factor of 4 higher than in the regional model, the regional condensation sink is about a factor of 3 higher than in the global model, while the concentrations of monoterpenes are within 10% (Supplementary Fig. A.3). The higher condensation sink results in around 50 times lower nucleation rate in the regional model. These numbers suggest that nucleation rate in the global model is higher than in the regional model in this deep convective environment due to the global model failing to resolve the small-scale spatial variations in trace gases, aerosols and clouds.

The percentage contribution of NPF to the Aitken mode particle concentration in the regional model is also dominant above 14 km in altitude, but is small below that height. Below 2 km (in the boundary layer), it is around 12%-19%. Between 14 and 15 km in altitude, around 51%-66% of the domain-averaged Aitken mode concentration is from NPF in the regional domain, and 25%-41% is from the global model NPF. The percentages do not sum to 100% because of the contribution from primary particles. At 5 km, NPF in the regional model accounts for 12% and outside the regional domain, the global model accounts for 78% of the Aitken mode concentration. This result supports the arguments that the extra Aitken mode aerosol that was seen in Fig. 3.6 when switching from BioOx to BioOxEm at 5 km in altitude were due to NPF in the global model (either at 5 km, or at other heights followed by vertical transport). The overall percentage contribution of NPF to Aitken mode aerosol in the regional domain is smaller than that of the nucleation mode aerosol because forming the Aitken mode aerosol requires a longer time and is affected by coagulation and scavenging.

The accumulation mode aerosol is the least dependent on NPF from the regional model. Above 15 km, the contribution of NPF in the regional domain to the accumulation mode aerosol is 49% and 20% is from global model NPF, meaning that the regional model is able to form some accumulation mode aerosol via NPF in the time available in the domain. In Fig. 3.6 more accumulation mode aerosol appear below 2 km in altitude as the biogenic nucleation rates were increased (from Bio to BioOx and from BioOx to BioOxEm). Fig. 3.10 confirms that NPF in the regional domain does not lead to the formation of the additional accumulation mode below 2 km because NPF actually slightly reduces the concentrations, showing that the regionally-formed Aitken mode particles do not grow to accumulation mode sizes at these heights. A few possible explanations for the slight reduction in concentrations due to NPF below 2 km are: that NPF causes the aerosol size distribution to shift to a smaller size as was reported in Sullivan et al. (2018); due to upward transport from the surface to higher altitudes; it could also be caused by the randomness of a different convection field. Further investigations of the issue of aerosol vertical transport are in Section 3.3.5.

Overall, the findings in this section show that in the regional domain below 2 km, Aitken and accumulation mode particles are dominated by NPF occurring outside of the regional domain and in this study, these particles come from the global model. It implies that the boundary layer CCN, which influence cloud droplet number concentrations, are originally transported

from outside the domain.

3.3.5 Convective transport of particles

Section 3.3.4 showed that NPF in the regional domain produces only around 10-20% of Aitken mode aerosol in the boundary layer and has a negligible effect on the accumulation mode. Here the reason why these regionally nucleated particles have a weak effect on boundary layer Aitken and accumulation mode particles is investigated. Five simulations are added in which NPF in the regional model is only allowed at specific altitudes (1-4 km, 4-7 km, 7-10 km, 10-13 km, and 13-16 km). Percentage differences are calculated using $100 \times (\text{NPF\_XXkm} - \text{off\_regNPF})/\text{NPF\_XXkm}$, where NPF_XXkm denotes one of the simulations with NPF switched on only between 1-4 km, 4-7 km, 7-10 km, 10-13 km, and 13-16 km.

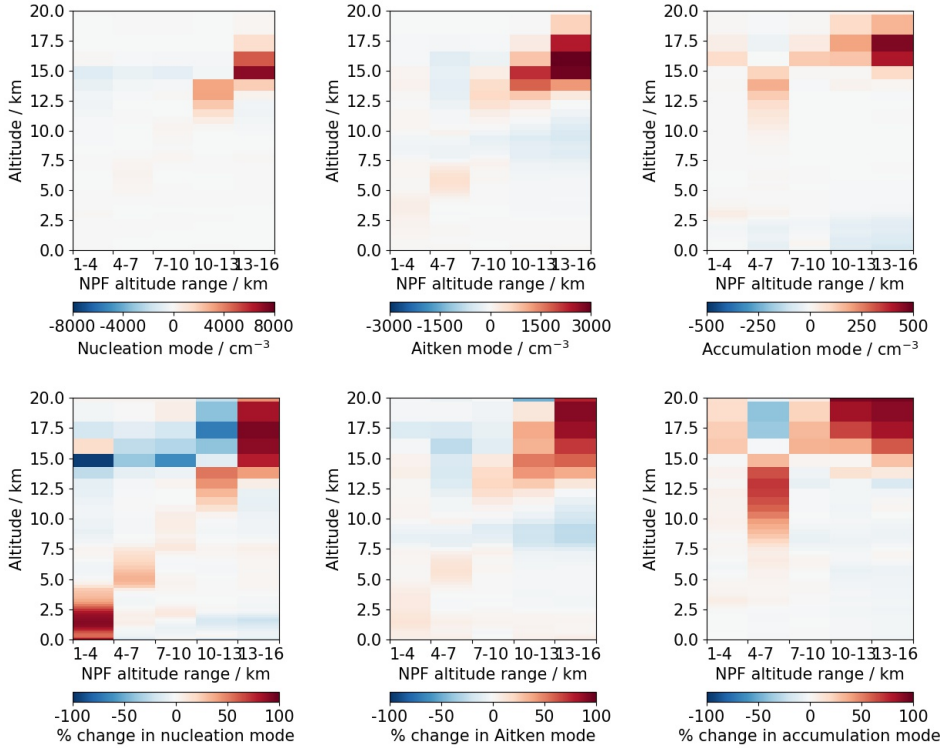

Figure 3.11: The absolute (upper row) and percentage (lower row) changes of the regional time- and domain-averaged profiles of ambient number concentrations of (left column) nucleation mode aerosol, (middle column) Aitken mode aerosol, and (right column) accumulation mode aerosol, between the simulations with NPF switched on at certain altitudes (NPF_1-4km, NPF_4-7km, NPF_7-10km, NPF_10-13km, and NPF_13-16km) and the simulation with no NPF in the regional domain (off_regNPF).

Figure 3.11 shows the absolute and percentage domain-average effects of NPF occurring in these altitude layers. The absolute differences are most significant for the nucleation and Aitken mode

above 10 km, and the accumulation mode above 15 km in altitude. NPF above 10 km (in the UT; NPF_10-13km and NPF_13-16km) perturbs particle concentrations almost entirely at or above the heights where it occurs. For example, in the NPF_13-16km simulation, the nucleation mode concentration changes by around 7200 cm^{-3} (79%) at these altitudes, the Aitken mode concentration changes by 3900 cm^{-3} (70%), and accumulation mode concentration changes by 470 cm^{-3} (83%). It again confirms that the regionally-formed nucleation mode particles grow and coagulate to form Aitken and accumulation mode aerosol within the domain. NPF between 13 and 16 km (NPF_13-16km) contributes to nucleation and Aitken mode particles between 12 and 20 km and to accumulation mode particles between 13 and 20 km. The vertical extent over which the perturbations occur implies that nucleation and Aitken mode particles are transported mostly upwards (but also downwards) from the altitudes where NPF takes place, while the accumulation mode particles in most of the time are only transported upwards.

NPF in the regional model UT contributes very little to particle concentrations below 2 km in the regional domain during the 3-day dry season simulation. The contributions of NPF above 10 km to particles below 2 km are -0.3 cm^{-3} (-0.01%) for the nucleation mode, 33 cm^{-3} (1.1%) for Aitken mode and -126 cm^{-3} (-4.2%) for the accumulation mode. In cloudy downdrafts below 2 km, Aitken mode concentrations resulting from NPF above 10 km occasionally reach a maximum of 100 cm^{-3} (but on average, it only account for 0.13% of the local concentration of all times) and a maximum of 60 cm^{-3} (on average contributing to 0.08% of the domain particles) for the accumulation mode. It shows that deep convection can transport particles that are formed in the regional UT to low altitudes when convective downdrafts are strong. However, these number concentrations have a negligible effect on the domain-mean number concentrations below 2 km because deep convection covers only around 4% of the domain below 2 km. Thus, even though NPF above 10 km in the regional model can form the Aitken and accumulation mode particles within the domain, the majority of the particles either stay in the UT or leave the domain by horizontal transport. These particles may be transported downwards on larger spatial scales, but not on the scale of around 1000 km simulated here.

NPF below 10 km produces fewer particles than NPF in the UT. NPF between 7 and 10 km causes a peak in the Aitken mode concentration up to around 590 cm^{-3} (20%) between 11 and 15 km, while there is no increase in Aitken mode in the 7-10 km height range where NPF is occurring. It shows that Aitken mode particles at 11-15 km are affected by ascent of nucleation

mode aerosol from lower altitudes followed by growth to Aitken mode sizes. NPF in all altitude layers contributes to accumulation mode particles in the 10-15.5 km layer, with domain- and time-mean increases as large as 180 cm^{-3} (65%). Overall, these results show that NPF below the UT can contribute to Aitken and accumulation mode particles in the UT.

The addition of NPF in the regional domain *reduces* the accumulation mode number concentrations below 4 km. It is likely due to enhanced nucleation that competes with particle growth for condensible gases (Sullivan et al. 2018), but these increases could also be due to model randomness.

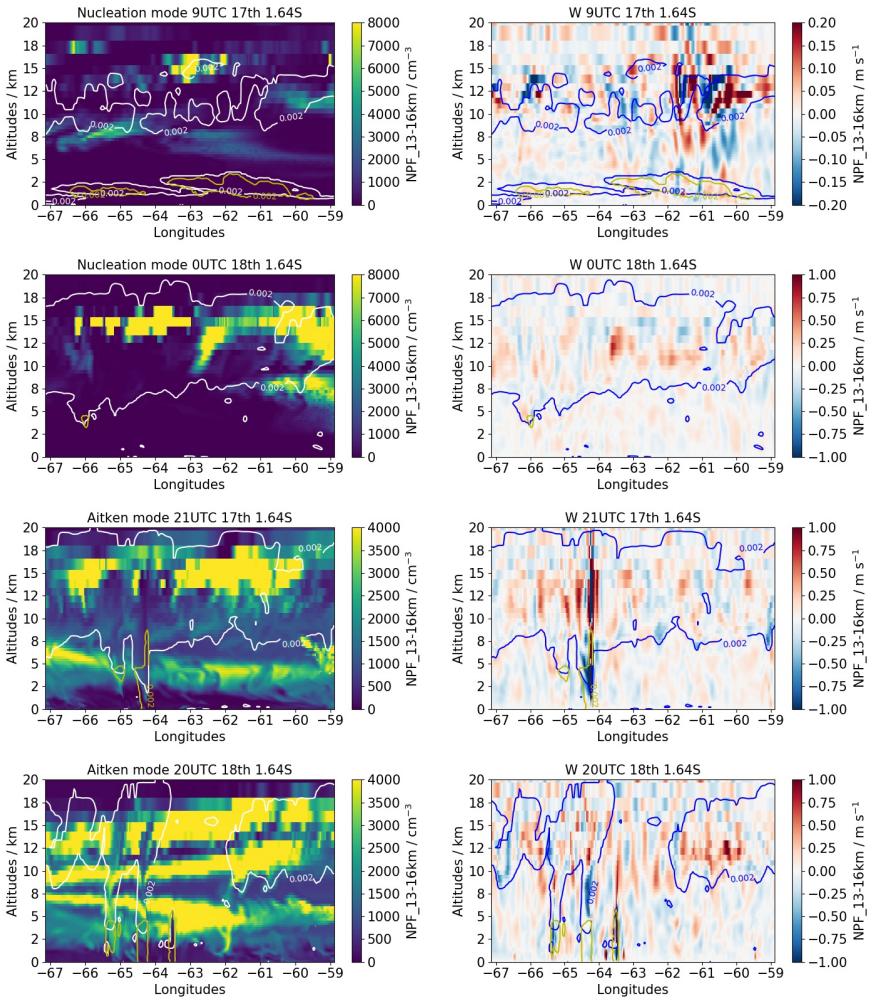

Figure 3.12: West to east vertical slices at 1.64 S of nucleation mode (first two rows), Aitken mode (lower two rows) number concentrations and the vertical velocity from the NPF_13-16km regional simulation at various times (see panel titles) in order to highlight vertical transport. Easterly winds were dominant. White and blue contours highlight clouds (liquid plus frozen water content = 0.002 g kg^{-1}) and yellow contours denote rain mass mixing ratios of 0.002 g kg^{-1}. Videos of the nucleation, Aitken and accumulation mode aerosol slices can be found in the supplementary.

Figure 3.12 shows the vertical slices of nucleation mode, Aitken mode particles and vertical velocity that exemplify the vertical transport. A plume of nucleation mode aerosol at 9 UTC on 17 September 2014 descends from around 10 km to 7 km between 64 W and 66 W and quickly exits the regional domain to the west (see videos of vertical transport in the appendix). Similarly, at 0 UTC on 18 September between 62 W and 63 W a 'finger' of nucleation mode aerosol extends from the UT down to around 9 km and is then diluted within three hours. The two slices also show clear downward transport of Aitken mode aerosol from around 7 km to below 2 km in altitude between 64 W and 66 W, which is associated with cloud (white contours). The downward motion of Aitken mode aerosol is a potential explanation for the excess accumulation mode seen below 2 km in BioOxEm compared to BioOx in Fig. 3.6 e (Section 3.3.2), namely that the additional nucleation in BioOxEm leads to more nucleation and Aitken mode aerosols in the global domain, which enters the regional domain below 7 km from the global model and those Aitken mode formed below 7 km within the regional domain, are transported downwards into the boundary layer by convection and then grows to accumulation mode sizes. The Aitken mode aerosol from the global model nucleation are mostly formed above around 2 km in altitude where nucleation rates start to significantly affect aerosol concentrations and grow to accumulation mode as they sink into lower altitudes (Supplementary Fig. A.3 and A.4).

Some transport-only passive tracers are implemented in the model to understand the vertical transport efficiency of air in the convective environment. The tracers were emitted within 9 vertical model layers using the same constant emission rate as the default monoterpenes emission rate from CMIP5 inventories with no deposition. Figure 3.13 shows the domain averaged tracer mixing ratios for the whole simulation period. Figure 3.14 shows maps of the instantaneous mixing ratio of the 14 km altitude tracer at different altitudes. The 9 tracers have the largest concentrations where they were emitted, but only those that are emitted below 6 km reach the surface. The tracers emitted at higher altitudes are redistributed both up- and downwards by around 5 km, creating bands with depths between 8-10 km. An example can be seen from the maps of tracer that is emitted at 14 km altitude (Fig. 3.14). Similar scales of vertical mixing of aerosols can also be seen from global model (Supplementary Fig. A.4). The tracer mixing ratios at 9 km, 5 km and 500 m to 14 km altitudes are compared in order to obtain the transport ability. The results show that on average less than 5% of the 14 km tracer reaches an altitude of 9 km, 0.13% reaches 5 km, and barely any is transported to 500 m altitude

(0.01%). Consequently, over a 3-day period, a convective environment of dimension 1000 km can transport air downward in sufficient quantities to significantly affect the domain mean by at most 5 to 8 km within the regional domain, but the influence is less than a few percent.

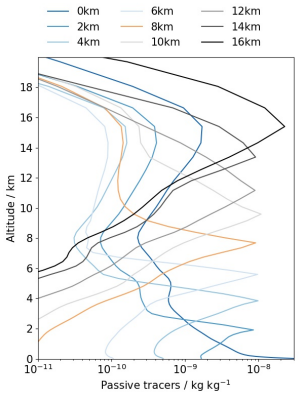

Figure 3.13: Regional time- and domain-averaged profiles of passive tracer mass mixing ratios emitted from 9 different model levels with vertical thicknesses ranging from 16 m at the surface (blue) to 2000 m at 16 km (black) in altitudes.

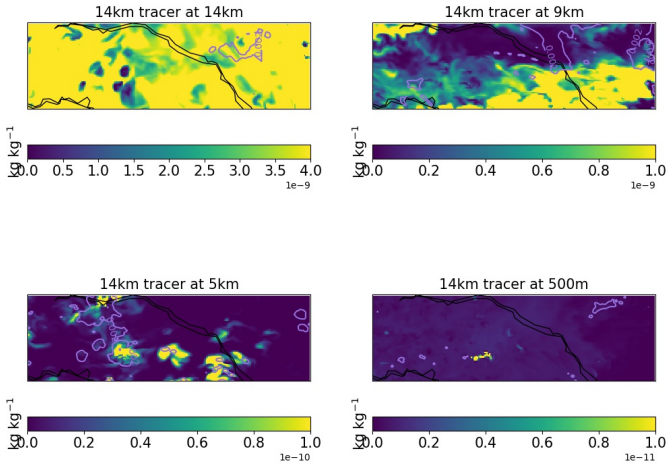

Figure 3.14: Maps of the mixing ratio of a passive tracer emitted at 13-16 km altitude. Mixing ratios are shown at 14 km, 9 km, 5 km, and 500 m at 21 UTC on 17 September 2014 (47 hours after the first release of the tracer). The upper limits in the four maps are different.

Amazonia in East-West direction is around a factor of 3 of the size of the regional domain. Therefore, if air masses keep the descending motion, the number of particles being transported into the boundary layer would be expected to increase. A regional simulation with a higher resolution would be likely to be more efficient at transporting aerosol vertically but such a simulation is not performed in this study in order to keep a reasonably large domain. In contrast, the model exhibits strong upward transport which allows substantial amount of tracers,

especially for those emitted below 4 km to reach 16 km in altitude. Other tracers are transported upward by around 0.5-4 km. Therefore, in the regional domain, the aerosol can be transported upward by as far as 16 km, but downward by at most 8 km.

3.4 Discussion and Conclusions

A a global model with a 4 km-resolution nested regional domain is used (of size 1080 km by 440 km) to study the influence of deep convection on new particle formation (NPF) and the budget of cloud-forming aerosol particles in Amazonian boundary layer.

The regional-scale simulations show that deep convection regulates the vertical distribution of trace gases and aerosol particles by efficiently transporting monoterpenes from the surface to the UT. In the UT, monoterpenes can be oxidised within a few hours, and with low temperature and condensation sink, new particles are efficiently formed. Consistent with observations (Andreae et al. 2018; Williamson et al. 2019) and global model simulations (Pierce and Adams 2007; Merikanto et al. 2009; Wang and Penner 2009; Dunne et al. 2016), the regional simulations of a convective environment show that NPF is strongest in the UT, leading to the greatest number concentrations of nucleation and Aitken mode particles (a total of more than 10000 cm^{-3}).

The rate of NPF in the UT is reduced and spatially strongly modulated by the condensation sink of trace gases and nuclei on cloud droplets and ice particles. When this additional 'cloud condensation sink' is included in the regional model, mean concentrations of nucleation and Aitken mode particles in the UT are reduced by 50%. The formation of particles primarily in detraining convective clouds is consistent with several observations (Clarke et al. 1998; Twohy et al. 2002; Andreae et al. 2018; Williamson et al. 2019). This localised cloud sink is straightforward to include in a convection-resolving model, but would be more difficult to include in a global model in which clear and cloudy air parcels in the UT are not explicitly simulated.

The typical vertical profiles of nucleation mode and Aitken mode particles, with peak concentrations in the UT, are created through NPF in the regional model on the timescale of a few days. With typical easterly winds in the simulated area, the nucleation and Aitken mode particle profiles in the UT are therefore created on spatial scale of a few hundred kilometres as air advects across the rainforest. However, below the UT the environmental conditions required to create the nucleation and Aitken mode profiles are not ideal in the regional domain. The

regional influence of NPF on the accumulation mode particle profile is important only at the highest altitudes in the UT (around 15 km) and is negligible at lower altitudes. Similarly, the influence of regional-domain NPF on Aitken mode aerosols is significant in the UT, but NPF accounts for only around 10-25% of particle concentrations in the boundary layer with the other more than 75% of the particles from the global model. This weak effect is because of the longer time taken to form the larger particles following NPF, which means that particles formed by NPF above the boundary layer are advected out of the domain before they reach the larger sizes or before they can be transported downwards.

Below approximately 10 km altitude, the regional model simulations show that nucleation and Aitken mode particles are not substantially affected by NPF on the timescale of 3 days. In the regional domain of size around 1000 km aligned with the mean easterly wind, aerosol in the boundary layer is mostly produced outside the region (in the global model) and advected into the domain below 10 km altitude. Consistent with previous global model studies, the results show that these advected particles were mostly formed by NPF, but on much larger spatial scales than the 1000 km domain in the simulations.

NPF is strongest above 10 km altitude, but the simulations show that it can affect particles below this altitude through vertical transport in the deep convective environment. The regional simulations show clear plumes of particles being transported in downdrafts, and these have been observed Wang et al. (2016). However, extremely few particles formed above 10 km altitude are transported all the way to the boundary layer (less than 1%) during the 3 days of the regional simulation. Rather, the simulations show that NPF-formed aerosol above 10 km altitude is transported only a few kilometres downwards (to around 8-10 km in altitude), while the aerosol entering the boundary layer originated from altitudes below 7 km. This lower-altitude aerosol was not formed by NPF during the 3-day simulation, but was advected into the regional domain and then transported downwards. Figure 3.15 shows a sketch of this vertical transport. This limited vertical transport, especially for Aitken and accumulation mode, is because the downdraft within one convective cycle in the regional domain is not strong enough to bring a large number of particles from the UT down to the boundary layer, not even for the passive tracers that are not scavenged during vertical transport. These results show that new aerosols that are formed within a 1080 km by 440 km regional domain in the Amazonian dry-to-wet season are not the major source of the boundary layer aerosol particles for such a domain.

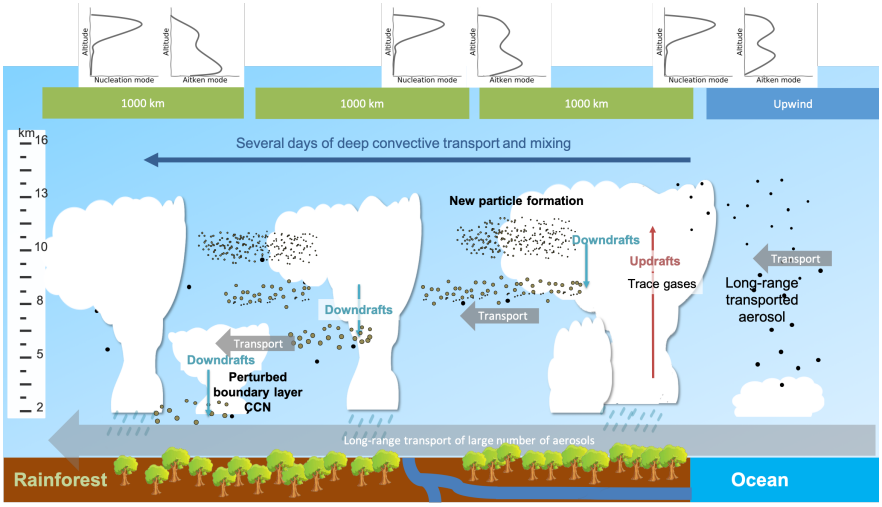

Figure 3.15: A schematic diagram of downward transport and mixing of aerosols associated with NPF. The nucleation and Aitken mode aerosol profiles in upper panels are example number concentrations in the upwind, within, and in the downwind of the simulated 1000 km by 400 km region.

The results are similar to those of Clarke et al. (2013), who reported that particles in the free troposphere are likely to be transported from thousands of km away before they finally contribute to boundary layer CCN. The extent of aerosol vertical transport in the simulations is in line with Gerken et al. (2016) who showed that O_3 from 2-7 km altitude may enter the boundary layer during convective storms occurring during GoAmazon2014/5. Other observational studies (Giangrande et al. 2016; Machado et al. 2021) also reported that downdrafts occurred most frequently below the freezing level (10 km) in Amazonia and that the horizontal extent of the downdraft decreased with increasing altitude. Similarly during GoAmazon2014/5, observations in Tang et al. (2016) showed that the air exhibited downward motion between around 700 hPa and the surface during the day (10-18 local time), and above around 700 hPa during the rest of the day, but these two periods were interrupted by the upward motion, inhibiting the downward motion from the UT to the boundary layer. The results do not show any significant increases in particle number concentrations below 2 km associated with convective downdrafts, which is consistent with the analysis of observations during GoAmazon2014/5 and ACRIDICON-CHUVA campaigns (Machado et al. 2021). Wang et al. (2016) reported rapid downward transport of free tropospheric aerosols that could have been formed in the cloud outflow. With ATTO tower data, Franco et al. (2022) found particles smaller than 50 nm to enter the boundary layer that was likely to be caused by gust front downdrafts or rain. The results of this chapter also show instantaneous increase of Aitken mode particles up to 100 cm^{-3} associated with cloudy down-

draft but only occurs occasionally. However, over the 3-day simulation of the 1000 km domain, these downward transported particles are negligible, making the downward transport efficiency small in the simulations.

In the dry-to-wet season transition, NPF in the boundary layer has a very limited effect on Aitken mode and accumulation mode particles below 2 km in altitude. Instead, in the wet season when the environment is less polluted, the percentage contribution of convective downdraft from UT to the boundary layer particles are likely to be greater. The small effect of NPF upon boundary layer CCN may be further weakened by strong biomass burning events that took place in September 2014, which would increase the aerosol condensation sink and suppress NPF. These events were not included in the simulations. This additional condensation sink may be less important in the wet season when biomass burning is rarer and the condensation sink is generally lower than the season studied here.

The results support the conclusion of Andreae et al. (2018) that NPF in the Amazonian UT is sustained by the upward transport of biogenic vapours in deep convection. The simulations show that very high particle concentrations above 10 km altitude are created within a few days of advection of air over the rainforest. However, the results show that these newly formed particles in the UT do not contribute to boundary layer particles via vertical mixing and transport on the timescale of a few days. The results agree with Andreae et al. (2018) and Wang et al. (2016) that Aitken mode particles can be transported downwards from the lower free troposphere into the boundary layer, and such downdraft events associated with convection are apparent in the model. However, on the timescale of a few days and a spatial scale of 1000 km, such transport has a small effect on mean particle concentrations in the boundary layer. This is even the case for passive tracers, so transport is the limiting factor, not aerosol microphysics. Although the results are consistent with Andreae et al. (2018) in that NPF in the free troposphere is an important overall source of CCN in Amazonian boundary layer, the results show that these particles are formed on spatial scales much larger than 1000 km, and not necessarily over Amazonia.

Overall, I have high confidence that, during the dry-to-wet transition season, Amazonian rainforest controls aerosol particle concentrations in the UT, and that the observed high concentrations are produced directly within regions of deep convection on the timescale of a few days. I have

moderate confidence that particle concentrations below the UT are controlled by processes occurring on much larger scales than 1000 km. Therefore, the concept of a cycle of trace gas vertical transport, particle formation, and subsequent CCN transport into the boundary layer is unlikely to be a 'closed loop' over the selected region in Amazonia which is around 1/3 of the forest in East-West direction, but is likely to be strongly influenced by advection of aerosol into this regional domain.

There are some limitations of the simulations that would need to be overcome to confirm the conclusions. In particular, the regional domain size and 4 km resolution may limit the generalisability of the results and understandings of the regional NPF to CCN link. The relatively coarse 4 km resolution may limit the extent of downward transport of aerosol from the UT to the boundary layer in distinct plumes. Nevertheless, there are thermodynamic limits on the extent to which air can be exchanged in this way. If the domain were larger, the particles would be allowed to grow and be transported in the domain for a longer time, then the number particles enters the boundary layer from UT may experience moderate increases. A domain covering the whole of Amazonia would be about 2-3 times larger in linear dimension than the domain in this chapter, which would provide about 2-3 times longer for vertical mixing assuming the same mean advection speed. This increase alone would not be sufficient to affect the conclusion that Amazonia is not a closed CCN production loop through new particle formation. Such a loop could exist in regions where air is stagnant over Amazonia or in the wet season with considerably more convection.

It is strongly recommended that future regional modelling studies of Amazonian particles include a driving global model to fully capture the long-range transport of aerosol. I also recommend that the regional nests use an increased resolution and domain size; and that more chemical complexity is included. Comparing the wet and dry season would be helpful to gain a complete picture of the evolution of the particle number concentrations and size distributions in Amazonia.

Chapter 4

The influence of Amazonian anthropogenic emissions on aerosol, cloud and surface rain

4.1 Introduction

Anthropogenic aerosols contribute a high fraction of uncertainty in radiative forcing of climate change by acting as cloud condensation nuclei (CCN) (Jones et al. 1994; Pierce and Adams 2007; Wang and Penner 2009; Merikanto et al. 2009; Kazil et al. 2010; Yu et al. 2013; Dunne et al. 2016; Gordon et al. 2016; Gordon et al. 2017). Several modelling studies have showed that anthropogenic emissions can affect aerosol concentrations and thus, CCN (Manktelow et al. 2009; Laakso et al. 2013; Yu et al. 2013; Shrivastava et al. 2019; Zhao et al. 2021). Changes in CCN concentration affect cloud properties such as cloud droplet number concentration (N_d), which then provides cloud adjustments of liquid water path (LWP) and cloud fraction (Twomey 1977; Albrecht 1989). Evidence for the effect of aerosol and pollution on cloud optical depth, cloud thickness, N_d and precipitation have been confirmed by observational studies (Kawamoto 2006; Sporre et al. 2012; Gonçalves et al. 2015; Fan et al. 2018; Douglas and L'Ecuyer 2021). However, it is hard to interpret and quantify the influences of anthropogenic emissions on clouds from observations, especially for deep convective clouds.

Satellite observations from MODIS (Moderate Resolution Imaging Spectroradiometer) show

that more aerosols could cause taller clouds and larger anvils for convective clouds (Koren et al. 2010). Observations from GoAmazon2014/5 (Observations and Modeling of the Green Ocean Amazon 2014-2015) showed that under polluted conditions, the warm-phase cloud droplet effective diameter undergoes changes of 10%-40% and N_d is increased by a factor of 10 compared to clean conditions (Cecchini et al. 2016).

Regional models and large-eddy simulations (LES) have widely been used to study aerosol-cloud interactions. Anthropogenic emissions as well as new particle formation (NPF) mechanisms are found to be likely to affect CCN concentration between preindustrial and present-day environments (Pierce and Adams 2009; Wang and Penner 2009; Makkonen et al. 2012; Gordon et al. 2016; Gordon et al. 2017). For deep clouds, increasing aerosol concentrations may produce more smaller sized cloud droplets and ice crystals which release extra latent heat, then the changed cloud microphysics will potentially affect cloud dynamics such as updraft velocity, cloud fraction etc. (Kawamoto 2006; Rosenfeld et al. 2008; Marinescu et al. 2021). The response of clouds to increasing aerosol concentrations may depend on aerosol sizes. A continuous supply of CCN can sustain a storm cloud and extra sub-micron aerosol activation was found to invigorate deep convective clouds (Ekman et al. 2004; Fan et al. 2018), while adding large particles to the environment can cause reduction of rain in mixed-phase clouds (Pan et al. 2022). A greater aerosol concentration can produce more ice number because of increased cloud droplets (Fan et al. 2013; Herbert et al. 2015; Grabowski and Morrison 2020). The effects of aerosol on precipitation in deep convective clouds vary with region, background aerosols, environmental conditions and model setups (Heever and Cotton 2007; Connolly et al. 2013; Heikenfeld et al. 2019; Dagan et al. 2022). Even the differences between deep convective clouds themselves affect the response of precipitation to aerosol changes, e.g. whether the rain events are light or heavy, warm or cold etc. (Qian et al. 2009; Li et al. 2011; Fan et al. 2012; Tao et al. 2012; Guo et al. 2014; Jiang et al. 2016; Barthlott and Hoose 2018). Nevertheless, the effects of anthropogenic emissions on clouds via NPF and aerosols are still not well understood.

Amazonia is one of the most pristine environments in present-day, especially during the wet season when rain cleans the air, but the environment is still affected by pollution from cities like Manaus in central Amazonia. Aircraft measurements over Manaus and the downwind forest have shown that around 20% of the total particulate matter at 1 μm diameter are composed of anthropogenic sources which include sulfates, nitrates and ammonium (Shilling et al. 2018)

and observations from a research tower downwind of Manaus showed that the total sub-micron particulate matter concentration is up to a factor of 2 higher in polluted conditions than in background conditions (Sá et al. 2018). Cirino et al. (2018) used observations from two towers downwind of Manaus to show that the fractional contribution of organic gas molecules to aerosol mass increased when the sites were further away from emission sources, implying the decreasing influences of pollution with longer distance from the emission source. Glicker et al. (2019) also reported higher particle concentrations during high-pollution days from observations and their back-trajectory model showed that the high concentrations were due to emissions from Manaus. Other modelling studies have also confirmed that anthropogenic emissions enhanced aerosol mass by a up to factor of 4 and enhanced concentrations by a factor of 5-25 downwind of Manaus (Shrivastava et al. 2019; Zhao et al. 2021). However, these studies did not investigate the effects of anthropogenic emissions on clouds in the convective environment.

Inspired by the aforementioned studies, which either studied effects of emissions on aerosols or investigated the effects of aerosols on clouds, this chapter aims to investigate the extent to which changes in aerosol concentrations caused by anthropogenic emissions affect cloud, rain, and the underlying mechanisms in the convective environment in Amazonia. Here, the anthropogenic emissions in this study are defined in Table 4.1. The atmosphere-only configuration of HadGEM3 (Hadley Centre Global Environment Model version 3) climate model with a nested regional domain that covers the Manaus region and most of the rainforest region will be run (720 km by 1200 km with 3 km resolution) under several regional emission scenarios, with the baseline model simulation evaluated against observations from the GoAmazon2014/5 campaign. The questions for this chapter are addressed as follows:

(1) What are the effects of anthropogenic emissions on aerosol, cloud and rain in Amazonia?

(2) What mechanisms drive the changes in cloud water and rain?

4.2 Methods

4.2.1 GoAmazon2014/5 campaign and G-1 aircraft observations

The observations used in this study are from the 2-year field campaign Observations and Modeling of the Green Ocean Amazon 2014-2015 (GoAmazon2014/5) in central Amazonia (Martin et al. 2016; Martin et al. 2017). The campaign aimed to study the response of Amazonian en-

vironment under pollution plumes transported from Manaus in 2014 and 2015. The campaign included aircraft measurements onboard a low-altitude G-159 Gulfstream I (G-1) in February, March, August, September and October 2014, and 9 fixed research sites that collected observations in various environments such as urban, forest, pasture, both upwind of Manaus and downwind transects of the pollution plume and the surrounding areas. The measured data include meteorology, aerosol, gas pollutants, and cloud properties (Martin et al. 2016; Martin et al. 2017).

The aircraft measurements of aerosol number concentrations onboard the G-1 aircraft on 11, 12, 14, 16 and 17 March 2014 were used. There were 15 flights available in February and March 2014. The selected five days are within the regional model simulation time (11-18 March 2014). Figure 4.1 shows the flight tracks of the selected five days and the measured regions are mainly the transects of the plume from Manaus. The measured aerosols with diameters greater than 3 nm ($N_{D>3nm}$), 10 nm ($N_{D>10nm}$) and 100 nm ($N_{D>100nm}$) are compared with the model. $N_{D>3nm}$ and $N_{D>10nm}$ were measured using a Condensation Particle Counter (CPC) with the cutoff diameters between 3 nm - 3 mm, and 10 nm - 3 mm for the two size ranges. $N_{D>100nm}$ was measured with a Passive Cavity Aerosol Spectrometer Probe (PCASP). Full details of the instruments can be found in Martin et al. (2016). During the five days, most of the measurements were made below 2 km altitude, and occasionally at 2-6 km altitude where particle number concentrations are between around 100 and 200 cm^{-3}, significantly lower than the concentrations in the lowest 2 km layer.

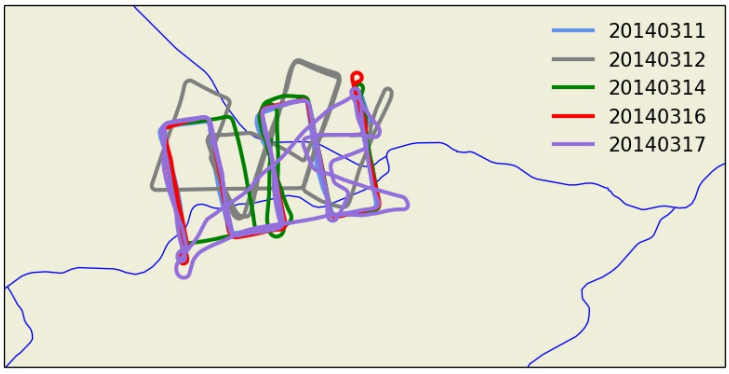

Figure 4.1: G-1 flight tracks on 11, 12, 14, 16 and 17 March 2014. The aircraft flew at below 2 km in altitude on 11, 12 and 16 March and reached around 6 km on 14 and 17 March 2014.

The 3-hourly precipitation rate measured by the S-band Amazon Protection National System radar between 11-17 March 2014 is also used in this chapter for comparison.

4.2.2 Global and regional model configurations

A configuration which has the regional model nested in a global model is used, and the global model is based on Unified Model version 11.6 with GA7.1 (Global Atmosphere v7.1), similar to the models in Chapter 3, and other details can be found in Chapter 2. The global model resolution is N96 (around 135 km) in the horizontal direction and there are 85 vertical levels up to 80 km in altitude. The regional domain is centred at (3.1° S, 62.7° W), downwind of Manaus. The domain is 1200 km (east to west direction) by 700 km (north to south direction) with 3-km horizontal resolution. There are 70 vertical model levels with the highest altitude at 40 km and the lowest 64 levels cover the vertical extent from the surface to 20 km in altitude, mainly where cloud and aerosol interact. Convection, cloud microphysics, aerosol microphysics in UKCA (United Kingdom Chemistry and Aerosol) and the coupling settings are described in Chapter 2.

UKCA uses monthly averaged emissions for natural gases. CMIP6 emission inventories provide CH_4. Monoterpene, isoprene and natural SO_2 are obtained from CMIP5 inventories. The marine source of DMS has been parameterised based on Lana et al. (2011) and the land source is biomass burning (Werf et al. 2006; Lamarque et al. 2010; Granier et al. 2011; Diehl et al. 2012). The emitted CH_4 from biomass burning data have been generated by the JULES (Joint UK Land Environment Simulator) model (Mangeon et al. 2016; Walters et al. 2019). Monoterpene and isoprene are obtained from monthly averaged emission inventories that include vegetation (Guenther et al. 1995; Pacifico et al. 2012). Natural SO_2 comes from volcano eruption (Stier et al. 2005).

Most of the emissions of anthropogenic gases and primary aerosols are obtained from the high-resolution (0.1° by 0.1°) EDGAR (Emissions Database for Global Atmospheric Research) inventories which allows us to better reproduce the locations and concentrations of aerosol (Janssens-Maenhout et al. 2015). The emissions used in the model are monthly averages for the year 2010 and Table 4.1 shows all the included species. Here, the emissions of BC (black carbon) and OC (organic carbon) are the sum of anthropogenic sources and biomass burning of each species. NVOC (non-volatile organic compounds) comes from the anthropogenic emission inventory, MACCity MEGAN (Monitoring Atmospheric Composition and Climate project, The Model of Emissions of Gases and Aerosols from Nature), and the emissions are read in and used as methanol in the UKCA model (Sindelarova et al. 2014). NO emission from CMIP6 inventory

includes the NO emitted during aircraft flights and biomass burning events (Hoesly et al. 2018). All biomass burning emissions are considered anthropogenic in this study. A temporal evolution is applied for NO, BC and OC to align with the traffic hours.

Table 4.1: Gaseous species and aerosol emissions that are anthropogenic

Species names			
BC	OC	SO_2	NH_3
NOx	CH_3CHO	CH_3COCH_3	CH_2O
CO	C_3H_8	C_2H_6	Biomass burning

UKCA uses a coupled chemistry scheme (StratTrop) which involves 84 species with 81 of them having chemical reactions (Archibald et al. 2020), including several chemical reactions with anthropogenic gas species (ammonia, ethane, nitrogen monoxide etc.). StratTrop chemistry scheme can better (than offline chemistry) represent reactions associated with pollution plumes from Manaus and the biogenic emissions from the surrounding forest in Amazonia, and subsequently affects NPF in this study. Here, monoterpenes are oxidised by the same oxidants (OH, O3 and NO_3) as described in Chapter 3, but the oxidants in StratTrop chemistry scheme can be transported, deposited as tracers, and vary the concentrations with chemical reactions. The StratTrop scheme has been used in global modelling studies (Mulcahy et al. 2020), and was firstly incorporated in regional modelling in the study of Gordon et al. (submitted).

4.2.3 New particle formation

In this chapter, the biogenic nucleation mechanism introduced in Chapter 2 and a nucleation scheme that includes sulfuric acid and organic gas molecules (BioOxOrg) (Riccobono et al. 2014; Kirkby et al. 2016) are used for new particle formation in UKCA.

The inorganic-organic (InorgOrg) nucleation mechanism has been established by CLOUD chamber experiments and parameterised in GLOMAP (Global Model of Aerosol Processes) (Riccobono et al. 2014). It produces particles at 1.7 nm in diameter with H_2SO_4 and BioOxOrg clusters. The BioOxOrg is an oxidation product of monoterpenes oxidised by OH (Riccobono et al. 2014). Nucleation rates at 1.7 nm in diameter are derived using the concentrations of BioOxOrg and H_2SO_4 (Eq. 4.1).

$$J_{\mathrm{InorgOrg}_{1.7\mathrm{nm}}} = \exp(-(T - T_0)/B_1) \times (B_2 \times k \times [H_2SO_4]^2 \times [\mathrm{BioOxOrg}]), \quad (4.1)$$

where, $J_{InorgOrg_{1.7nm}}$ represents nucleation rate at 1.7 nm in cm^{-3} s^{-1}, T is temperature in K, T_0 is a constant temperature (278 K), [BioOxOrg] and [H_2SO_4] represent the concentrations in molecules per cm^{-3}, k is kinetic factor with a constant value (3.27×10^{-21} cm^6 s^{-1}) (Riccobono et al. 2014). The nucleation rate is also applied with the dimensionless constant B_2 (equals to 0.5) and a temperature dependency $\exp(-(T - T_0)/B_1)$ (equals to 10).

4.2.4 Simulation details

The global and regional models were run from 11 to 18 March 2014, in the Amazonia wet season and covering the days of 5 research flights during GoAmazon2014/5 (Martin et al. 2016; Martin et al. 2017). The global model was run 70 days prior to the start of the regional simulation for the initialisation of the aerosol fields.

Table 4.2: A table of simulations with different anthropogenic emissions and nucleation mechanisms.

	Gas emission	Primary aerosol emission	Biogenic nucleation	InorgOrg nucleation
CTL	✓	✓	✓	✓
offREG			✓	almost off
0.5×emis	✓0.5×	✓0.5×	✓	✓
1.5×emis	✓1.5×	✓1.5×	✓	✓
2×emis	✓2×	✓2×	✓	✓
5×emis	✓5×	✓5×	✓	✓
Prim_emis		✓	✓	
0.25×aero	✓	✓	✓	✓
CTL 1-month	✓	✓	✓	✓
offREG 1-month			✓	almost off

almost off: The InorgOrg nucleation makes use of H_2SO_4, which is an anthropogenic gas for nucleation. When anthropogenic emissions within the domain are set to zero, nucleation from InorgOrg scheme only depends on H_2SO_4 from the global model advection. In this case, the height and domain averaged InorgOrg nucleation rate at 100 m - 1 km in the regional domain is reduced by a factor of 3000 resulting in a nucleation rate that is not strong enough to produce aerosols. Therefore, it is marked as 'almost off'.

Table 4.2 shows the simulations in this study. For all the simulations, the NPF mechanisms were limited to above 100 m altitude so that unrealistic surface nucleation is avoided (Shilling et al. 2018; Wimmer et al. 2018); nucleation above 1 km altitude is disabled so that the model has a better representation of the observed particle number concentration in the CTL simulation which uses default anthropogenic emissions from EDGAR and CMIP6 emission inventories. In the test simulations, switching on nucleation in the upper troposphere always caused overestimations of the observed particle number concentrations by factors of more than 20 in the free

troposphere. Thus, all nucleation above 1 km altitude is switched off. The reason for this large overestimation, which was not seen in Chapter 3, has not been diagnosed. As shown below, the aerosol vertical profile has extremely (and unusually) low concentrations above the boundary layer, which differ substantially from those observed in the dry-wet transition season (Chapter 3). Two explanations may be that precipitation constantly removes aerosol particles in the free troposphere or because of much less biomass burning events during the wet season.

In all simulations, cloud condensation sink is used, as described in Chapter 2.

The default emission set simulation (CTL) uses both anthropogenic gas and primary aerosol emissions and the offREG (off regional) simulation has anthropogenic emissions switched off in the regional domain. The regionally switched off species can be found in Table 4.1, as well as NO, NVOC from anthropogenic sources, BC and OC. Because the InorgOrg nucleation mechanism is strongly controlled by the concentrations of H_2SO_4 and that global transport cannot supply enough H_2SO_4 below 1 km to this region for nucleation, switching off emissions in the regional domain almost disables this nucleation process. All anthropogenic emissions were perturbed by factors of 0.5, 1.5, 2 and 5 in additional simulations to understand the sensitivity of aerosols and cloud properties to the changes. The effects of primary anthropogenic aerosol emissions to the environment can be identified in Prim_emis (primary emission) simulation where only anthropogenic primary aerosol emissions are kept and the InorgOrg nucleation is switched off in the regional domain. The primary aerosol contribution to the total particle concentration and cloud properties can be roughly derived with the equation $100\% \times (\text{Prim\_emis} - \text{offREG})/\text{CTL}$. An extra simulation with the number of total CCN that is passed from UKCA to CASIM (CLoud-AeroSol Interacting Microphysics) aerosol activation process being scaled down by a factor 4 (simulation 0.25×aero) was run to understand whether the environment has a significant response with 75% less aerosols available for activation. As shown below, the 7-day simulations of the six emission scenarios showed an insignificant response of cloud properties to reductions in aerosol emissions, therefore the CTL and offREG simulations were also run for a month so that a longer-term effect for the clouds could be quantified.

4.3 Results

4.3.1 Comparison with observations

Figure 4.2 shows the time series of the observed and modelled particle number concentrations with diameters greater than 3 nm ($N_{D>3nm}$), 10 nm ($N_{D>10nm}$) and 100 nm ($N_{D>100nm}$) on 5 days from 11 to 17 March 2014. As shown in Fig. 4.1, the G-1 aircraft measured particle number concentrations in Manaus pollution plumes and for most of the time flew downwind of the city. Therefore, several peaks in particle number concentrations were observed during the flights. The modelled results in the CTL and offREG simulations are interpolated according to the flight time, coordinates and altitude for comparison with the observations.

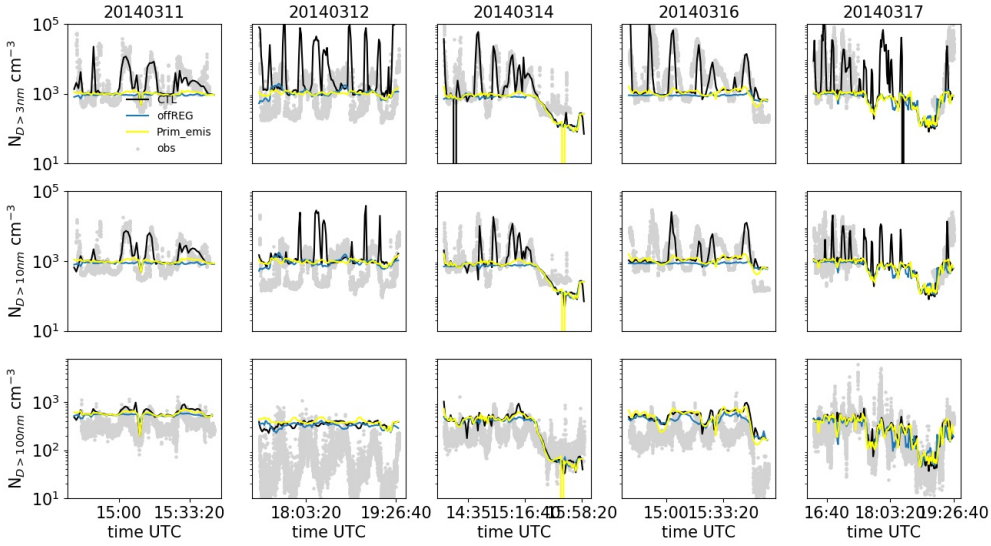

Figure 4.2: Time series of observed (grey dots) and modelled (CTL, offREG and Prim_emis; solid lines) particles number concentrations with diameters greater than 3 nm (upper row), 10 nm (middle row) and 100 nm (lower row) on 11, 12, 14, 16 and 17 March 2014. The observations were measured onboard the G-1 aircraft during GoAmazon2014/5 campaign and model data are interpolated according to the time, coordinates and altitudes of the G-1 flight tracks. Black solid lines are for the CTL simulation, blue lines are for the offREG simulation where anthropogenic emissions are switched off, and yellow lines are for the Prim_emis simulation where anthropogenic gas emissions and the InorgOrg nucleation are switched off in the regional domain.

All the observed particle concentrations ($N_{D>3nm}$, $N_{D>10nm}$ and $N_{D>100nm}$) exhibit strong temporal as well as spatial variations that are related to pollution plumes from Manaus. Among the five days of measurement, 16 and 17 March have the greatest number concentrations for all particle size ranges (around 11000 cm^{-3} for $N_{D>3nm}$, 3200 cm^{-3} for $N_{D>10nm}$, 270 cm^{-3} for

$N_{D>100nm}$ averaged over time) which implies that the downwind air was most polluted on 16 and 17 September and was most distinct from the surrounding environments. The background particles are around 1000 cm^{-3} for $N_{D>3nm}$ and $N_{D>10nm}$, and around 300 cm^{-3} for $N_{D>100nm}$ during the five days. The least polluted day is 12 March when the time averaged particle number concentrations are 1300 cm^{-3} ($N_{D>3nm}$), 900 cm^{-3} ($N_{D>10nm}$), and 75 cm^{-3} ($N_{D>100nm}$), and the range of $N_{D>3nm}$ is more than 8 times smaller than that of the 16 and 17 March. On the other two days (11 and 14 March), the time averaged particle number concentrations are factors of 2-4 greater than 12 March, and are equivalent to factors of around 0.3-0.6 of the particle concentrations on 16 and 17 March for $N_{D>3nm}$ and $N_{D>10nm}$, and factors of 0.9-1.6 for $N_{D>100nm}$.

The interpolated model results in the CTL simulation reproduce most of the observed peak number concentrations for $N_{D>3nm}$ and $N_{D>10nm}$, and the most of the temporal evolution for $N_{D>100nm}$. The modelled particle concentrations of the three size ranges well reproduce the observations on 11, 14, 16, and 17 March 2014, but the particle concentrations are overestimated on 12 March 2014. Of all the five days, the modelled results are the closest to the observations on 11 March, with an averaged underestimation of the observed $N_{D>3nm}$ by -8%; for $N_{D>10nm}$ the mean differences between model and observations are around -3%; the modelled results overestimate $N_{D>100nm}$ by 70%. On 14 and 16 March, compared to the observations the particle number concentrations are generally overestimated by the model, by between 15% and 20% for $N_{D>3nm}$, underestimated by around -25% to -28% for $N_{D>10nm}$, and between 63% and 130% for $N_{D>100nm}$, but overall, the model captures the spatial and temporal variations well in these two days. On 17 March 2014, the observed particles larger than 3 nm and 10 nm are underestimated by around -20 % and -40 %, and are on average overestimated by 10 % for particles larger than 100 nm. The comparisons are worse on 12 March for all three size ranges, with the modelled particle concentrations being factors of 11 ($N_{D>3nm}$), 2 ($N_{D>10nm}$) and 3.6 ($N_{D>100nm}$) too high. This discrepancy is likely to be caused by the residuals of particles from 11 March that have not been scavenged for all 3 size modes on 12 March because the background particle concentrations are around a factor of 3 higher than observed, or because the surface emission in UKCA on 12 March is higher than reality. For the former hypothesis, the precipitation measurement by S-band radar during GoAmazon2014/5 shows that precipitation rate reaches approximately 2.6 mm hr^{-1} on 11 March at around 3.2°S, 60.6°W, and it could

remove aerosol (Fig. 4.3). In the CTL simulation, surface precipitation averaged over the radar domain (approximately 2° by 2° W domain that centres at 3.2° S, 60.6° W) shows precipitation rate at relatively similar magnitude, but whether the modelled rain removed equivalent amount of aerosols remains unknown. The modelled results reproduce most of the observed temporal and spatial variations for $N_{D>100nm}$ during the five days, but with some overestimations. Although the number concentrations of $N_{D>100nm}$ are less associated with NPF, there are still simultaneous peak concentrations of $N_{D>100nm}$, $N_{D>3nm}$ and $N_{D>10nm}$ on most of the days. It indicates the fast NPF and particle growth processes.

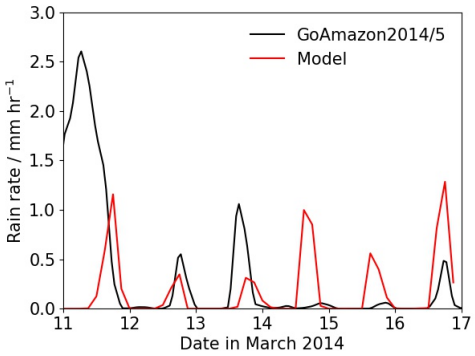

Figure 4.3: Precipitation rate observed by S-band Amazon Protection National System radar at 3.2° S, 60.6° W during GoAmazon2014/5 from 11 to 17 March 2014 (black) and precipitation rate from the model in CTL simulation (red) averaged over the radar domain (approximately 2° by 2° W domain that centres at 3.2° S, 60.6° W).

The model is able to match the temporal and spatial evolution of the observations. Thus, this simulation (CTL) is used as a baseline for the sensitivity test to anthropogenic emissions.

4.3.2 Effects of anthropogenic emissions on aerosol

In this section, the influence of anthropogenic emissions along the G-1 aircraft flight tracks on $N_{D>3nm}$, $N_{D>10nm}$ and $N_{D>100nm}$ particles is investigated. The effects of emissions on aerosol and cloud profiles in the regional domain but only the areas that are affected by pollution are studied. Polluted regions are defined according to the instantaneous column integrated sulfur from H_2SO_4 and SO_2 in the lowest 2 km in the CTL simulation. Polluted, high-sulfur air is defined as having a total sulfur column of 6×10^{-5} g m^{-2}. The column-integrated sulfur is calculated with $\int_{z=0}^{z=2}(1000\rho_z S_z)\,dz$, where z is altitude, ρ_z is air density at a height of z, and S_z denotes sulfur mass mixing ratio obtained from H_2SO_4 and SO_2. The same high-sulfur regions of the CTL simulation are used for the other simulations for consistency (offREG,

0.5×emis, 1.5×emis, 2×emis 5×emis and 0.25×aero), irrespective of the sulfur content in the five simulations. Here, only the data to the west of the red line in the domain are analysed for each simulation (Fig. 4.4) because it represents the area affected by Manaus pollution. The areas to the east of the red line are not included in the following analyses because these regions are not necessarily affected by emissions from Manaus, but are needed as a part of the regional domain in order to allow space for the regional domain boundary conditions to evolve before air masses advect into the the regions of interest. Here, sulfur alone may not be able to mark all the regions that are affected by anthropogenic emission in the domain, but it has the closest relationship to NPF of all the emissions. Figure 4.4 shows example definitions of where the high-sulfur (within the contours) are at 21 UTC on 14 March 2014; most of the high-sulfur regions are around the Amazon river. Although the high-sulfur regions evolve with time, Manaus, Tapauá and other river-side areas (where most of the cities are located) are always the most polluted areas in the regional domain.

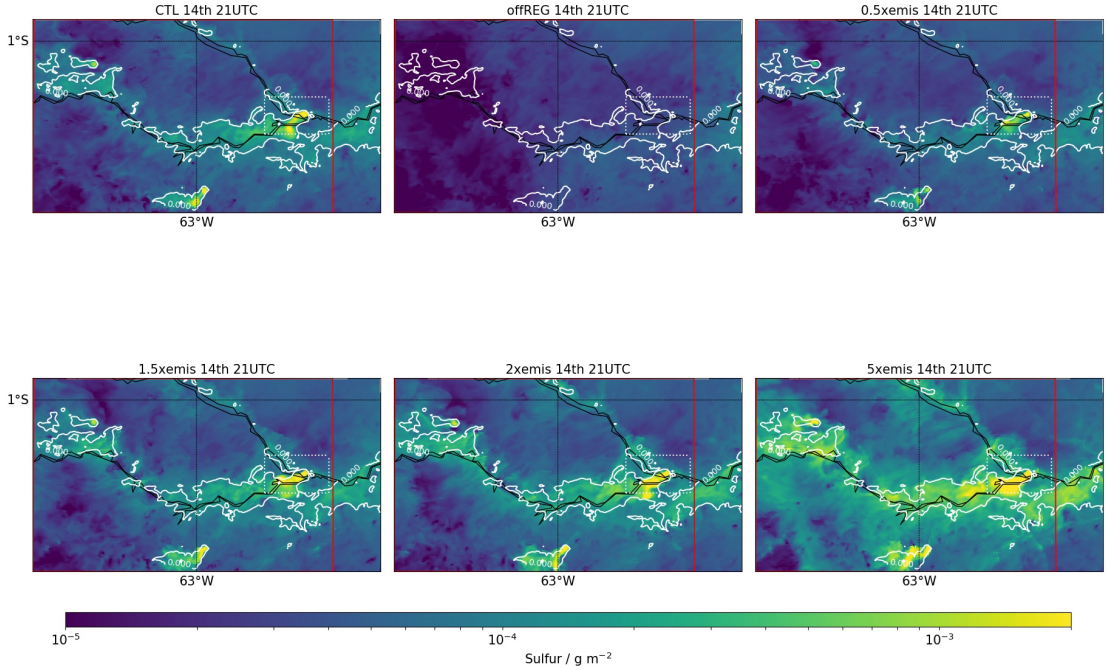

Figure 4.4: Maps of instantaneous column integrated sulfur (g m^{-2}) at 21 UTC on 14 March 2014 in CTL, offREG, 0.5×emis, 1.5×emis, 2×emis and 5×emis simulations. The contours in both maps denote column integrated sulfur equal to 6×10^{-5} g m^{-2} in the CTL simulation. The sulfur content is integrated from surface to 2 km in altitude where most of the pollutants persist. The dotted rectangles mark where the G-1 aircraft flew in March 2014 with the red line marking the eastern edge of that region. For the rest of the chapter, only the region to the west of the red line is analysed.

Figure 4.2 also shows the particle number concentrations along the flight tracks when both

anthropogenic gas and primary aerosol emissions are switched off in the regional domain (offREG simulation) and when anthropogenic gas emission and InorgOrg nucleation are switched off in the regional domain (Prim_emis simulation). In offREG simulation, the temporal and spatial variations of $N_{D>3nm}$ and $N_{D>10nm}$ are very small compared to the concentrations in the CTL simulation. Although $N_{D>100nm}$ in offREG simulations captures the background values, it misses most of the peak values in $N_{D>3nm}$ and $N_{D>10nm}$. The lack of temporal and spatial variability in the offREG simulation indicates that the variability shown in the CTL simulation is caused by emission and NPF in the region, especially for $N_{D>3nm}$ which is reduced by between -70% and -90% and $N_{D>10nm}$ which is reduced by between -50% and -70% during the 5 days compared to the CTL simulation. $N_{D>100nm}$ is least affected (-6% to -20% reduction). Apart from primary anthropogenic aerosol emissions, the response of $N_{D>100nm}$ to anthropogenic emissions are also associated with NPF as well as the subsequent particle growth. Switching off anthropogenic emissions causes the averaged nucleation rates (biogenic and InorgOrg) along the track to decrease by up to a factor of 2.4×10^5 (16 March). On the same day, condensation sink is reduced by a factor of 125 in the offREG simulation, suggesting the significant effects of anthropogenic emission in affecting nucleation. $N_{D>100nm}$ has both increases and reductions in number concentrations when anthropogenic emissions are switched off and the reductions dominate for most of the time. The increases in $N_{D>100nm}$ at certain times may be caused by the suppression of NPF when there are no anthropogenic emissions, which thereby allows more condensable gases for particle growth (Sullivan et al. 2018). The occurrence of both increases and decreases in $N_{D>100nm}$ for CTL vs offREG implies that the effect of anthropogenic emissions in the simulations on CCN is quite variable.

The temporal and spatial variations of $N_{D>3nm}$ and $N_{D>10nm}$ in Prim_emis simulation are similar to offREG simulation (Fig. 4.2). During most of the time, Prim_emis simulation is able to reproduce the $N_{D>100nm}$ while missing some peak values. Compared to offREG simulation, the Prim_emis simulation has a few more overlaps with the CTL for $N_{D>10nm}$ and $N_{D>100nm}$, indicating the contribution of large primary anthropogenic aerosol particles. The missing peak concentrations in Prim_emis show that the discrepancies between Prim_emis and CTL simulation are mainly caused by the anthropogenic emissions induced NPF (InorgOrg mechanism). The contribution of primary aerosols to the environment is less than 3 % for $N_{D>3nm}$, between 1 % and 10 % for $N_{D>10nm}$, and less than 20 % for $N_{D>100nm}$, and the overall it contributes

to around 0.5% of the height-averaged total particle concentrations below 4 km altitude in the polluted regions (Fig. 4.5). Thus, the majority of the changes in concentrations are caused by the combination of precursor gas emission and NPF.

The modelled NPF is shown to be aware of and sensitive to the locations of the plume from urban cities. Consequently, to better understand the response of aerosols and clouds to anthropogenic emissions using the UKCA-CASIM model, it is necessary to amplify the difference in emissions between the offREG, Prim_emis and CTL simulations in the additional simulations (0.5×emis, 1.5×emis, 2×emis, and 5×emis). Here, the effects of anthropogenic emissions on aerosol and cloud properties are analysed by taking the ratios of the changes in aerosol and cloud from the baseline CTL simulation to the changes in anthropogenic emissions. Then, the changes of aerosol and cloud due to each unit increase of anthropogenic emissions are derived. I compare the changes to CTL simulation because it has the default anthropogenic emissions and the particles in the CTL simulation are most close to the real environment.

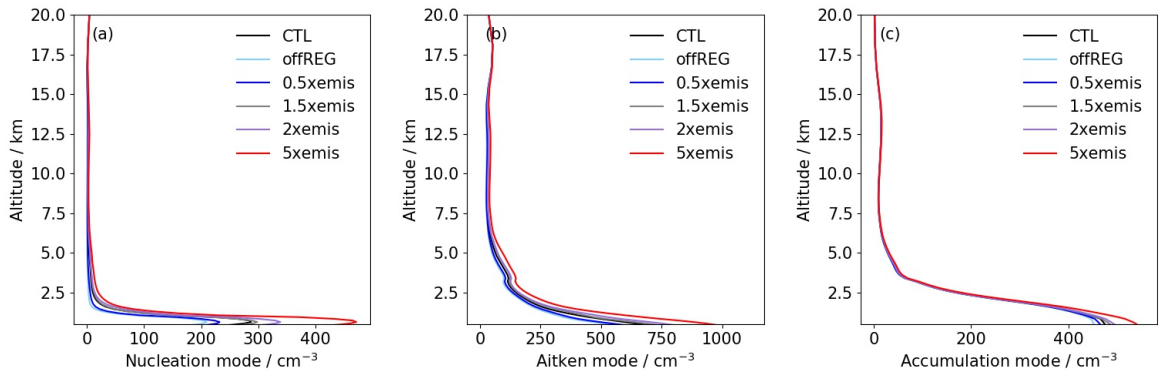

Figure 4.5: Profiles of (a) nucleation, (b) Aitken and (c) accumulation mode aerosol number concentrations, averaged over time and the area of the high-sulfur region in the CTL (black), offREG (light blue), 0.5×emis (blue), 1.5×emis (grey), 2×emis (light purple), and 5×emis (red) simulations. The high-sulfur regions are areas with column integrated sulfur greater than 6×10^{-5} g m^{-2} in the CTL simulation.

Figure 4.5 shows the vertical profiles of aerosol number concentrations averaged over the high-sulfur regions. The concentrations have similar variations with height in all the six simulations. The number concentrations are the greatest below 2 km for all three modes of aerosol in the six simulations. For example, in the CTL simulation the height-averaged concentrations below 2 km are 130 cm^{-3} for nucleation mode, 530 cm^{-3} for Aitken mode, and 430 cm^{-3} for accumulation mode. Above 2 km, the aerosol number concentration quickly falls to very low concentrations at 6 km in altitude and remains at very low concentrations above 6 km in the CTL simulation.

The differences in aerosol number concentrations among the six simulations are evident below around 4 km where aerosols are affected by emissions at the surface and NPF between 100 m - 1 km, and higher anthropogenic emission produces more aerosols. The height-averaged nucleation mode aerosol number concentration below 4 km altitude increases by 29 cm^{-3} (29% of the CTL simulation) for each unit increase in anthropogenic emissions. Similarly, Aitken mode increases by 68 cm^{-3} (16%) and accumulation mode increases by 12 cm^{-3} (4%) for each unit increase in anthropogenic emissions. For the total aerosol number which also includes the insoluble Aitken mode and coarse mode, the increase is around 113 cm^{-3} (13% or by a factor of around 1.1) with anthropogenic emissions.

4.3.3 Effects of anthropogenic emissions on cloud

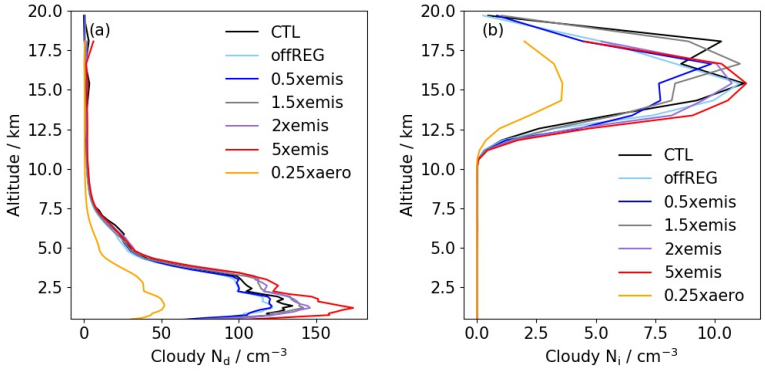

Figure 4.6: Profiles of (a) N_d and (b) N_i, averaged over time and over the cloudy area of the high-sulfur region in the CTL (black), offREG (light blue), 0.5×emis (blue), 1.5×emis (grey), 2×emis (light purple), 5×emis (red), and 0.25×aero (orange) simulations. The high-sulfur regions are areas with column integrated sulfur greater than 6×10^{-5} g m^{-2} in the CTL simulation, and the cloudy areas have total cloud liquid and ice content greater than 0.1 g kg^{-1}.

Figure 4.6 shows the profiles of N_d and N_i (ice number concentration) averaged over time and the cloudy areas in high-sulfur regions. The cloudy areas are defined as grid cells with total cloud water mass greater than 0.1 g kg^{-1} for each simulation. In the CTL simulation, the averaged N_d in cloudy areas increases with height until around 1.3 km where it reaches a maximum of 135 cm^{-3}, then the concentration decreases until around 10 km altitude. N_d in other simulations also has similar vertical variations. Most of the differences that are caused by anthropogenic emissions exist below 4 km and the relative magnitude follows the aerosol concentrations. The height-averaged N_d below 4 km altitude are similar in CTL (95 cm^{-3}), offREG (84 cm^{-3}), 0.5×emis (87 cm^{-3}), 1.5×emis (98 cm^{-3}), and 2×emis (102 cm^{-3}) simulations, and the 5×emis simulation produces 120 cm^{-3} N_d. The greatest change in N_d in the lowest 4 km layer occurs

in 5×emis simulation, with an averaged increase in concentration of 26% relative to the CTL simulation. Concluding from all the six simulations, the time and cloudy domain in high-sulfur regions averaged N_d increases by 9 cm^{-3} (9% of the CTL simulation) for each unit increase in anthropogenic emissions. Below 4 km altitude, the 0.25×aero simulation has an averaged N_d of 36 cm^{-3}, which is a factor of approximately 0.38 of the CTL simulation. This simulation has (36% of the CTL simulation) stronger change in N_d than 5×emis simulation because of the significant change of CCN concentration in 0.25×aero simulation and likely because N_d has a greater response to aerosol reductions than increases in the Amazonia.

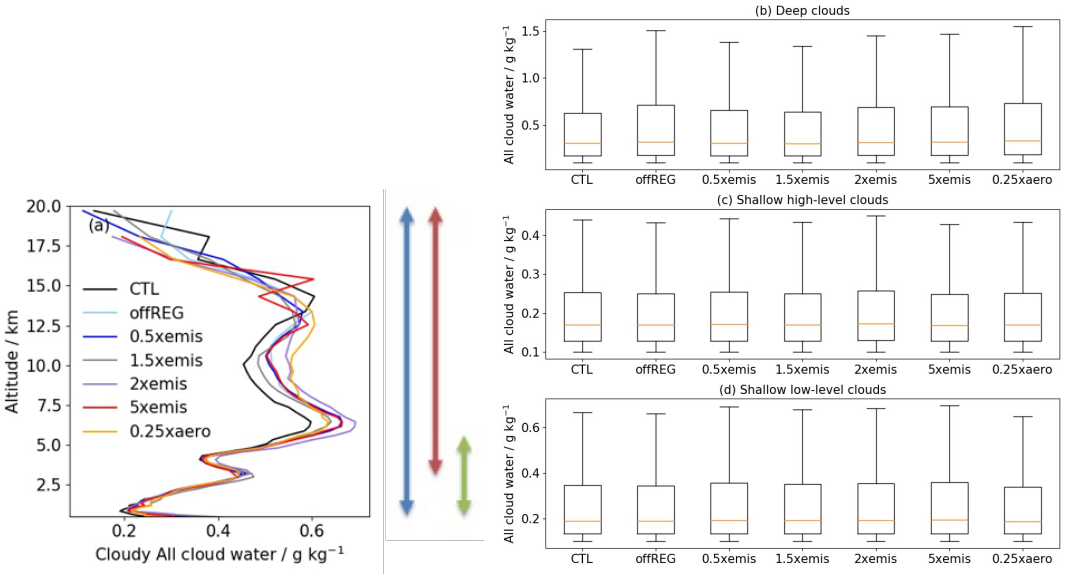

Figure 4.7: Profiles of (a) total cloud water mass mixing ratio (cloud liquid, ice crystal, snow, and graupel), averaged over time and over the cloudy area of the high-sulfur region in the CTL (black), offREG (light blue), 0.5×emis (blue), 1.5×emis (grey), 2×emis (light purple), 5×emis (red) and 0.25×aero (orange) simulations. The high-sulfur regions are areas with column integrated sulfur greater than 6×10^{-5} g m^{-2} in the CTL simulation, and the cloudy areas have total cloud liquid and ice content greater than 0.1 g kg^{-1}. The box plots of total cloud water mass mixing ratios from all the 3-hourly instantaneous output in the high-sulfur regions in five simulations for (b) deep clouds (cloud thickness greater than 3 km), (c) shallow clouds at high altitude (cloud thickness smaller than 3 km and at above 4 km in altitude), and (d) shallow clouds at low altitude (cloud thickness smaller than 3 km and at below 5 km in altitude). The three arrows indicate the vertical extent of the data that are used to identify deep cloud (blue), shallow cloud at high altitude (red), and shallow clouds at low altitude (green).

In-cloud N_i is negligible from surface to around 11 km in altitude, from which height it increases and peaks at around 15 km (11 cm^{-3} in the CTL simulation) and then decreases until 20 km in the seven simulations. Changing the anthropogenic emissions in the regional domain does not cause evident differences in N_i between 10-20 km. Averaged over height between 10-20 km, N_i in the simulations with six emission scenarios have similar values (roughly 6 cm^{-3}) and

the differences are negligible and are likely caused by natural variability. While in 0.25×aero simulation, N_i is on average reduced by a factor of 3 compared to CTL simulation. Therefore, clouds are expected to have a greater response under a clean than polluted environment.

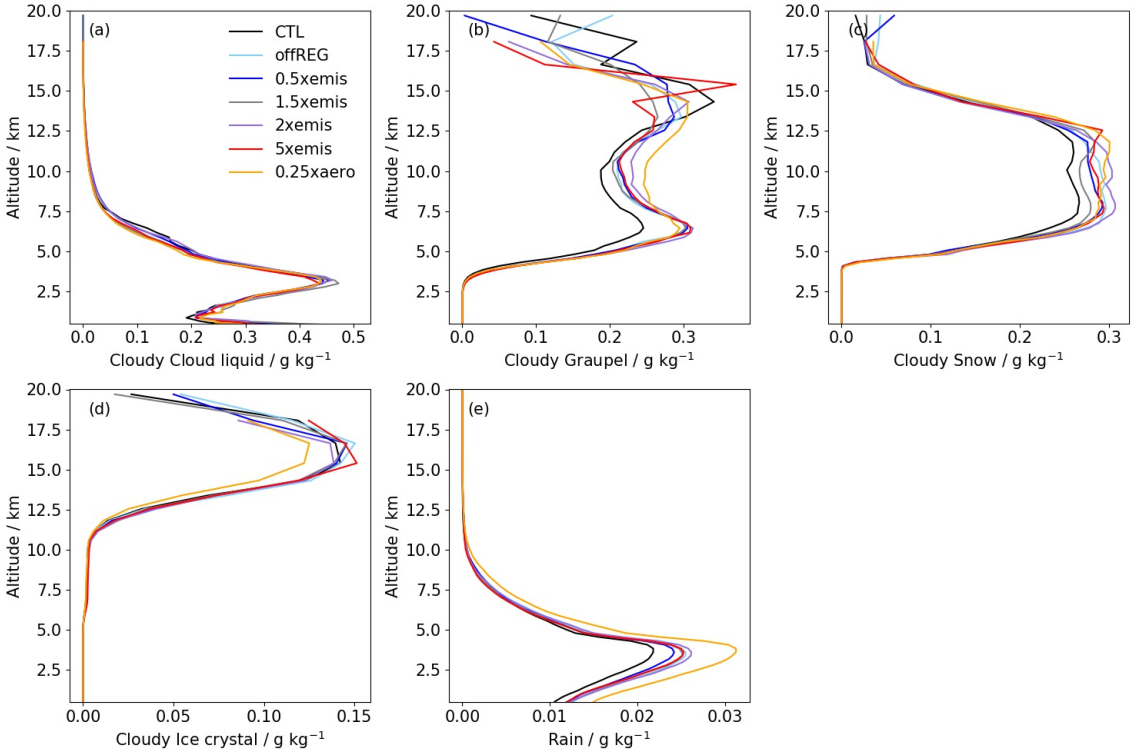

Figure 4.8: Profiles of (a) cloud liquid, (b) graupel, (c) snow and (d) ice crystal mass mixing ratio, averaged over time and over the cloudy area of the high-sulfur region in the CTL (black), offREG (light blue), 0.5×emis (blue), 1.5×emis (grey), 2×emis (light purple), 5×emis (red), and 0.25×aero (orange) simulations. Profiles of (e) rain mass mixing ratio are averaged over time and the area of the high-sulfur region for the seven simulations. The high-sulfur regions are areas with column integrated sulfur greater than 6×10^{-5} g m^{-2} in the CTL simulation, and the cloudy areas have total cloud liquid and ice content greater than 0.1 g kg^{-1}.

The profiles of in-cloud liquid and ice mass mixing ratios averaged over the high-sulfur regions exhibit several peaks at 3 km, 6 km and around 13 km in altitude for the seven simulations (Fig. 4.7.a). The cloud water is liquid phase below 4 km altitude, mixed phase between 4 and 10 km, and ice phase above 10 km altitude (Fig. 4.8). Cloud liquid water mass mixing ratio is similar among the seven simulations and it quickly increases with altitude from 1 to 3 km reaching a maximum (0.46 g kg^{-1}), then it keeps decreasing with height. Some clearer (but still random) differences among the seven simulations are shown for cloud ice mass mixing ratio which exists above about 5 km altitude, allowing the mixed-phase cloud to reach 0.6 g kg^{-1} at around 6 km and cloud ice mass to become 0.61 g kg^{-1} at 14 km altitude. The results show that the variations of cloud ice with height are not affected by changes in anthropogenic emissions by

factors between 0 and 5 within the regional domain, or when CCN concentrations are reduced by a factor of 4.

The box plots (Fig. 4.7.b-d) show the distribution of total cloud liquid and ice mass mixing ratios from all the 3-hourly instantaneous output in the six emission scenarios and 0.25×aero simulation separated into deep clouds (thickness greater than 3 km), shallow clouds (thickness smaller than 3 km) situated below 5 km altitude, and shallow clouds situated above 4 km altitude. All three cloud types have the same cloud water mass mixing ratio for the lower whiskers (minimums of the data) (0.1 g kg^{-1}). For deep clouds, the lower whisker (the edge of the lower 25 % of the data), lower quartile and median values in the seven simulations generally differ by less than 0.03 g kg^{-1}, while the upper quartile values differ by at most 0.08 g kg^{-1} and upper whisker values differ by 0.2 g kg^{-1}. The greatest values for the upper quartile (the edge of the upper 75 % of the data) and upper whisker (maximums of the data) for deep clouds occur in the offREG and 0.25×aero simulations which have the least cloud droplets due to the least number of CCN. For shallow cloud situated at high altitudes, the whisker, quartile and median values of all seven simulations are almost the same, with differences among the simulations to be within 0.02 g kg^{-1}. For shallow clouds situated at low altitudes, the whiskers, quartiles and median values are also similar (differences within 0.04 g kg^{-1}) and simulations with higher cloud droplets number concentrations generally have greater cloud water mass. Overall the box plots show that the occurrence of 'extreme' values is random under varied anthropogenic emissions.

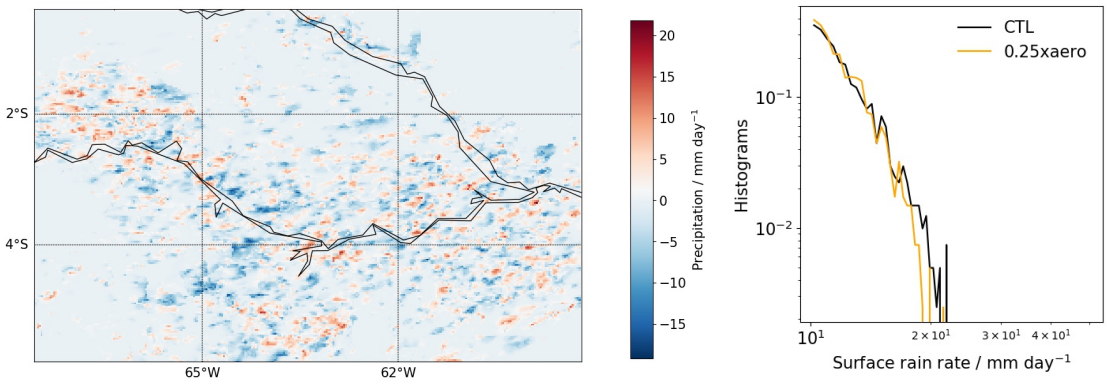

Figure 4.9: The map (left) of the differences between CTL and 0.25×aero simulations for the time averaged surface rain rate in the high-sulfur regions that have appeared at all time between 12 and 18 March 2014. The histograms (right) of surface rain rate in high-sulfur regions in the CTL (black) and 0.25×aero (orange) simulations.

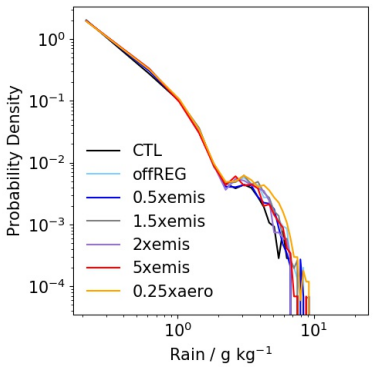

Figure 4.10: The histograms of surface rain mass mixing ratios in high-sulfur regions in the CTL (black), offREG (light blue), 0.5×emis (blue), 1.5×emis (grey), 2×emis (light purple), 5×emis (red), and 0.25×aero (orange) simulations. The high-sulfur regions are areas with column integrated sulfur greater than 6×10^{-5} g m^{-2} in the CTL simulation.

Figure 4.9 shows a map of the time-averaged differences in surface rain rate between the CTL and 0.25×aero simulations for the simulation period (12-18 March 2014) and the histograms of the surface rain rate. The map shows all the locations that rain has ever occurred in high-sulfur regions during the 7-day simulation. The changes in surface rain mostly occur close to the Amazon river where cities are located. Averaged over time, the surface rain in high-sulfur regions is increased by 0.16 mm day^{-1} (4% of the CTL simulation) when the number of CCN to enter CASIM activation by a factor of 4 (0.25×aero minus CTL). The changes in rain rate is twice as much as the changes in offREG from CTL simulation. The histograms of surface rain rate do not show strong differences between CTL and 0.25×aero simulations, except for the upper end of the distribution. Similarly, the histograms of surface rain mass mixing ratios for all the seven simulations (Fig. 4.10) show that the changes are only clear for the maximum values (greater than 2 g kg^{-1}), while light rain is rarely affected. Neither do the histograms show clear relationship between the level of anthropogenic emissions nor surface rain mass mixing ratio in the six anthropogenic emission simulations, except for 0.25×aero simulation which has relatively a greater rain mass mixing ratio. However, the profiles of rain mass mixing ratio averaged over time and the high-sulfur regions show that 0.25×aero simulation exhibits the statistically significant changes (p value is 0.04) that are twice as much as those in other emission scenarios from the baseline CTL simulation (Fig. 4.8). Overall, reducing the total CCN concentration (0.25×aero) produces the greatest changes in rain, implying the suppression of rain in the six simulations with varied emissions, and that the role of anthropogenic emissions is limited in influencing rain.

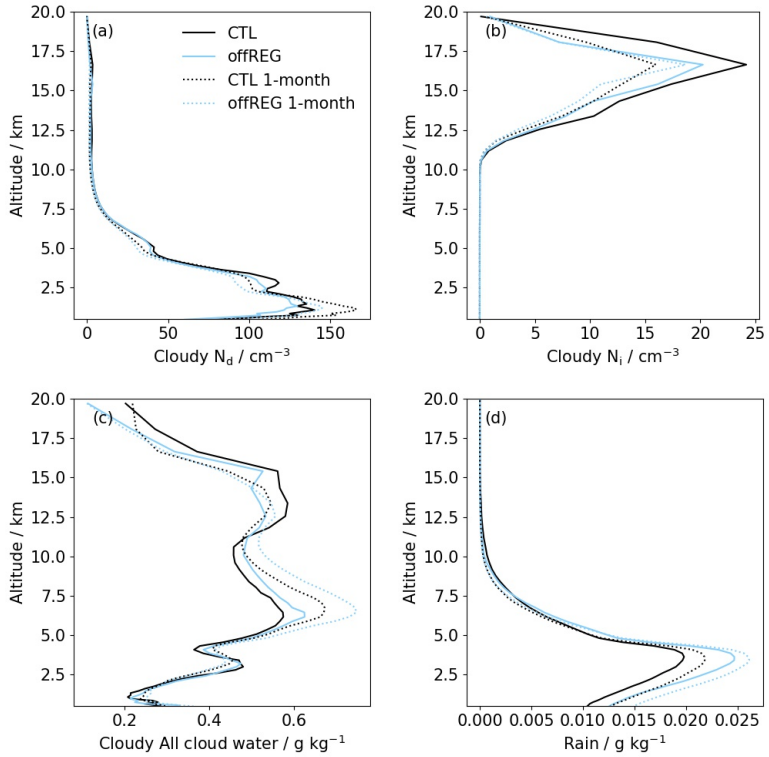

Figure 4.11: Profiles of (a) CDNC, (b) INC and (c) total cloud water mass mixing ratio, averaged over time and over the cloudy area of the high-sulfur region in the CTL (solid black) and offREG (solid light blue) simulations that are run for 7 days (solid), and two extra simulations that are run for 1 month, CTL 1-month (dotted black), and offREG 1-month (dotted light blue). Profiles of rain mass mixing ratio (d) are averaged over time and the area of the high-sulfur region for the four simulations. Here, the high-sulfur regions are areas with column integrated sulfur greater than 6×10^{-5} g m^{-2} in the CTL simulation, and the cloudy areas have total cloud liquid and ice content greater than 0.1 g kg^{-1}.

The differences in cloud properties between the simulations with perturbed anthropogenic emissions are very small and not significant over the 7 day simulations. Two 1-month CTL and offREG simulations were therefore run from 11 March to 10 April 2014 to investigate whether the changes in cloud liquid and ice water mass mixing ratio and rain are different for a longer time (Fig. 4.11). The results are similar to the six 1-week simulations that N_d, ice and liquid cloud mass mixing ratio and rain mass mixing ratio are not significantly different between CTL 1-month and offREG 1-month simulations. For example, the differences of N_d between the CTL 1-month and offREG 1-month simulations are 10 cm^{-3} (10% of the CTL 1-month simulation) when averaged over time, height below 10 km altitude, and cloudy area of the high-sulfur regions. The mean difference for N_i above 10 km altitude is -0.2 cm^{-3} (-31%) and total cloud mass mixing ratio at all altitudes is -0.03 g kg^{-1} (-7.2%). Rain mass mixing ratio differences are 0.002 g kg^{-1} (16%) below 10 km altitude in the high-sulfur regions.

4.4 Discussion and conclusions

The influences of anthropogenic emissions on aerosol particles, clouds and rain in central Amazonia are investigated with a regional model nested within a global atmosphere-only model, and the regional domain is perturbed with several anthropogenic emission scenarios relative to a control simulation. The baseline simulation (CTL) with high-resolution emissions compared well with the observations in the areas where G-1 aircraft flew (mostly below 2 km), and the averaged observation-model differences in the regional domain of all the 5 days are between -8% and a factor of 11 for the 3 nm ($N_{D>3nm}$), -40% to a factor of 2 ($N_{D>10nm}$) and 11% to a factor of 3.6 ($N_{D>100nm}$) particles (Martin et al. 2016; Martin et al. 2017). Upper tropospheric nucleation, along with subsequent downward transport, has been proven to be important for determining low-level particle concentrations (Clarke et al. 1998; Clarke et al. 1999a; Clarke et al. 1999b; Clarke and Kapustin 2002; Pierce and Adams 2007; Merikanto et al. 2009; Wang and Penner 2009; Weigel et al. 2011; Wang et al. 2016; Williamson et al. 2019), and it is important for Amazonia during the dry season (Andreae et al. 2018). However, in the test simulations, switching on upper tropospheric nucleation caused an overestimation of particle concentrations compared to the observations which are available mostly below 2 km altitude and occasionally at 2-6 km altitude. Because there are not enough observations to identify or evaluate the strength of new particle formation in the free and upper troposphere during the wet season, nucleation above 1 km is disabled to achieve consistency between the model and observations in March 2014.

Switching off anthropogenic emissions in the regional domain (CTL to offREG simulation) causes reductions of aerosol number concentrations along the flight track by -70% to -90% of the observed $N_{D>3nm}$, -50% to -70% for $N_{D>10nm}$, and reductions of up to -20% for $N_{D>100nm}$ particles. The reduced aerosols involve both primary and nucleated particles with the latter being the dominant source of the changes. Primary aerosol has very small contribution to the smallest particles ($N_{D>3nm}$) and has moderate contributions to $N_{D>10nm}$ and $N_{D>100nm}$, but overall only contributes to around 0.5% of the total particle concentrations in the polluted regions. In this study, both the pure biogenic nucleation mechanism and the nucleation mechanism that additionally uses H_2SO_4 (InorgOrg) create new particles. The simulations show that it is mainly the InorgOrg nucleation rate that responds to changes in anthropogenic emissions (SO_2 that forms H_2SO_4) at lower altitudes. The InorgOrg nucleation mechanism is therefore

the more important factor in controlling the particle concentration variations along the flight tracks. The enhancement of particle number concentrations in Amazonia due to anthropogenic emissions was also found in Shrivastava et al. (2019) and Zhao et al. (2021).

To quantify the effects of anthropogenic emissions, I focused on the regions that are strongly affected by anthropogenic emissions in the regional domain (termed high-sulfur regions) defined as an instantaneous column-integrated sulfur column (from H_2SO_4 and SO_2) below 2 km altitude that exceeds than 6×10^{-5} g m^{-2} in the CTL simulation. Then, the changes in aerosol, cloud and rain properties among the simulations in the high-sulfur regions are compared. The high-sulfur regions are dependent on the time and intensity of emissions as well as the wind fields.

For each unit increase in anthropogenic emissions in the regional domain (e.g. from CTL to 2×emis), the equivalent total aerosol number concentrations in the high-sulfur region increase by approximately 13% averaged over time. The positive relationship between aerosol and anthropogenic emissions has also been found from an observational study in which days of clean and polluted air in Amazonia were compared (Glicker et al. 2019) and are found in the modelling studies (Shrivastava et al. 2019; Zhao et al. 2021).

In the lowest 4 km altitude, the cloudy N_d increases by 9% for each unit increase of anthropogenic emissions. Higher anthropogenic emissions result in more cloud droplets because greater aerosol concentrations can produce more CCN which subsequently form cloud droplets (Polonik et al. 2020; Pöhlker et al. 2021). Reducing the aerosol concentration causes a reduction of N_d by a factor of 2 in the 0.25×aero simulation compared with the CTL simulation. For ice particle number concentrations (N_i), reductions are only found in 0.25×aero simulation which is caused by a smaller N_d, which allows fewer droplets to freeze, while the rest of the simulations have similar N_i because of similar N_d. The correlation between N_i and N_d in the results is consistent with previous studies that have shown that ice nucleation is affected by cloud droplet concentrations (Fan et al. 2013; Herbert et al. 2015; Grabowski and Morrison 2020).

The simulations explored how changes in aerosol affect cloud and rain water mass mixing ratios. The responses of total cloud water and rain mass mixing ratios are not statistically different among the various perturbation simulations. The results are not too different when the CTL and offREG simulations are run for three more weeks. Cloud droplets should be much smaller

in size under higher N_d conditions in high-sulfur regions making clouds less likely to rain or delaying the onset of rain (Albrecht 1989; Ackerman et al. 2004; Kawamoto 2006; Xue and Feingold 2006; Hill et al. 2008; Xue et al. 2008), which may subsequently lead to increases in cloud water content. However, no such clear and systematic increases were found in cloud liquid water mass mixing ratio or reductions in precipitation in the six emission scenarios (offREG, 0.5×emis, CTL, 1.5×emis, 2×emis, and 5×emis). It can be explained by the complex processes of aerosol-deep convection interactions. Connolly et al. (2013) stated that aerosols affected deep convective clouds in an non-linear way which caused contrasting changes for cloud and rain. Similar complexity has been addressed by Ekman et al. (2007) and Heever and Cotton (2007). Compared to idealised simulations, Dagan et al. (2022) showed that changes in specific humidity due to aerosol were much smaller when the models are constrained by realistic large-scale forcing for both shallow and deep convective clouds. The strength of large-scale forcings also affects the response of convective clouds to aerosol changes (Kipling et al. 2020). In the 0.25×aero simulation, the liquid cloud mass mixing ratios averaged over the cloudy areas of the high-sulfur regions are similar to the CTL simulation, indicating insensitive cloud water content to a significant reduction of CCN concentration.

For surface rain, the results show that the frequencies of occurrence among the six emission scenarios are very similar for surface rain rate and are similar when rain mass mixing ratios are smaller than 2 g kg^{-1} but vary in a manner that is inconsistent with the emission changes when the rain is heavier. This similarity in frequencies and no correlation to emissions for heavy rain suggest that the changes to rain induced by changes in anthropogenic emissions are negligible in the six simulations (offREG, 0.5×emis, CTL, 1.5×emis, 2×emis, and 5×emis) because other environmental factors such as atmospheric conditions have stronger influences on clouds. Gonçalves et al. (2015) used radar data and found that atmospheric instability has a significant influence on how aerosol particles affect cloud and rain in Amazonia. It has also been shown that other factors such as wind shear, cloud structure and air humidity may have a large influence on aerosols to alter precipitation (Khain et al. 2008).

In contrast, reducing the concentrations of aerosol by a factor of 4 in the activation process (0.25×aero simulation) produces at least a factor of 2 greater changes in N_d and N_i than the rest of the emission scenarios from the baseline CTL simulation. It increases the averaged rain rate by around 4% of the CTL simulation in the high-sulfur regions, although the histograms of

rain rate do not show significant differences between CTL and 0.25×aero simulation. The much greater response implies that the perturbations to aerosol and N_d are not large enough in the six anthropogenic emission scenarios to trigger significant changes, and therefore the differences in the simulations were caused by natural variability. The results also show significant changes to the domain- and time-averaged profiles of rain mass mixing ratio in the polluted regions because the reductions of N_d are large enough in this extremely low-aerosol condition, while the other extreme scenario, 5×emis does not show such effects, even though it has around 26% more N_d than in CTL. The increase in rain mass mixing indicates the suppression of rain in CTL than in 0.25×aero simulation due to greater aerosol concentrations. Therefore, it is likely that rain has already been suppressed as much as it can be or because a 26% increase is too small to significantly affect clouds. The latter could suggest that, in this study, the changes in anthropogenic emissions in the regional domain are not large enough to cause effective perturbations to N_d and thus, the clouds and rain are not significantly affected.

Review studies (Rosenfeld et al. 2008; Tao et al. 2012; Fan et al. 2016) have highlighted more complex potential relationships among aerosol, clouds, and precipitation, and similar messages have been conveyed by some modelling studies although the focus was not on the environment in Amazonia (Seifert et al. 2012; Fan et al. 2016; Alizadeh-Choobari 2018; Barthlott et al. 2022; Furtado and Field 2022). For example, Alizadeh-Choobari (2018) investigated mid-latitude cloud systems and pointed out that aerosols could cause a redistribution of rain and that the response of rain to aerosol loadings depended on rain intensity. Also for mid-latitude clouds, Barthlott et al. (2022) used the ICON (Icosahedral Nonhydrostatic) model and found that the microphysical effects of higher CCN caused narrower cloud droplet distributions and reduced rain water content. However, using the COSMO (Consortium for Small-scale Modeling) weather forecast model, Seifert et al. (2012) found that aerosols had a negligible effect on surface precipitation over Germany. Over the Asia monsoon region, the changes in clouds caused by aerosols were also found to be complex (Furtado and Field 2022).

Overall, the relationships between anthropgoenic emission, aerosol, cloud and rain are complex and no clear correlations were found for changes in cloud liquid water, cloud ice water or rain to any changes in anthropogenic emissions. The insensitivity is caused by the already polluted environment and the small perturbations of N_d as a result of small changes in aerosols, because distinct responses of clouds were found when the number of aerosols were reduced by a factor

of 4 and the subsequent change in N_d is a factor of 2. It means that clouds as well as rain will be significantly changed if the cloud droplet concentrations are significantly affected.

The limitation of this study lies in the missing upper tropospheric NPF mechanism and missing aerosol interactive heterogeneous ice nucleation microphysics. NPF is disabled outside of the layer between 100 m and 1 km in altitude so that the regional model has a better representation of the observed aerosol particle concentrations. The compromise inhibits the descent of newly formed aerosols from the upper troposphere and their possible interactions with deep convection in the free and upper troposphere (Ekman et al. 2004; Yin et al. 2005; Fan et al. 2018). Lacking the aerosol-dependent heterogeneous ice nucleation causes the ice water content changes to be not directly related to aerosol concentration. Thus, this study may not fully represent response of cloud to changes in aerosol. It is also recommended that future studies can focus on the response of a single cloud to anthropogenic emissions in order to better understand the physical processes of the affected cloud, similar to the study of Miltenberger et al. (2018b) which developed an ensemble to evaluate the response of cloud properties. Nevertheless, this study provides new insights of small effects of anthropogenic emissions and NPF to clouds and rain.

Chapter 5

Effects of model resolution on non-linear biogenic new particle formation in Amazonia

5.1 Introduction

Observations found strong new particle formation (NPF) in the upper troposphere (UT) and global modelling studies have proved that the newly-formed particles are important sources for aerosol particles in the boundary layer (Merikanto et al. 2009; Clarke et al. 1998; Clarke et al. 1999a; Clarke et al. 1999b; Clarke and Kapustin 2002; Weigel et al. 2011; Williamson et al. 2019). NPF is affected by the intercorrelated factors which include gas precursor volatility, concentrations, condensation sink, and the surrounding environment. In Amazonia, NPF that involves biogenic sources is generally supported by deep convection which transports insoluble gas precursors (e.g. monoterpene) from the surface to the UT, then their oxidation products can nucleate (Thornton et al. 1997; Twohy et al. 2002; Kulmala et al. 2006; Andreae et al. 2018). The concentrations of the oxidised BVOCs are used to derive nucleation rate. Apart from condensation sink from aerosol particles, nucleation is also suppressed by cloud hydrometeors which have relatively larger surface areas than particles, and thus, suppresses nucleation rate by generating a condensation sink that allows gases to condense on existing surfaces rather than form new particles (Kulmala et al. 2001b; Kulmala et al. 2001a; Dal Maso et al. 2002; Kazil et al. 2011). Deep convection is found to perturb the temperature fields and moisture in

the UT (Sassi et al. 2001; Johnston et al. 2018) which affect the efficiency of NPF (Zhao et al. 2020; Simon et al. 2020).

NPF supported by deep convection occurs in many tropical regions (Andreae et al. 2018; Williamson et al. 2019) and has a large-scale effect on CCN. It is therefore important to understand how well this process is simulated by a large-scale (global) model compared to a much higher resolution regional model that explicitly resolves convection and the cloud-scale processes, including gas transport and removal. The global model used in this thesis has a coarse resolution that is much larger than cloud scales, and it uses a parameterised convection scheme (Fritsch and Chappell 1980; Gregory and Rowntree 1990; Stratton et al. 2009; Derbyshire et al. 2011; Walters et al. 2019), which simplifies the sub-grid transport processes. Even though sub-grid parameterisation produces approximations for the 'transported' gas as well as for convection, rain, cloud fraction etc., the spatial variability within each global model grid box (e.g. 100 km) is not fully represented. This is because the global model uses cloud, rain, particle concentrations and gas concentrations for each grid box, which creates a homogeneous region, while in reality the grid box is representing several unresolved cloud systems that vary within each grid box. Gas fields that are significantly affected by convective transport may not be correctly represented by global model approximations.

The high spatial variability of trace gases and aerosols has been demonstrated by observations of black carbon which has a spatial scale of around 85-155 km (Weigum et al. 2012), approximately the resolution of a global climate model can capture. WRF-Chem model results showed that sub-grid variability of the 75 km resolution is most significant near the sources of the gases and may not be well represented by 75 km grid spacing (Qian et al. 2010). Effects of resolution have been investigated in the modelling study of Weigum et al. (2016). The results showed that 80 km resolution WRF-Chem simulations can cause large discrepancies in aerosol optical depth and CCN concentrations compared to 10 km resolution simulations, via differences in aerosol and gas processes (Weigum et al. 2016). The study also pointed out that convective transport exaggerated the discrepancies in gas and aerosol concentrations (Weigum et al. 2016), indicating the potential effects of deep convection in enhancing spatial variability. Therefore, missing the sub-grid variability may result in incorrect gas and aerosol fields which will subsequently affect nucleation rates because nucleation is a non-linear process, eventually affecting aerosol radiative forcing (Gustafson Jr. et al. 2011).

The chemical lifetime of gases may partly determine whether the concentrations vary greatly within an area equivalent to a coarse global model grid box that is perturbed by clouds. The chemical lifetime represents the time for the species to be removed (Seinfeld and Pandis 2012). The key consideration is the chemical lifetime versus the rate of creation of concentration gradients caused by convective transport and mixing. In Amazonian UT, gases such as SO_2 usually have relatively long chemical lifetimes (more than 1 day) and the concentrations within a region will therefore mainly depend on long-range transport, meaning that the concentrations may quickly return to equilibrium after being perturbed. However, monoterpene, which is used as a NPF precursor gas in the UKCA model (United Kingdom Chemistry and Aerosol model), usually has chemical lifetime of less than a few hours against oxidation (less than 10 hours) (Yáñez-Serrano et al. 2018), which is a similar timescale of deep convective transport and mixing. In reality, monoterpene represents several biogenic terpene species (α-pinene, β-pinene, Limonene etc.) with different chemical lifetimes. In the UKCA nucleation process, monoterpenes are treated similar to α-pinene based on the results from CLOUD experiments (Kirkby et al. 2016) and model parameterisation (Gordon et al. 2016), thus, 10 hours is a rough estimate according to the lifetime of α-pinene (Yáñez-Serrano et al. 2018). Therefore, the spatial distributions of short-lived monoterpene concentrations over a region will be significantly affected by deep convection, because they may not live long enough to be evenly distributed over a region, or reach the regions of low condensation sink, before being oxidised. A short lifetime also affects whether biogenic vapours can be efficiently transported by deep convection upward (Li et al. 2017), and partly affects the amount of monoterpenes to eventually reach the upper troposphere. Because NPF is non-linear to monoterpene concentrations, and high spatial variability of the short-lived gas precursor (monoterpene) caused by deep convection, NPF rates are likely to be spatially non-linear due to insufficient mixing, and thus may not be well represented by coarse resolutions. Whether NPF rates are sensitive to the precursor gas (monoterpene) lifetime needs to be understood.

To understand how coarse resolutions in the global models may affect the spatially non-linear NPF, this chapter uses output from high-resolution regional model simulations and applies averaging to imitate the the lower resolution of a global model, and investigate how nucleation rate changes. The averaging method may not fully represent processes in the global model, but is a simplified step that resembles some of the deficiencies of a global model. The benefit

of comparing high-resolution results and the averaged results is that only the effect of spatial resolution of the chemical fields is tested while the other factors including convection, cloud microphysics, model time step, resolutions of the emissions and regional model boundary conditions that all affect the spatial distribution of monoterpene are kept under control. Questions for this chapter are addressed as follows:

(1) How are nucleation rates affected by averaging the input variables?

(2) What are the causes of the changes in nucleation rates by averaging?

(3) How will monoterpene oxidation rate affect the spatially non-linear nucleation rate?

5.2 Methods

5.2.1 Global and regional model configurations

This chapter uses the same model configuration in Chapter 4, which includes a nested regional model in a global model based on Unified Model version 11.6 with GA7.1 (Global Atmosphere v7.1). Other details can be found in Chapter 2. The global model resolution is N96 (135 km) with 85 vertical levels up to 80 km in altitude. The regional domain is centred at (3.1° S, 62.7° W) in central Amazonia at 3 km resolution horizontally. The region covers around 1200 km in the east to west direction and around 700 km in the north to south direction. There are 70 vertical model levels with the highest altitude at 40 km and the lowest 64 levels cover the vertical extent from the surface to 20 km in altitude, mainly where cloud and aerosol interact. The regional model uses explicit convection and CASIM microphysics (Shipway and Hill 2012; Hill et al. 2015; Grosvenor et al. 2017; Miltenberger et al. 2018a; Gordon et al. 2020; Field et al. 2023). Details of the convection, cloud microphysics, aerosol microphysics in UKCA and the coupling settings are described in Chapter 2.

UKCA uses monthly mean emissions for gases and aerosols. CMIP6 emission inventories provide CH_4, and anthropogenic BC, OC and SO_2 for the year 2014 (Eyring et al. 2016; Walters et al. 2019). Monoterpene, isoprene and natural SO_2 are obtained from CMIP5 inventories for the year 2000. The marine source of DMS has been parameterised based on Lana et al. (2011) and the land source is biomass burning (Werf et al. 2006; Lamarque et al. 2010; Granier et al. 2011; Diehl et al. 2012). The emitted CH_4 from biomass burning data have been generated by the JULES (Joint UK Land Environment Simulator) model (Mangeon et al. 2016; Walters et al.

2019). BC and OC are from biofuel, biomass burning and fossil fuel burning events (Marle et al. 2017; Hoesly et al. 2018). Monoterpene and isoprene are obtained from monthly averaged emission inventories that include vegetation (Guenther et al. 1995; Pacifico et al. 2012). Natural and anthropogenic SO_2 comes from volcanic eruption, biomass burning, biofuel and fossil fuel burning (Andres and Kasgnoc 1998; Stier et al. 2005; Lamarque et al. 2010; Hoesly et al. 2018).

The same coupled chemistry scheme (StratTrop) is used as introduced in Chapter 4.

5.2.2 New particle formation

In this chapter, the biogenic nucleation mechanism introduced in Chapter 2 is used for NPF in UKCA. Similar to Chapter 3, NPF only occurs above 100 m altitude to prevent unrealistic boundary layer nucleation. The parameterisation produces new particles at 3 nm in diameter with oxidised organic gas molecules (highly-oxygenated molecules, HOMs) (Kirkby et al. 2016).

The parameterisation of biogenic nucleation in UKCA allows HOMs to be oxidised from monoterpenes by OH and O_3 (Gordon et al. 2016), but monoterpenes are first oxidised to SecOrg by OH, O_3 and NO_3, then the rest of the monoterpene in the environment is used to derive HOM concentrations as has been showed in Fig. 2.1. The concentration of HOMs is derived with Eq. 5.1 based on the study of Gordon et al. (2016).

$$[\mathrm{HOM}] = (1.2\% \times [\mathrm{OH}] \times [\mathrm{MT}] \times \mathrm{k_1} + 2.9\% \times [\mathrm{O_3}] \times [\mathrm{MT}] \times \mathrm{k_2})/\mathrm{CS1}, \tag{5.1}$$

where [HOM] is the concentrations of pure biogenic nucleation gas in molec cm^{-3}, [OH] and $[O_3]$ are the concentrations of the oxidants, OH and O_3, in molec cm^{-3}, [MT] represents the concentrations of monoterpene in molec cm^{-3}, T is temperature in K, and CS1 is condensation sink in s^{-1}. The constant 1.2 % represents that yields of HOM are 1.2% when α-pinenes are oxidised by OH, 2.9 % is the yields of HOM when α-pinenes are oxidised by O_3, k_1 and k_2 are the rate constants in cm^3 $molec^{-1}$ s^{-1} taken from Gordon et al. (2016), which was based on CLOUD chamber experiments. k_1 is equal to 1.2×10^{-11} multiplied by a dimensionless temperature dependence $\exp(440/\mathrm{T})$. k_2 is 8.05×10^{-16} multiplied by a dimensionless temperature dependence $\exp(-640/\mathrm{T})$, As α-pinene is a subset of monoterpene (Yáñez-Serrano et al. 2018), monoterpene is used as α-pinene in UKCA when producing [HOM].

Equation 5.2 is the same as in Chapter 2 (Eq. 2.1) to derive nucleation rate at 1.7 nm diameter

(Gordon et al. 2016).

$$J_{Bio_{1.7nm}} = \exp(-(T - T_0)/B_1) \times (A_1 \times ([HOM]/B_2)^{A_2 + \frac{A_5}{[HOM]/10^7}} + [Ion] \times A_3 \times ([HOM]/B_2)^{A_4 + \frac{A_5}{[HOM]/B_2}}), \quad (5.2)$$

where $J_{Bio_{1.7nm}}$ is the NPF rate at 1.7 nm in cm^{-3} s^{-1}, T is the temperature in K, T_0 is 278 K, A_{1-5}, B_1 (equals to 10) and B_2 (equals to 10^7) are constant parameters, [Ion] is the assumed constant ion concentrations (400 cm^{-3}) (Gordon et al. 2016). Both neutral and ion-induced rates are multiplied with a dimensionless temperature dependency $\exp(-(T-T_0)/B_1))$ (Gordon et al. 2016; Simon et al. 2020).

Then, the nucleation rate at 3 nm diameter (Eq. 5.3) is parameterised according to Kerminen and Kulmala (2002) equation.

$$J_{Bio_{3nm}} = J_{Bio_{1.7nm}} \times \exp(\gamma \times ({d_1}^{-1} - {d_2}^{-1}) \times CS2/GR, \quad (5.3)$$

where $J_{Bio_{3nm}}$ is the nucleation rate at 3 nm in cm^{-3} s^{-1}, γ is a constant factor (0.23 nm^2 m^2 s^{-1}), d_1 and d_2 are particle diameters in nm, CS2 is the condensation sink in m^{-2}, and GR is growth rate in m s^{-1}, and GR is derived with $[H_2SO_4]$ and H_2SO_4 concentrations (molec cm^{-3}). CS1 and CS2 are both condensation sink but in different units ($CS1 = 4\pi D_v \times CS2$, D_v is the diffusion coefficient).

The equations above show that NPF rate at 3 nm diameter is determined by concentrations of the intercorrelated gases, strength of condensation sink and temperature ([monoterpene], [OH], $[O_3]$, $[H_2SO_4]$, CS1, CS2, and T), and NPF rate is a non-linear function to the variations of these variables. Affected by deep convection, the spatial homogeneity of these input variables may contribute to extra non-linearity for NPF rate.

5.2.3 Simulation details

The global and regional models were run from 16 to 18 September 2014. The global model ran a spin-up from 1 to 15 September 2014 in order to initialise the aerosol fields.

Two simulations with different oxidation rates of monoterpene are used in this chapter, BioEmCCS (faster oxidation) and Bio0.1OxEmCCS (slower oxidation). The biogenic nucleation mechanism in Bio0.1OxEmCCS simulation is the same as BioOxEmCCS simulation in Chapter 3, but

Bio0.1OxEmCCS simulation is based on coupled chemistry. In Bio0.1OxEmCCS simulation, oxidation rates of monoterpenes (oxidised by OH, O_3 and NO_3) are reduced by a factor of 10 (slower), and monoterpene emission rate is increased by a factor of 10. Reducing the oxidation rate allows monoterpene to stay in the upper troposphere for longer than 12 hours. The simulation BioEmCCS used default (faster) monoterpene oxidation rate in UKCA and increased monoterpene emission rate by a factor of 10. With varied oxidation rates, the response of NPF rate at 3 nm diameter to averaged fields can be investigated under different monoterpene lifetimes.

The purpose of increasing monoterpene emission rates by a factor of 10 in both simulations is to allow UKCA to generate at least some moderate nucleation rates in the UT. Chapter 3 has shown that very few particles were produced with default monoterpene emission and oxidation rate. Therefore, to enable nucleation to occur in the UT, monoterpene emission rate is increased by a factor of 10 in both simulations.

Cloud condensation sink is used in both simulations, as described in Chapter 2.

5.2.4 Methods for analyses

Degraded resolution and offline nucleation rate

Based on the 3 km resolution results from the regional model, this chapter uses three additional degraded resolutions (30 km, 60 km, and 120 km) to calculate nucleation rate at 3 nm diameter offline. The 3 km, 400 by 240 regional model domain is split into 40 by 24 for 30 km resolution, 20 by 12 for 60 km resolution, and 10 by 6 for 120 km resolution (Table 5.1). Each of the cells at the first degraded resolution (30 km) contains 100 (10 by 10) original model grid boxes at 3 km resolution; second degraded resolution (60 km) has 400 (20 by 20) original model grid boxes; and the third degraded resolution (120 km) contains 1600 (40 by 40) original model grid boxes. Then, the 3 km resolution output within each degraded cell are averaged, and the newly averaged values of the model output represent the results for degraded resolutions. The outcome of the degraded resolutions by averaging is shown in Fig. 5.3 and 5.4.

Table 5.1: A table of original model resolution, degraded resolutions and the number of grid boxes within each degraded cell

Resolution	3 km	30 km	60 km	120 km
Number of grids/cells in the domain	400 by 240	40 by 24	20 by 12	10 by 6
Number of 3 km grids in each of the cells with degraded resolutions	—	10 by 10	20 by 20	40 by 40

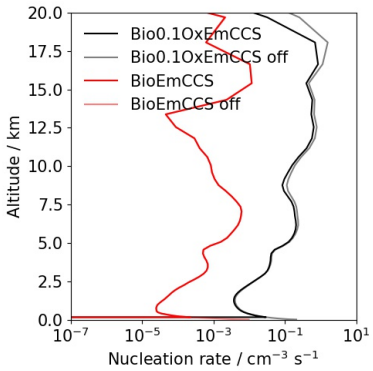

Figure 5.1: Profiles of modelled (black and red lines) and offline calculated (grey and light red) nucleation rate averaged over time and 3-km resolution domain in Bio0.1OxEmCCS (black and grey) and BioEmCCS (red colors) simulations.

Deriving the nucleation rate at 3 nm diameter offline allows us to examine the effects of averaging to influence nucleation rate. The time- and domain-mean offline nucleation is comparable to the nucleation rate from model output (Fig. 5.1). The offline nucleation rate at 3 nm diameter ($J_{Bio_{3nm}}$) is calculated with Eq. 5.1, Eq. 5.2, and Eq. 5.3 by feeding input variables ([monoterpene], [OH], [O_3], [H_2SO_4], CS1, CS2, and T) from the model output at 3 km resolution, averaged variables at 30 km resolution, averaged variables at 60 km resolution, and averaged variables at 120 km resolution.

Kernel Distribution Estimation and idealised offline nucleation rate

Probability densities of monoterpene concentrations and condensation sink (CS1) at 14 km altitude are derived with Gaussian kernel distribution estimation (KDE) method (Scott 2012). KDE uses a smoothing method to derive the densities of probability of the dataset. Each smoothed probability density is derived with weighted averaged data. Using KDE method allows us to understand the probability densities of monoterpene concentrations and condensation sink.

Both monoterpene concentrations and condensation sink are divided into 1000 bins, which are then fed into the equations (Eq. 5.1, 5.2, and 5.3) to derive idealised offline nucleation rate at 3

nm diameter while keeping the rest of the variables constant ([OH], [O_3], [H_2SO_4], CS2, and T). The constants are the medians of the 3 km resolution model output when CS1 is smaller than 0.02 s^{-1}, because particle production is more likely to occur under such environment (Table 5.2). The same constants are used for idealised offline nucleation rate at all four resolutions for each simulation. Such application will show how nucleation rate varies with monoterpene concentrations and condensation sink specifically.

Table 5.2: Constant values of OH, O_3, H_2SO_4, CS2, and T used to derive idealised offline nucleation rate at 3 nm diameter that varies with only monoterpene concentration and condensation sink in Bio0.1OxEmCCS and BioEmCCS simulations

Variables	Bio0.1OxEmCCS	BioEmCCS
[OH]	22781.075520	21588.492811
[O_3]	7.687413×10^{11}	7.518136×10^{11}
[H_2SO_4]	287.078880	1691.777106
CS2	43.240222	35.329285
T	265.299960	268.680637

The justifications of choosing the variables CS1 and [monoterpene] to be examined are described in Section 5.3.

Weighted NPF

The idealised offline nucleation rate (Section 5.2.4) takes account of the binned monoterpene concentration and condensation sink, but it does not consider the probability densities of the input variables (monoterpene concentration and condensation sink). Therefore, multiplying the idealised offline nucleation rate with the probability densities gives the weighted NPF at 3 nm diameter, indicating the relative importance and magnitude of NPF to occur under various combinations of monoterpene concentration and condensation sink.

5.3 Results

5.3.1 Offline nucleation rates with degraded resolutions

Figure 5.2 shows the vertical profiles of time- and domain-mean nucleation rate at 3 nm diameter that is calculated offline with Eq. 5.1, 5.2, and 5.3 and input variables ([monoterpene], [OH], [O_3], [H_2SO_4], CS1, CS2, and T), at the original 3 km resolution and three degraded resolutions (30 km, 60 km, and 120 km) in the Bio0.1OxEmCCS and BioEmCCS simulations.

In the simulation with reduced oxidation rate of monoterpene (Bio0.1OxEmCCS), offline nucleation rate in the original 3 km resolution decreases with height from surface until around 1 km, then gradually increases up to 11-18 km altitude, where it reaches a maximum of 1.6 cm^{-3} s^{-1}. The offline nucleation rate calculated with input variables at degraded resolutions have similar profiles as the original 3 km resolution, but as resolution becomes lower, the discrepancies are greater from the original 3 km resolution. Degraded resolutions produce smaller nucleation rate at most of the altitudes. In the simulation with reduced oxidation rate (Bio0.1OxEmCCS), the ratios of the rates in degraded resolutions to the original 3 km resolution are 0.7 (30 km resolution), 0.6 (60 km resolution), and 0.4 (120 km resolution) averaged over height, indicating that averaging the input variables causes nucleation rate to shift away from the high-resolution results.

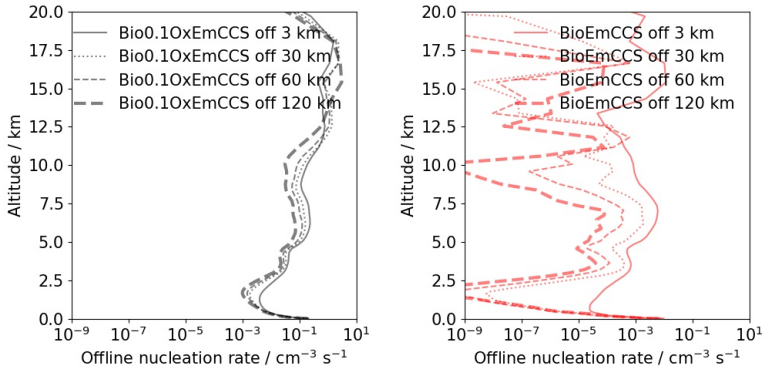

Figure 5.2: Profiles of offline calculated nucleation rate using the original model resolution (3 km, solid), degraded resolution (30 km, dotted), degraded resolution (60 km, thin dashed), and degraded resolution (120 km, thick dashed) in the simulations Bio0.1OxEmCCS (black) and BioEmCCS (red).

In the simulation with default monoterpene oxidation rate (BioEmCCS), offline nucleation rate at 3 km resolution are around a factor of 100 smaller than Bio0.1OxEmCCS simulation, because monoterpene in BioEmCCS simulation is oxidised at faster rates and thus is less likely to contribute to NPF. The offline nucleation rate decreases from surface until around 100 m altitude where it starts to increase with height and reaches a maxima at 7 km altitude (0.006 cm^{-3} s^{-1}), then nucleation rate decreases with height until 12 km (0.0003 cm^{-3} s^{-1}) and eventually increases up to 15-17 km altitude (0.012 cm^{-3} s^{-1}). Calculated with inputs from degraded resolutions, offline nucleation rate shows reductions at most of the heights except for around 12 km altitude. Lower resolutions generally produce smaller offline nucleation rates from the original 3 km resolution, the height-averaged ratios of the rates in the degraded resolutions to

the original 3 km resolutions are 1×10^{-5} (30 km resolution), 4×10^{-5} (60 km resolution) and 4×10^{-6} (120 km resolution) in BioEmCCS simulation, which represent more significant changes than Bio0.1OxEmCCS simulation with a slower oxidation rate.

The occurrence of differences between degraded resolutions and original resolution is caused by averaging within each degraded cell in 30 km, 60 km, and 120 km resolution, indicating a spatially non-linear nucleation rate as a result of input variables that vary across the horizontal domain. The cause of inhomogeneous gas, temperature and condensation sink fields is convection, especially deep convection which can efficiently transport sufficient amount of monoterpenes upwards from surface, affects oxidants, temperature and condensation sink at higher altitude.

In 30 km, 60 km, and 120 km domain, lower resolutions are associated with stronger averaging of the original 3 km resolution input variables, which causes discrepancies between the original offline nucleation rate profiles. The degraded resolutions produce stronger or similar nucleation rates than the original 3 km domain at around 11-17 km altitude in Bio0.1OxEmCCS simulation with reduced oxidation rate, and around 12 km altitude in BioEmCCS simulation with default oxidation rate. It is partly caused by the existence of very low monoterpene concentrations at these altitudes in the 3 km regional domain (e.g. empty areas in Fig. 5.3). When some grid boxes with low monoterpene concentrations are averaged with the surrounding grid boxes, the resulted nucleation rate in degraded cells can be larger than the averaged nucleation rate in the same area, because of the loss of extremely low nucleation rates at 3 km resolution. Overall, at most of the altitudes, simulations Bio0.1OxEmCCS and BioEmCCS show that a greater degradation of resolution usually produces smaller offline nucleation rates. The discrepancies caused by averaging to degraded resolutions and the magnitudes of discrepancies in each degraded resolutions are investigated in Section 5.3.2.

The discrepancies between degraded resolutions and original resolutions are different for simulations Bio0.1OxEmCCS and BioEmCCS, with the latter (a faster monoterpene oxidation rate) having greater changes relative to the original 3 km resolution results. Reducing the oxidation rate of monoterpene by a factor of 10 in Bio0.1OxEmCCS simulation extends the lifetime of monoterpenes so that they persist for a longer time before being oxidised by OH, O_3 and NO_3. Consequently, more monoterpene molecules can survive longer, so that they can be well mixed

after being detrained from clouds, and eventually contribute to NPF where condensation sink is low. Then, a well mixed region is less likely affected by averaging. A longer lifetime also allows more monoterpene molecules to be transported from surface to the upper troposphere by deep convection, which also affects the nucleation rates calculated with averaged concentrations in each degraded cell. However, in the BioEmCCS simulation where default (faster) monoterpene oxidation rate is used, monoterpenes have shorter lifetime, and thus fewer will escape clouds and have time to be well mixed with the surrounding environment. Insufficient mixing due to shorter lifetime causes a less homogeneous distribution, therefore averaging within the degraded resolutions causes larger discrepancies of offline nucleation rates in BioEmCCS than Bio0.1OxEmCCS simulation. Similarly, fewer monoterpene molecules reach regions of low condensation sink in BioEmCCS simulation, which leads to generally lower nucleation rates than Bio0.1OxEmCCS simulation.

5.3.2 Spatial variability of monoterpene and condensation sink

Here I investigate how convection introduces significant spatial variability for gas, condensation sink and temperature fields and thereby affects calculated nucleation rates at 3 nm diameter. Monoterpene concentrations and condensation sink in the UT, which determine the nucleation rate, are controlled by convection. Therefore, in the following analyses, the effects of averaging on monoterpene concentrations and condensation sink (CS1) at around 14 km altitude are investigated. The condensation sink is used for further investigation because CS1 is used to derive the concentrations of HOMs and subsequently indirectly affects nucleation rate at 3 nm diameter, while CS2 is used to derive nucleation rate from 1.7 nm to 3 nm (Section 5.2.2). The condensation sink in the following sections refer to CS1.

Figure 5.3 and 5.4 show maps of monoterpene and condensation sink at all four resolutions in the simulations Bio0.1OxEmCCS and BioEmCCS. Monoterpene concentration and condensation sink are roughly positively correlated, because monoterpenes are transported by convection and condensation sink is determined by the cloud water content formed by convection. Thus, high monoterpene concentrations usually occur at the same locations of high condensation sink in the maps.

In the simulation with reduced oxidation rate (Bio0.1OxEmCCS), monoterpene concentrations are generally between 10^8 and 10^{12} molec cm^{-3} (or higher) with some lower concentrations at

the edge of the clouds, likely caused by the entrained air from higher altitude. Lower monoterpene concentrations also occur in the cloud-free regions indicated by white patches. Here, the white colour means that the concentrations are smaller than the lower limit (1 molec cm^{-3}) of the maps. Averaging to degraded domains reduces the contrasts of the high and low concentrations as the resolution becomes coarser, and the smoothing effect is stronger when more 3 km grid boxes are averaged within each degraded cell. Eventually monoterpenes in the 120 km resolution are almost homogeneously distributed at 14 km altitude in Bio0.1OxEmCCS simulation. Condensation sink in Bio0.1OxEmCCS simulation, which takes into account of the contribution from clouds, is higher in the clouds than outside at 14 km altitude, showing a great spatial variability. In Bio0.1OxEmCCS simulation, the smoothing effect is similar for condensation sink, which reduces high condensation sink while increases low condensation sink in the region. Different from monoterpenes which can mix with the surrounding air, high condensation sink (> 0.1 s^{-1}) which can completely prevent nucleation, usually occurs in clouds. The gradients of condensation sink in- and outside the clouds are large, meaning that nucleation may rarely occur in the clouds. Therefore, degrading the resolutions will generally cause reduced condensation sink in clouds, but should hardly affect nucleation rate in the cloudy regions. Unless at 120 km resolution in which each grid box covers an area greater than the clouds, then the nucleation rates outside the cloud region at 3 km resolution will be affected.

BioEmCCS simulation with default oxidation rate has in general lower monoterpene concentrations than Bio0.1OxEmCCS simulation because monoterpenes are more rapidly oxidised and less likely to create a region of homogeneous concentrations, or less likely to reach the UT in this environment. Due to rapid oxidation rate, monoterpene concentrations at the original 3 km resolution in BioEmCCS simulation show a wider range of concentrations in log-scale and significant spatial variability across the domain. Averaged monoterpene concentrations in degraded resolutions show increasingly more homogeneous concentrations as the resolution becomes coarser, but the log-scale maps still appear less homogeneous than Bio0.1OxEmCCS simulation which has a slower oxidation rate. The maps of condensation sink in BioEmCCS simulation at the original 3 km resolution and degraded resolutions are similar to the maps in Bio0.1OxEmCCS simulation, because condensation sink in the low-aerosol UT is primarily driven by clouds which are hardly affected by different NPF mechanism (see also Chapter 3).

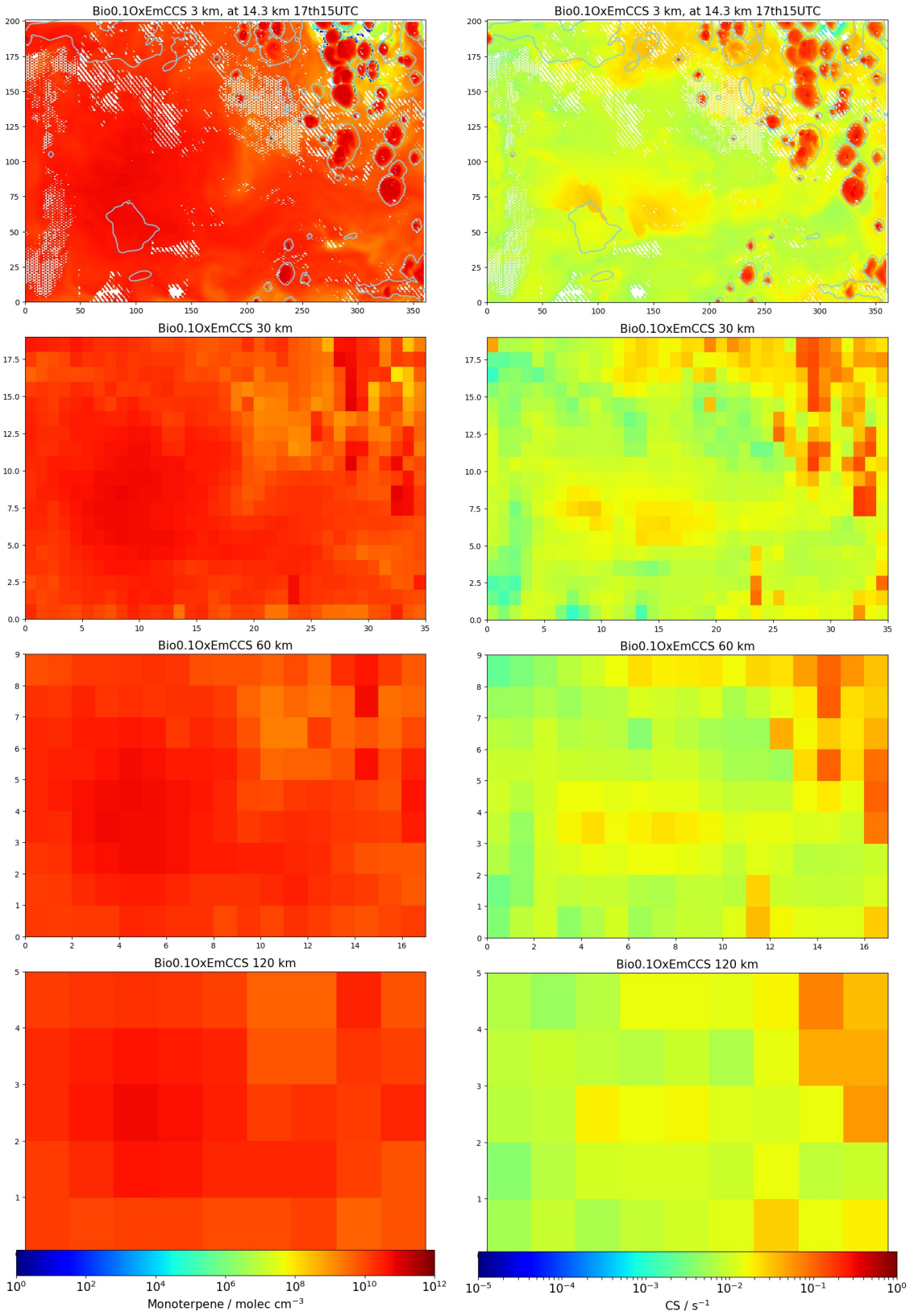

Figure 5.3: Maps of monoterpene (left) and condensation sink (right) at 14 km altitude in Bio0.1OxEmCCS simulation. The maps in each column use the same colour scale shown at the bottom. Maps in the first row are at the original 3 km resolution and the contours highlight the locations of clouds and are drawn where the cloud water content is equal to 0.002 g kg^{-1}, in the second row are at 30 km resolution, in the third row are at 60 km resolution, and in the fourth row are at 120 km resolution.

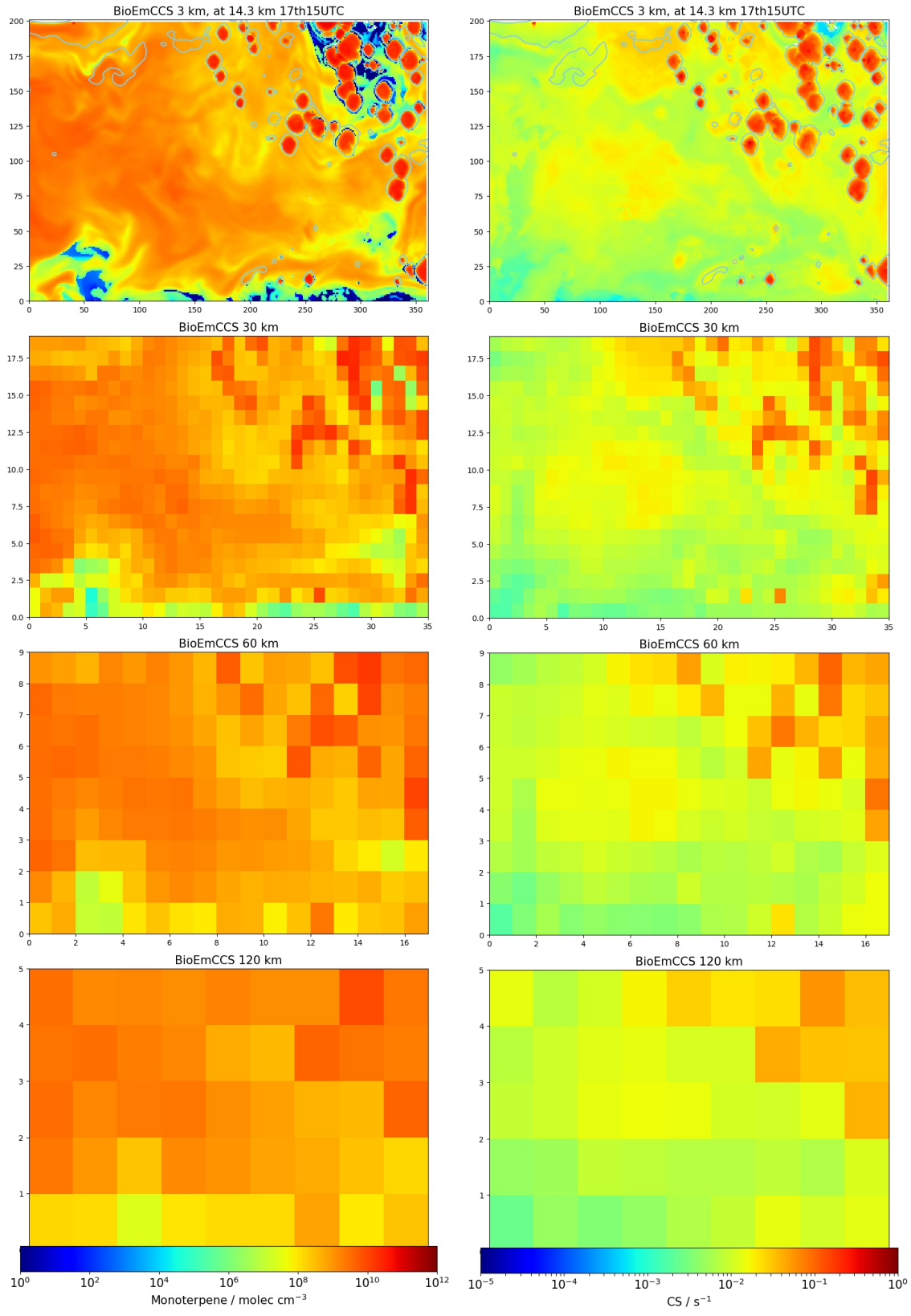

Figure 5.4: Maps of monoterpene (left) and condensation sink (right) at 14 km altitude in BioEmCCS simulation. The maps in each column use the same colour scale shown at the bottom. Maps in the first row are at the original 3 km resolution and the contours highlight the locations of clouds and are drawn where the cloud water content is equal to 0.002 g kg^{-1}, in the second row are at 30 km resolution, in the third row are at 60 km resolution, and in the fourth row are at 120 km resolution.

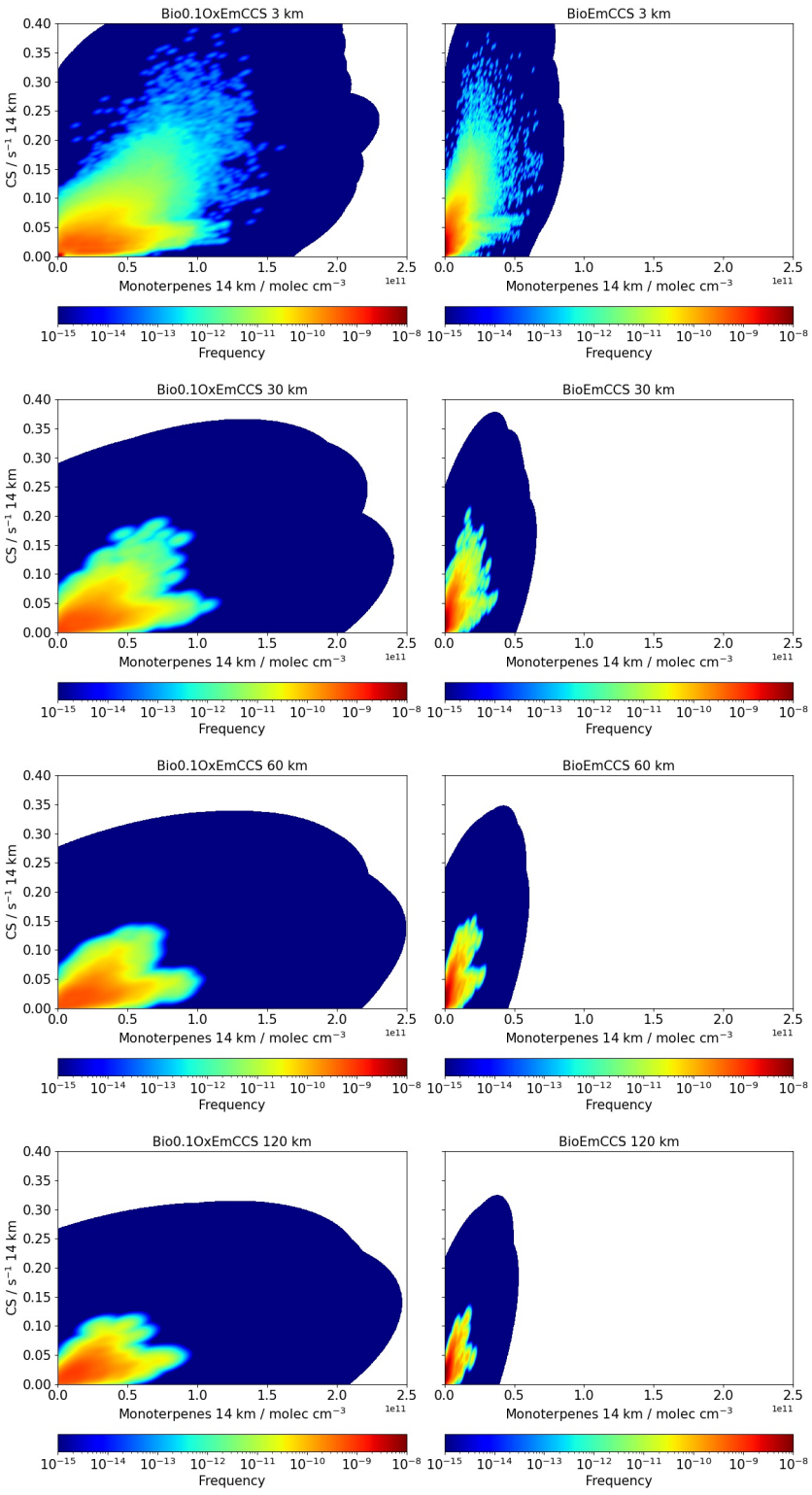

Figure 5.5: Probability densities of the occurrence of monoterpene and condensation sink in the Bio0.1OxEmCCS (left) and BioEmCCS (right) simulation at 14 km altitude for all the instantaneous output in the original model resolution (3 km, first row), 30 km resolution (second row), 60 km resolution (third row), and 120 km resolution (fourth row). The frequency in the color bars denotes probability densities.

Figure 5.5 shows the 2-dimensional probability densities for occurrence of monoterpene con-

centrations and condensation sink in Bio0.1OxEmCCS and BioEmCCS simulations for the four resolutions. The KDE method is used and introduced in Section 5.2.4. Figure 5.5 at the original 3 km resolution show that the monoterpene concentrations and condensation sink have great spatial variability for both Bio0.1OxEmCCS and BioEmCCS simulations, indicated as the range of the results of each colour being relatively large and the edge of the colours being far from the neighbouring colours. At the 3 km resolution, higher probability densities (orange and red colours) are shown for monoterpene concentrations smaller than around 0.7 molec cm^{-3} and condensation sink smaller than 0.08 s^{-1} in Bio0.1OxEmCCS simulation; in BioEmCCS simulation, higher probability densities are shown for monoterpene concentrations smaller than 0.2 molec cm^{-3} and condensation sink smaller than 0.11 cm^{-3}; meaning that distributions in both simulations are generally skewed to lower monoterpene concentration and condensation sink at 14 km altitude. However, the ranges in light blue and green in the two simulations show that there are still many grid boxes with relatively higher monoterpene concentration and condensation sink which can be easily lost due to coarse resolutions.

The ranges of the 14-km altitude colour map at 3 km resolution is greater in Bio0.1OxEmCCS simulation because in general, it has a slower oxidation rate which causes higher monoterpene concentrations than BioEmCCS simulation, and thus, the colour map of probability density is narrower in BioEmCCS simulation in the axis of monoterpene.

Averaging to the degraded resolutions in Bio0.1OxEmCCS simulation reduces the range of the colour maps especially for the light blue-to-green regions, meaning that the 3 km resolution grid boxes that contain monoterpene concentrations and condensation sink that fall into the light blue-to-green range are much greater than their surrounding grid boxes. Then, the degraded resolutions lose many high monoterpene concentrations and condensation sink due to averaging. As resolutions become coarser, many more grid boxes are averaged from 30 km to 120 km resolution, then the range of the colour maps becomes smaller. Most of the changes occur when condensation sink is greater than 0.1 s^{-1} which are in the clouds as indicated in the maps (Fig. 5.3 and 5.4), and nucleation rates are zero or extremely low in the clouds. Thus, if these extreme nucleation rates exist in the cloudy regions of 3 km resolution, they will be lost with degraded resolution, but will not significantly affect the domain averaged nucleation rates. The edge of the colours are also more smoothed with degraded resolutions. Interestingly, the orange and red colours, which represent relatively higher probability densities of occurrence,

cover larger ranges of condensation sink (up to 0.1 s^{-1}) when the resolutions are degraded. It is because more grid boxes, which have even higher condensation sink in the original 3 km resolution, after averaging, now become smaller and are grouped into condensation sink ranges that are lower than 0.1 s^{-1}. Therefore, the probability densities are increased for monoterpene concentration and condensation sink that are below the condensation sink threshold (0.1 s^{-1}) in 30 km, 60 km, and 120 km resolutions. The changes in orange and red colour ranges may have great effects on nucleation rates due to a large number of grid boxes.

Similar to Bio0.1OxEmCCS simulation, averaging to the degraded resolutions in BioEmCCS simulation also produces smaller colour maps especially for the relatively high monoterpene concentration and condensation sink in light blue-to-green colours; the edges of the colours are more smoothed after averaging; the probability densities represented by orange and red colours now reach higher condensation sink (0.13 s^{-1}). However, the percentage shrinkage of the range of the colour maps as resolution degrades is more significant in BioEmCCS than in Bio0.1OxEmCCS simulation, which results in greater changes in offline nucleation rate as shown in Fig. 5.2.

Both simulations with default and slowed-down monoterpene oxidation rate show that averaging to the degraded resolutions generally reduces monoterpene concentrations and condensation sink. Although, other variables ([OH], $[O_3]$, $[H_2SO_4]$, CS2, T) that are used to derive nucleation rates are not shown in maps, they are expected to be changed in a similar way during averaging.

Figure 5.6 shows the same probability densities plots as in Fig. 5.5 but with lines of idealised offline nucleation rate derived with binned monoterpene concentrations and condensation sink, with the rest of the input variables as constants (see Section 5.2.4). It is referred to as idealised offline nucleation rate. In reality, other variables used to calculate nucleation rate ([OH], $[O_3]$, $[H_2SO_4]$, CS2, and T) should also change when monoterpene concentration and condensation sink (CS1) vary, but they are kept constant to simplify the processes.

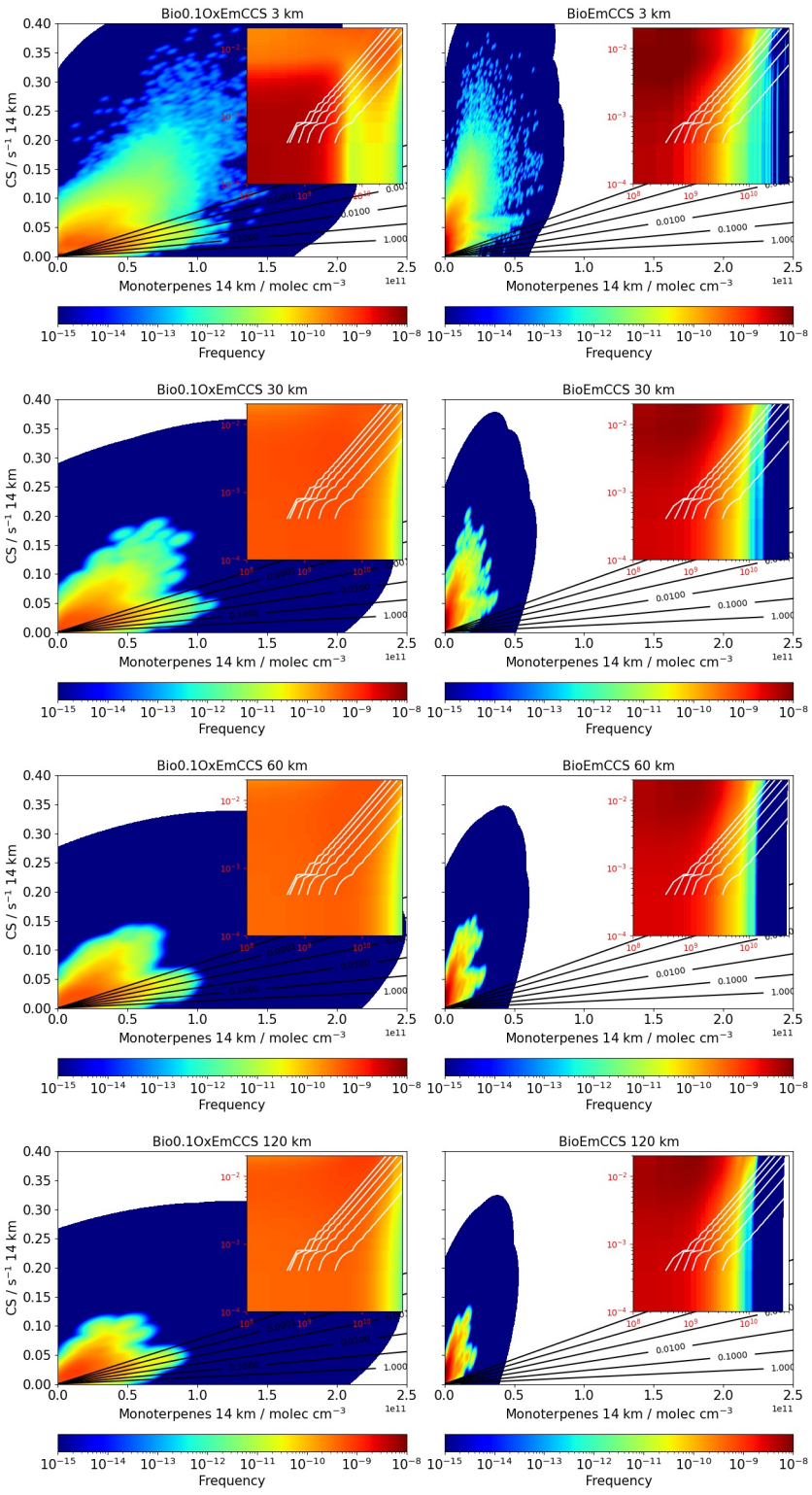

Figure 5.6: The same probability densities plots of monoterpene and condensation sink (same as Fig. 5.5) in the Bio0.1OxEmCCS (left) and BioEmCCS (right) simulation at 14 km altitude for all the instantaneous output in the original model resolution (3 km, first row), 30 km resolution (second row), 60 km resolution (third row), and 120 km resolution (fourth row). The additional lines represent idealised offline nucleation rate calculated with binned monoterpene concentration and condensation sink and assumed [OH], [O_3], [H_2SO_4], CS2, and T to be constant (see Section 5.2.4). The inset figures are the same but zoomed in to below 5×10^{10} molec cm^{-3} for monoterpene and below 0.02 s^{-1} for condensation sink. The frequency in the color bars denotes probability densities.

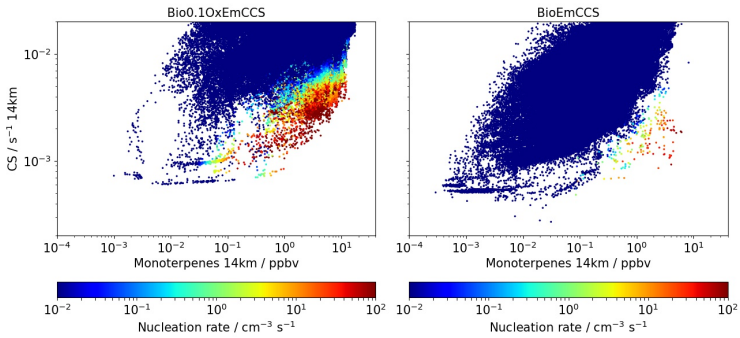

Figure 5.7: Correlation scatters of nucleation rate (colour map), monoterpene (x-axis), and condensation sink (y-axis) for all the modelled output at 14 km altitude in Bio0.1OxEmCCS (left) and BioEmCCS (right) simulations.

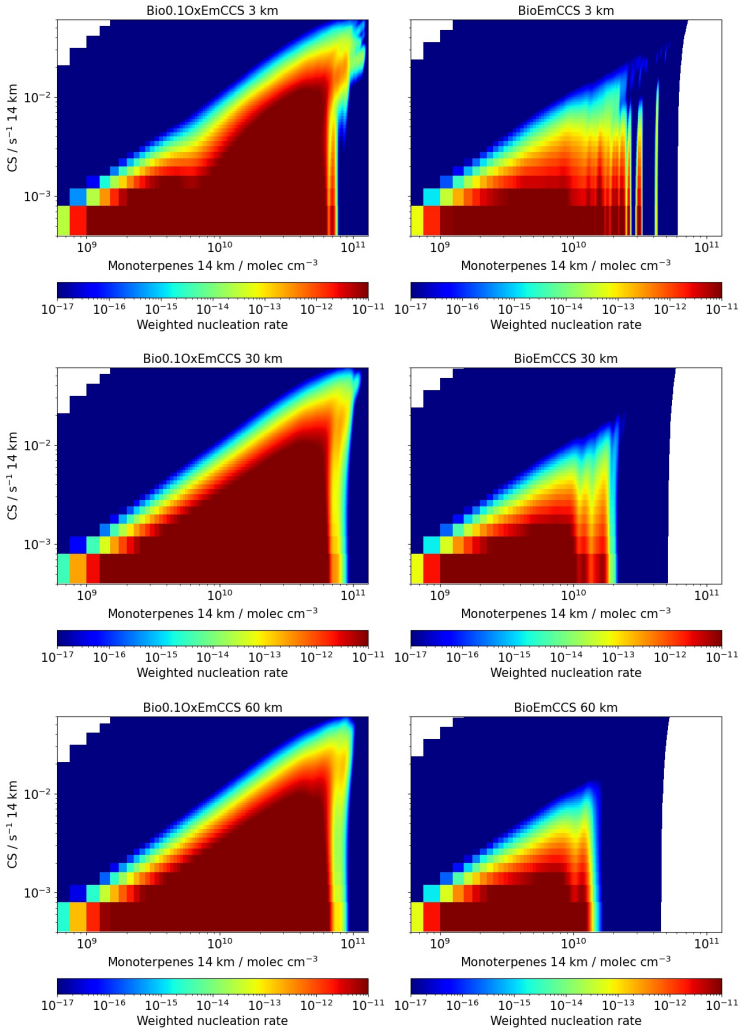

Figure 5.8: Idealised offline nucleation rate weighted by the probability densities in Fig. 5.5 (probability density × idealised nucleation rate), plotted against monoterpene and condensation sink in Bio0.1OxEmCCS (left) and BioEmCCS (right) at 14 km altitude in the original model resolution (3 km, first row), 30 km resolution (second row), and 60 km resolution (third row). The idealised offline nucleation rates are calculated with binned monoterpene concentration and condensation sink and assumed the [OH], [O_3], [H_2SO_4], CS2, and T to be constant (see Section 5.2.4). Weighted NPF can indicate show the probability of occurrence of NPF.

The idealised offline nucleation rate lines are the same for the degraded resolutions (30 km, 60 km, and 120 km) because the four probability density plots use the same bins for monoterpene concentration and condensation sink for clear comparisons. But the side effect of using same bins for all four resolutions is that it does not take into account of individual distributions for each simulation and resolution, and thereby results in the same idealised offline nucleation rate lines for each resolution. Idealised offline nucleation rate does not show up when condensation sink is smaller than 0.0004 s^{-1}. It is because lack of number of bins to plot the figure. Figure 5.7 shows the correlation scatter plots of condensation sink, monoterpene and nucleation rate from model output in Bio0.1OxEmCCS and BioEmCCS simulations. NPF does occur in the model when condensation sink is smaller than 0.0004 s^{-1}, although very rare and at low rates, because lower condensation sink is usually associated with lower monoterpene concentrations which are not ideal for high NPF rates to occur.

Lines of smaller idealised offline nucleation rates have greater slopes, and intersect with the edge of the colour maps at relatively higher condensation sink, which is consistent to the fact that condensation sink suppresses NPF. The areas under the lines are greater in Bio0.1OxEmCCS than in BioEmCCS simulation because slower oxidation rate of monoterpene increases the probability of NPF to occur. Interestingly, the 'slopes' are greater in BioEmCCS than Bio0.1OxEmCCS simulation when idealised offline nucleation rate is smaller than 0.001 cm^{-3} s^{-1}, which seems to suggest that nucleation could occur under higher condensation sink in BioEmCCS than in Bio0.1OxEmCCS simulation. However, the intersect points of the lines with the colours show that the idealised offline nucleation rates are constrained by the monoterpene concentrations and condensation sink. Accounting for the extent of the colour maps, BioEmCCS simulation still produces idealised offline nucleation rates much less efficiently than Bio0.1OxEmCCS simulation.

The calculation of idealised offline nucleation rates are not associated with the probability densities of the occurrence of different monoterpene concentrations and condensation sink in Fig. 5.6. Therefore, weighted NPF is calculated by multiplying the idealised offline nucleation rates with the probability densities in Fig. 5.5 (see also Section 5.2.4). The weighted NPF then links idealised offline nucleation rates with realistic occurrence of monoterpene concentrations and condensation sink in Fig. 5.8. Weighted NPF is able to show the probability of occurrence of NPF within a range of realistic monoterpene concentration and condensation sink.

Combining the idealised offline nucleation rate and the probability densities of monoterpene concentration and condensation sink, the weighted NPF in monoterpene-CS space shows similar triangle shapes for Bio0.1OxEmCCS and BioEmCCS simulations at the four resolutions (Fig. 5.8). The colour maps in Bio0.1OxEmCCS simulation cover greater ranges than BioEmCCS simulation. This is because Bio0.1OxEmCCS simulation uses a smaller oxidation rate which is more likely to allow NPF to occur because of reduced monoterpene volatility (Fig. 5.9), and eventually contribute to nucleation rates that can occur in a wider range of condensation sink. A slower oxidation rate also results in a region with more homogeneously distributed monoterpene concentrations. It additionally causes more monoterpene molecules being able to survive for a longer time, then, accumulate to higher concentrations everywhere. At the original 3 km resolution, the weighted NPF is greater than 1×10^{-15} for almost all monoterpene concentrations but only exceeds 1×10^{-15} when condensation sink is smaller than 0.06 s^{-1} (Bio0.1OxEmCCS) and 0.02 s^{-1} (BioEmCCS) which are outside the clouds (Fig. 5.3 and 5.4). The weighted NPF is skewed to higher monoterpene concentrations and lower condensation sink. Weighted NPF distributions are skewed because nucleation rates are positively correlated with monoterpene concentration and negatively correlated with condensation sink. In the dark blue regions, NPF also occurs, but with much lower probabilities, because very few cells have very high monoterpene concentration and very low condensation sink at the same time, or low monoterpene concentration and high condensation sink. Because monoterpenes are transported by deep convection and condensation sink is calculated with cloud water content formed by convection, the monotepene concentrations and condensation sink are positively correlated.

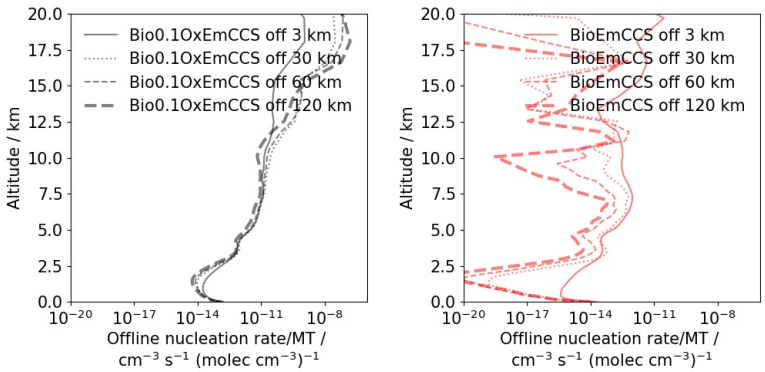

Figure 5.9: Profiles of offline calculated (grey and light red) nucleation rate divided by monoterpene concentrations (MT), averaged over time and domain in Bio0.1OxEmCCS (grey) and BioEmCCS (red) simulations at 3 km (solid), 30 km (dotted), 60 km (thin dashed), and 120 km (thick dashed) resolution.

The original 3 km resolution and the three degraded resolutions are very similar in the simulation with slower oxidation rates (Bio0.1OxEmCCS), with the range of colours of high monoterpene concentration and relatively high condensation sink being reduced after averaging. The reductions of the coloured ranges are mainly sensitive to changes in monoterpene concentrations, because Fig. 5.8 has already filtered out the range of condensation sink that is significantly affected by resolution (> 0.1 s^{-1}) while the rest (< 0.06 s^{-1}) are less likely affected by resolution. In each condensation sink range (e.g. 0.0004-0.0008 s^{-1}), weighted NPF in red colour band tends to be narrower as resolution degrades, converging to a certain middle point of monoterpene concentration by losing the high and low concentrations with averaging. The overall similar ranges of weighted NPF that are greater than 1×10^{-15} implies that the nucleation rates are less significantly affected by averaging to degraded resolutions in Bio0.1OxEmCCS simulation.

In contrast, weighted NPF in BioEmCCS simulation changes significantly due to averaging to degraded resolutions. The upper limit for light blue colour in 3 km resolution is around 4×10^{10} molec cm^{-3} for monoterpene concentration and 0.02 s^{-1} for condensation sink (Fig. 5.8). At 30 km resolution, the upper limits are reduced to around 2×10^{10} molec cm^{-3} and 0.018 s^{-1} which means that NPF is likely to occur within a smaller range of monoterpene concentration and condensation sink at degraded resolutions, and is accompanied by a smaller range of the colour map. Both upper limits and ranges of the colour maps are reduced further in 60 km and 120 km resolutions. Narrowing of the bands caused by averaging to degraded resolutions becomes clearer in BioEmCCS simulation, especially for the lowest condensation sink bin (0.0004-0.0008 s^{-1}) where the weighted NPF ranges tend to converge to the monoterpene concentration range between 2×10^{9} and 8×10^{9}, which is approximately where the orange-to-yellow band of probability densities (3×10^{-11}-3×10^{-10}) in Fig. 5.5 at 14 km altitude. The overall changes show that averaging causes narrowing of the weighted NPF, restricting NPF to occur in a smaller range of monoterpene concentration and condensation sink by averaging out the extreme monoterpene and condensation sink. Then, it can prevent extreme nucleation rates to occur.

BioEmCCS simulation shows more significant changes in colour maps of weighted NPF with resolution than Bio0.1OxEmCCS simulation, because of faster oxidation rates. Faster oxidation rates cause monoterpene to be less likely to contribute to NPF, have great spatial variability over the regional domain, and have generally lower concentrations. In conclusion, the faster oxidation rate of monoterpene, the stronger reductions of the likelihood of NPF to occur, especially

for extremely high and low nucleation rates.

5.4 Discussions and Conclusions

The effect of deep convection on the non-linear relationship of NPF (nucleation) rate, monoterpene and condensation sink is investigated with the output from a high-resolution regional model (grid spacing 3 km) with two monoterpene oxidation rates differing by a factor of 10 (Bio0.1OxEmCCS and BioEmCCS simulations). Both simulations use additional condensation sink from clouds to suppress in-cloud NPF. The simulations were carried out in September 2014, in a domain covering part of Amazonia where the oxidised biogenic gases can efficiently produce particles in the UT, as was observed during ACRIDICON-CHUVA campaign Andreae et al. (2018) and shown in modelled results in Chapter 3. Model output variables (gas concentrations, oxidant concentrations, condensation sink and temperature) were used to calculate nucleation rates offline for a range of degraded resolutions (30 km, 60 km, and 120 km) in order to understand how the non-linear dependence of nucleation rates on these variables are affected by averaging.

The changes across the four resolutions show that the time- and domain-mean nucleation rate is reduced in degraded resolutions in the Bio0.1OxEmCCS simulation which has slower monoterpene oxidation rates, while changes are much more significant in BioEmCCS simulation which has faster monoterpene oxidation rates. The changes in offline nucleation rates due to degraded resolution are caused by inhomogeneous gas, condensation sink and other meteorological fields modulated by clouds. It highlights the potentially significant effect of deep convection on NPF in the UT. At around 14 km altitude, averaging to degraded-resolution cells leads to a more homogeneous domain at the expense of losing extremely high and low input values which may produce extreme nucleation rates, and degrading the resolutions produces smaller time- and domain-mean nucleation rates at most of the altitudes. The overall nucleation rates are shown to be reduced at degraded resolutions along with reduced monoterpene concentrations and condensation sink. Although nucleation rate is positively correlated with monoterpene concentrations, it is suppressed by condensation sink, indicating the non-linearity of nucleation rate to monoterpene and condensation sink when the two are related. Thus, nucleation rates will be sensitive to the spatially inhomogeneous distribution of monoterpene concentration and condensation sink which are shown in the maps (Fig. 5.3 and 5.4).

Seen from the probability densities of the occurrence of monoterpene concentrations and condensation sink in Fig. 5.5, the distributions are skewed to lower monoterpene concentrations and condensation sink, indicating the significant variability and meaning that there are much less high monoterpene concentrations and condensation sink. Then, it implies that the likelihood of losing high values is greater than losing low values during averaging. The maps and weighted NPF (Fig. 5.3, Fig. 5.4 and Fig. 5.8) show that the high condensation sinks (> 0.1 s^{-1}) that are lost due to degraded resolutions do not necessarily affect the overall nucleation rates, because NPF rarely occurs in regions of high condensation sink. Consequently, comparing to condensation sink, the reduced monoterpene concentrations in degraded resolutions may play an important role in affecting nucleation rates. However, other input variables that are all correlated ([OH], $[O_3]$, $[H_2SO_4]$, CS2, and T) in the degraded resolutions may also affect nucleation rate but are not investigated in detail (see Section 5.2.2).

The idealised offline nucleation rate calculated with binned monoterpene concentrations and condensation sink show positive correlation of nucleation rate with monoterpene and negative correlation with condensation sink, but the idealised offline nucleation rates need to be weighted by realistic probability densities of the occurrence of monoterpene concentrations and condensation sink. The weighted NPF directly shows reductions of the ranges of the colour maps as a result of averaging monoterpene concentration and condensation sink. The weighted NPF ranges reduce to smaller ranges of both variables in degraded resolutions and the reduction is intensified when more 3 km resolutions grid boxes are averaged within each degraded cell. Additionally, the weighted NPF ranges tend to converge to a narrower set of conditions of monoterpene concentrations and condensation sink, approximately where the probability densities of occurrence of monoterpene concentrations and condensation sink are between 3×10^{-11}-3×10^{-10}. It also happens to be close to the edge of the probability densities which cover relatively similar ranges in the four resolutions, i.e. the edge inside which the range is hardly affected by averaging. Consequently, nucleation rates are incorrectly represented with averaging which restricts nucleation rates to occur for smaller ranges of monoterpene concentrations and condensation sink.

The results show that losing the spatial variability by averaging to degraded cells affects BioEmCCS simulation more significantly than Bio0.1OxEmCCS simulation. It can be speculated that a 10 times faster oxidation rate of monoterpene in BioEmCCS simulation reduces the probability of monoterpene concentrations to be homogeneous in a region, because of insufficient mixing.

Consequently, monoterpenes can be easily lost during transport from surface to the UT and detraining by deep convection, because they are oxidised to SecOrg. While in Bio0.1OxEmCCS simulation, monoterpene has relatively longer lifetime and can become more homogeneously distributed across the domain because monoterpene in Bio0.1OxEmCCS has more time to be transported and mixed to the surrounding environment. Therefore, it is expected that nucleation rates will not be affected by averaging if monoterpene has a lifetime that is long enough against transport and mixing. Then, monoterpene will be more dependent on long-range transport like SO_2 which has chemical lifetime longer than a day. Consequently, the spatial variability of monoterpene concentration at 3 km resolution is more strongly affected by averaging to 30 km, 60 km, and 120 km resolutions in BioEmCCS simulation than Bio0.1OxEmCCS simulation, because reduced oxidation rates allow substantial amount monoterpene molecules to be more evenly distributed. Thus, averaging to degraded resolutions for Bio0.1OxEmCCS simulation does not significantly affect the nucleation rates as it does for BioEmCCS simulation.

The simulation with slower oxidation rates (Bio0.1OxEmCCS simulation) produces greater nucleation rates than with faster oxidation rates (BioEmCCS simulation) because two factors affected by a reduction in oxidation rate. First, monoterpenes are less volatile which makes NPF rate more efficient per monoterpene at the level of detrainment (Fig. 5.9). It is similar to previous studies which found that BVOC species usually had a wide range of volatility and those with lower vapour volatility were more likely to form new particles (Tröstl et al. 2016; Simon et al. 2020). Second, a slower oxidation rate will allow more monoterpene molecules to be transported to the upper troposphere by deep convection, causing higher concentrations which can additionally enhance nucleation rate. The efficiency of vertical transport are also consistent to the findings of Li et al. (2017) and Bardakov et al. (2020) which found that BVOCs, especially isoprene and alpha-pinene could be more efficiently transported by convection.

Investigating the non-linear nucleation rate with monoterpene concentrations and condensation sink by averaging shows a general picture that deep convection can perturb the UT by transporting monoterpenes from the surface (Thornton et al. 1997; Yin et al. 2001; Yin et al. 2002; Twohy et al. 2002; Devine et al. 2006; Kulmala et al. 2006; Andreae et al. 2018), form cloud condensation sink to suppress HOM production and nucleation rate (Kazil et al. 2011), and cause a domain with significant spatial variability that can be less well represented by coarse resolutions, even though algorithms such as probability density functions and sub-grid

parameterisations have been used in global models. Then, averaging or using a coarse grid spacing to represent a relatively large region will result in nucleation rate with great uncertainties, especially when the lifetime of a gas precursor is relatively short (a few hours), because much important sub-grid variability will be smoothed out, NPF will occur over a smaller range of monoterpene and condensation sink, and thereby hamper our understandings of NPF-deep convection interactions.

There are limitations of the work presented in this chapter. First, only two sets of monoterpene oxidation rates were investigated, while increasing monoterpene oxidation rates from the default state, interpolating the rates between the two sets, or doing both are expected to provide new insights. Second, variables other than monoterpene concentrations and condensation sink were not investigated. Including the probability density analyses of [OH], [O_3], [H_2SO_4], CS2, and T may present a more complete picture of the non-linear nucleation rates affected by deep convection. Therefore, it is recommended for future studies to use ensemble simulations to investigate nucleation rates affected by the spatial variability of [monoterpene], [OH], [O_3], [H_2SO_4], CS1, CS2, and T under a wider range of monoterpene oxidation rates. It is also recommended to investigate how binary nucleation which depends on longer-lived gas precursor SO_2 will be affected by spatial variability, as well as comparing the high-resolution regional model results with a global model.

Chapter 6

Conclusions

A global model with a regional nested domain over central Amazonia has been used to investigate NPF-aerosol-cloud interactions. Both models are coupled to the UKCA aerosol-chemistry model and the regional model with explicit convection is additionally coupled with CASIM two-moment cloud microphysics. The study first quantified the NPF and particle concentrations under the influence of deep convection during the dry-to-wet transition season in a 1000 km region of Amazonia (Chapter 3). Second, effects of anthropogenic emissions on aerosol and cloud in the Manaus and downwind region and the underlying mechanism were studied (Chapter 4). Finally, the non-linear relationship of nucleation rate in the Amazonian upper troposphere and the influencing factors of condensation sink and monoterpenes were investigated (Chapter 5).

Overall, the PhD thesis provides new insights concerning the origins of particles in the Amazonia region, the efficiency of transport of particles by deep convection, and an improved understanding of the NPF-cloud interactions in the convective environment of Amazonia. A summary of the major findings is presented below in response to the questions raised in section 1.2.

6.1 Summary of major findings

6.1.1 Chapter 3: The contribution of regional aerosol nucleation and transport to low-level CCN in an Amazonian deep convective environment

(1) How do NPF-deep convection interactions on regional scales (around 1000 km) affect the vertical distributions of particles in the Amazonian tropical rainforest?

Deep convection can efficiently transport monoterpene, which is an insoluble nucleation precursor gas that can be oxidised within a few hours, from the surface to the upper troposphere. Because of low temperature and generally low condensation sink, NPF is strongest in the upper troposphere (above 10 km altitude, 3.5 cm^{-3} s^{-1}) and thus produces higher total particle concentrations there (more than 10000 cm^{-3}) than at lower altitudes. The profiles of the total particle concentrations are consistent with the observations during ACRIDICON-CHUVA (Andreae et al. 2018). (Section 3.3.1, 3.3.2 and 3.3.3)

Clouds suppress nucleation by creating a large condensation sink from droplets and ice (cloud condensation sink) for nucleating vapours and particles smaller than 3 nm. Therefore, NPF is spatially strongly modulated by clouds. Over a horizontal domain in the upper troposphere, the averaged nucleation and Aitken mode particle concentrations are reduced by 50% with the addition of a cloud condensation sink. (Section 3.3.3)

(2) How much does NPF occurring on a regional scale affect the CCN budget of the region? What fraction of CCN is created regionally versus being transported into a region from outside?

Within a 1000 km regional domain, NPF from the regional model contributes more than 50% of the nucleation and Aitken mode particle concentrations in the upper troposphere where nucleation rates are the greatest. The smaller particle diameters, the larger fraction of particle concentrations are formed by NPF in the regional upper troposphere. However, the contribution of NPF occurring in the regional domain to particles is negligible below 10 km altitude. The rest of the NPF-induced particles have been formed from outside the domain in the global model before they enter the 1000 km regional domain, and this fraction is more than 75% for Aitken and accumulation mode below 2 km altitude. Thus, only a small fraction of CCN are formed by NPF in the regional domain, with the rest being transported from outside. (Section 3.3.4)

The weak contribution of NPF in the relatively polluted regional domain to CCN below 2 km altitude is partly because most of the newly formed particles do not have enough time to grow to CCN sizes before they are transported outside the domain. Air in the Amazonian 1000 km domain has an average residence time of 20-40 hours with typical easterly wind speeds. However, a few days are needed for the whole process of nucleation and subsequent growth to Aitken

and accumulation mode sizes, longer than the residence time of air mass in the domain.

(3) How effective is deep convection at transporting particles downwards to low-levels?

In the Amazonian deep convective environment, particles from the upper troposphere can be transported downward to around 8-10 km altitude within a day and then are transported outside the domain by the easterlies, but the particles below 2 km altitude (75% in question (2)) were formed in the global model, then entered the regional domain at altitudes below 7 km. Less than 1% of the instantaneous domain-mean total particle concentrations in the lowest 2 km altitude are due to downward transport by deep convection from the upper troposphere to the boundary layer in the 1000 km regional domain during the 3-day simulation. The small vertical transport shows that one convective cycle of deep convection is not long enough to transport significant amount of particles from upper troposphere to the boundary layer. (Section 3.3.5)

(4) How are particle concentrations, nucleation and growth rates in the regional domain sensitive to changes in nucleation mechanisms?

Several NPF mechanisms have been used to test the sensitivity of nucleation rate, growth rate and particle concentrations, including binary nucleation which forms new particles with sulfuric acid and water clusters with default nucleation rate, binary nucleation rate increased by a factor of 10, biogenic nucleation, biogenic nucleation with reduced oxidation rate of monoterpene ($\div$10), and biogenic nucleation with reduced oxidation ($\div$10) and emission rates of monoterpenes were also increased by a factor of 10. (Section 3.3.1, 3.3.2 and 3.3.3)

Particle concentrations of various sizes and nucleation rates are not significantly affected when binary nucleation rates are increased by a factor of 10. Only minor differences are shown for nucleation rate, nucleation mode, and Aitken mode particles above 10 km altitude. The smaller effect compared to biogenic nucleation is because binary nucleation is determined by the SO_2 trace gas field that, due to its long lifetime relative to monoterpenes, is more controlled by the global model.

The three biogenic nucleation mechanisms have more significant effects on the particles and rates at all altitudes. It implies that organic molecules in Amazonia are important for NPF as has been stated by the observational study Andreae et al. (2018). In the upper troposphere

where NPF is the strongest, the biogenic nucleation and growth rates are increased by up to a factor of 1800 and 10 respectively when oxidation and emission rates are both changed from default values. Subsequently, the nucleation mode concentration is enhanced by a factor of 18 due to the changed oxidation and emission rates. In the boundary layer, Aitken and accumulation mode aerosols are significantly affected by biogenic nucleation mechanisms (factors of 3-5). Particle concentrations, especially nucleation and Aitken mode, are very sensitive to biogenic nucleation is because the biogenic nucleation mechanism precursor, monoterpene, can be quickly transported and mixed by deep convection, and oxidised within a few hours.

6.1.2 Chapter 4: The influence of Amazonian anthropogenic emissions on aerosol, cloud and surface rain

(1) What are the effects of anthropogenic emissions on aerosol, cloud and rain in Amazonia?

In this chapter, six simulations with varied anthropogenic emission scenarios by factors of 0-5 in a regional domain in Amazonia were performed. The simulation with default emission setup is used as a baseline simulation. The biogenic nucleation mechanism of (Kirkby et al. 2016) and a nucleation mechanism that involves sulfuric acid and organic gas molecules (Riccobono et al. 2014) are used for all simulations in Chapter 4. Such a combination of nucleation mechanisms was determined based on the observations from GoAmazon2014/5 which measured aerosols of various sizes below 2 km in altitude (Martin et al. 2016). Aerosol particle number concentrations have a positive relationship with anthropogenic emissions. Increasing anthropogenic emission enhances total particle concentrations by providing more H_2SO_4, which subsequently determines the nucleation rate based on the study of Riccobono et al. (2014). The ratios of the change in total particle concentrations to the change in emission rate show that the total particle concentration increases by 13% (relative to the baseline simulation) for each unit increase in anthropogenic emission in the polluted regions. The changes in aerosol concentrations are mainly driven by anthropogenic gas emissions within the regional domain, while anthropogenic primary aerosol emissions change the total aerosol concentrations by only 0.5% of the total particle concentrations averaged below 4 km altitude. It again confirms the results in Chapter 3 that particle concentrations in the Amazonian boundary layer are strongly dependent on long-range transport and that NPF in the regional domain has a limited effect on particle population

even when anthropogenic emissions are involved. (Section 4.3.2)

Cloud droplets are positively correlated with anthropogenic emissions, but cloud water and rain mass mixing ratios are not sensitive to the change in anthropogenic emissions. Cloud droplet number concentration increases by 9% in the cloudy area of the polluted regions as a result of 13% more aerosol particles. However, ice number concentration and total cloud water mass mixing ratio show random changes that are not correlated with anthropogenic emissions but rather likely caused by natural variability of different clouds. Surface rain in the six emission scenarios are similar with slight differences for the greatest rain water mass mixing ratios. The results of cloud and rain here help rule out the potential effects of rain scavenging in affecting total particle concentrations in the boundary layer during the dry-to-wet season in Chapter 3, and show that the changes in total particle concentrations are primarily caused by nucleation. (Section 4.3.3)

(2) What mechanisms drive the changes in cloud water and rain?

NPF associated with pollution plumes causes the increases in the total particle concentrations, which enhance CCN concentrations. Consequently, through microphysics, cloud droplet number concentrations are enhanced in the cloudy area of the polluted regions.

The insensitivity of cloud water and rain mass mixing ratio to anthropogenic emissions is either because the changes to anthropogenic emission do not efficiently affect cloud droplet concentrations, or because there are a lot of particles that have already suppressed rain in Amazonia, then additional particles formed by increasing anthropogenic emissions are buffered, and cloud and rain mass mixing ratio appear to be barely affected with additional aerosol particles in the environment. (Section 4.3.3)

6.1.3 Chapter 5: Effects of model resolution on non-linear biogenic new particle formation in Amazonia

(1) How are nucleation rates affected by averaging the input variables?

Chapter 3 and observations (Andreae et al. 2018) have demonstrated the significant number of particles that are produced by upper tropospheric NPF and the role of deep convection in supporting and affecting the NPF process. This chapter aimed to understand NPF in the upper troposphere and how it is affected by horizontal resolution by applying averaging. By calcu-

lating nucleation rates offline with averaged input values of the variables that control NPF, Chapter 5 found that the time- and domain-mean nucleation rates are generally reduced by spatial averaging, and are increased at a few altitudes. The changes vary with the assumed monoterpene oxidation rate. A slower monoterpene oxidation rate, which increases the length of time that monoterpenes can stay in the upper troposphere to at least more than 12 hours, shows smaller changes in nucleation rates after averaging. While a faster oxidation rate that only allows monoterpenes to persist for only around less than 10 hours, results in more significant changes (mostly reductions) in nucleation rates. The reductions in offline nucleation rates increase as resolutions decrease. (Section 5.3.1)

(2) What are the causes of the changes in nucleation rates by averaging?

In an horizontal domain of Amazonian upper troposphere, the monoterpene concentration and condensation sink are not homogeneously distributed because of deep convection and the inhomogeneity of monoterpenes are affected by a relatively short lifetime of monoterpene. Averaging to degraded resolutions smooths out the spatial variability of monoterpene and condensation sink. Because NPF rate is an non-linear function of spatially inhomogeneous monoterpene concentration and condensation sink, averaging causes changes in nucleation rates. Due to averaging, nucleation rate only occurs for smaller ranges of monoterpene concentration and condensation sink compared with high-resolution results, and thus coarse resolutions are not ideal for representing nucleation rates from monoterpenes.

The results show that averaging first smooths the domain by reducing the spatial variability of monoterpene and condensation sink which are not homogeneously distributed in Amazonian region because of deep convection. Second, averaging to degraded resolutions mostly leads to reduced and sometimes increased monoterpene and condensation sink. As resolution becomes lower, the changes in monoterpene concentration and condensation sink are stronger. It is because the distributions of monoterpene concentrations and condensation sink are skewed to lower values, suggesting that higher monoterpene and condensation sink are more likely to be lost due to averaging than the lower ones. As resolutions degrade, monoterpene concentrations and condensation sink tend to be more homogeneous over a region because larger areas are smoothed. (Section 5.3.2)

(3) How will the monoterpene oxidation rate affect the spatially non-linear nucle-

ation rate?

Inhomogeneous gas and condensation sink fields exist for both slow and fast monoterpene oxidation rates, but offline nucleation rates are more significantly affected by averaging to degraded resolutions when monoterpenes a have faster oxidation rate or a shorter lifetime. Short-lived monoterpenes have greater spatial variability because they do not have enough time to be well mixed with the surrounding air after being transported from surface and detrained by deep convection. Then, averaging to degraded resolutions will significantly smooth out the spatial variability of the concentrations, and will subsequently cause the domain averaged nucleation rates with relatively higher levels of uncertainties at coarser resolutions. However, when monoterpenes have a lifetime that is long enough, nucleation rates are less affected by averaging and monoterpenes will depend more on long-range transport instead of deep convective transport. (Section 5.3.2)

6.2 Limitations of this thesis and future work

Chapter 3 aimed to understand the sensitivity of particle concentrations of various sizes to NPF within a 1000 km regional domain and the role of deep convection in supporting NPF in the upper troposphere and transporting particles downward. This chapter uses a 1000 km regional domain at 4 km resolution. The size and resolution of the regional domain will limit our understandings of NPF that occurs within a regional scale to affect CCN and the efficiency of deep convection to transport aerosol particles vertically. Apart from affecting the vertical transport efficiency, resolution may also significantly influence nucleation rates in the region studied in Chapter 5. Thus, future studies are recommended to use a larger domain size and a higher resolution. It is also recommended to investigate both dry and wet seasons in Amazonia to better understand the particles in this environment. Additionally, more complex chemistry can be used in models to fully represent the chemical reactions for biogenic precursor gases and interactive oxidant chemistry in Amazonia, which is similar to Chapter 4 where a more realistic oxidant field was simulated. As chapter 3 pointed out, the importance of long-range transport for sustaining boundary layer CCN means that it is advantageous to use a driving global model or realistic time-varying chemical boundary conditions so that high-resolution regional models can better reproduce CCN concentrations in Amazonia. Unrealistic boundary conditions will dominate aerosol simulations over domains of the 1000 km and smaller.

Chapter 4 aimed to study the effects of anthropogenic emissions on aerosol and cloud in an Amazonian convective environment. In contrast to Chapter 3, Chapter 4 uses the biogenic nucleation mechanism with the default monoterpene oxidation and emission rates, and it also uses a mechanism that takes into account H_2SO_4 to allow nucleation to be affected by anthropogenic emissions. Additionally, NPF is only allowed between 100 m and 1 km in altitude. These choices were made to both include the effect of anthropogenic emissions on NPF and to match the modelled particle concentrations ($N_{D>3nm}$, $N_{D>10nm}$ and $N_{D>100nm}$) to the observations, but caused some limitations for the study. One of the limitations is that NPF in the upper troposphere was not included. The reasons for this were partly related to the data availability which were below around 2 km altitude in GoAmazon2014/5, while the observations in the ACRIDICON-CHUVA campaign in Chapter 3 were available in the upper troposphere, so that what happens in the upper troposphere in the wet season is unknown. Despite the lack of availability of observations, Chapter 3 as well as previous studies (Andreae et al. 2018; Williamson et al. 2019) have shown that NPF in the tropical upper troposphere can produce a significant number of new aerosol particles and can potentially supply boundary layer CCN (Merikanto et al. 2009). Consequently, removing upper tropospheric nucleation may cause a misrepresentation of the total particle concentrations in the region. Another limitation lies in the monoterpene oxidation rate, which was shown in Chapter 3 to significantly affect NPF in Amazonia. Although, Chapter 3 and 5 have shown that monoterpenes with a smaller oxidation rate can significantly enhance NPF compared to a faster oxidation rate, whether or how the oxidation rate is different between the dry and wet seasons is not clear. The influence of background aerosol and pollutant (biomass burning in dry-to-wet season and anthropogenic emission in wet season) is also not well understood. Thus, the choices of nucleation mechanism and monoterpene oxidation rate are uncertain for this region. Therefore, it is recommended for future studies to investigate the cause of inconsistency in modelled and observed $N_{D>3nm}$, $N_{D>10nm}$ and $N_{D>100nm}$ with the addition of upper tropospheric NPF and improve the NPF mechanism if necessary. It is also recommended that future studies focus on the response of a single cloud to anthropogenic emissions in order to understand the physical processes of an individual cloud and include heterogeneous ice nucleation microphysics.

In Chapter 5, two monoterpene oxidation rates were simulated and only the effects of monoterpene concentrations and condensation sink on nucleation rates were investigated in detail.

Therefore, the analyses may benefit from extra simulations with a faster oxidation rate, although some test simulations in Chapter 3 have indicated suppressed nucleation rate under this circumstance. The fifth chapter can also benefit from analysing the sensitivity of nucleation rate to the variation of the other input variables (concentrations of OH, O_3, H_2SO_4, and temperature) that are used to calculate nucleation rates. It is recommended for future regional modelling studies to further investigate the oxidation rate in a wider range and ideally a sequence of oxidation rates to produce a range of nucleating vapours, similar to the study of Murphy et al. (2015) which defined four ranges of volatility for organic vapours to form particles (extremely low volatility, low volatility, semivolatile, and intermediate volatility). Additionally, bringing oxidants, sulfuric acid and temperature fields that influence nucleation rates to the analyses will help understand the non-linear nucleation rates as a full picture. Thus, ensemble simulations which perturb all the input variables (monoterpene, oxidants, sulfuric acid, condensation sink and temperature) that affect nucleation at various resolutions are recommended to fully understand the nucleation in convective environment. It is also recommended to investigate how binary nucleation which depends on longer-lived gas precursor (SO_2) will be affected by spatial variability. Comparing NPF-deep convection interactions between a regional model and a global model is also recommended.

6.3 Implications of the research

The thesis shows the importance of using a regional model with high resolution and resolved convection to investigate NPF under the support of and interacts with deep convection in Amazonia, which can be achieved with a global model, but will be difficult because global models will need extra work on parameterisations, validations or tunings.

Chapter 3 showed the unique benefit of using a nested regional model which was driven by a global model through the model boundary conditions. The relative contribution of Amazonian particles from the region itself and from long-range transport were quantified. The results highlight the importance of long-range transport to sustain the majority of the boundary layer CCN, and also show the dominance of NPF in the regional domain to form particles in the upper troposphere.

With explicit convection, Chapter 3 was able to simulate cloud-scale processes, and allowed

transport of aerosols and gases by convection. Chapter 3 simulated biogenic NPF which is significantly affected by the vertically transported biogenic gas precursors (monoterpenes in the model). Transporting the right amount of monoterpene molecules by deep convection is vital because it will eventually affect the subsequently calculated NPF rates. Convection in the regional model allows the monoterpenes to quickly reach the upper troposphere, and allows monoterpene concentrations to vary across the heights from surface to 20 km altitude, and thereby affecting nucleation rates at different altitudes. Subsequently, the results show significant effect of deep convection to support NPF when it transports monoterpenes to the upper troposphere in this convective environment. Chapter 3 also shows that including explicit convection and advanced cloud microphysics (CASIM) will form clouds which can contribute to cloud condensation sink and suppress in-cloud NPF, while a global model may not be able to generate the right amount of cloud condensates to suppress NPF. Regional model results show the importance of including cloud condensation sink because it will affect nucleation and Aitken mode concentrations in the upper troposphere by 50%. Then, with explicit convection, only a few of the newly formed particles in the upper troposphere were found to be transported into the boundary layer in convective downdrafts within the 1000 km regional domain and occasionally account for less than 1% of the instantaneous boundary layer total particle concentrations. It indicated that particles could travel through a few convective cycles before they could be transported from upper troposphere to the boundary layer.

Chapter 4 and Chapter 5 show the importance of using both high-resolution and explicit convection in the models. Regional model simulations in Chapter 4 quantified the aerosol and cloud properties affected by six anthropogenic emission scenarios in the regional domain. High-resolution pollution plumes emitted from Manaus city were included, and the analyses focused precisely in the polluted regions. The results show that convective clouds were not sensitive to changes in regional anthropogenic emissions in this complex convective environment unless cloud droplet number concentrations are significantly changed. Or the rain has already been suppressed by large number of particles in the pristine Amazonia, thereby causing insensitive response of clouds to increments in anthropogenic emissions. The results improved our understandings of aerosol-cloud interactions under the influence of regional anthropogenic emissions within a complex convective environment.

Chapter 5 made use of high-resolution model output and investigated effects of coarse resolu-

tions on non-linear biogenic nucleation rate under the influence of spatially inhomogeneous gas precursors, oxidants, condensation sink and temperature in the Amazonian upper troposphere. The results highlight the importance of using high resolution models with resolved convection to simulate biogenic nucleation in the upper troposphere. It is because NPF rate is a non-linear function of the above variables and is affected by the significant spatial variability of condensation sink and gas precursor concentrations. The spatial variability of condensation sink was caused by deep convection which contributes to cloud condensation sink. The spatial variability of gas precursors was significant because gas precursors were transported by deep convection, and because the short-lived monoterpenes do not have enough time to be homogeneously distributed in the upper troposphere and to reach the regions of low condensation to contribute to NPF. In contrast, the global models with coarse resolutions may not well represent the sub-grid spatial variability, subsequently the global models may produce less accurate domain-mean nucleation rates, and eventually it will affect the production of particle number concentrations.

In conclusion, this thesis investigated the processes that happen in a regional model under the influence of global long-range transport, and thus uniquely provides new insights for the Amazonian region and for many other regions. Aerosol populations and anthropogenic emissions in the regional model are also affected by processing in the global model outside of the domain, since aerosols and gases enter the regional domain through the boundary conditions that are set by the global model. The effect from the global model is found to have a significant influence on the processes in the selected Amazonian regional model domain. This is because the global model can simulate longer time periods and represents connected regions over larger scales than are possible with regional model domains. However, many sub-grid scale processes may not be well-represented by global models, and the rough estimation by the global models may substantially change the results (e.g. nucleation rate) over the global scale. In the thesis, deep convection is found to strongly modulate processes such as vertical transport, oxidation of short-lived species (monoterpenes) and nucleation which usually occurs over spatiotemporal scales of a few hours and a few kilometers. Then, these features are difficult for global models with coarse resolution and parameterised convection to simulate, which may subsequently increase the level of uncertainty in driving the regional models. Such uncertainty can be reduced by performing global models at a high enough resolution to explicitly simulate convection which would resolve the cloud-scale processes, as has been reported in Stevens et al. (2019). However,

two-moment aerosol microphysics would need to be added to the already expensive simulations to achieve aerosol-cloud interactions. Therefore, this thesis shows that it is necessary to improve the global models with regards to clouds, biogenic nucleation and vertical transport in order to gain a better understanding of the global scale.

References

Abdul-Razzak, Hayder and Ghan, Steven J (2000). "A parameterization of aerosol activation: 2. Multiple aerosol types". In: *Journal of Geophysical Research: Atmospheres* 105.D5, pp. 6837–6844. DOI: https://doi.org/10.1029/1999JD901161.

Ackerman, Andrew S, Kirkpatrick, Michael P, Stevens, David E, and Toon, Owen B (2004). "The impact of humidity above stratiform clouds on indirect aerosol climate forcing". In: *Nature* 432.7020, p. 1014. DOI: https://doi.org/10.1038/nature03174.

Ajith, T.C., Kompalli, Sobhan Kumar, Nair, Vijayakumar S., and Babu, S. Suresh (2022). "Mesoscale variations of the chemical composition of submicron aerosols and its influence on the cloud condensation nuclei activation". In: *Atmospheric Environment* 268, p. 118778. DOI: https://doi.org/10.1016/j.atmosenv.2021.118778.

Albrecht, Bruce A (1989). "Aerosols, cloud microphysics, and fractional cloudiness". In: *Science* 245.4923, pp. 1227–1230. DOI: 10.1126/science.245.4923.1227.

Alizadeh-Choobari, O. (2018). "Impact of aerosol number concentration on precipitation under different precipitation rates". In: *Meteorological Applications* 25.4, pp. 596–605. DOI: https://doi.org/10.1002/met.1724. eprint: https://rmets.onlinelibrary.wiley.com/doi/pdf/10.1002/met.1724.

Almeida, João, Schobesberger, Siegfried, Kürten, Andreas, Ortega, Ismael K, Kupiainen-Määttä, Oona, Praplan, Arnaud P, Adamov, Alexey, Amorim, Antonio, Bianchi, Federico, Breitenlechner, Martin, et al. (2013). "Molecular understanding of sulphuric acid–amine particle nucleation in the atmosphere". In: *Nature* 502.7471, p. 359. DOI: https://doi.org/10.1038/nature12663.

Andreae, M. O. (2009). "Correlation between cloud condensation nuclei concentration and aerosol optical thickness in remote and polluted regions". In: *Atmospheric Chemistry and Physics* 9.2, pp. 543–556. DOI: 10.5194/acp-9-543-2009.

Andreae, M. O., Andreae, T. W., Ditas, F., and Pöhlker, C. (2022). "Frequent new particle formation at remote sites in the subboreal forest of North America". In: *Atmospheric Chemistry and Physics* 22.4, pp. 2487–2505. DOI: 10.5194/acp-22-2487-2022.

Andreae, Meinrat O, Afchine, Armin, Albrecht, Rachel, Holanda, Bruna Amorim, Artaxo, Paulo, Barbosa, Henrique MJ, Borrmann, Stephan, Cecchini, Micael A, Costa, Anja, Dollner, Maximilian, et al. (2018). "Aerosol characteristics and particle production in the upper troposphere over the Amazon Basin". In: *Atmospheric Chemistry and Physics* 18.2, pp. 921–961. DOI: https://doi.org/10.5194/acp-18-921-2018.

Andres, R. J. and Kasgnoc, A. D. (1998). "A time-averaged inventory of subaerial volcanic sulfur emissions". In: *Journal of Geophysical Research: Atmospheres* 103.D19, pp. 25251–25261. DOI: https://doi.org/10.1029/98JD02091. eprint: https://agupubs.onlinelibrary.wiley.com/doi/pdf/10.1029/98JD02091.

Andronache, C (2003). "Estimated variability of below-cloud aerosol removal by rainfall for observed aerosol size distributions". In: *Atmospheric Chemistry and Physics* 3.1, pp. 131–143. DOI: https://doi.org/10.5194/acp-3-131-2003.

Ångström, Anders (1929). "On the Atmospheric Transmission of Sun Radiation and on Dust in the Air". In: *Geografiska Annaler* 11.2, pp. 156–166. DOI: 10.1080/20014422.1929.11880498. eprint: https://doi.org/10.1080/20014422.1929.11880498.

Archibald, A. T., O'Connor, F. M., Abraham, N. L., Archer-Nicholls, S., Chipperfield, M. P., Dalvi, M., Folberth, G. A., Dennison, F., Dhomse, S. S., Griffiths, P. T., Hardacre, C., Hewitt, A. J., Hill, R. S., Johnson, C. E., Keeble, J., Köhler, M. O., Morgenstern, O., Mulcahy, J. P., Ordóñez, C., Pope, R. J., Rumbold, S. T., Russo, M. R., Savage, N. H., Sellar, A., Stringer, M., Turnock, S. T., Wild, O., and Zeng, G. (2020). "Description and evaluation of the UKCA stratosphere–troposphere chemistry scheme (StratTrop vn 1.0) implemented in UKESM1". In: *Geoscientific Model Development* 13.3, pp. 1223–1266. DOI: 10.5194/gmd-13-1223-2020.

Arias, P.A., Bellouin, N., Coppola, E., Jones, R.G., Krinner, G., Marotzke, J., Naik, V., Palmer, M.D., Plattner, G.-K., Rogelj, J., Rojas, M., Sillmann, J., Storelvmo, T., Thorne, P.W., Trewin, B., Achuta Rao, K., Adhikary, B., Allan, R.P., Armour, K., Bala, G., Barimalala, R., Berger, S., Canadell, J.G., Cassou, C., Cherchi, A., Collins, W., Collins, W.D., Connors, S.L., Corti, S., Cruz, F., Dentener, F.J., Dereczynski, C., Di Luca, A., Diongue Niang, A., Doblas-Reyes, F.J., Dosio, A., Douville, H., Engelbrecht, F., Eyring, V., Fischer, E., Forster, P., Fox-Kemper, B., Fuglestvedt, J.S., Fyfe, J.C., Gillett, N.P., Goldfarb, L., Gorodetskaya, I., Gutierrez, J.M., Hamdi, R., Hawkins, E., Hewitt, H.T., Hope, P., Islam, A.S., Jones, C., Kaufman, D.S., Kopp, E.E., Kosaka, Y., Kossin, J., Krakovska, S., Lee, J.-Y., Li, J., Mauritsen, T., Maycock, T.K., Meinshausen, M., Min, S.-K., Monteiro, P.M.S., Ngo-Duc, T., Otto, F., Pinto, I., Pirani, A., Raghavan, K., Ranasinghe, R., Ruane, A.C., Ruiz, L., Sallée, J.-B., Samset, B.H., Sathyendranath, S., Seneviratne, S.I., Sörensson, A.A., Szopa, S., Takayabu, I., Tréguier, A.-M., Hurk, B. van den, Vautard, R., Schuckmann, K. von, Zaehle, S., Zhang, X., and Zickfeld, K. (2021). *IPCC, 2021: Technical Summary*. Tech. rep. Cambridge University Press, Cambridge, United Kingdom and New York, NY, USA: Climate Change 2021: The Physical Science Basis. Contribution of Working Group I to the Sixth Assessment Report of the Intergovernmental Panel on Climate Change [Masson-Delmotte, V., P. Zhai, A. Pirani, S.L. Connors, C. Péan, S. Berger, N. Caud, Y. Chen, L. Goldfarb, M.I. Gomis, M. Huang, K. Leitzell, E. Lonnoy, J.B.R. Matthews, T.K. Maycock, T. Waterfield, O. Yelekçi, R. Yu, and B. Zhou (eds.)], pp. 33–144.

Asmi, E., Kivekäs, N., Kerminen, V.-M., Komppula, M., Hyvärinen, A.-P., Hatakka, J., Viisanen, Y., and Lihavainen, H. (2011). "Secondary new particle formation in Northern Finland Pallas site between the years 2000 and 2010". In: *Atmospheric Chemistry and Physics* 11.24, pp. 12959–12972. DOI: 10.5194/acp-11-12959-2011.

Baklanov, Alexander, Elperin, Tov, Fominykh, Andrew, and Krasovitov, Boris (2013). "Cell model of in-cloud scavenging of highly soluble gases". In: *Journal of Atmospheric and Solar-Terrestrial Physics* 97, pp. 135–142. DOI: https://doi.org/10.1016/j.jastp.2013.02.018.

Bardakov, Roman, Riipinen, Ilona, Krejci, Radovan, Savre, Julien, Thornton, Joel A, and Ekman, Annica ML (2020). "A novel framework to study trace gas transport in deep convective clouds". In: *Journal of Advances in Modeling Earth Systems* 12.5, e2019MS001931.

Barth, Mary C., Cantrell, Christopher A., Brune, William H., Rutledge, Steven A., Crawford, James H., Huntrieser, Heidi, Carey, Lawrence D., MacGorman, Donald, Weisman, Morris, Pickering, Kenneth E., Bruning, Eric, Anderson, Bruce, Apel, Eric, Biggerstaff, Michael, Campos, Teresa, Campuzano-Jost, Pedro, Cohen, Ronald, Crounse, John, Day, Douglas A., Diskin, Glenn, Flocke, Frank, Fried, Alan, Garland, Charity, Heikes, Brian, Honomichl, Shawn, Hornbrook, Rebecca, Huey, L. Gregory, Jimenez, Jose L., Lang, Timothy, Lichtenstern, Michael, Mikoviny, Tomas, Nault, Benjamin, O'Sullivan, Daniel, Pan, Laura L., Peischl, Jeff, Pollack, Ilana, Richter, Dirk, Riemer, Daniel, Ryerson, Thomas, Schlager, Hans, Clair, Jason St., Walega, James, Weibring, Petter, Weinheimer, Andrew, Wennberg, Paul, Wisthaler, Armin, Wooldridge, Paul J., and Ziegler, Conrad (2015). "The Deep Convective Clouds and Chemistry (DC3) Field Campaign". In: *Bulletin of the American Meteorological Society* 96.8, pp. 1281–1309. DOI: 10.1175/BAMS-D-13-00290.1.

Barthlott, C., Zarboo, A., Matsunobu, T., and Keil, C. (2022). "Importance of aerosols and shape of the cloud droplet size distribution for convective clouds and precipitation". In: *Atmospheric Chemistry and Physics* 22.3, pp. 2153–2172. DOI: 10.5194/acp-22-2153-2022.

Barthlott, Christian and Hoose, Corinna (2018). "Aerosol Effects on Clouds and Precipitation over Central Europe in Different Weather Regimes". In: *Journal of the Atmospheric Sciences* 75.12, pp. 4247–4264. DOI: 10.1175/JAS-D-18-0110.1.

Bela, Megan M, Barth, Mary C, Toon, Owen B, Fried, Alan, Homeyer, Cameron R, Morrison, Hugh, Cummings, Kristin A, Li, Yunyao, Pickering, Kenneth E, Allen, Dale J, et al. (2016). "Wet scavenging of soluble gases in DC3 deep convective storms using WRF-Chem simulations and aircraft observations". In: *Journal of Geophysical Research: Atmospheres* 121.8, pp. 4233–4257. DOI: https://doi.org/10.1002/2015JD024623.

Bela, Megan M, Barth, Mary C, Toon, Owen Brian, Fried, Alan, Ziegler, Conrad, Cummings, Kristin A, Li, Yunyao, Pickering, Kenneth E, Homeyer, Cameron R, Morrison, Hugh, et al. (2018). "Effects of scavenging, entrainment, and aqueous chemistry on peroxides and

formaldehyde in deep convective outflow over the central and Southeast United States". In: *Journal of Geophysical Research: Atmospheres* 123.14, pp. 7594–7614. DOI: https://doi.org/10.1029/2018JD028271.

Beydoun, H. and Hoose, C. (2019). "Aerosol-Cloud-Precipitation Interactions in the Context of Convective Self-Aggregation". In: *Journal of Advances in Modeling Earth Systems* 11.4, pp. 1066–1087. DOI: https://doi.org/10.1029/2018MS001523. eprint: https://agupubs.onlinelibrary.wiley.com/doi/pdf/10.1029/2018MS001523.

Bianchi, F, Junninen, H, Bigi, A, Sinclair, VA, Dada, L, Hoyle, CR, Zha, Q, Yao, L, Ahonen, LR, Bonasoni, P, et al. (2020). "Biogenic particles formed in the Himalaya as an important source of free tropospheric aerosols". In: *Nature Geoscience*, pp. 1–6. DOI: https://doi.org/10.1038/s41561-020-00661-5.

Bianchi, Federico, Kurtén, Theo, Riva, Matthieu, Mohr, Claudia, Rissanen, Matti P., Roldin, Pontus, Berndt, Torsten, Crounse, John D., Wennberg, Paul O., Mentel, Thomas F., Wildt, Jürgen, Junninen, Heikki, Jokinen, Tuija, Kulmala, Markku, Worsnop, Douglas R., Thornton, Joel A., Donahue, Neil, Kjaergaard, Henrik G., and Ehn, Mikael (Mar. 2019). "Highly Oxygenated Organic Molecules (HOM) from Gas-Phase Autoxidation Involving Peroxy Radicals: A Key Contributor to Atmospheric Aerosol". In: *Chemical Reviews* 119.6, pp. 3472–3509. DOI: 10.1021/acs.chemrev.8b00395.

Bianchi, Federico, Tröstl, Jasmin, Junninen, Heikki, Frege, Carla, Henne, Stephan, Hoyle, Christopher R, Molteni, Ugo, Herrmann, Erik, Adamov, Alexey, Bukowiecki, Nicolas, et al. (2016). "New particle formation in the free troposphere: A question of chemistry and timing". In: *Science* 352.6289, pp. 1109–1112. DOI: 10.1126/science.aad5456.

Boucher, O., Randall, D., Artaxo, P., Bretherton, C., Feingold, G., Forster, P., Kerminen, V.-M., Kondo, Y., Liao, H., Lohmann, U., Rasch, P., Satheesh, S.K., Sherwood, S., Stevens, B., and Zhang, X.Y. (2013). "Clouds and Aerosols". In: *Climate Change 2013: The Physical Science Basis. Contribution of Working Group I to the Fifth Assessment Report of the Intergovernmental Panel on Climate Change*. Ed. by T.F. Stocker, D. Qin, G.-K. Plattner, M. Tignor, S.K. Allen, J. Boschung, A. Nauels, Y. Xia, V. Bex, and P.M. Midgley. Cambridge, United

Kingdom and New York, NY, USA: Cambridge University Press. Chap. 7, pp. 571–658. DOI: 10.1017/CBO9781107415324.016.

Boucher, Olivier (2015). *Atmospheric aerosols: Properties and climate impacts*. Springer. DOI: https://doi.org/10.1007/978-94-017-9649-1_2.

Cahalan, Robert F., Ridgway, William, Wiscombe, Warren J., Bell, Thomas L., and Snider, Jack B. (1994). "The Albedo of Fractal Stratocumulus Clouds". In: *Journal of Atmospheric Sciences* 51.16, pp. 2434–2455. DOI: 10.1175/1520-0469(1994)051<2434:TAOFSC>2.0.CO;2.

Carrio, G. G. and Cotton, W. R. (2011). "Investigations of aerosol impacts on hurricanes: virtual seeding flights". In: *Atmospheric Chemistry and Physics* 11.6, pp. 2557–2567. DOI: 10.5194/acp-11-2557-2011.

Carslaw, Ken S., ed. (2022). *Aerosols and Climate*. San Diego: Elsevier.

Cecchini, M. A., Machado, L. A. T., Comstock, J. M., Mei, F., Wang, J., Fan, J., Tomlinson, J. M., Schmid, B., Albrecht, R., Martin, S. T., and Artaxo, P. (2016). "Impacts of the Manaus pollution plume on the microphysical properties of Amazonian warm-phase clouds in the wet season". In: *Atmospheric Chemistry and Physics* 16.11, pp. 7029–7041. DOI: 10.5194/acp-16-7029-2016.

Charlson, R. J., Schwartz, S. E., Hales, J. M., Cess, R. D., Coakley, J. A., Hansen, J. E., and Hofmann, D. J. (1992). "Climate Forcing by Anthropogenic Aerosols". In: *Science* 255.5043, pp. 423–430. DOI: 10.1126/science.255.5043.423. eprint: https://www.science.org/doi/pdf/10.1126/science.255.5043.423.

Chen, Q., Koren, I., Altaratz, O., Heiblum, R. H., Dagan, G., and Pinto, L. (2017). "How do changes in warm-phase microphysics affect deep convective clouds?" In: *Atmospheric Chemistry and Physics* 17.15, pp. 9585–9598. DOI: 10.5194/acp-17-9585-2017.

Chen, Xiao and Xie, Shaocheng (Jan. 1996). "armbecldrad". In: DOI: 10.5439/1333228.

Chen, Ying, Haywood, Jim, Wang, Yu, Malavelle, Florent, Jordan, George, Partridge, Daniel, Fieldsend, Jonathan, De Leeuw, Johannes, Schmidt, Anja, Cho, Nayeong, Oreopoulos, Lazaros,

Platnick, Steven, Grosvenor, Daniel, Field, Paul, and Lohmann, Ulrike (2022). "Machine learning reveals climate forcing from aerosols is dominated by increased cloud cover". In: *Nature Geoscience* 15.8, pp. 609–614. DOI: 10.1038/s41561-022-00991-6.

Cirino, Glauber, Brito, Joel, Barbosa, Henrique MJ, Rizzo, Luciana V, Tunved, Peter, Sá, Suzane S de, Jimenez, Jose L, Palm, Brett B, Carbone, Samara, Lavric, Jost V, et al. (2018). "Observations of Manaus urban plume evolution and interaction with biogenic emissions in GoAmazon 2014/5". In: *Atmospheric Environment* 191, pp. 513–524. DOI: https://doi.org/10.1016/j.atmosenv.2018.08.031.

Clarke, A. D., Freitag, S., Simpson, R. M. C., Hudson, J. G., Howell, S. G., Brekhovskikh, V. L., Campos, T., Kapustin, V. N., and Zhou, J. (2013). "Free troposphere as a major source of CCN for the equatorial pacific boundary layer: long-range transport and teleconnections". In: *Atmospheric Chemistry and Physics* 13.15, pp. 7511–7529. DOI: https://doi.org/10.5194/acp-13-7511-2013.

Clarke, AD, Eisele, F, Kapustin, VN, Moore, Ko, Tanner, D, Mauldin, L, Litchy, M, Lienert, B, Carroll, MA, and Albercook, G (1999a). "Nucleation in the equatorial free troposphere: Favorable environments during PEM-Tropics". In: *Journal of Geophysical Research: Atmospheres* 104.D5, pp. 5735–5744. DOI: https://doi.org/10.1029/98JD02303.

Clarke, AD, Kapustin, VN, Eisele, FL, Weber, RJ, and McMurry, Peter H (1999b). "Particle production near marine clouds: Sulfuric acid and predictions from classical binary nucleation". In: *Geophysical Research Letters* 26.16, pp. 2425–2428. DOI: https://doi.org/10.1029/1999GL900438.

Clarke, AD, Varner, JL, Eisele, F, Mauldin, RL, Tanner, D, and Litchy, M (1998). "Particle production in the remote marine atmosphere: Cloud outflow and subsidence during ACE 1". In: *Journal of Geophysical Research: Atmospheres* 103.D13, pp. 16397–16409. DOI: https://doi.org/10.1029/97JD02987.

Clarke, Antony D and Kapustin, Vladimir N (2002). "A Pacific aerosol survey. Part I: A decade of data on particle production, transport, evolution, and mixing in the troposphere". In: *Journal of the atmospheric sciences* 59.3, pp. 363–382. DOI: https://doi.org/10.1175/1520-0469(2002)059<0363:APASPI>2.0.CO;2.

Cofala, Janusz, Amann, Markus, and Mechler, Reinhard (2005). "Scenarios of World Anthropogenic Emissions of Air Pollutants and Methane up to 2030. International Institute for Applied Systems Analysis. Laxemburg, Austria". In: *Tech. rep., International Institute for Applied Systems Analysis (IIASA), Laxenburg, Austria.*

Collow, Allison B Marquardt, Miller, Mark A, and Trabachino, Lynne C (2016). "Cloudiness over the Amazon rainforest: Meteorology and thermodynamics". In: *Journal of Geophysical Research: Atmospheres* 121.13, pp. 7990–8005. DOI: https://doi.org/10.1002/2016JD024848.

Connolly, PJ, Vaughan, G, May, PT, Chemel, C, Allen, G, Choularton, TW, Gallagher, MW, Bower, KN, Crosier, J, and Dearden, C (2013). "Can aerosols influence deep tropical convection? Aerosol indirect effects in the Hector island thunderstorm". In: *Quarterly Journal of the Royal Meteorological Society* 139.677, pp. 2190–2208. DOI: https://doi.org/10.1002/qj.2083.

Cotton, William R. and Walko, Robert (2021). "Examination of Aerosol-Induced Convective Invigoration Using Idealized Simulations". In: *Journal of the Atmospheric Sciences* 78.1, pp. 287–298. DOI: 10.1175/JAS-D-20-0023.1.

Crumeyrolle, S., Kontkanen, J., Rose, C., Velasquez Garcia, A., Bourrianne, E., Catalfamo, M., Riffault, V., Tison, E., Ferreira de Brito, J., Visez, N., Ferlay, N., Auriol, F., and Chiapello, I. (2022). "Measurement report: Atmopsheric new particle formation in a peri-urban site in Lille, Northern France". In: *Atmospheric Chemistry and Physics Discussions* 2022, pp. 1–35. DOI: 10.5194/acp-2022-436.

Cui, Zhiqiang and Carslaw, Kenneth S (2006). "Enhanced vertical transport efficiency of aerosol in convective clouds due to increases in tropospheric aerosol abundance". In: *Journal of Geophysical Research: Atmospheres* 111.D15. DOI: https://doi.org/10.1029/2005JD006781.

Dagan, Guy, Stier, Philip, Spill, George, Herbert, Ross, Heikenfeld, Max, Heever, Susan C. van den, and Marinescu, Peter J. (2022). "Boundary conditions representation can determine simulated aerosol effects on convective cloud fields". In: *Communications Earth & Environment* 3.1, p. 71. DOI: 10.1038/s43247-022-00399-5.

Dal Maso, M, Kulmala, M, Lehtinen, Kari EJ, Mäkelä, JM, Aalto, P, and O'Dowd, CD (2002). "Condensation and coagulation sinks and formation of nucleation mode particles in coastal and boreal forest boundary layers". In: *Journal of Geophysical Research: Atmospheres* 107.D19, PAR–2. DOI: https://doi.org/10.1029/2001JD001053.

Das, Sampa, Harshvardhan, H., Bian, Huisheng, Chin, Mian, Curci, Gabriele, Protonotariou, Anna P., Mielonen, Tero, Zhang, Kai, Wang, Hailong, and Liu, Xiaohong (2017). "Biomass burning aerosol transport and vertical distribution over the South African-Atlantic region". In: *Journal of Geophysical Research: Atmospheres* 122.12, pp. 6391–6415. DOI: https://doi.org/10.1002/2016JD026421. eprint: https://agupubs.onlinelibrary.wiley.com/doi/pdf/10.1002/2016JD026421.

Derbyshire, S. H., Maidens, A. V., Milton, S. F., Stratton, R. A., and Willett, M. R. (2011). "Adaptive detrainment in a convective parametrization". In: *Quarterly Journal of the Royal Meteorological Society* 137.660, pp. 1856–1871. DOI: https://doi.org/10.1002/qj.875. eprint: https://rmets.onlinelibrary.wiley.com/doi/pdf/10.1002/qj.875.

Devine, GM, Carslaw, KS, Parker, DJ, and Petch, JC (2006). "The influence of subgrid surface-layer variability on vertical transport of a chemical species in a convective environment". In: *Geophysical research letters* 33.15. DOI: https://doi.org/10.1029/2006GL025986.

Dias, A., Ehrhart, S., Vogel, A., Williamson, C., Almeida, J., Kirkby, J., Mathot, S., Mumford, S., and Onnela, A. (2017). "Temperature uniformity in the CERN CLOUD chamber". In: *Atmospheric Measurement Techniques* 10.12, pp. 5075–5088. DOI: 10.5194/amt-10-5075-2017.

Dickerson, R. R., Huffman, G. J., Luke, W. T., Nunnermacker, L. J., Pickering, K. E., Leslie, A. C. D., Lindsey, C. G., Slinn, W. G. N., Kelly, T. J., Daum, P. H., Delany, A. C., Greenberg, J. P., Zimmerman, P. R., Boatman, J. F., Ray, J. D., and Stedman, D. H. (1987). "Thunderstorms: An Important Mechanism in the Transport of Air Pollutants". In: *Science* 235.4787, pp. 460–465. DOI: 10.1126/science.235.4787.460. eprint: https://www.science.org/doi/pdf/10.1126/science.235.4787.460.

Diehl, T., Heil, A., Chin, M., Pan, X., Streets, D., Schultz, M., and Kinne, S. (2012). "Anthropogenic, biomass burning, and volcanic emissions of black carbon, organic carbon, and

$SO_2 from 1980 to 2010 for hindcast model experiments$". In: *Atmospheric Chemistry and Physics Discussions* 12, pp. 24895–24954. DOI: 10.5194/acpd-12-24895-2012.

Dingilian, Kayane K., Lippe, Martina, Kubečka, Jakub, Krohn, Jan, Li, Chenxi, Halonen, Roope, Keshavarz, Fatemeh, Reischl, Bernhard, Kurtén, Theo, Vehkamäki, Hanna, Signorell, Ruth, and Wyslouzil, Barbara E. (May 2021). "New Particle Formation from the Vapor Phase: From Barrier-Controlled Nucleation to the Collisional Limit". In: *The Journal of Physical Chemistry Letters* 12.19, pp. 4593–4599. DOI: 10.1021/acs.jpclett.1c00762.

Donahue, N. M., Robinson, A. L., Stanier, C. O., and Pandis, S. N. (Apr. 2006). "Coupled Partitioning, Dilution, and Chemical Aging of Semivolatile Organics". In: *Environmental Science & Technology* 40.8, pp. 2635–2643. DOI: 10.1021/es052297c.

Douglas, A. and L'Ecuyer, T. (2021). "Global evidence of aerosol-induced invigoration in marine cumulus clouds". In: *Atmospheric Chemistry and Physics* 21.19, pp. 15103–15114. DOI: 10.5194/acp-21-15103-2021.

Dunne, Eimear M, Gordon, Hamish, Kürten, Andreas, Almeida, João, Duplissy, Jonathan, Williamson, Christina, Ortega, Ismael K, Pringle, Kirsty J, Adamov, Alexey, Baltensperger, Urs, et al. (2016). "Global atmospheric particle formation from CERN CLOUD measurements". In: *Science* 354.6316, pp. 1119–1124. DOI: 10.1126/science.aaf2649.

Duplissy, Jonathan, Merikanto, J, Franchin, A, Tsagkogeorgas, G, Kangasluoma, J, Wimmer, D, Vuollekoski, H, Schobesberger, S, Lehtipalo, K, Flagan, RC, et al. (2016). "Effect of ions on sulfuric acid-water binary particle formation: 2. Experimental data and comparison with QC-normalized classical nucleation theory". In: *Journal of Geophysical Research: Atmospheres* 121.4, pp. 1752–1775. DOI: https://doi.org/10.1002/2015JD023539.

Dye, J. E., Ridley, B. A., Skamarock, W., Barth, M., Venticinque, M., Defer, E., Blanchet, P., Thery, C., Laroche, P., Baumann, K., Hubler, G., Parrish, D. D., Ryerson, T., Trainer, M., Frost, G., Holloway, J. S., Matejka, T., Bartels, D., Fehsenfeld, F. C., Tuck, A., Rutledge, S. A., Lang, T., Stith, J., and Zerr, R. (2000). "An overview of the Stratospheric-Tropospheric Experiment: Radiation, Aerosols, and Ozone (STERAO)-Deep Convection experiment with results for the July 10, 1996 storm". In: *Journal of Geophysical Research:*

Atmospheres 105.D8, pp. 10023–10045. DOI: https://doi.org/10.1029/1999JD901116. eprint: https://agupubs.onlinelibrary.wiley.com/doi/pdf/10.1029/1999JD901116.

Eguchi, K., Uno, I., Yumimoto, K., Takemura, T., Shimizu, A., Sugimoto, N., and Liu, Z. (2009). "Trans-pacific dust transport: integrated analysis of NASA/CALIPSO and a global aerosol transport model". In: *Atmospheric Chemistry and Physics* 9.9, pp. 3137–3145. DOI: 10.5194/acp-9-3137-2009.

Ehn, Mikael, Thornton, Joel A., Kleist, Einhard, Sipilä, Mikko, Junninen, Heikki, Pullinen, Iida, Springer, Monika, Rubach, Florian, Tillmann, Ralf, Lee, Ben, Lopez-Hilfiker, Felipe, Andres, Stefanie, Acir, Ismail-Hakki, Rissanen, Matti, Jokinen, Tuija, Schobesberger, Siegfried, Kangasluoma, Juha, Kontkanen, Jenni, Nieminen, Tuomo, Kurtén, Theo, Nielsen, Lasse B., Jørgensen, Solvejg, Kjaergaard, Henrik G., Canagaratna, Manjula, Maso, Miikka Dal, Berndt, Torsten, Petäjä, Tuukka, Wahner, Andreas, Kerminen, Veli-Matti, Kulmala, Markku, Worsnop, Douglas R., Wildt, Jürgen, and Mentel, Thomas F. (2014). "A large source of low-volatility secondary organic aerosol". In: *Nature* 506.7489, pp. 476–479. DOI: 10.1038/nature13032.

Ekman, A. M. L., Engström, A., and Wang, C. (2007). "The effect of aerosol composition and concentration on the development and anvil properties of a continental deep convective cloud". In: *Quarterly Journal of the Royal Meteorological Society* 133.627, pp. 1439–1452. DOI: https://doi.org/10.1002/qj.108. eprint: https://rmets.onlinelibrary.wiley.com/doi/pdf/10.1002/qj.108.

Ekman, AML, Wang, Chen, Wilson, J, and Ström, J (2004). "Explicit simulations of aerosol physics in a cloud-resolving model: A sensitivity study based on an observed convective cloud". In: *Atmospheric Chemistry and Physics* 4.3, pp. 773–791. DOI: https://doi.org/10.5194/acp-4-773-2004.

Elperin, Tov, Fominykh, Andrew, and Krasovitov, Boris (2015). "Precipitation scavenging of gaseous pollutants having arbitrary solubility in inhomogeneous atmosphere". In: *Meteorology and Atmospheric Physics* 127.2, pp. 205–216. DOI: 10.1007/s00703-014-0358-9.

– (2017). “Wet precipitation scavenging of soluble atmospheric trace gases due to chemical absorption in inhomogeneous atmosphere”. In: *Meteorology and Atmospheric Physics* 129.1, pp. 1–15. DOI: 10.1007/s00703-016-0449-x.

Eyring, V., Bony, S., Meehl, G. A., Senior, C. A., Stevens, B., Stouffer, R. J., and Taylor, K. E. (2016). “Overview of the Coupled Model Intercomparison Project Phase 6 (CMIP6) experimental design and organization”. In: *Geoscientific Model Development* 9.5, pp. 1937–1958. DOI: 10.5194/gmd-9-1937-2016.

Fan, Jiwen, Leung, L Ruby, Li, Zhanqing, Morrison, Hugh, Chen, Hongbin, Zhou, Yuquan, Qian, Yun, and Wang, Yuan (2012). “Aerosol impacts on clouds and precipitation in eastern China: Results from bin and bulk microphysics”. In: *Journal of Geophysical Research: Atmospheres* 117.D16. DOI: https://doi.org/10.1029/2011JD016537.

Fan, Jiwen, Leung, L Ruby, Rosenfeld, Daniel, Chen, Qian, Li, Zhanqing, Zhang, Jinqiang, and Yan, Hongru (2013). “Microphysical effects determine macrophysical response for aerosol impacts on deep convective clouds”. In: *Proceedings of the National Academy of Sciences* 110.48, E4581–E4590. DOI: https://doi.org/10.1073/pnas.1316830110.

Fan, Jiwen, Rosenfeld, Daniel, Zhang, Yuwei, Giangrande, Scott E, Li, Zhanqing, Machado, Luiz AT, Martin, Scot T, Yang, Yan, Wang, Jian, Artaxo, Paulo, et al. (2018). “Substantial convection and precipitation enhancements by ultrafine aerosol particles”. In: *Science* 359.6374, pp. 411–418. DOI: 10.1126/science.aan8461.

Fan, Jiwen, Wang, Yuan, Rosenfeld, Daniel, and Liu, Xiaohong (2016). “Review of aerosol–cloud interactions: mechanisms, significance, and challenges”. In: *Journal of the Atmospheric Sciences* 73.11, pp. 4221–4252. DOI: https://doi.org/10.1175/JAS-D-16-0037.1.

Fan, Jiwen, Zhang, Renyi, Li, Guohui, and Tao, Wei-Kuo (2007). “Effects of aerosols and relative humidity on cumulus clouds”. In: *Journal of Geophysical Research: Atmospheres* 112.D14.

Field, Paul R., Hill, Adrian, Shipway, Ben, Furtado, Kalli, Wilkinson, Jonathan, Miltenberger, Annette, Gordon, Hamish, Grosvenor, Daniel P., Stevens, Robin, and Van Weverberg, Kwinten (2023). “Implementation of a Double Moment Cloud Microphysics Scheme in the UK Met Office Regional Numerical Weather Prediction Model”. In: *Quarterly Journal of the*

Royal Meteorological Society n/a.n/a. DOI: https://doi.org/10.1002/qj.4414. eprint: https://rmets.onlinelibrary.wiley.com/doi/pdf/10.1002/qj.4414.

Franco, M. A., Ditas, F., Kremper, L. A., Machado, L. A. T., Andreae, M. O., Araújo, A., Barbosa, H. M. J., Brito, J. F. de, Carbone, S., Holanda, B. A., Morais, F. G., Nascimento, J. P., Pöhlker, M. L., Rizzo, L. V., Sá, M., Saturno, J., Walter, D., Wolff, S., Pöschl, U., Artaxo, P., and Pöhlker, C. (2022). "Occurrence and growth of sub-50 nm aerosol particles in the Amazonian boundary layer". In: *Atmospheric Chemistry and Physics* 22.5, pp. 3469–3492. DOI: 10.5194/acp-22-3469-2022.

Fritsch, J. M. and Chappell, C. F. (1980). "Numerical Prediction of Convectively Driven Mesoscale Pressure Systems. Part I: Convective Parameterization". In: *Journal of Atmospheric Sciences* 37.8, pp. 1722–1733. DOI: 10.1175/1520-0469(1980)037<1722:NPOCDM>2.0.CO;2.

Fuchs, N.A. and Sutugin, A.G. (1971). "High-dispersed aerosols". In: *Topics in Current Aerosol Research*. Ed. by G.M. Hidy and J.R. Brock. International Reviews in Aerosol Physics and Chemistry. Pergamon, p. 1. DOI: https://doi.org/10.1016/B978-0-08-016674-2.50006-6.

Furtado, K. and Field, P. (2022). "A strong statistical link between aerosol indirect effects and the self-similarity of rainfall distributions". In: *Atmospheric Chemistry and Physics* 22.5, pp. 3391–3407. DOI: 10.5194/acp-22-3391-2022.

Gelbard, Fred and Seinfeld, John H (1979). "The general dynamic equation for aerosols. Theory and application to aerosol formation and growth". In: *Journal of Colloid and Interface Science* 68.2, pp. 363–382. DOI: https://doi.org/10.1016/0021-9797(79)90289-3.

– (1978). "Numerical solution of the dynamic equation for particulate systems". In: *Journal of Computational Physics* 28.3, pp. 357–375. DOI: https://doi.org/10.1016/0021-9991(78)90058-X.

Gerken, Tobias, Wei, Dandan, Chase, Randy J, Fuentes, Jose D, Schumacher, Courtney, Machado, Luiz AT, Andreoli, Rita V, Chamecki, Marcelo, Souza, Rodrigo A Ferreira de, Freire, Livia S, et al. (2016). "Downward transport of ozone rich air and implications for atmospheric

chemistry in the Amazon rainforest". In: *Atmospheric Environment* 124, pp. 64–76. DOI: https://doi.org/10.1016/j.atmosenv.2015.11.014.

Giangrande, Scott E., Toto, Tami, Jensen, Michael P., Bartholomew, Mary Jane, Feng, Zhe, Protat, Alain, Williams, Christopher R., Schumacher, Courtney, and Machado, Luiz (2016). "Convective cloud vertical velocity and mass-flux characteristics from radar wind profiler observations during GoAmazon2014/5". In: *Journal of Geophysical Research: Atmospheres* 121.21, pp. 12, 891–12, 913. DOI: https://doi.org/10.1002/2016JD025303. eprint: https://agupubs.onlinelibrary.wiley.com/doi/pdf/10.1002/2016JD025303.

Glicker, H. S., Lawler, M. J., Ortega, J., Sá, S. S. de, Martin, S. T., Artaxo, P., Vega Bustillos, O., Souza, R. de, Tota, J., Carlton, A., and Smith, J. N. (2019). "Chemical composition of ultrafine aerosol particles in central Amazonia during the wet season". In: *Atmospheric Chemistry and Physics* 19.20, pp. 13053–13066. DOI: 10.5194/acp-19-13053-2019.

Gonçalves, W. A., Machado, L. A. T., and Kirstetter, P.-E. (2015). "Influence of biomass aerosol on precipitation over the Central Amazon: an observational study". In: *Atmospheric Chemistry and Physics* 15.12, pp. 6789–6800. DOI: 10.5194/acp-15-6789-2015.

Gordon, H., Carslaw, K.S., Hill, A.A., Field, P.R., Abraham, N.L., Beyersdorf, A., Corr-Limoges, C., Ghosh, P., Hemmings, J., Sanchez, C., Wang, X., and Wilkinson, J. (submitted). "Description of the multi-scale regional chemistry-climate setup of the Met Office Unified Model, and evaluation with KORUS-AQ data". In.

Gordon, Hamish, Field, Paul R, Abel, Steven J, Barrett, Paul, Bower, Keith, Crawford, Ian, Cui, Zhiqiang, Grosvenor, Daniel P, Hill, Adrian A, Taylor, Jonathan, et al. (2020). "Development of aerosol activation in the double-moment Unified Model and evaluation with CLARIFY measurements". In: *Atmospheric Chemistry and Physics* 20.18, pp. 10997–11024. DOI: https://doi.org/10.5194/acp-20-10997-2020.

Gordon, Hamish, Field, Paul R, Abel, Steven J, Dalvi, Mohit, Grosvenor, Daniel P, Hill, Adrian A, Johnson, Ben T, Miltenberger, Annette K, Yoshioka, Masaru, and Carslaw, Ken S (2018). "Large simulated radiative effects of smoke in the south-east Atlantic". In: *Atmospheric Chemistry and Physics* 18.20, pp. 15261–15289. DOI: https://doi.org/10.5194/acp-18-15261-2018.

Gordon, Hamish, Kirkby, Jasper, Baltensperger, Urs, Bianchi, Federico, Breitenlechner, Martin, Curtius, Joachim, Dias, Antonio, Dommen, Josef, Donahue, Neil M, Dunne, Eimear M, et al. (2017). "Causes and importance of new particle formation in the present-day and preindustrial atmospheres". In: *Journal of Geophysical Research: Atmospheres* 122.16, pp. 8739–8760. DOI: https://doi.org/10.1002/2017JD026844.

Gordon, Hamish, Sengupta, Kamalika, Rap, Alexandru, Duplissy, Jonathan, Frege, Carla, Williamson, Christina, Heinritzi, Martin, Simon, Mario, Yan, Chao, Almeida, João, et al. (2016). "Reduced anthropogenic aerosol radiative forcing caused by biogenic new particle formation". In: *Proceedings of the National Academy of Sciences* 113.43, pp. 12053–12058. DOI: https://doi.org/10.1073/pnas.1602360113.

Grabowski, Wojciech W. and Morrison, Hugh (2020). "Do Ultrafine Cloud Condensation Nuclei Invigorate Deep Convection?" In: *Journal of the Atmospheric Sciences* 77.7, pp. 2567–2583. DOI: 10.1175/JAS-D-20-0012.1.

Granier, Claire, Bessagnet, Bertrand, Bond, Tami, D'Angiola, Ariela, Denier van der Gon, Hugo, Frost, Gregory J., Heil, Angelika, Kaiser, Johannes W., Kinne, Stefan, Klimont, Zbigniew, Kloster, Silvia, Lamarque, Jean-François, Liousse, Catherine, Masui, Toshihiko, Meleux, Frederik, Mieville, Aude, Ohara, Toshimasa, Raut, Jean-Christophe, Riahi, Keywan, Schultz, Martin G., Smith, Steven J., Thompson, Allison, Aardenne, John van, Werf, Guido R. van der, and Vuuren, Detlef P. van (2011). "Evolution of anthropogenic and biomass burning emissions of air pollutants at global and regional scales during the 1980–2010 period". In: *Climatic Change* 109.1, p. 163. DOI: 10.1007/s10584-011-0154-1.

Gregory, D. and Rowntree, P. R. (1990). "A Mass Flux Convection Scheme with Representation of Cloud Ensemble Characteristics and Stability-Dependent Closure". In: *Monthly Weather Review* 118.7, pp. 1483–1506. DOI: 10.1175/1520-0493(1990)118<1483:AMFCSW>2.0.CO;2.

Grosvenor, Daniel P, Field, Paul R, Hill, Adrian A, and Shipway, Benjamin J (2017). "The relative importance of macrophysical and cloud albedo changes for aerosol-induced radiative effects in closed-cell stratocumulus: insight from the modelling of a case study". In: *Atmospheric Chemistry and Physics* 17.8, pp. 5155–5183. DOI: https://doi.org/10.5194/acp-17-5155-2017.

Guenther, Alex, Hewitt, C. Nicholas, Erickson, David, Fall, Ray, Geron, Chris, Graedel, Tom, Harley, Peter, Klinger, Lee, Lerdau, Manuel, Mckay, W. A., Pierce, Tom, Scholes, Bob, Steinbrecher, Rainer, Tallamraju, Raja, Taylor, John, and Zimmerman, Pat (1995). "A global model of natural volatile organic compound emissions". In: *Journal of Geophysical Research: Atmospheres* 100.D5, pp. 8873–8892. DOI: https://doi.org/10.1029/94JD02950. eprint: https://agupubs.onlinelibrary.wiley.com/doi/pdf/10.1029/94JD02950.

Guida, R., Carrié, P., De Menezes, L., Duplissy, J., Fayet, F., Haider, S., Kirkby, J., Mathot, S., Minginette, P., Onnela, A., Rochez, J., Thomas, G., Wasem, A., and Wilhelmsson, M. (2013). "Development of the gas system for the CLOUD experiment at CERN". In: *2013 IEEE Nuclear Science Symposium and Medical Imaging Conference (2013 NSS/MIC)*, pp. 1–5. DOI: 10.1109/NSSMIC.2013.6829603.

Guo, Jianping, Deng, Minjun, Fan, Jiwen, Li, Zhanqing, Chen, Qian, Zhai, Panmao, Dai, Zhijian, and Li, Xiaowen (2014). "Precipitation and air pollution at mountain and plain stations in northern China: Insights gained from observations and modeling". In: *Journal of Geophysical Research: Atmospheres* 119.8, pp. 4793–4807. DOI: https://doi.org/10.1002/2013JD021161. eprint: https://agupubs.onlinelibrary.wiley.com/doi/pdf/10.1002/2013JD021161.

Gustafson Jr., William I., Qian, Yun, and Fast, Jerome D. (2011). "Downscaling aerosols and the impact of neglected subgrid processes on direct aerosol radiative forcing for a representative global climate model grid spacing". In: *Journal of Geophysical Research: Atmospheres* 116.D13. DOI: https://doi.org/10.1029/2010JD015480. eprint: https://agupubs.onlinelibrary.wiley.com/doi/pdf/10.1029/2010JD015480.

Halmer, M.M., Schmincke, H.-U., and Graf, H.-F. (2002). "The annual volcanic gas input into the atmosphere, in particular into the stratosphere: a global data set for the past 100 years". In: *Journal of Volcanology and Geothermal Research* 115.3, pp. 511–528. DOI: https://doi.org/10.1016/S0377-0273(01)00318-3.

Hamed, A., Joutsensaari, J., Mikkonen, S., Sogacheva, L., Dal Maso, M., Kulmala, M., Cavalli, F., Fuzzi, S., Facchini, M. C., Decesari, S., Mircea, M., Lehtinen, K. E. J., and Laaksonen,

A. (2007). “Nucleation and growth of new particles in Po Valley, Italy”. In: *Atmospheric Chemistry and Physics* 7.2, pp. 355–376. DOI: 10.5194/acp-7-355-2007.

Hamed, Amar, Korhonen, Hannele, Sihto, Sanna-Liisa, Joutsensaari, Jorma, Järvinen, Heikki, Petäjä, Tuukka, Arnold, Frank, Nieminen, Tuomo, Kulmala, Markku, Smith, James N., Lehtinen, Kari E. J., and Laaksonen, Ari (2011). “The role of relative humidity in continental new particle formation”. In: *Journal of Geophysical Research: Atmospheres* 116.D3. DOI: https://doi.org/10.1029/2010JD014186. eprint: https://agupubs.onlinelibrary.wiley.com/doi/pdf/10.1029/2010JD014186.

He, Xu-Cheng et al. (2021). “Role of iodine oxoacids in atmospheric aerosol nucleation”. In: *Science* 371.6529, pp. 589–595. DOI: 10.1126/science.abe0298. eprint: https://www.science.org/doi/pdf/10.1126/science.abe0298.

Heever, Susan C. van den and Cotton, William R. (2007). “Urban Aerosol Impacts on Downwind Convective Storms”. In: *Journal of Applied Meteorology and Climatology* 46.6, pp. 828–850. DOI: 10.1175/JAM2492.1.

Heikenfeld, M., White, B., Labbouz, L., and Stier, P. (2019). “Aerosol effects on deep convection: the propagation of aerosol perturbations through convective cloud microphysics”. In: *Atmospheric Chemistry and Physics* 19.4, pp. 2601–2627. DOI: 10.5194/acp-19-2601-2019.

Herbert, Ross J., Murray, Benjamin J., Dobbie, Steven J., and Koop, Thomas (2015). “Sensitivity of liquid clouds to homogenous freezing parameterizations”. In: *Geophysical Research Letters* 42.5, pp. 1599–1605. DOI: https://doi.org/10.1002/2014GL062729. eprint: https://agupubs.onlinelibrary.wiley.com/doi/pdf/10.1002/2014GL062729.

Hill, AA, Dobbie, S, and Yin, Y (2008). “The impact of aerosols on non-precipitating marine stratocumulus. I: Model description and prediction of the indirect effect”. In: *Quarterly Journal of the Royal Meteorological Society: A journal of the atmospheric sciences, applied meteorology and physical oceanography* 134.634, pp. 1143–1154. DOI: https://doi.org/10.1002/qj.278.

Hill, AA, Shipway, BJ, and Boutle, IA (2015). "How sensitive are aerosol-precipitation interactions to the warm rain representation?" In: *Journal of Advances in Modeling Earth Systems* 7.3, pp. 987–1004. DOI: https://doi.org/10.1002/2014MS000422.

Hoesly, R. M., Smith, S. J., Feng, L., Klimont, Z., Janssens-Maenhout, G., Pitkanen, T., Seibert, J. J., Vu, L., Andres, R. J., Bolt, R. M., Bond, T. C., Dawidowski, L., Kholod, N., Kurokawa, J.-I., Li, M., Liu, L., Lu, Z., Moura, M. C. P., O'Rourke, P. R., and Zhang, Q. (2018). "Historical (1750–2014) anthropogenic emissions of reactive gases and aerosols from the Community Emissions Data System (CEDS)". In: *Geoscientific Model Development* 11.1, pp. 369–408. DOI: 10.5194/gmd-11-369-2018.

Igel, Adele L. and Heever, Susan C. van den (2021). "Invigoration or Enervation of Convective Clouds by Aerosols?" In: *Geophysical Research Letters* 48.16. e2021GL093804 2021GL093804, e2021GL093804. DOI: https://doi.org/10.1029/2021GL093804. eprint: https://agupubs.onlinelibrary.wiley.com/doi/pdf/10.1029/2021GL093804.

Janssens-Maenhout, G., Crippa, M., Guizzardi, D., Dentener, F., Muntean, M., Pouliot, G., Keating, T., Zhang, Q., Kurokawa, J., Wankmüller, R., Denier van der Gon, H., Kuenen, J. J. P., Klimont, Z., Frost, G., Darras, S., Koffi, B., and Li, M. (2015). "HTAP v2.2: a mosaic of regional and global emission grid maps for 2008 and 2010 to study hemispheric transport of air pollution". In: *Atmospheric Chemistry and Physics* 15.19, pp. 11411–11432. DOI: 10.5194/acp-15-11411-2015.

Jiang, Mengjiao, Li, Zhanqing, Wan, Bingcheng, and Cribb, Maureen (2016). "Impact of aerosols on precipitation from deep convective clouds in eastern China". In: *Journal of Geophysical Research: Atmospheres* 121.16, pp. 9607–9620. DOI: https://doi.org/10.1002/2015JD024246. eprint: https://agupubs.onlinelibrary.wiley.com/doi/pdf/10.1002/2015JD024246.

Johnston, Benjamin R., Xie, Feiqin, and Liu, Chuntao (2018). "The Effects of Deep Convection on Regional Temperature Structure in the Tropical Upper Troposphere and Lower Stratosphere". In: *Journal of Geophysical Research: Atmospheres* 123.3, pp. 1585–1603. DOI: https://doi.org/10.1002/2017JD027120. eprint: https://agupubs.onlinelibrary.wiley.com/doi/pdf/10.1002/2017JD027120.

Jones, A., Roberts, D. L., and Slingo, A. (1994). "A climate model study of indirect radiative forcing by anthropogenic sulphate aerosols". In: *Nature* 370.6489, pp. 450–453. DOI: 10.1038/370450a0.

Kanakidou, M, Seinfeld, JH, Pandis, SN, Barnes, I, Dentener, FJ, Facchini, MC, Dingenen, R Van, Ervens, B, Nenes, ANCJSE, Nielsen, CJ, et al. (2005). "Organic aerosol and global climate modelling: a review". In: *Atmospheric Chemistry and Physics* 5.4, pp. 1053–1123. DOI: https://doi.org/10.5194/acp-5-1053-2005.

Kang, L., Marchand, R. T., Wood, R., and McCoy, I. L. (2022). "Coalescence Scavenging Drives Droplet Number Concentration in Southern Ocean Low Clouds". In: *Geophysical Research Letters* 49.7. e2022GL097819 2022GL097819, e2022GL097819. DOI: https://doi.org/10.1029/2022GL097819. eprint: https://agupubs.onlinelibrary.wiley.com/doi/pdf/10.1029/2022GL097819.

Kawamoto, Kazuaki (2006). "Relationships between cloud properties and precipitation amount over the Amazon basin". In: *Atmospheric Research* 82.1. 14th International Conference on Clouds and Precipitation, pp. 239–247. DOI: https://doi.org/10.1016/j.atmosres.2005.10.007.

Kawamoto, Kazuaki and Suzuki, Kentaroh (2012). "Microphysical transition in water clouds over the Amazon and China derived from space-borne radar and radiometer data". In: *Journal of Geophysical Research: Atmospheres* 117.D5. DOI: https://doi.org/10.1029/2011JD016412. eprint: https://agupubs.onlinelibrary.wiley.com/doi/pdf/10.1029/2011JD016412.

Kazil, J, Wang, H, Feingold, G, Clarke, AD, Snider, Jefferson Robert, and Bandy, AR (2011). "Modeling chemical and aerosol processes in the transition from closed to open cells during VOCALS-REx". In: *Atmospheric Chemistry and Physics* 11.15, pp. 7491–7514. DOI: https://doi.org/10.5194/acp-11-7491-2011.

Kazil, J., Stier, P., Zhang, K., Quaas, J., Kinne, S., O'Donnell, D., Rast, S., Esch, M., Ferrachat, S., Lohmann, U., and Feichter, J. (2010). "Aerosol nucleation and its role for clouds and Earth's radiative forcing in the aerosol-climate model ECHAM5-HAM". In: *Atmospheric Chemistry and Physics* 10.22, pp. 10733–10752. DOI: 10.5194/acp-10-10733-2010.

Kerminen, Veli-Matti and Kulmala, Markku (2002). "Analytical formulae connecting the "real" and the "apparent" nucleation rate and the nuclei number concentration for atmospheric nucleation events". In: *Journal of Aerosol Science* 33.4, pp. 609–622. DOI: https://doi.org/10.1016/S0021-8502(01)00194-X.

Khain, A., Rosenfeld, D., Pokrovsky, A., Blahak, U., and Ryzhkov, A. (2011). "The role of CCN in precipitation and hail in a mid-latitude storm as seen in simulations using a spectral (bin) microphysics model in a 2D dynamic frame". In: *Atmospheric Research* 99.1, pp. 129–146. DOI: https://doi.org/10.1016/j.atmosres.2010.09.015.

Khain, A. P., BenMoshe, N., and Pokrovsky, A. (2008). "Factors Determining the Impact of Aerosols on Surface Precipitation from Clouds: An Attempt at Classification". In: *Journal of the Atmospheric Sciences* 65.6, pp. 1721–1748. DOI: 10.1175/2007JAS2515.1.

Kipling, Z, Stier, P, Schwarz, JP, Perring, AE, Spackman, JR, Mann, GW, Johnson, CE, and Telford, PJ (2013). "Constraints on aerosol processes in climate models from vertically-resolved aircraft observations of black carbon". In: *Atmospheric Chemistry and Physics* 13.12, pp. 5969–5986. DOI: https://doi.org/10.5194/acp-13-5969-2013.

Kipling, Zak, Labbouz, Laurent, and Stier, Philip (2020). "Global response of parameterised convective cloud fields to anthropogenic aerosol forcing". In: *Atmospheric Chemistry and Physics* 20.7, pp. 4445–4460. DOI: https://doi.org/10.5194/acp-20-4445-2020.

Kirkby, Jasper, Curtius, Joachim, Almeida, João, Dunne, Eimear, Duplissy, Jonathan, Ehrhart, Sebastian, Franchin, Alessandro, Gagné, Stéphanie, Ickes, Luisa, Kürten, Andreas, et al. (2011). "Role of sulphuric acid, ammonia and galactic cosmic rays in atmospheric aerosol nucleation". In: *Nature* 476.7361, p. 429. DOI: https://doi.org/10.1038/nature10343.

Kirkby, Jasper, Duplissy, Jonathan, Sengupta, Kamalika, Frege, Carla, Gordon, Hamish, Williamson, Christina, Heinritzi, Martin, Simon, Mario, Yan, Chao, Almeida, João, et al. (2016). "Ion-induced nucleation of pure biogenic particles". In: *Nature* 533.7604, p. 521. DOI: https://doi.org/10.1038/nature17953.

Köhler, Hilding (1936). "The nucleus in and the growth of hygroscopic droplets". In: *Transactions of the Faraday Society* 32, pp. 1152–1161. DOI: https://doi.org/10.1039/TF9363201152.

Koren, I., Remer, L. A., Altaratz, O., Martins, J. V., and Davidi, A. (2010). "Aerosol-induced changes of convective cloud anvils produce strong climate warming". In: *Atmospheric Chemistry and Physics* 10.10, pp. 5001–5010. DOI: 10.5194/acp-10-5001-2010.

Koren, Ilan, Dagan, Guy, and Altaratz, Orit (2014). "From aerosol-limited to invigoration of warm convective clouds". In: *Science* 344.6188, pp. 1143–1146. DOI: 10.1126/science.125259.

Koren, Ilan, Kaufman, Yoram J, Rosenfeld, Daniel, Remer, Lorraine A, and Rudich, Yinon (2005). "Aerosol invigoration and restructuring of Atlantic convective clouds". In: *Geophysical Research Letters* 32.14. DOI: https://doi.org/10.1029/2005GL023187.

Kreidenweis, Sonya M and Seinfeld, John H (1988). "Nucleation of sulfuric acid-water and methanesulfonic acid-water solution particles: implications for the atmospheric chemistry of organosulfur species". In: *Atmospheric Environment (1967)* 22.2, pp. 283–296. DOI: https://doi.org/10.1016/0004-6981(88)90034-0.

Krejci, Radovan, Ström, Johan, Reus, Marian de, Hoor, Peter, Williams, Jonathan, Fischer, Horst, and Hansson, Hans-Christen (2003). "Evolution of aerosol properties over the rain forest in Surinam, South America, observed from aircraft during the LBA-CLAIRE 98 experiment". In: *Journal of Geophysical Research: Atmospheres* 108.D18. DOI: https://doi.org/10.1029/2001JD001375. eprint: https://agupubs.onlinelibrary.wiley.com/doi/pdf/10.1029/2001JD001375.

Kuhn, U, Andreae, Meinrat O, Ammann, Christoph, Araújo, AC, Brancaleoni, Enzo, Ciccioli, Paolo, Dindorf, Tamara, Frattoni, Massimiliano, Gatti, Luciana Vanni, Ganzeveld, L, et al. (2007). "Isoprene and monoterpene fluxes from Central Amazonian rainforest inferred from tower-based and airborne measurements, and implications on the atmospheric chemistry and the local carbon budget". In: *Atmospheric Chemistry and Physics Discussions* 7.1, pp. 642–708. DOI: https://doi.org/10.5194/acp-7-2855-2007.

Kulmala, M., Hämeri, K., Aalto, P. P., Mäkelä, J. M., Pirjola, L., Nilsson, E. Douglas, Buzorius, G., Rannik, Ü., Maso, M. Dal, Seidl, W., Hoffman, T., Janson, R., Hansson, H.-C., Viisanen, Y., Laaksonen, A., and O'Dowd, C. D. (2001a). "Overview of the international project on biogenic aerosol formation in the boreal forest (BIOFOR)". In: *Tellus B* 53.4, pp. 324–343. DOI: https://doi.org/10.1034/j.1600-0889.2001.530402.x. eprint: https://onlinelibrary.wiley.com/doi/pdf/10.1034/j.1600-0889.2001.530402.x.

Kulmala, M., Maso, M. Dal, Mäkelä, J. M., Pirjola, L., Väkevä, M., Aalto, P., Miikkulainen, P., Hämeri, K., and O'Dowd, C. D. (2001b). "On the formation, growth and composition of nucleation mode particles". In: *Tellus B* 53.4, pp. 479–490. DOI: https://doi.org/10.1034/j.1600-0889.2001.530411.x. eprint: https://onlinelibrary.wiley.com/doi/pdf/10.1034/j.1600-0889.2001.530411.x.

Kulmala, Markka, Laaksonen, Ari, and Pirjola, Liisa (1998). "Parameterizations for sulfuric acid/water nucleation rates". In: *Journal of Geophysical Research: Atmospheres* 103.D7, pp. 8301–8307. DOI: https://doi.org/10.1029/97JD03718.

Kulmala, Markku, Reissell, Anni, Sipilä, Mikko, Bonn, Boris, Ruuskanen, Taina M, Lehtinen, Kari EJ, Kerminen, Veli-Matti, and Ström, Johan (2006). "Deep convective clouds as aerosol production engines: Role of insoluble organics". In: *Journal of Geophysical Research: Atmospheres* 111.D17. DOI: https://doi.org/10.1029/2005JD006963.

Kwok, Eric SC and Atkinson, Roger (1995). "Estimation of hydroxyl radical reaction rate constants for gas-phase organic compounds using a structure-reactivity relationship: an update". In: *Atmospheric Environment* 29.14, pp. 1685–1695. DOI: https://doi.org/10.1016/1352-2310(95)00069-B.

Laakso, L., Anttila, T., Lehtinen, K. E. J., Aalto, P. P., Kulmala, M., Hõrrak, U., Paatero, J., Hanke, M., and Arnold, F. (2004). "Kinetic nucleation and ions in boreal forest particle formation events". In: *Atmospheric Chemistry and Physics* 4.9/10, pp. 2353–2366. DOI: 10.5194/acp-4-2353-2004.

Laakso, L., Mäkelä, J. M., Pirjola, L., and Kulmala, M. (2002). "Model studies on ion-induced nucleation in the atmosphere". In: *Journal of Geophysical Research: Atmospheres* 107.D20,

AAC 5-1-AAC 5–19. DOI: https://doi.org/10.1029/2002JD002140. eprint: https://agupubs.onlinelibrary.wiley.com/doi/pdf/10.1029/2002JD002140.

Laakso, L., Merikanto, J., Vakkari, V., Laakso, H., Kulmala, M., Molefe, M., Kgabi, N., Mabaso, D., Carslaw, K. S., Spracklen, D. V., Lee, L. A., Reddington, C. L., and Kerminen, V.-M. (2013). "Boundary layer nucleation as a source of new CCN in savannah environment". In: *Atmospheric Chemistry and Physics* 13.4, pp. 1957–1972. DOI: 10.5194/acp-13-1957-2013.

Lamarque, J.-F., Bond, T. C., Eyring, V., Granier, C., Heil, A., Klimont, Z., Lee, D., Liousse, C., Mieville, A., Owen, B., Schultz, M. G., Shindell, D., Smith, S. J., Stehfest, E., Van Aardenne, J., Cooper, O. R., Kainuma, M., Mahowald, N., McConnell, J. R., Naik, V., Riahi, K., and Vuuren, D. P. van (2010). "Historical (1850–2000) gridded anthropogenic and biomass burning emissions of reactive gases and aerosols: methodology and application". In: *Atmospheric Chemistry and Physics* 10.15, pp. 7017–7039. DOI: 10.5194/acp-10-7017-2010.

Lana, A., Bell, T. G., Simó, R., Vallina, S. M., Ballabrera-Poy, J., Kettle, A. J., Dachs, J., Bopp, L., Saltzman, E. S., Stefels, J., Johnson, J. E., and Liss, P. S. (2011). "An updated climatology of surface dimethlysulfide concentrations and emission fluxes in the global ocean". In: *Global Biogeochemical Cycles* 25.1. DOI: https://doi.org/10.1029/2010GB003850. eprint: https://agupubs.onlinelibrary.wiley.com/doi/pdf/10.1029/2010GB003850.

Lee, S-H, Wilson, JC, Baumgardner, D, Herman, RL, Weinstock, EM, LaFleur, BG, Kok, G, Anderson, B, Lawson, P, Baker, B, et al. (2004). "New particle formation observed in the tropical/subtropical cirrus clouds". In: *Journal of Geophysical Research: Atmospheres* 109.D20. DOI: https://doi.org/10.1029/2004JD005033.

Lee, Seoung Soo, Kim, Byung-Gon, Lee, Chulkyu, Yum, Seong Soo, and Posselt, Derek (2014). "Effect of aerosol pollution on clouds and its dependence on precipitation intensity". In: *Climate Dynamics* 42.3, pp. 557–577. DOI: 10.1007/s00382-013-1898-2.

Li, Wenhong and Fu, Rong (2004). "Transition of the Large-Scale Atmospheric and Land Surface Conditions from the Dry to the Wet Season over Amazonia as Diagnosed by the ECMWF Re-Analysis". In: *Journal of Climate* 17.13, pp. 2637–2651. DOI: 10.1175/1520-0442(2004)017<2637:TOTLAA>2.0.CO;2.

Li, Yang, Barth, Mary C, Patton, Edward G, and Steiner, Allison L (2017). "Impact of In-Cloud Aqueous Processes on the Chemistry and Transport of Biogenic Volatile Organic Compounds". In: *Journal of Geophysical Research: Atmospheres* 122.20. DOI: https://doi.org/10.1002/2017JD026688.

Li, Zhanqing, Niu, Feng, Fan, Jiwen, Liu, Yangang, Rosenfeld, Daniel, and Ding, Yanni (2011). "Long-term impacts of aerosols on the vertical development of clouds and precipitation". In: *Nature Geoscience* 4.12, pp. 888–894. DOI: 10.1038/ngeo1313.

Lipsky, Eric M. and Robinson, Allen L. (Jan. 2006). "Effects of Dilution on Fine Particle Mass and Partitioning of Semivolatile Organics in Diesel Exhaust and Wood Smoke". In: *Environmental Science & Technology* 40.1, pp. 155–162. DOI: 10.1021/es050319p.

Loftus, A.M. and Cotton, W.R. (2014). "Examination of CCN impacts on hail in a simulated supercell storm with triple-moment hail bulk microphysics". In: *Atmospheric Research* 147-148, pp. 183–204. DOI: https://doi.org/10.1016/j.atmosres.2014.04.017.

Loosmore, Gwen A and Cederwall, Richard T (2004). "Precipitation scavenging of atmospheric aerosols for emergency response applications: testing an updated model with new real-time data". In: *Atmospheric Environment* 38.7, pp. 993–1003. DOI: https://doi.org/10.1016/j.atmosenv.2003.10.055.

Machado, L. A. T., Franco, M. A., Kremper, L. A., Ditas, F., Andreae, M. O., Artaxo, P., Cecchini, M. A., Holanda, B. A., Pöhlker, M. L., Saraiva, I., Wolff, S., Pöschl, U., and Pöhlker, C. (2021). "How weather events modify aerosol particle size distributions in the Amazon boundary layer". In: *Atmospheric Chemistry and Physics* 21.23, pp. 18065–18086. DOI: 10.5194/acp-21-18065-2021.

Mäkelä, J. M., Aalto, P., Jokinen, V., Pohja, T., Nissinen, A., Palmroth, S., Markkanen, T., Seitsonen, K., Lihavainen, H., and Kulmala, M. (1997). "Observations of ultrafine aerosol particle formation and growth in boreal forest". In: *Geophysical Research Letters* 24.10, pp. 1219–1222. DOI: https://doi.org/10.1029/97GL00920. eprint: https://agupubs.onlinelibrary.wiley.com/doi/pdf/10.1029/97GL00920.

Makkonen, R., Asmi, A., Kerminen, V.-M., Boy, M., Arneth, A., Hari, P., and Kulmala, M. (2012). "Air pollution control and decreasing new particle formation lead to strong climate warming". In: *Atmospheric Chemistry and Physics* 12.3, pp. 1515–1524. DOI: 10.5194/acp-12-1515-2012.

Mangeon, S., Voulgarakis, A., Gilham, R., Harper, A., Sitch, S., and Folberth, G. (2016). "INFERNO: a fire and emissions scheme for the UK Met Office's Unified Model". In: *Geoscientific Model Development* 9.8, pp. 2685–2700. DOI: 10.5194/gmd-9-2685-2016.

Manktelow, P. T., Carslaw, K. S., Mann, G. W., and Spracklen, D. V. (2009). "Variable CCN formation potential of regional sulfur emissions". In: *Atmospheric Chemistry and Physics* 9.10, pp. 3253–3259. DOI: 10.5194/acp-9-3253-2009.

Mann, GW, Carslaw, KS, Spracklen, DV, Ridley, DA, Manktelow, PT, Chipperfield, MP, Pickering, SJ, and Johnson, CE (2010). "Description and evaluation of GLOMAP-mode: A modal global aerosol microphysics model for the UKCA composition-climate model". In: *Geoscientific Model Development* 3.2, pp. 519–551. DOI: https://doi.org/10.5194/gmd-3-519-2010.

Marinescu, Peter J., Heever, Susan C. van den, Heikenfeld, Max, Barrett, Andrew I., Barthlott, Christian, Hoose, Corinna, Fan, Jiwen, Fridlind, Ann M., Matsui, Toshi, Miltenberger, Annette K., Stier, Philip, Vie, Benoit, White, Bethan A., and Zhang, Yuwei (2021). "Impacts of Varying Concentrations of Cloud Condensation Nuclei on Deep Convective Cloud Updrafts—A Multimodel Assessment". In: *Journal of the Atmospheric Sciences* 78.4, pp. 1147–1172. DOI: 10.1175/JAS-D-20-0200.1.

Marle, M. J. E. van, Kloster, S., Magi, B. I., Marlon, J. R., Daniau, A.-L., Field, R. D., Arneth, A., Forrest, M., Hantson, S., Kehrwald, N. M., Knorr, W., Lasslop, G., Li, F., Mangeon, S., Yue, C., Kaiser, J. W., and Werf, G. R. van der (2017). "Historic global biomass burning emissions for CMIP6 (BB4CMIP) based on merging satellite observations with proxies and fire models (1750–2015)". In: *Geoscientific Model Development* 10.9, pp. 3329–3357. DOI: 10.5194/gmd-10-3329-2017.

Martin, S. T., Artaxo, P., Machado, L., Manzi, A. O., Souza, R. A. F., Schumacher, C., Wang, J., Biscaro, T., Brito, J., Calheiros, A., Jardine, K., Medeiros, A., Portela, B., Sá, S. S. de,

Adachi, K., Aiken, A. C., Albrecht, R., Alexander, L., Andreae, M. O., Barbosa, H. M. J., Buseck, P., Chand, D., Comstock, J. M., Day, D. A., Dubey, M., Fan, J., Fast, J., Fisch, G., Fortner, E., Giangrande, S., Gilles, M., Goldstein, A. H., Guenther, A., Hubbe, J., Jensen, M., Jimenez, J. L., Keutsch, F. N., Kim, S., Kuang, C., Laskin, A., McKinney, K., Mei, F., Miller, M., Nascimento, R., Pauliquevis, T., Pekour, M., Peres, J., Petäjä, T., Pöhlker, C., Pöschl, U., Rizzo, L., Schmid, B., Shilling, J. E., Dias, M. A. Silva, Smith, J. N., Tomlinson, J. M., Tóta, J., and Wendisch, M. (2017). "The Green Ocean Amazon Experiment (GoAmazon2014/5) Observes Pollution Affecting Gases, Aerosols, Clouds, and Rainfall over the Rain Forest". In: *Bulletin of the American Meteorological Society* 98.5, pp. 981–997. DOI: 10.1175/BAMS-D-15-00221.1.

Martin, ST, Artaxo, P, Machado, LAT, Manzi, AO, Souza, RAF, Schumacher, C, Wang, J, Andreae, MO, Barbosa, HMJ, Fan, J, et al. (2016). "Introduction: Observations and modeling of the green ocean Amazon (GoAmazon2014/5)". In: *Atmospheric Chemistry and Physics* 16.8. DOI: https://doi.org/10.5194/acp-16-4785-2016.

McCoy, Isabel L., Bretherton, Christopher S., Wood, Robert, Twohy, Cynthia H., Gettelman, Andrew, Bardeen, Charles G., and Toohey, Darin W. (2021). "Influences of Recent Particle Formation on Southern Ocean Aerosol Variability and Low Cloud Properties". In: *Journal of Geophysical Research: Atmospheres* 126.8. e2020JD033529 2020JD033529, e2020JD033529. DOI: https://doi.org/10.1029/2020JD033529. eprint: https://agupubs.onlinelibrary.wiley.com/doi/pdf/10.1029/2020JD033529.

McMurry, P.H (1983). "New particle formation in the presence of an aerosol: Rates, time scales, and sub-0.01 m size distributions". In: *Journal of Colloid and Interface Science* 95.1, pp. 72–80. DOI: https://doi.org/10.1016/0021-9797(83)90073-5.

McMurry, P.H. and Friedlander, S.K. (1979). "New particle formation in the presence of an aerosol". In: *Atmospheric Environment (1967)* 13.12, pp. 1635–1651. DOI: https://doi.org/10.1016/0004-6981(79)90322-6.

Merikanto, J, Spracklen, DV, Mann, GW, Pickering, SJ, and Carslaw, KS (2009). "Impact of nucleation on global CCN". In: *Atmospheric Chemistry and Physics* 9.21, pp. 8601–8616. DOI: https://doi.org/10.5194/acp-9-8601-2009.

Miltenberger, Annette K, Field, Paul R, Hill, Adrian A, Rosenberg, Phil, Shipway, Ben J, Wilkinson, Jonathan M, Scovell, Robert, and Blyth, Alan M (2018a). "Aerosol–cloud interactions in mixed-phase convective clouds–Part 1: Aerosol perturbations". In: *Atmospheric Chemistry and Physics* 18.5, pp. 3119–3145. DOI: https://doi.org/10.5194/acp-18-3119-2018.

Miltenberger, Annette K, Field, Paul R, Hill, Adrian A, Shipway, Ben J, and Wilkinson, Jonathan M (2018b). "Aerosol–cloud interactions in mixed-phase convective clouds–Part 2: Meteorological ensemble". In: *Atmospheric Chemistry and Physics* 18.4, pp. 10593–10613.

Mulcahy, J. P., Johnson, C., Jones, C. G., Povey, A. C., Scott, C. E., Sellar, A., Turnock, S. T., Woodhouse, M. T., Abraham, N. L., Andrews, M. B., Bellouin, N., Browse, J., Carslaw, K. S., Dalvi, M., Folberth, G. A., Glover, M., Grosvenor, D. P., Hardacre, C., Hill, R., Johnson, B., Jones, A., Kipling, Z., Mann, G., Mollard, J., O'Connor, F. M., Palmiéri, J., Reddington, C., Rumbold, S. T., Richardson, M., Schutgens, N. A. J., Stier, P., Stringer, M., Tang, Y., Walton, J., Woodward, S., and Yool, A. (2020). "Description and evaluation of aerosol in UKESM1 and HadGEM3-GC3.1 CMIP6 historical simulations". In: *Geoscientific Model Development* 13.12, pp. 6383–6423. DOI: 10.5194/gmd-13-6383-2020.

Murphy, Benjamin N, Julin, Jan, Riipinen, Ilona, and Ekman, Annica ML (2015). "Organic aerosol processing in tropical deep convective clouds: Development of a new model (CRM-ORG) and implications for sources of particle number". In: *Journal of Geophysical Research: Atmospheres* 120.19, pp. 10–441. DOI: https://doi.org/10.1002/2015JD023551.

Oshima, N., Koike, M., Kondo, Y., Nakamura, H., Moteki, N., Matsui, H., Takegawa, N., and Kita, K. (2013). "Vertical transport mechanisms of black carbon over East Asia in spring during the A-FORCE aircraft campaign". In: *Journal of Geophysical Research: Atmospheres* 118.23, pp. 13, 175–13, 198. DOI: https://doi.org/10.1002/2013JD020262. eprint: https://agupubs.onlinelibrary.wiley.com/doi/pdf/10.1002/2013JD020262.

Pacifico, F., Folberth, G. A., Jones, C. D., Harrison, S. P., and Collins, W. J. (2012). "Sensitivity of biogenic isoprene emissions to past, present, and future environmental conditions and implications for atmospheric chemistry". In: *Journal of Geophysical Research: Atmospheres*

117.D22. DOI: https://doi.org/10.1029/2012JD018276. eprint: https://agupubs.onlinelibrary.wiley.com/doi/pdf/10.1029/2012JD018276.

Pan, Zengxin, Mao, Feiyue, Rosenfeld, Daniel, Zhu, Yannian, Zang, Lin, Lu, Xin, Thornton, Joel A., Holzworth, Robert H., Yin, Jianhua, Efraim, Avichay, and Gong, Wei (2022). "Coarse sea spray inhibits lightning". In: *Nature Communications* 13.1, p. 4289. DOI: 10.1038/s41467-022-31714-5.

Pan, Zengxin, Rosenfeld, Daniel, Zhu, Yannian, Mao, Feiyue, Gong, Wei, Zang, Lin, and Lu, Xin (2021). "Observational Quantification of Aerosol Invigoration for Deep Convective Cloud Lifecycle Properties Based on Geostationary Satellite". In: *Journal of Geophysical Research: Atmospheres* 126.9. e2020JD034275 2020JD034275, e2020JD034275. DOI: https://doi.org/10.1029/2020JD034275. eprint: https://agupubs.onlinelibrary.wiley.com/doi/pdf/10.1029/2020JD034275.

Peltola, M., Rose, C., Trueblood, J. V., Gray, S., Harvey, M., and Sellegri, K. (2022). "New particle formation in coastal New Zealand with a focus on open-ocean air masses". In: *Atmospheric Chemistry and Physics* 22.9, pp. 6231–6254. DOI: 10.5194/acp-22-6231-2022.

Pierce, J. R. and Adams, P. J. (2009). "Uncertainty in global CCN concentrations from uncertain aerosol nucleation and primary emission rates". In: *Atmospheric Chemistry and Physics* 9.4, pp. 1339–1356. DOI: 10.5194/acp-9-1339-2009.

Pierce, JR (2017). "Cosmic rays, aerosols, clouds, and climate: Recent findings from the CLOUD experiment". In: *Journal of Geophysical Research: Atmospheres* 122.15, pp. 8051–8055. DOI: https://doi.org/10.1002/2017JD027475.

Pierce, JR and Adams, PJ (2007). "Efficiency of cloud condensation nuclei formation from ultrafine particles". In: *Atmospheric Chemistry and Physics* 7.5, pp. 1367–1379. DOI: https://doi.org/10.5194/acp-7-1367-2007.

Pierce, JR, Croft, B, Kodros, JK, D'Andrea, SD, and Martin, RV (2015). "The importance of interstitial particle scavenging by cloud droplets in shaping the remote aerosol size distribution and global aerosol-climate effects". In: *Atmospheric Chemistry and Physics* 15, pp. 6147–6158. DOI: https://doi.org/10.5194/acp-15-6147-2015.

Pillai, Priya, Khlystov, Andrey, Walker, John, and Aneja, Viney (2013). "Observation and Analysis of Particle Nucleation at a Forest Site in Southeastern US". In: *Atmosphere* 4.2, pp. 72–93. DOI: 10.3390/atmos4020072.

Pirjola, Liisa and Kulmala, Markku (1998). "Modelling the formation of H2SO4–H2O particles in rural, urban and marine conditions". In: *Atmospheric Research* 46.3, pp. 321–347. DOI: https://doi.org/10.1016/S0169-8095(97)00072-0.

Pirjola, Liisa, O'Dowd, Colin D, Brooks, Ian M, and Kulmala, Markku (2000). "Can new particle formation occur in the clean marine boundary layer?" In: *Journal of Geophysical Research: Atmospheres* 105.D21, pp. 26531–26546. DOI: https://doi.org/10.1029/2000JD900310.

Planche, Celine, Mann, Graham W, Carslaw, Kenneth S, Dalvi, Mohit, Marsham, John H, and Field, Paul R (2017). "Spatial and temporal CCN variations in convection-permitting aerosol microphysics simulations in an idealised marine tropical domain". In: *Atmospheric Chemistry and Physics* 17.5, pp. 3371–3384. DOI: https://doi.org/10.5194/acp-17-3371-2017.

Pöhlker, M. L., Pöhlker, C., Ditas, F., Klimach, T., Hrabe de Angelis, I., Araújo, A., Brito, J., Carbone, S., Cheng, Y., Chi, X., Ditz, R., Gunthe, S. S., Kesselmeier, J., Könemann, T., Lavrič, J. V., Martin, S. T., Mikhailov, E., Moran-Zuloaga, D., Rose, D., Saturno, J., Su, H., Thalman, R., Walter, D., Wang, J., Wolff, S., Barbosa, H. M. J., Artaxo, P., Andreae, M. O., and Pöschl, U. (2016). "Long-term observations of cloud condensation nuclei in the Amazon rain forest – Part 1: Aerosol size distribution, hygroscopicity, and new model parametrizations for CCN prediction". In: *Atmospheric Chemistry and Physics* 16.24, pp. 15709–15740. DOI: 10.5194/acp-16-15709-2016.

Pöhlker, M. L., Zhang, M., Campos Braga, R., Krüger, O. O., Pöschl, U., and Ervens, B. (2021). "Aitken mode particles as CCN in aerosol- and updraft-sensitive regimes of cloud droplet formation". In: *Atmospheric Chemistry and Physics* 21.15, pp. 11723–11740. DOI: 10.5194/acp-21-11723-2021.

Pöhlker, Mira L, Ditas, Florian, Saturno, Jorge, Klimach, Thomas, Hrabě de Angelis, Isabella, Araùjo, Alessandro C, Brito, Joel, Carbone, Samara, Cheng, Yafang, Chi, Xuguang, et al. (2018). "Long-term observations of cloud condensation nuclei over the Amazon rain forest–Part 2: Variability and characteristics of biomass burning, long-range transport, and pristine

rain forest aerosols". In: *Atmospheric Chemistry and Physics* 18.14, pp. 10289–10331. DOI: https://doi.org/10.5194/acp-18-10289-2018.

Polonik, P., Knote, C., Zinner, T., Ewald, F., Kölling, T., Mayer, B., Andreae, M. O., Jurkat-Witschas, T., Klimach, T., Mahnke, C., Molleker, S., Pöhlker, C., Pöhlker, M. L., Pöschl, U., Rosenfeld, D., Voigt, C., Weigel, R., and Wendisch, M. (2020). "The challenge of simulating the sensitivity of the Amazonian cloud microstructure to cloud condensation nuclei number concentrations". In: *Atmospheric Chemistry and Physics* 20.3, pp. 1591–1605. DOI: 10.5194/acp-20-1591-2020.

Qi, X. M., Ding, A. J., Nie, W., Petäjä, T., Kerminen, V.-M., Herrmann, E., Xie, Y. N., Zheng, L. F., Manninen, H., Aalto, P., Sun, J. N., Xu, Z. N., Chi, X. G., Huang, X., Boy, M., Virkkula, A., Yang, X.-Q., Fu, C. B., and Kulmala, M. (2015). "Aerosol size distribution and new particle formation in the western Yangtze River Delta of China: 2 years of measurements at the SORPES station". In: *Atmospheric Chemistry and Physics* 15.21, pp. 12445–12464. DOI: 10.5194/acp-15-12445-2015.

Qian, Y., Gustafson Jr., W. I., and Fast, J. D. (2010). "An investigation of the sub-grid variability of trace gases and aerosols for global climate modeling". In: *Atmospheric Chemistry and Physics* 10.14, pp. 6917–6946. DOI: 10.5194/acp-10-6917-2010.

Qian, Yun, Gong, Daoyi, Fan, Jiwen, Leung, L. Ruby, Bennartz, Ralf, Chen, Deliang, and Wang, Weiguo (2009). "Heavy pollution suppresses light rain in China: Observations and modeling". In: *Journal of Geophysical Research: Atmospheres* 114.D7. DOI: https://doi.org/10.1029/2008JD011575. eprint: https://agupubs.onlinelibrary.wiley.com/doi/pdf/10.1029/2008JD011575.

Riccobono, Francesco, Schobesberger, Siegfried, Scott, Catherine E, Dommen, Josef, Ortega, Ismael K, Rondo, Linda, Almeida, João, Amorim, Antonio, Bianchi, Federico, Breitenlechner, Martin, et al. (2014). "Oxidation products of biogenic emissions contribute to nucleation of atmospheric particles". In: *Science* 344.6185, pp. 717–721. DOI: 10.1126/science.1243527.

Rissler, J., Vestin, A., Swietlicki, E., Fisch, G., Zhou, J., Artaxo, P., and Andreae, M. O. (2006). "Size distribution and hygroscopic properties of aerosol particles from dry-season

biomass burning in Amazonia". In: *Atmospheric Chemistry and Physics* 6.2, pp. 471–491. DOI: 10.5194/acp-6-471-2006.

Rizzo, L.V., Artaxo, P., Karl, T., Guenther, A.B., and Greenberg, J. (2010). "Aerosol properties, in-canopy gradients, turbulent fluxes and VOC concentrations at a pristine forest site in Amazonia". In: *Atmospheric Environment* 44.4, pp. 503–511. DOI: https://doi.org/10.1016/j.atmosenv.2009.11.002.

Rizzo, Luciana Varanda, Roldin, Pontus, Brito, Joel, Backman, John, Swietlicki, Erik, Krejci, Radovan, Tunved, Peter, Petäjä, Tuukka, Kulmala, Markku, Artaxo, Paulo, et al. (2018). "Multi-year statistical and modeling analysis of submicrometer aerosol number size distributions at a rain forest site in Amazonia". In: *Atmospheric Chemistry and Physics*. DOI: https://doi.org/10.5194/acp-18-10255-2018.

Rosenfeld, Daniel, Lohmann, Ulrike, Raga, Graciela B, O'dowd, Colin D, Kulmala, Markku, Fuzzi, Sandro, Reissell, Anni, and Andreae, Meinrat O (2008). "Flood or drought: How do aerosols affect precipitation?" In: *science* 321.5894, pp. 1309–1313. DOI: 10.1126/science.1160606.

Sá, S. S. de, Palm, B. B., Campuzano-Jost, P., Day, D. A., Hu, W., Isaacman-VanWertz, G., Yee, L. D., Brito, J., Carbone, S., Ribeiro, I. O., Cirino, G. G., Liu, Y., Thalman, R., Sedlacek, A., Funk, A., Schumacher, C., Shilling, J. E., Schneider, J., Artaxo, P., Goldstein, A. H., Souza, R. A. F., Wang, J., McKinney, K. A., Barbosa, H., Alexander, M. L., Jimenez, J. L., and Martin, S. T. (2018). "Urban influence on the concentration and composition of submicron particulate matter in central Amazonia". In: *Atmospheric Chemistry and Physics* 18.16, pp. 12185–12206. DOI: 10.5194/acp-18-12185-2018.

Sassi, Fabrizio, Salby, Murry, and Read, William G. (2001). "Relationship between upper tropospheric humidity and deep convection". In: *Journal of Geophysical Research: Atmospheres* 106.D15, pp. 17133–17146. DOI: https://doi.org/10.1029/2001JD900121. eprint: https://agupubs.onlinelibrary.wiley.com/doi/pdf/10.1029/2001JD900121.

Schulz, Christiane, Schneider, Johannes, Amorim Holanda, Bruna, Appel, Oliver, Costa, Anja, Sá, Suzane S de, Dreiling, Volker, Fütterer, Daniel, Jurkat-Witschas, Tina, Klimach, Thomas, et al. (2018). "Aircraft-based observations of isoprene-epoxydiol-derived secondary organic

aerosol (IEPOX-SOA) in the tropical upper troposphere over the Amazon region". In: *Atmospheric Chemistry and Physics* 18.20, pp. 14979–15001. DOI: https://doi.org/10.5194/acp-18-14979-2018.

Scott, David W. (2012). "Multivariate Density Estimation and Visualization". In: *Handbook of Computational Statistics: Concepts and Methods*. Ed. by James E. Gentle, Wolfgang Karl Härdle, and Yuichi Mori. Berlin, Heidelberg: Springer Berlin Heidelberg, pp. 549–569. DOI: 10.1007/978-3-642-21551-3_19.

Sebastian, M., Kompalli, S. K., Kumar, V. A., Jose, S., Babu, S. S., Pandithurai, G., Singh, S., Hooda, R. K., Soni, V. K., Pierce, J. R., Vakkari, V., Asmi, E., Westervelt, D. M., Hyvärinen, A.-P., and Kanawade, V. P. (2022). "Observations of particle number size distributions and new particle formation in six Indian locations". In: *Atmospheric Chemistry and Physics* 22.7, pp. 4491–4508. DOI: 10.5194/acp-22-4491-2022.

Seifert, A., Köhler, C., and Beheng, K. D. (2012). "Aerosol-cloud-precipitation effects over Germany as simulated by a convective-scale numerical weather prediction model". In: *Atmospheric Chemistry and Physics* 12.2, pp. 709–725. DOI: 10.5194/acp-12-709-2012.

Seiki, Tatsuya and Nakajima, Teruyuki (2014). "Aerosol effects of the condensation process on a convective cloud simulation". In: *Journal of the Atmospheric Sciences* 71.2, pp. 833–853. DOI: https://doi.org/10.1175/JAS-D-12-0195.1.

Seinfeld, John H and Pandis, Spyros N (2012). *Atmospheric chemistry and physics: from air pollution to climate change*. John Wiley & Sons.

Sheffield, Amanda M., Saleeby, Stephen M., and Heever, Susan C. van den (2015). "Aerosol-induced mechanisms for cumulus congestus growth". In: *Journal of Geophysical Research: Atmospheres* 120.17, pp. 8941–8952. DOI: https://doi.org/10.1002/2015JD023743. eprint: https://agupubs.onlinelibrary.wiley.com/doi/pdf/10.1002/2015JD023743.

Shilling, John E, Pekour, Mikhail S, Fortner, Edward C, Artaxo, Paulo, Sá, Suzane de, Hubbe, John M, Longo, Karla M, Machado, Luiz AT, Martin, Scot T, Springston, Stephen R, et al. (2018). "Aircraft observations of the chemical composition and aging of aerosol in the

Manaus urban plume during GoAmazon 2014/5". In: *Atmospheric Chemistry and Physics* 18.14, pp. 10773–10797. DOI: https://doi.org/10.5194/acp-18-10773-2018.

Shipway, BJ and Hill, AA (2012). "Diagnosis of systematic differences between multiple parametrizations of warm rain microphysics using a kinematic framework". In: *Quarterly Journal of the Royal Meteorological Society* 138.669, pp. 2196–2211. DOI: https://doi.org/10.1002/qj.1913.

Shrivastava, Manish, Andreae, Meinrat O, Artaxo, Paulo, Barbosa, Henrique MJ, Berg, Larry K, Brito, Joel, Ching, Joseph, Easter, Richard C, Fan, Jiwen, Fast, Jerome D, et al. (2019). "Urban pollution greatly enhances formation of natural aerosols over the Amazon rainforest". In: *Nature Communications* 10.1, p. 1046. DOI: https://doi.org/10.1038/s41467-019-08909-4.

Shrivastava, Manish K., Lipsky, Eric M., Stanier, Charles O., and Robinson, Allen L. (Apr. 2006). "Modeling Semivolatile Organic Aerosol Mass Emissions from Combustion Systems". In: *Environmental Science & Technology* 40.8, pp. 2671–2677. DOI: 10.1021/es0522231.

Simon, Mario, Dada, Lubna, Heinritzi, Martin, Scholz, Wiebke, Stolzenburg, Dominik, Fischer, Lukas, Wagner, Andrea C, Kürten, Andreas, Rörup, Birte, He, Xu-Cheng, et al. (2020). "Molecular understanding of new-particle formation from α-pinene between- 50 and+ 25 ° C". In: *Atmospheric Chemistry and Physics* 20.15, pp. 9183–9207. DOI: https://doi.org/10.5194/acp-20-9183-2020.

Sindelarova, K., Granier, C., Bouarar, I., Guenther, A., Tilmes, S., Stavrakou, T., Müller, J.-F., Kuhn, U., Stefani, P., and Knorr, W. (2014). "Global data set of biogenic VOC emissions calculated by the MEGAN model over the last 30 years". In: *Atmospheric Chemistry and Physics* 14.17, pp. 9317–9341. DOI: 10.5194/acp-14-9317-2014.

Sotiropoulou, REP, Tagaris, E, Pilinis, C, Anttila, T, and Kulmala, M (2006). "Modeling new particle formation during air pollution episodes: Impacts on aerosol and cloud condensation nuclei". In: *Aerosol Science and Technology* 40.7, pp. 557–572. DOI: https://doi.org/10.1080/02786820600714346.

Sporre, Moa K., Glantz, Paul, Tunved, Peter, Swietlicki, Erik, Kulmala, Markku, and Lihavainen, Heikki (2012). "A study of the indirect aerosol effect on subarctic marine liquid low-level clouds using MODIS cloud data and ground-based aerosol measurements". In: *Atmospheric Research* 116. Remote Sensing of Clouds and Aerosols: Techniques and Applications - Atmospheric Research, pp. 56–66. DOI: https://doi.org/10.1016/j.atmosres.2011.09.014.

Spracklen, DV, Carslaw, KS, Kulmala, M, Kerminen, V-M, Mann, GW, and Sihto, S-L (2006). "The contribution of boundary layer nucleation events to total particle concentrations on regional and global scales". In: *Atmospheric Chemistry and Physics* 6.12, pp. 5631–5648. DOI: https://doi.org/10.5194/acp-6-5631-2006.

Spracklen, DV, Pringle, KJ, Carslaw, KS, Chipperfield, MP, and Mann, GW (2005). "A global off-line model of size-resolved aerosol microphysics: I. Model development and prediction of aerosol properties". In: *Atmospheric Chemistry and Physics* 5.8, pp. 2227–2252. DOI: https://doi.org/10.5194/acp-5-2227-2005.

Stevens, Bjorn and Feingold, Graham (2009). "Untangling aerosol effects on clouds and precipitation in a buffered system". In: *Nature* 461.7264, p. 607. DOI: https://doi.org/10.1038/nature08281.

Stevens, Bjorn, Satoh, Masaki, Auger, Ludovic, Biercamp, Joachim, Bretherton, Christopher S., Chen, Xi, Düben, Peter, Judt, Falko, Khairoutdinov, Marat, Klocke, Daniel, Kodama, Chihiro, Kornblueh, Luis, Lin, Shian-Jiann, Neumann, Philipp, Putman, William M., Röber, Niklas, Shibuya, Ryosuke, Vanniere, Benoit, Vidale, Pier Luigi, Wedi, Nils, and Zhou, Linjiong (2019). "DYAMOND: the DYnamics of the Atmospheric general circulation Modeled On Non-hydrostatic Domains". In: *Progress in Earth and Planetary Science* 6.1, p. 61. DOI: 10.1186/s40645-019-0304-z.

Stier, P., Feichter, J., Kinne, S., Kloster, S., Vignati, E., Wilson, J., Ganzeveld, L., Tegen, I., Werner, M., Balkanski, Y., Schulz, M., Boucher, O., Minikin, A., and Petzold, A. (2005). "The aerosol-climate model ECHAM5-HAM". In: *Atmospheric Chemistry and Physics* 5.4, pp. 1125–1156. DOI: 10.5194/acp-5-1125-2005.

Stocker, T.F., Qin, D., Plattner, G.-K., Alexander, L.V., Allen, S.K., Bindoff N.L. and. Bréon, F.-M, Church, J.A., Cubasch, U., Emori, S., Forster, P., Friedlingstein, P., Gillett, N., Gregory, J.M., Hartmann, D.L., Jansen, E., Kirtman, B., Knutti, R., Krishna Kumar, K., Lemke, P., Marotzke, J., Masson-Delmotte, V., Meehl, G.A., Mokhov, I.I., Piao, S., Ramaswamy, V., Randall, D., Rhein, M., Rojas, M., Sabine, C., Shindell, D., Talley, L.D., Vaughan, D.G., and Xie, S.-P. (2013). *IPCC, 2013: Technical Summary*. Tech. rep. Cambridge University Press, Cambridge, United Kingdom and New York, NY, USA.: Climate Change 2013: The Physical Science Basis. Contribution of Working Group I to the Fifth Assess- ment Report of the Intergovernmental Panel on Climate Change [Stocker, T.F., D. Qin, G.-K. Plattner, M. Tignor, S.K. Allen, J. Boschung, A. Nauels, Y. Xia, V. Bex and P.M. Midgley (eds.)]

Stolzenburg, Dominik, Fischer, Lukas, Vogel, Alexander L, Heinritzi, Martin, Schervish, Meredith, Simon, Mario, Wagner, Andrea C, Dada, Lubna, Ahonen, Lauri R, Amorim, Antonio, et al. (2018). "Rapid growth of organic aerosol nanoparticles over a wide tropospheric temperature range". In: *Proceedings of the National Academy of Sciences* 115.37, pp. 9122–9127. DOI: https://doi.org/10.1073/pnas.1807604115.

Stratton, RA, Stirling, A, and Derbyshire, S (2009). "Changes and developments to Convective Momentum Transport (CMT) parametrization based on analysis of CRM and SCM". In: *Met Office R&D Tech. Rep* 530.

Sullivan, Ryan C, Crippa, Paola, Matsui, Hitoshi, Leung, L Ruby, Zhao, Chun, Thota, Abhinav, and Pryor, Sara C (2018). "New particle formation leads to cloud dimming". In: *npj Climate and Atmospheric Science* 1.1, pp. 1–9. DOI: https://doi.org/10.1038/s41612-018-0019-7.

Tang, S., Xie, S., Zhang, Y., Zhang, M., Schumacher, C., Upton, H., Jensen, M. P., Johnson, K. L., Wang, M., Ahlgrimm, M., Feng, Z., Minnis, P., and Thieman, M. (2016). "Large-scale vertical velocity, diabatic heating and drying profiles associated with seasonal and diurnal variations of convective systems observed in the GoAmazon2014/5 experiment". In: *Atmospheric Chemistry and Physics* 16.22, pp. 14249–14264. DOI: 10.5194/acp-16-14249-2016.

Tao, Wei-Kuo, Chen, Jen-Ping, Li, Zhanqing, Wang, Chien, and Zhang, Chidong (2012). "Impact of aerosols on convective clouds and precipitation". In: *Reviews of Geophysics* 50.2. DOI: https://doi.org/10.1029/2011RG000369.

Thornton, D. C., Bandy, A. R., Blomquist, B. W., Bradshaw, J. D., and Blake, D. R. (1997). "Vertical transport of sulfur dioxide and dimethyl sulfide in deep convection and its role in new particle formation". In: *Journal of Geophysical Research: Atmospheres* 102.D23, pp. 28501–28509. DOI: https://doi.org/10.1029/97JD01647. eprint: https://agupubs.onlinelibrary.wiley.com/doi/pdf/10.1029/97JD01647.

Tröstl, Jasmin, Chuang, Wayne K, Gordon, Hamish, Heinritzi, Martin, Yan, Chao, Molteni, Ugo, Ahlm, Lars, Frege, Carla, Bianchi, Federico, Wagner, Robert, et al. (2016). "The role of low-volatility organic compounds in initial particle growth in the atmosphere". In: *Nature* 533.7604, p. 527. DOI: https://doi.org/10.1038/nature18271.

Twohy, Cynthia H., Clement, Charles F., Gandrud, Bruce W., Weinheimer, Andrew J., Campos, Teresa L., Baumgardner, Darrel, Brune, William H., Faloona, Ian, Sachse, Glen W., Vay, Stephanie A., and Tan, David (2002). "Deep convection as a source of new particles in the midlatitude upper troposphere". In: *Journal of Geophysical Research: Atmospheres* 107.D21, AAC 6-1-AAC 6–10. DOI: https://doi.org/10.1029/2001JD000323. eprint: https://agupubs.onlinelibrary.wiley.com/doi/pdf/10.1029/2001JD000323.

Twomey, S. (1977). "The Influence of Pollution on the Shortwave Albedo of Clouds". In: *Journal of Atmospheric Sciences* 34.7, pp. 1149–1152. DOI: 10.1175/1520-0469(1977)034<1149:TIOPOT>2.0.CO;2.

Tyson, P.D. (1997). "Atmospheric transport of aerosols and trace gases over southern Africa". In: *Progress in Physical Geography: Earth and Environment* 21.1, pp. 79–101. DOI: 10.1177/030913339702100105. eprint: https://doi.org/10.1177/030913339702100105.

Van Der Werf, Guido R, Randerson, James T, Collatz, G James, and Giglio, Louis (2003). "Carbon emissions from fires in tropical and subtropical ecosystems". In: *Global Change Biology* 9.4, pp. 547–562. DOI: https://doi.org/10.1046/j.1365-2486.2003.00604.x.

Vehkamäki, H., Dal Maso, M., Hussein, T., Flanagan, R., Hyvärinen, A., Lauros, J., Merikanto, P., Mönkkönen, M., Pihlatie, K., Salminen, K., Sogacheva, L., Thum, T., Ruuskanen, T. M., Keronen, P., Aalto, P. P., Hari, P., Lehtinen, K. E. J., Rannik, Ü., and Kulmala, M. (2004). "Atmospheric particle formation events at Värriö measurement station in Finnish Lapland 1998-2002". In: *Atmospheric Chemistry and Physics* 4.7, pp. 2015–2023. DOI: 10.5194/acp-4-2015-2004.

Vehkamäki, Hanna, Kulmala, Markku, Napari, Ismo, Lehtinen, Kari EJ, Timmreck, Claudia, Noppel, Madis, and Laaksonen, Ari (2002). "An improved parameterization for sulfuric acid–water nucleation rates for tropospheric and stratospheric conditions". In: *Journal of Geophysical Research: Atmospheres* 107.D22. DOI: https://doi.org/10.1029/2002JD002184.

Vehkamäki, Hanna, Paatero, Pentti, Kulmala, Markku, and Laaksonen, Ari (1994). "Binary nucleation kinetics: A matrix method". In: *The Journal of chemical physics* 101.11, pp. 9997–10002. DOI: https://doi.org/10.1063/1.468421.

Vijayakumar, K., Safai, P.D., Devara, P.C.S., Rao, S. Vijaya Bhaskara, and Jayasankar, C.K. (2016). "Effects of agriculture crop residue burning on aerosol properties and long-range transport over northern India: A study using satellite data and model simulations". In: *Atmospheric Research* 178-179, pp. 155–163. DOI: https://doi.org/10.1016/j.atmosres.2016.04.003.

Wagner, Robert, Yan, Chao, Lehtipalo, Katrianne, Duplissy, Jonathan, Nieminen, Tuomo, Kangasluoma, Juha, Ahonen, Lauri R, Dada, Lubna, Kontkanen, Jenni, Manninen, Hanna E, et al. (2017). "The role of ions in new particle formation in the CLOUD chamber". In: *Atmospheric Chemistry and Physics* 17.24, pp. 15181–15197. DOI: https://doi.org/10.5194/acp-17-15181-2017.

Wallace, John M and Hobbs, Peter V (2006). *Atmospheric science: an introductory survey*. Vol. 92. Elsevier.

Walters, D., Baran, A. J., Boutle, I., Brooks, M., Earnshaw, P., Edwards, J., Furtado, K., Hill, P., Lock, A., Manners, J., Morcrette, C., Mulcahy, J., Sanchez, C., Smith, C., Stratton, R., Tennant, W., Tomassini, L., Van Weverberg, K., Vosper, S., Willett, M., Browse, J., Bushell, A., Carslaw, K., Dalvi, M., Essery, R., Gedney, N., Hardiman, S., Johnson, B., Johnson, C., Jones, A., Jones, C., Mann, G., Milton, S., Rumbold, H., Sellar, A., Ujiie, M., Whitall, M.,

Williams, K., and Zerroukat, M. (2019). "The Met Office Unified Model Global Atmosphere 7.0/7.1 and JULES Global Land 7.0 configurations". In: *Geoscientific Model Development* 12.5, pp. 1909–1963. DOI: 10.5194/gmd-12-1909-2019.

Wang, Jian, Krejci, Radovan, Giangrande, Scott, Kuang, Chongai, Barbosa, Henrique MJ, Brito, Joel, Carbone, Samara, Chi, Xuguang, Comstock, Jennifer, Ditas, Florian, et al. (2016). "Amazon boundary layer aerosol concentration sustained by vertical transport during rainfall". In: *Nature* 539.7629, p. 416. DOI: https://doi.org/10.1038/nature19819.

Wang, M. and Penner, J. E. (2009). "Aerosol indirect forcing in a global model with particle nucleation". In: *Atmospheric Chemistry and Physics* 9.1, pp. 239–260. DOI: 10.5194/acp-9-239-2009.

Wang, Nanchao, Zhang, Kai, Shen, Xue, Wang, Yuan, Li, Jing, Li, Chencai, Mao, Jietai, Malinka, Aleksey, Zhao, Chuanfeng, Russell, Lynn M., Guo, Jianping, Gross, Silke, Liu, Chong, Yang, Jing, Chen, Feitong, Wu, Lingyun, Chen, Sijie, Ke, Ju, Xiao, Da, Zhou, Yudi, Fang, Jing, and Liu, Dong (2022). "Dual-field-of-view high-spectral-resolution lidar: Simultaneous profiling of aerosol and water cloud to study aerosol–cloud interaction". In: *Proceedings of the National Academy of Sciences* 119.10, e2110756119. DOI: 10.1073/pnas.2110756119. eprint: https://www.pnas.org/doi/pdf/10.1073/pnas.2110756119.

Wang, Y., Wan, Q., Meng, W., Liao, F., Tan, H., and Zhang, R. (2011). "Long-term impacts of aerosols on precipitation and lightning over the Pearl River Delta megacity area in China". In: *Atmospheric Chemistry and Physics* 11.23, pp. 12421–12436. DOI: 10.5194/acp-11-12421-2011.

Weber, R. J., Marti, J. J., McMurry, P. H., Eisele, F. L., Tanner, D. J., and Jefferson, A. (1997). "Measurements of new particle formation and ultrafine particle growth rates at a clean continental site". In: *Journal of Geophysical Research: Atmospheres* 102.D4, pp. 4375–4385. DOI: https://doi.org/10.1029/96JD03656. eprint: https://agupubs.onlinelibrary.wiley.com/doi/pdf/10.1029/96JD03656.

Weber, RJ, McMurry, PH, Eisele, FL, and Tanner, DJ (1995). "Measurement of expected nucleation precursor species and 3–500-nm diameter particles at Mauna Loa observatory, Hawaii".

In: *Journal of Atmospheric Sciences* 52.12, pp. 2242–2257. DOI: https://doi.org/10.1175/1520-0469(1995)052<2242:MOENPS>2.0.CO;2.

Weigel, R, Borrmann, S, Kazil, J, Minikin, A, Stohl, A, Wilson, JC, Reeves, JM, Kunkel, D, De Reus, M, Frey, W, et al. (2011). "In situ observations of new particle formation in the tropical upper troposphere: the role of clouds and the nucleation mechanism". In: *Atmospheric Chemistry and Physics* 11.18, pp. 9983–10010. DOI: https://doi.org/10.5194/acp-11-9983-2011.

Weigum, N., Schutgens, N., and Stier, P. (2016). "Effect of aerosol subgrid variability on aerosol optical depth and cloud condensation nuclei: implications for global aerosol modelling". In: *Atmospheric Chemistry and Physics* 16.21, pp. 13619–13639. DOI: 10.5194/acp-16-13619-2016.

Weigum, N. M., Stier, P., Schwarz, J. P., Fahey, D. W., and Spackman, J. R. (2012). "Scales of variability of black carbon plumes over the Pacific Ocean". In: *Geophysical Research Letters* 39.15. DOI: https://doi.org/10.1029/2012GL052127. eprint: https://agupubs.onlinelibrary.wiley.com/doi/pdf/10.1029/2012GL052127.

Wellmann, C., Barrett, A. I., Johnson, J. S., Kunz, M., Vogel, B., Carslaw, K. S., and Hoose, C. (2018). "Using Emulators to Understand the Sensitivity of Deep Convective Clouds and Hail to Environmental Conditions". In: *Journal of Advances in Modeling Earth Systems* 10.12, pp. 3103–3122. DOI: https://doi.org/10.1029/2018MS001465. eprint: https://agupubs.onlinelibrary.wiley.com/doi/pdf/10.1029/2018MS001465.

Wendisch, Manfred, Pöschl, Ulrich, Andreae, Meinrat O, Machado, Luiz AT, Albrecht, Rachel, Schlager, Hans, Rosenfeld, Daniel, Martin, Scot T, Abdelmonem, Ahmed, Afchine, Armin, et al. (2016). "ACRIDICON–CHUVA campaign: Studying tropical deep convective clouds and precipitation over Amazonia using the new German research aircraft HALO". In: *Bulletin of the American Meteorological Society* 97.10, pp. 1885–1908. DOI: https://doi.org/10.1175/BAMS-D-14-00255.1.

Werf, G. R. van der, Randerson, J. T., Giglio, L., Collatz, G. J., Kasibhatla, P. S., and Arellano Jr., A. F. (2006). "Interannual variability in global biomass burning emissions from 1997 to

2004". In: *Atmospheric Chemistry and Physics* 6.11, pp. 3423–3441. DOI: 10.5194/acp-6-3423-2006.

West, R. E. L., Stier, P., Jones, A., Johnson, C. E., Mann, G. W., Bellouin, N., Partridge, D. G., and Kipling, Z. (2014). "The importance of vertical velocity variability for estimates of the indirect aerosol effects". In: *Atmospheric Chemistry and Physics* 14.12, pp. 6369–6393. DOI: 10.5194/acp-14-6369-2014.

Williamson, Christina J, Kupc, Agnieszka, Axisa, Duncan, Bilsback, Kelsey R, Bui, ThaoPaul, Campuzano-Jost, Pedro, Dollner, Maximilian, Froyd, Karl D, Hodshire, Anna L, Jimenez, Jose L, et al. (2019). "A large source of cloud condensation nuclei from new particle formation in the tropics". In: *Nature* 574.7778, pp. 399–403. DOI: https://doi.org/10.1038/s41586-019-1638-9.

Wilson, Damian R. and Ballard, Susan P. (1999). "A microphysically based precipitation scheme for the UK meteorological office unified model". In: *Quarterly Journal of the Royal Meteorological Society* 125.557, pp. 1607–1636. DOI: https://doi.org/10.1002/qj.49712555707. eprint: https://rmets.onlinelibrary.wiley.com/doi/pdf/10.1002/qj.49712555707.

Wimmer, Daniela, Buenrostro Mazon, Stephany, Manninen, Hanna Elina, Kangasluoma, Juha, Franchin, Alessandro, Nieminen, Tuomo, Backman, John, Wang, Jian, Kuang, Chongai, Krejci, Radovan, et al. (2018). "Ground-based observation of clusters and nucleation-mode particles in the Amazon". In: *Atmospheric Chemistry and Physics* 18.17, pp. 13245–13264. DOI: https://doi.org/10.5194/acp-18-13245-2018.

Wu, Zhijun, Hu, Min, Liu, Shang, Wehner, Birgit, Bauer, Stefan, Ma ßling, Andreas, Wiedensohler, Alfred, Petäjä, Tuukka, Dal Maso, Miikka, and Kulmala, Markku (2007). "New particle formation in Beijing, China: Statistical analysis of a 1-year data set". In: *Journal of Geophysical Research: Atmospheres* 112.D9. DOI: https://doi.org/10.1029/2006JD007406. eprint: https://agupubs.onlinelibrary.wiley.com/doi/pdf/10.1029/2006JD007406.

Wurzler, S., Flossmann, A. I., Pruppacher, H. R., and Schwartz, S. E. (1995). "The scavenging of nitrate by clouds and precipitation". In: *Journal of Atmospheric Chemistry* 20.3, pp. 259–280. DOI: 10.1007/BF00694497.

Wurzler, Sabine (1998). "The scavenging of nitrogen compounds by clouds and precipitation:: Part II. The effects of cloud microphysical parameterization on model predictions of nitric acid scavenging by clouds". In: *Atmospheric Research* 47-48, pp. 219–233. DOI: https://doi.org/10.1016/S0169-8095(97)00091-4.

Wyant, Matthew C., Bretherton, Christopher S., Wood, Robert, Blossey, Peter N., and McCoy, Isabel L. (2022). "High Free-Tropospheric Aitken-Mode Aerosol Concentrations Buffer Cloud Droplet Concentrations in Large-Eddy Simulations of Precipitating Stratocumulus". In: *Journal of Advances in Modeling Earth Systems* 14.6. e2021MS002930 2021MS002930, e2021MS002930. DOI: https://doi.org/10.1029/2021MS002930. eprint: https://agupubs.onlinelibrary.wiley.com/doi/pdf/10.1029/2021MS002930.

Xue, Huiwen and Feingold, Graham (2006). "Large-eddy simulations of trade wind cumuli: Investigation of aerosol indirect effects". In: *Journal of the atmospheric sciences* 63.6, pp. 1605–1622. DOI: https://doi.org/10.1175/JAS3706.1.

Xue, Huiwen, Feingold, Graham, and Stevens, Bjorn (2008). "Aerosol Effects on Clouds, Precipitation, and the Organization of Shallow Cumulus Convection". In: *Journal of the Atmospheric Sciences* 65.2, pp. 392–406. DOI: 10.1175/2007JAS2428.1.

Yáñez-Serrano, Ana Maria, Nölscher, Anke Christine, Bourtsoukidis, Efstratios, Alves, Eliane Gomes, Ganzeveld, Laurens, Bonn, Boris, Wolff, Stefan, Sa, Marta, Yamasoe, Marcia, Williams, Jonathan, et al. (2018). "Monoterpene chemical speciation in a tropical rainforest: variation with season, height, and time of day at the Amazon Tall Tower Observatory (ATTO)". In: *Atmospheric Chemistry and Physics* 18.5, pp. 3401–3418. DOI: https://doi.org/10.5194/acp-18-3403-2018.

Yang, Qing, Easter, Richard C, Campuzano-Jost, Pedro, Jimenez, Jose L, Fast, Jerome D, Ghan, Steven J, Wang, Hailong, Berg, Larry K, Barth, Mary C, Liu, Ying, et al. (2015). "Aerosol transport and wet scavenging in deep convective clouds: A case study and model evaluation using a multiple passive tracer analysis approach". In: *Journal of Geophysical Research: Atmospheres* 120.16, pp. 8448–8468. DOI: https://doi.org/10.1002/2015JD023647.

Yin, Y, Carslaw, KS, and Feingold, G (2005). "Vertical transport and processing of aerosols in a mixed-phase convective cloud and the feedback on cloud development". In: *Quarterly*

Journal of the Royal Meteorological Society: A journal of the atmospheric sciences, applied meteorology and physical oceanography 131.605, pp. 221–245. DOI: https://doi.org/10.1256/qj.03.186.

Yin, Y, Carslaw, KS, and Parker, DJ (2002). "Redistribution of trace gases by convective clouds-mixed-phase processes". In: *Atmospheric Chemistry and Physics* 2.4, pp. 293–306. DOI: https://doi.org/10.5194/acp-2-293-2002.

Yin, Y, Parker, DJ, and Carslaw, KS (2001). "Simulation of trace gas redistribution by convective clouds-Liquid phase processes". In: *Atmospheric Chemistry and Physics* 1.1, pp. 19–36. DOI: https://doi.org/10.5194/acp-1-19-2001.

Yin, Yan, Chen, Qian, Jin, Lianji, Chen, Baojun, Zhu, Shichao, and Zhang, Xiaopei (2012). "The effects of deep convection on the concentration and size distribution of aerosol particles within the upper troposphere: A case study". In: *Journal of Geophysical Research: Atmospheres* 117.D22. DOI: https://doi.org/10.1029/2012JD017827.

Yu, F., Luo, G., Nadykto, A. B., and Herb, J. (2017). "Impact of temperature dependence on the possible contribution of organics to new particle formation in the atmosphere". In: *Atmospheric Chemistry and Physics* 17.8, pp. 4997–5005. DOI: 10.5194/acp-17-4997-2017.

Yu, F., Luo, G., Nair, A. A., Schwab, J. J., Sherman, J. P., and Zhang, Y. (2020). "Wintertime new particle formation and its contribution to cloud condensation nuclei in the Northeastern United States". In: *Atmospheric Chemistry and Physics* 20.4, pp. 2591–2601. DOI: 10.5194/acp-20-2591-2020.

Yu, Fangqun, Ma, Xiaoyan, and Luo, Gan (May 2013). "Anthropogenic contribution to cloud condensation nuclei and the first aerosol indirect climate effect". In: *Environmental Research Letters* 8.2, p. 024029. DOI: 10.1088/1748-9326/8/2/024029.

Yu, Pengfei, Froyd, Karl D, Portmann, Robert W, Toon, Owen B, Freitas, Saulo R, Bardeen, Charles G, Brock, Charles, Fan, Tianyi, Gao, Ru-Shan, Katich, Joseph M, et al. (2019). "Efficient In-cloud Removal of Aerosols by Deep Convection". In: *Geophysical Research Letters*. DOI: https://doi.org/10.1029/2018GL080544.

Zannoni, Nora, Leppla, Denis, Assis, Pedro Ivo Lembo Silveira de, Hoffmann, Thorsten, Sá, Marta, Araújo, Alessandro, and Williams, Jonathan (2020). "Surprising chiral composition changes over the Amazon rainforest with height, time and season". In: *Communications Earth and Environment* 1.1, pp. 1–11. DOI: https://doi.org/10.1038/s43247-020-0007-9.

Zhang, Leiming, Vet, Robert, and Michelangeli, Diane V. (2006). "Numerical Investigation of Gas Scavenging by Weak Precipitation". In: *Journal of Atmospheric Chemistry* 54.3, pp. 203–231. DOI: 10.1007/s10874-005-9010-x.

Zhang, Y., Fan, J., Li, Z., and Rosenfeld, D. (2021). "Impacts of cloud microphysics parameterizations on simulated aerosol–cloud interactions for deep convective clouds over Houston". In: *Atmospheric Chemistry and Physics* 21.4, pp. 2363–2381. DOI: 10.5194/acp-21-2363-2021.

Zhao, Bin, Fast, Jerome D, Donahue, Neil M, Shrivastava, Manish, Schervish, Meredith, Shilling, John E, Gordon, Hamish, Wang, Jian, Gao, Yang, Zaveri, Rahul A, et al. (2021). "Impact of Urban Pollution on Organic-Mediated New-Particle Formation and Particle Number Concentration in the Amazon Rainforest". In: *Environmental Science & Technology* 55.8, pp. 4357–4367. DOI: https://doi.org/10.1021/acs.est.0c07465.

Zhao, Bin, Shrivastava, Manish, Donahue, Neil M, Gordon, Hamish, Schervish, Meredith, Shilling, John E, Zaveri, Rahul A, Wang, Jian, Andreae, Meinrat O, Zhao, Chun, et al. (2020). "High concentration of ultrafine particles in the Amazon free troposphere produced by organic new particle formation". In: *Proceedings of the National Academy of Sciences* 117.41, pp. 25344–25351. DOI: https://doi.org/10.1073/pnas.2006716117.

Zhao, Chunsheng, Tie, Xuexi, Brasseur, Guy, Noone, Kevin J., Nakajima, Teruyuki, Zhang, Qiang, Zhang, Renyi, Huang, Mengyu, Duan, Ying, Li, Gelun, and Ishizaka, Yutaka (2006). "Aircraft measurements of cloud droplet spectral dispersion and implications for indirect aerosol radiative forcing". In: *Geophysical Research Letters* 33.16. DOI: https://doi.org/10.1029/2006GL026653. eprint: https://agupubs.onlinelibrary.wiley.com/doi/pdf/10.1029/2006GL026653.

Zheng, Guangjie, Wang, Yang, Wood, Robert, Jensen, Michael P., Kuang, Chongai, McCoy, Isabel L., Matthews, Alyssa, Mei, Fan, Tomlinson, Jason M., Shilling, John E., Zawadowicz, Maria A., Crosbie, Ewan, Moore, Richard, Ziemba, Luke, Andreae, Meinrat O., and Wang,

Jian (2021). "New particle formation in the remote marine boundary layer". In: *Nature Communications* 12.1, p. 527. DOI: 10.1038/s41467-020-20773-1.

Zhou, Jingchuan, Swietlicki, Erik, Hansson, Hans Christen, and Artaxo, Paulo (2002). "Submicrometer aerosol particle size distribution and hygroscopic growth measured in the Amazon rain forest during the wet season". In: *Journal of Geophysical Research: Atmospheres* 107.D20, LBA 22-1-LBA 22–10. DOI: https://doi.org/10.1029/2000JD000203. eprint: https://agupubs.onlinelibrary.wiley.com/doi/pdf/10.1029/2000JD000203.

Zhou, Y., Hakala, S., Yan, C., Gao, Y., Yao, X., Chu, B., Chan, T., Kangasluoma, J., Gani, S., Kontkanen, J., Paasonen, P., Liu, Y., Petäjä, T., Kulmala, M., and Dada, L. (2021). "Measurement report: New particle formation characteristics at an urban and a mountain station in northern China". In: *Atmospheric Chemistry and Physics* 21.23, pp. 17885–17906. DOI: 10.5194/acp-21-17885-2021.

Zhu, Jialei, Penner, Joyce E, Yu, Fangqun, Sillman, Sanford, Andreae, Meinrat O, and Coe, Hugh (2019). "Decrease in radiative forcing by organic aerosol nucleation, climate, and land use change". In: *Nature Communications* 10.1, pp. 1–7. DOI: https://doi.org/10.1038/s41467-019-08407-7.

Appendix A

Appendix for Chapter 3: The contribution of regional aerosol nucleation and transport to low-level CCN in an Amazonian deep convective environment

The videos to show the vertical transport of nucleation, Aitken and accumulation mode aerosols in the regional model from the NPF_13-16km simulation can be accessed from below.

https://drive.google.com/file/d/1DTWCyaevqFDTk5UfkMrxDjArjaNq3-TY/view?usp=sharing

https://drive.google.com/file/d/19JnwQNFG-NjUETIpcaWD620kXGx0bGF0/view?usp=sharing

https://drive.google.com/file/d/10v5Ygb8zDje8GpoH00pbbBIC4aGpPJ_z/view?usp=sharing

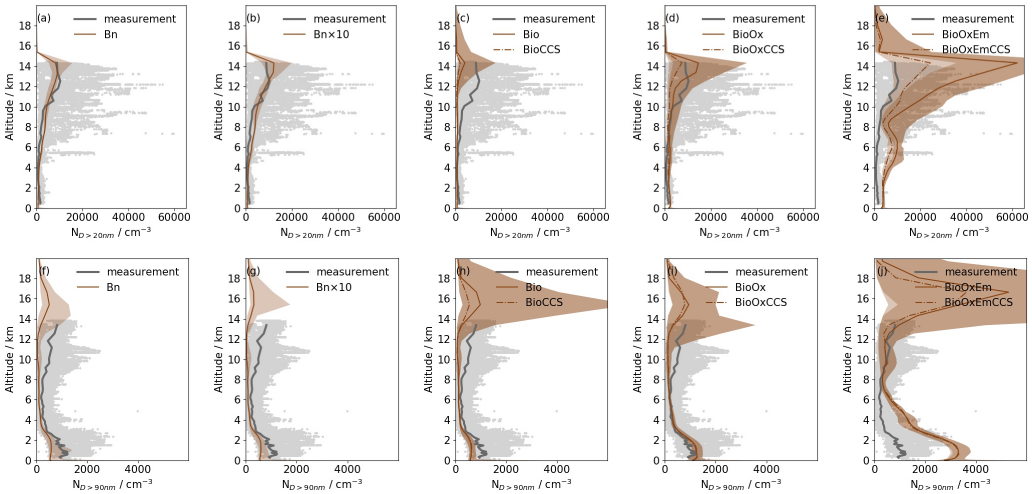

Figure A.1: The observed and modelled vertical profiles of median number concentrations of particles with diameters >20 nm ($N_{D>20nm}$, top) and >90 nm ($N_{D>90nm}$, bottom). The observations are shown in dots and grey line (repeated for all panels), and the modelled results are from the regional simulations averaged from 0 UTC on 17 September to 23 UTC on 18 September 2014, (a) Bn, (b) Bn×10, (c) Bio and BioCCS (dashed line), (d) BioOx and BioOxCCS (dashed line), and (e) BioOxEm and BioOxEmCCS (dashed line), corrected to standard temperature and pressure (Eq. 3.1). The shading represents 2.5% and 97.5% percentiles from the modelling results. The grey dots are individual observations from all flights during ACRIDICON-CHUVA with a time resolution of 1 minute, and the thick grey lines are the medians of the observations binned within the same height ranges as the regional model levels.

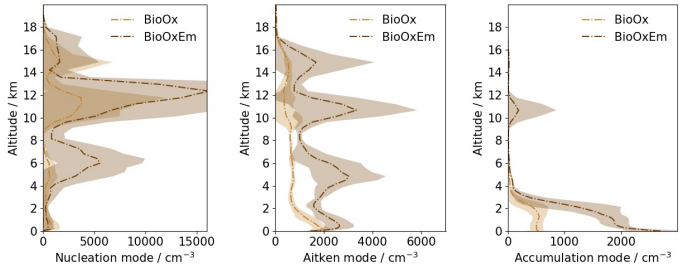

Figure A.2: The time- and domain-averaged profiles of the nucleation, Aitken and accumulation mode aerosol in the simulations BioOx, and BioOxEm from the global model in the upwind (East) of the regional domain.

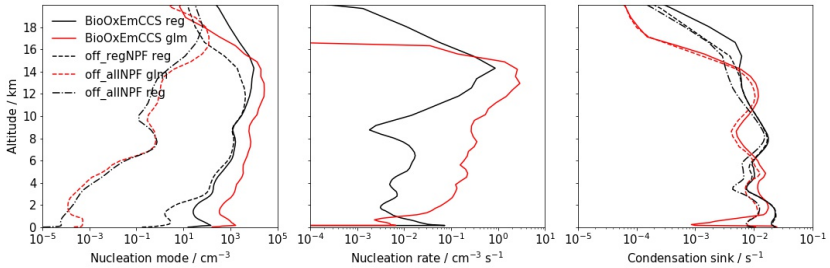

Figure A.3: The time- and regional domain-averaged profiles of nucleation mode aerosol concentrations, nucleation rate and condensation sink in the simulations BioOxEmCCS (solid), off_allNPF (dotted dashed), and off_regNPF (dashed) in the global model (red) and regional model (black).

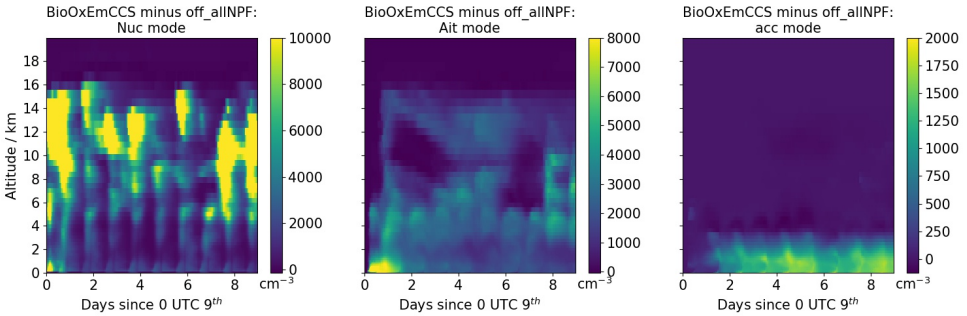

Figure A.4: Time series of the global domain averaged aerosol number concentrations at the same location of the regional domain. The number concentrations are the differences between the BioOxEmCCS and off_allNPF simulations.